

**Development of Self-assembled Layer-by-layer Polymeric Carriers to  
Deliver Small and Macromolecule Therapeutics**

**THESIS**

Submitted in partial fulfillment  
of the requirements for the degree of

**DOCTOR OF PHILOSOPHY**

by

**M. PRAVEEN KUMAR**

**ID. No. 2010PHXF429H**

Under the supervision of

**Dr. VENKATA VAMSI KRISHNA VENUGANTI**



**BITS Pilani**

Pilani | Dubai | Goa | Hyderabad

**BIRLA INSTITUTE OF TECHNOLOGY AND SCIENCE, PILANI**

**2015**

**CERTIFICATE**

This is to certify that the thesis entitled “**Development of Self-assembled Layer-by-layer Polymeric Carriers to Deliver Small and Macromolecule Therapeutics**” and submitted by **M. Praveen Kumar** ID. No. **2010PHXF429H** for award of Ph. D. of the Institute embodies original work done by him under my supervision.

Signature of the supervisor :

Name in capital letters : VENKATA VAMSI KRISHNA VENUGANTI

Designation : Assistant Professor

Date :

## ACKNOWLEDGEMENTS

Words cannot express my heartfelt gratitude to my mentor and guide, Dr. Venkata Vamsi Krishna Venuganti, Assistant Professor, Department of Pharmacy, BITS Pilani, Hyderabad Campus. He has been a constant source of support and inspiration to me throughout my course of work. His boundless enthusiasm coupled with his sharp intellectual abilities has left an indelible mark on me. His moral support and timely advice at crucial times are unforgettable. I am highly indebted to him and sincerely acknowledge his help at all times.

I am extremely obliged to Prof. Shrikanth Y Charde, Associate Professor and Head, Department of Pharmacy and Prof. Punnarao Ravi, Department of Pharmacy, BITS-Pilani Hyderabad, who acted as Doctoral Advisory Committee (DAC) members and gave their valuable comments whenever needed. My sincere thanks to Prof. Bijendra Nath Jain, Prof. M. M. S. Anand, Registrar, Prof. S. K. Verma, Dean, Academic Research (Ph.D. Programme) BITS-Pilani, Pilani, Prof. V. S. Rao, Director, Prof. M. B. Srinivas, Dean, General Administration and Prof. Vidya Rajesh, Associate Dean, Academic Research (Ph.D. Programme) BITS-Pilani, Hyderabad, for providing necessary support to accomplish my research work. I am grateful to Prof. D. Sriram and Prof. P. Yogeewari, Department of Pharmacy, BITS-Pilani Hyderabad for for sharing their vast experience and technical knowledge with me at needy times. I also thank Dr. Swathi Biswas, Asst. Professor, Convener, Departmental Research Committee (DRC) for her invaluable support.

My lab mates Mr. Suman, Mr. Anup, Ms. Shubhmita, Mr. Shailender, Mr. Omkar, Ms. Preeti, Mr. Vishnu deserve special thanks for making congenial environment in the lab. It would be incomplete if I failed to thank my fellow scholars Dr. Aditya, Dr. Rahul Vats, Dr. Mallika, Mr. Madhu babu, Mr. Saketh, Mr. Mahibalan, Mr. Srikanth, Mr. Brahmam, Mr.

Koushik, Ms. Rukaiyya S Khan and Mr. Gangadhar for giving me overwhelming support all these days. My heartfelt thanks to supporting staff Mrs. Saritha, Mr. Rajesh, Mr. Venkat, Mrs. Shalini, Mr. Ramana Babu, Mr. Uppalaya and Mr. Praveen for their extra-ordinary support.

I appreciate the Council for Scientific and Industrial Research (CSIR)-New Delhi for awarding Senior Research Fellowship to pursue doctoral studies. I also thank SERB, Department of Science and Technology (DST), Indian Council of Medical Research (ICMR) and Centre for International Co-operation in science (CICS) for providing travel assistance to present my research work at various conferences in abroad.

This section would be incomplete without thanking my family for their unwavering support throughout this period. My heartfelt thanks to my parents, Mr Rajaiah and Mrs Laxmi and my brothers Mr. Venu and Mr. Srinivas for being pillars of my life and for providing me with unconditional support at all times. I can hardly find words to express my gratitude to my wife Pravalika for her patience and sacrifice.

**Praveen Kumar M**

July, 2015



## ABSTRACT

Rapid growth in the drug discovery science resulted in the development of potential small molecule drugs and biotechnology based drugs including proteins and nucleic acids. However, the clinical application of many new therapeutics is limited by inefficient drug delivery systems. There is a need for development of drug carriers which can deliver the cargo in a stable and efficient manner. Recently, the self-assembled delivery systems have shown potential as drug carriers with improved solubilisation of drugs, stimuli-responsive targeted delivery, reduced toxicity, achieving controlled release and protection of therapeutic agent against biological degradation. Among the various self-assembly approaches reported for the fabrication of drug delivery carriers, the layer-by-layer (LbL) technique has gained greater interest. LbL assembly is a highly versatile technique, where polymers can be coated on different sizes, shapes and surface chemistry. Essentially, the LbL technique involves sequential adsorption of oppositely charged polyelectrolytes on a template. A planar template would result in the formation of a thin film, while a spherical sacrificial template would result in the formation of a nano- or microcapsule.

This dissertation explored the development of novel drug delivery carriers including microcapsules and thin films using layer-by-layer technology for delivery of small and macro-molecule therapeutics. To this end, the overall objective of the study is fabrication and characterization of layer-by-layer assembled microcapsules for systemic application and layer-by-layer thin films for topical application.

The first objective was to investigate the influence of physical and chemical properties of active molecules on encapsulation in LbL-MC. Layer-by-layer microcapsules (LbL-MC) were prepared by sequential adsorption of poly(styrene sulfonate) (PSS) and poly(ethyleneimine) (PEI) on calcium carbonate sacrificial templates. Model small molecules

with varying charge, anionic - ascorbic acid, indomethacin; cationic – imatinib mesylate, rhodamine; and neutral – 5-fluorouracil, estradiol were encapsulated in LbL-MC; whereas, bovine serum albumin (BSA) was used as a model protein. To achieve pH-responsive LbL-MC, we used poly(styrene sulfonic acid) and polyallylamine hydrochloride polymers for layering. Encapsulation efficiency of BSA in LbL-MC was studied by co-precipitation and physical adsorption methods. The influence of pH on encapsulation and release of model small molecules and BSA in LbL-MC was studied at pH 2-10. The blank and active molecules loaded LbL-MC were characterized using scanning electron microscope, zetasizer, FTIR spectroscope and differential scanning calorimeter (DSC). Cell viability in the presence of blank and imatinib mesylate loaded LbL-MC was studied in B16F10 murine melanoma cells. Biodistribution of imatinib mesylate loaded LbL-MC before and after PEGylation was studied in BALB/c mice. The stability of BSA entrapped in LbL-MC was studied after incubation with trypsin using sodium dodecyl sulphate polyacrylamide gel electrophoresis (SDS-PAGE).

Results showed spherical LbL-MC with average particle size of  $3.0 \pm 0.4 \mu\text{m}$  diameter. The zeta-potential was found to be  $11.2 \pm 0.9$  and  $-7.4 \pm 0.7$  mV for blank LbL-MC and BSA loaded LbL-MC, respectively. For small molecule entrapment, the encapsulation efficiency (% EE) of LbL-MC increased with the increase in solute concentration. Increase in pH from 2-6 increased the encapsulation of charged molecules in LbL-MC. Charged molecules showed greater EE in LbL-MC compared to neutral molecule. In adsorption method, BSA encapsulation in LbL-MC was found to be greater at pH 6.5 and 0.2M NaCl. Co-precipitation of BSA with  $\text{CaCO}_3$  resulted in 4-fold greater encapsulation efficiency (%) of BSA in LbL-MC compared with adsorption method. In-vitro studies showed pH dependent release of BSA from LbL-MC. At pH 4, BSA release was controlled up to 120h, whereas at pH 7.4 and 9.0, 100% release was achieved within 36h. SDS-PAGE showed that BSA encapsulated in LbL-

MC through co-precipitation method is stable towards trypsin treatment, while BSA encapsulated through adsorption method showed degradation. Free imatinib mesylate showed significantly ( $p < 0.05$ ) more cytotoxicity compared with IM loaded LbL-MC studied in B16F10 cells. Bio-distribution studies showed that PEGylation of LbL-MC decreased the liver and spleen uptake of IM encapsulated LbL-MC. Overall, LbL-MC can be developed as a potential carrier for small molecules and proteins depending on their physical and chemical properties.

The second objective of the study was to fabricate and characterize the drug loaded LbL thin films and evaluate their potential in excisional dermal wound management. Pirfenidone (PFD) was used as a small model molecule, while siRNA and epidermal growth factor (EGF) were model macromolecules. The rationale for selection of PFD and transforming growth factor-beta (TGF- $\beta$ ) siRNA was to suppress TGF- $\beta$  induced collagen secretion and fibrosis within wound tissue. Polyelectrolyte multilayer films were prepared by LbL sequential adsorption of chitosan and sodium alginate on a glass template. The prepared LbL thin films were characterized using UV-spectroscopy, FTIR and DSC. The physical and mechanical properties including thickness, swelling, porosity, tensile strength and adhesion strength were studied. In-vitro cell adhesion and cell viability studies in the presence of LbL thin film was performed in A431 human epidermoid carcinoma cells. The effect of PFD on excisional dermal wounds when delivered using LbL films was studied in C57BL/6 mouse model. LbL film (1 cm<sup>2</sup>) containing 1 mg of PFD was applied once daily for 12 days on the wounded site. The wound tissue was collected after sacrificing the mice on 3, 6, 9 and 12<sup>th</sup> day. Then the samples were analyzed for total protein, collagen and TGF- $\beta$  expression. Furthermore, siRNA against TGF- $\beta$  and EGF were loaded as the final two layers of LbL thin film. The entrapment and release of siRNA and EGF was studied using SDS-PAGE and dialysis membrane method. These films were applied daily (EGF loaded film) or alternate

days (siRNA loaded film) on excisional wounds. Samples were collected and analyzed for total protein, collagen and TGF- $\beta$  suppression.

The UV-spectroscopy, FTIR and DSC studies confirmed the LbL thin film formation. The thickness of LbL thin film was found to be  $15\pm 2$   $\mu\text{m}$ . Each  $\text{cm}^2$  area of film contained 1 mg PFD, 3  $\mu\text{g}$  siRNA and 3  $\mu\text{g}$  EGF. A431 cell adhesion study showed an average of  $3.75\times 10^3$  and  $4.61\times 10^3$  cells/ $\text{mm}^2$  adhered to the chitosan and alginate surfaces of LbL thin film, respectively after 48 h incubation. In-vivo wound healing studies showed an accelerated (<9 days) wound contraction after treatment with the PFD, siRNA and EGF loaded LbL thin film compared with blank films and control siRNA (12 days). Furthermore, the collagen fraction on 12<sup>th</sup> day was significantly ( $p<0.05$ ) decreased after treatment with the PFD and siRNA loaded LbL thin films compared to control groups. After 12 days, the collagen content was found to be  $39.6 \pm 5.3$ ,  $30.2 \pm 2.5$  and  $24.8 \pm 1.2$  mg/g tissue for control (without any treatment), blank film and scrambled siRNA control film, respectively. The collagen content decreased to  $5.45 \pm 1.07$ ,  $3.4 \pm 1.2$  and  $3.7 \pm 0.8$  mg/g tissue after treatment with PFD, siRNA and combination of siRNA and EGF. Western blot analysis confirmed the TGF- $\beta$  suppression after treatment with the PFD and siRNA loaded film. PFD treatment group showed 50, 66.7, 96.6 and 99.2% TGF- $\beta$  suppression after 3, 6, 9 and 12<sup>th</sup> day of excisional wound, respectively. Taken together, LbL strategy can be utilized to fabricate microcapsules and thin films for effective delivery of small and macromolecules for systemic and topical applications.

## TABLE OF CONTENTS

<i>Certificate</i> .....	<i>i</i>
<i>Acknowledgements</i> .....	<i>ii</i>
<i>Abstract</i> .....	<i>iv</i>
<i>List of table</i> .....	<i>x</i>
<i>List of figures</i> .....	<i>xi</i>
<i>List of abbreviations/symbols</i> .....	<i>xv</i>
<b>Chapter 1 Introduction</b> .....	<b>1-65</b>
1.1 Self-assembly.....	1
1.2 Drug delivery systems prepared through self-assembly.....	10
1.3 Basic principles of layer-by-layer assembly.....	20
1.4 Strategies for layer-by-layer assembly.....	32
1.5 Layer-by-layer self-assembled micro- and nanocapsules.....	44
1.6 Layer-by-layer self-assembled thin films.....	52
1.7 Objectives.....	63
<b>Chapter 2 Layer-by-layer microcapsules for small molecule delivery</b> .....	<b>66-96</b>
2.1 Introduction.....	66
2.2 Materials and methods.....	68
2.3 Results.....	75
2.4 Discussion.....	91
2.5 Conclusion.....	96
<b>Chapter 3 Layer-by-layer microcapsules for protein delivery</b> .....	<b>97-116</b>
3.1 Introduction.....	97

3.2	Materials and methods.....	98
3.3	Results.....	104
3.4	Discussion.....	114
3.5	Conclusion.....	116
<b>Chapter 4 Layer-by-layer thin films for small molecule delivery.....</b>		<b>117-155</b>
4.1	Introduction.....	117
4.2	Materials and methods.....	119
4.3	Results.....	132
4.4	Discussion.....	152
4.5	Conclusion.....	155
<b>Chapter 5 Layer-by-layer thin films for macromolecule delivery.....</b>		<b>156-172</b>
5.1	Introduction.....	156
5.2	Materials and methods.....	158
5.3	Results.....	163
5.4	Discussion.....	169
5.5	Conclusion.....	172
<b>Chapter 6 Summary and Conclusions.....</b>		<b>173-174</b>
	Future scope and directions.....	175
	References.....	176
	List of Publications and Presentations.....	216
	Brief Biography of the Candidate.....	219
	Brief Biography of the Supervisor.....	219

## LIST OF TABLES

Table 1.1	List of polyelectrolytes used for layer-by-layer assembly.....	24
Table 2.1	Physico-chemical properties of polymers and model small molecules used in the present study.....	70
Table 2.2	Optimized parameters for entrapment of molecules in LbL-MC.....	84
Table 2.3	Correlation coefficients from regression analysis after model fitting of the release profiles for model molecules.....	86
Table 2.4	Physical constants from Freundlich adsorption isotherm.....	87
Table 3.1	Particle size and zeta-potential measurement of BSA encapsulated LbL-MC.....	106
Table 3.2	Zeta-potential measurements of free BSA and free LbL-MC at different pH conditions and NaCl concentrations.....	111
Table 4.1	Physical and mechanical characteristics of LbL thin films.....	135
Table 4.2	Pharmacokinetic parameters calculated after topical application of PFD loaded LbL thin film.....	151
Table 5.1	Different treatment groups studied for application of TGF-beta siRNA and EGF loaded LbL thin films.....	162

## LIST OF FIGURES

Fig. 1.1	An illustration showing the noncovalent interactions involved in supramolecular chemistry and their strength.....	03
Fig. 1.2	Synthetic and biological building blocks used in supramolecular self-assembly and their potential biomedical applications.....	09
Fig. 1.3	Schematic representation of self-assembled micelles.....	12
Fig. 1.4	Illustration of self-assembled structures (micelles or vesicles) trapped in hydrogels.....	14
Fig. 1.5	Schematic representation of self-assembled micro-emulsion.....	15
Fig. 1.6	Schematic representation of liposome vesicles (a) and liposomes with functionalized or covalently modified amphiphiles (b).....	17
Fig. 1.7	Schematic representation of self-assembled cubosomes.....	18
Fig. 1.8	Schematic representation of polyelectrolyte films and hollow capsules prepared by layer-by-layer assembly.....	20
Fig. 1.9	Classification of substrates used in fabrication of layer-by-layer assembly.....	22
Fig. 1.10	Layer-by-layer assembly of nanofilms for preparing functional materials.....	33
Fig. 1.11	Layer-by-layer assembly using immersive technique.....	35
Fig. 1.12	Layer-by-layer assembly using spin assembly.....	37
Fig. 1.13	Layer-by-layer assembly using spray assembly.....	39
Fig. 1.14	Layer-by-layer assembly using electromagnetic assembly.....	41
Fig. 1.15	Layer-by-layer assembly using fluidic assembly.....	43
Fig. 1.16	Schematic representation of layer-by-layer micro/nanocapsules preparation.....	44
Fig. 1.17	Schematic representation of layer-by-layer thin film formation.....	52
Fig. 2.1	Structure of polymers and model small molecules used in the present study.....	71



Fig. 2.2	Characterization of LbL-MC. Scanning electron micrographs of CaCO <sub>3</sub> (a), blank LbL-MC (b), light microscopic images of LbL-MC before (c) and after disintegration (d) of CaCO <sub>3</sub> . (e) zeta-potential obtained for CaCO <sub>3</sub> and sequential layers of polymers.....	76
Fig. 2.3a	Characterization of LbL-MC. FTIR spectra of CaCO <sub>3</sub> , PSS, PEI, LbL coated CaCO <sub>3</sub> and LbL-MC.....	79
Fig. 2.3b	Characterization of LbL-MC. FTIR spectra of free and LbL-MC encapsulated model molecule.....	80
Fig. 2.4a	DSC thermograms of CaCO <sub>3</sub> , PSS, PEI, LbL coated CaCO <sub>3</sub> and LbL-MC.....	81
Fig. 2.4b	DSC thermograms of free and LbL-MC encapsulated model molecule...	82
Fig. 2.5	Factors influencing encapsulation of molecules into LbL-MC.....	85
Fig. 2.6	In-vitro cumulative release profiles of (a) neat solutions and molecules encapsulated in LbL-MC (b).....	86
Fig. 2.7	B16F10 cell viability after incubation with free IM and IM encapsulated LbL-MC.....	87
Fig. 2.8	Biodistribution of free IM, IM encapsulated LbL-MC and IM encapsulated in PEGylated LbL-MC after intravenous administration in BALB/c mice.....	89
Fig. 2.9	Representative HPLC chromatograms of deionized water (a), IM in deionized water (b), mouse plasma sample (c), IM in mouse plasma sample (d).....	89
Fig. 2.10	<sup>1</sup> H NMR spectrum of mPEG-PEI copolymer.....	90
Fig. 2.11	DSC thermograms of mPEG, PEI and mPEG-PEI copolymer.....	90
Fig. 2.12	FTIR spectra of mPEG, PEI and mPEG-PEI copolymer.....	91
Fig. 3.1	Schematic of BSA encapsulation in LbL-MC through adsorption and co-precipitation methods.....	101
Fig 3.2	SEM images of CaCO <sub>3</sub> (a), CaCO <sub>3</sub> co-precipitated BSA (b), free LbL-MC (c), BSA encapsulated LbL-MC through co-precipitation (d). Fluorescence micrographs of FITC labelled BSA encapsulated in LbL-MC through co-precipitation (e) and adsorption (f) methods.....	105
Fig 3.3	FTIR spectra of neat CaCO <sub>3</sub> , neat PSS, neat PAH, blank LbL- MC, BSA and BSA encapsulated in LbL-MC prepared by co-precipitation and adsorption method.....	107

Fig. 3.4	DSC thermograms of neat CaCO <sub>3</sub> , neat PSS, neat PAH, blank LbL- MC, BSA and BSA encapsulated in LbL-MC prepared by co-precipitation and adsorption method.....	108
Fig. 3.5	Encapsulation of BSA in LbL-MC. Influence of encapsulation technique (a), pH on BSA adsorption (b) and NaCl concentration on BSA adsorption (c).....	110
Fig. 3.6	In-vitro cumulative release profiles of free BSA solutions (a); BSA encapsulated in LbL-MC prepared by co-precipitation method (b) and adsorption method (c). Release studies were performed in different buffers including citrate (pH 4), phosphate buffered saline (pH 7.4) and tris buffer (pH 9) at 37°C.....	112
Fig. 3.7	Stability of BSA encapsulated in LbL-MC in presence of trypsin determined using SDS-PAGE.....	113
Fig. 4.1	Molecular mechanisms of Pirfenidone.....	118
Fig. 4.2	Characterization of LbL assembly using UV-visible spectro photometer (a,b) and FTIR (c); SEM image (d) and (e) digital photograph of LbL Thin film.....	134
Fig. 4.3	Representative graphs of the burst strength (a), tensile strength (b), stress-strain curve (c) and mouse skin adhesion strength (d) of LbL thin film.....	136
Fig. 4.4	A representative FTIR spectra of neat CS, SA and PFD, physical mixture, blank film and PFD loaded film.....	138
Fig. 4.5	A representative DSC thermograms of neat CS, SA and PFD, physical mixture, blank film and PFD loaded film.....	139
Fig. 4.6	Photographs of bacterial zone of inhibition method after incubation with tetracycline (TE), chloramphenicol (C) and streptomycin (S) (a, b) and CS and LbL thin film (c, d) for <i>S. aureus</i> (a, c) and <i>E. coli</i> (b, d).....	141
Fig. 4.7	Growth curves of <i>S. aureus</i> ( a) and <i>E. coli</i> (b) in the presence of controls, CS, SA and LbL thin films at different time points, (c) Percentage growth inhibition for <i>S. aureus</i> and <i>E. coli</i> in the presence of tetracyclin (TE), CS, SA, LbL films.....	142
Fig. 4.8	A431 cell viability in the presence of LbL thin film.....	143
Fig. 4.9	Cumulative percent release of pirfenidone in PBS from LbL film and ointment.....	144
Fig. 4.10	Fluorescence micrographs of A431 cell adhesion of the chitosan-alginate LbL thin film.....	145

Fig. 4.11	Effect of topical application of the blank LbL thin film, mice treated PFD loaded LbL thin film, PFD ointment and povidone ointment on wound contraction (a), total protein (b) and collagen content (c) compared with control (without any treatment).....	147
Fig. 4.12	Digital photographs of excisional wounds on day 0, 3, 6, 9 and 12 after topical application of the blank LbL thin film, mice treated PFD loaded LbL thin film, PFD ointment and povidone ointment.....	148
Fig. 4.13	Western blot analysis of TGF-beta protein expression in skin samples after PFD treatment.....	149
Fig. 4.14	The plasma concentration – time profile of PFD in the wounded and non-wounded C57BL/6 mice after topical application of the PFD loaded LbL thin film.....	150
Fig. 5.1	Schematic representation of layer-by-layer thin film loaded with siRNA (a), EGF (b) and combination of siRNA and EGF (c).....	159
Fig. 5.2	Cumulative percent release of a) TGF-beta siRNA and b) EGF in PBS from LbL thin film.....	163
Fig. 5.3	Integrity of siRNA release samples characterized by gel electrophoresis.	164
Fig. 5.4	Effect of topical application of the blank LbL film, EGF ointment, EGF loaded film, siRNA alone and in combination with EGF and scrambled siRNA control film on wound contraction (a), total protein (b) and collagen content (c) compared with control.....	167
Fig. 5.5	Digital photographs of wound healing and reepithelialization in mice after treatment with all groups at 0, 3, 6, 9 and 12 post wounding.....	168
Fig. 5.6	TGF-beta protein analysis in excisional wounds from day 0 to day 12 after treatment with LbL thin films loaded with TGF-beta siRNA and EGF.....	169

## LIST OF ABBREVIATIONS AND SYMBOLS

µg	Microgram
5-FU	5-fluorouracil
AA	Ascorbic acid
AUC	Area under concentration versus time curve
BSA	Bovine serum albumin
CaCl <sub>2</sub>	Calcium chloride
CaCO <sub>3</sub>	Calcium carbonate
DLS	Dynamic light scattering
DMEM	Dulbecco's modified eagle's medium
DSC	Differential scanning calorimeter
EDTA	Ethylene diamine tetra acetic acid
EE	Encapsulation efficiency
EGF	Epidermal growth factor
FBS	Fetal bovine serum
FDA	Food and drug administration
FTIR	Fourier transform infrared spectroscopy
G	Gram
H	Hour
HPLC	High performance liquid chromatography
IAEC	Institutional animal ethics committee
ICH	International conference on harmonization
IM	Imatinib mesylate

J	Joules
L	Litre
LbL	Layer-by-layer
LbL MC	Layer-by-layer microcapsules
Log P	Log of oil/water partition coefficient
M	Molar
mg	Milligram
min	Minute
mm	Millimeter
mPEG	Methoxy polyethylene glycol
MW	Molecular weight
N	Newton
Na <sub>2</sub> CO <sub>3</sub>	Sodium carbonate anhydrous
°C	Degree centigrade
PAH	Poly(allylamine) hydrochloride
PBS	Phosphate buffered saline
PDI	Polydispersity index
PEI	Polyethylene imine
PFD	Pirfenidone
PLL	Poly-L-lysine
PSS	Poly(styrene-4-sulphonic acid)
R <sup>2</sup>	Regression coefficient
RNAi	Ribonucleic acid interference

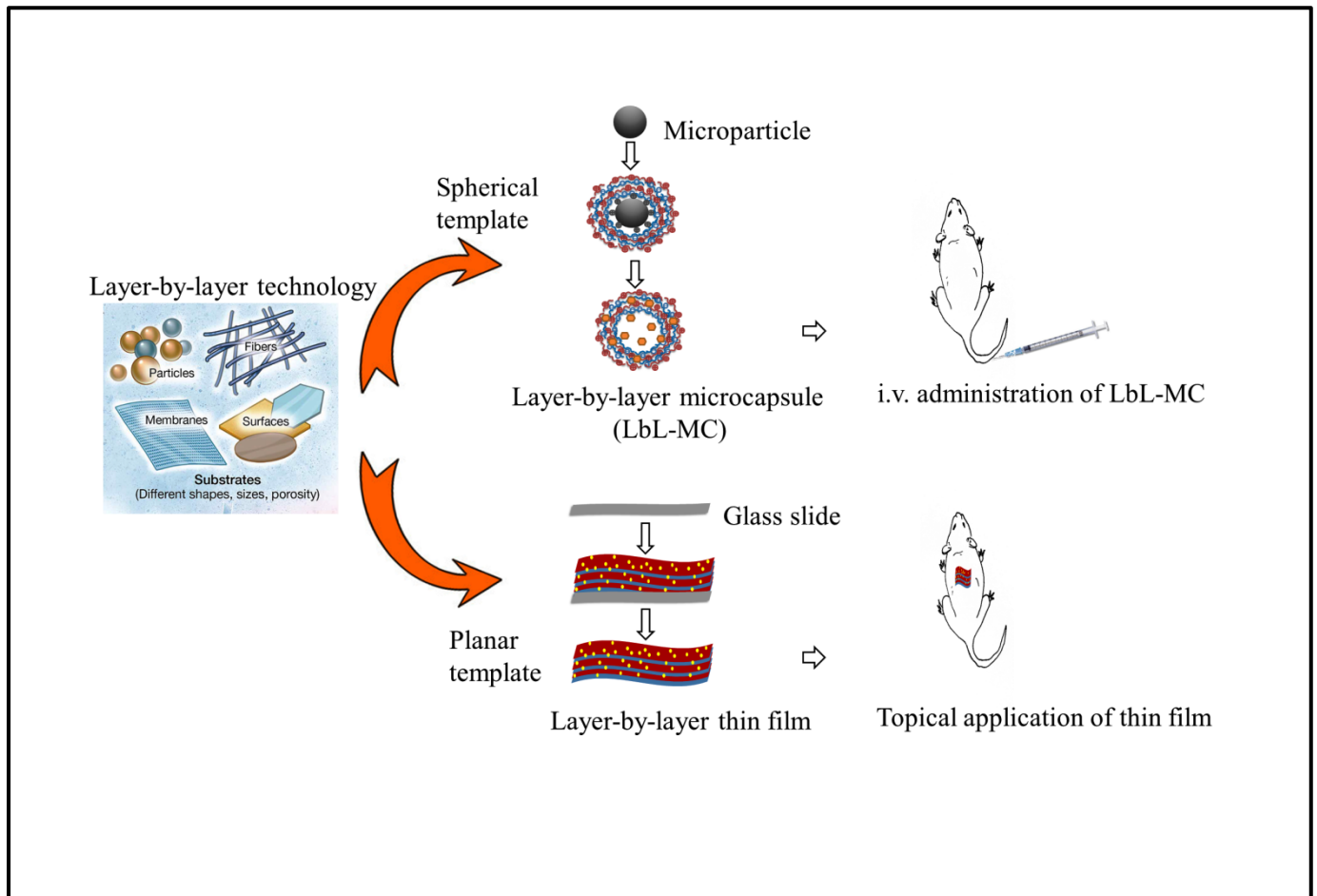
RP-HPLC	Reverse phase – high performance liquid chromatography
RT	Room temperature ( $25 \pm 2$ °C/ $60 \pm 5$ % RH)
s	Seconds
SA	Sodium alginate
SD	Standard deviation
SDS	Sodium dodecyl sulfate
SDS-PAGE	Sodium dodecyl sulfate polyacrylamide gel electrophoresis
SEM	Scanning electron microscopy
siRNA	Small or short interfering ribonucleic acid
$T_{1/2}$	Half-life
TBE	Tris Borate EDTA buffer
TEM	Transmission electron microscopy
TEMED	N, N' tetramethyl ethylene diamine
TGF-beta	Transforming growth factor-beta
TNF-alpha	Tumor necrosis factor-alpha
UV	Ultraviolet
$\Delta H$	Melting enthalpy
$\epsilon$	Epsilon
$\zeta$ -potential	Zeta-potential
$\lambda_{\max}$	Wavelength maxima for UV-absorbance

# Chapter 1

## Introduction

---

## Outline



Schematic representation of the preparation of layer-by-layer assembled carriers (microcapsules and thin films) for the delivery of therapeutic agents.



## INTRODUCTION

### 1.1. Self-assembly

Self-assembly (SA) is defined as the spontaneous and reversible organization of molecular units into ordered structures (spatial and/or temporal order) by non-covalent interactions without external control (Grzybowski et al., 2009; Whitesides et al., 2005). The spontaneity of the self-assembly process is due to electrostatic, hydrogen bond, hydrophobic and van der Waal interactions, which act strictly on local level. Supramolecular chemistry provides the basis of self-assembly, the way how larger entities assemble is coded in the structural motifs of individual molecules (Boncheva et al., 2005). Molecular self-assembly consists of a group of molecules or segments of a molecule which interact with each other and those molecular segments may be the same or different. The interaction starts from a less ordered state (a solution, disordered aggregate or random coil) to more ordered state (crystal).

Self-assembly is classified into two main classes, static and dynamic assembly (Grzybowski et al., 2009). In static self-assembly, components form ordered static structures as the system approaches equilibrium (structure does not change in time) without energy exchange with the environment. In contrast, dynamic self-assembly refers to ordered non-equilibrium structures, which are far from equilibrium and with an input of external energy.

#### 1.1.1. Supramolecular interactions for molecular self-assembly

The supramolecular interactions responsible for molecular self-assembly are non-covalent forces, such as electrostatic, hydrophobic, hydrogen bonding, van der Waal interactions, aromatic stacking and metal coordination (**Fig.1.1.**). Generally, all these interactions are individually weak when compared to covalent bonds but still they can generate stable self-assemblies if they are available in sufficient number or collectively.

#### 1.1.1.1. Electrostatic interactions

Electrostatic interactions between electrically charged particles are nonselective interactions that can result in attractive or repulsive effects. Ionic self-assembly has been employed as a straightforward and reliable method for the organization of different building blocks such as polyelectrolytes, charged surfactants, peptides, and lipids.

#### 1.1.1.2. Hydrophobic interactions

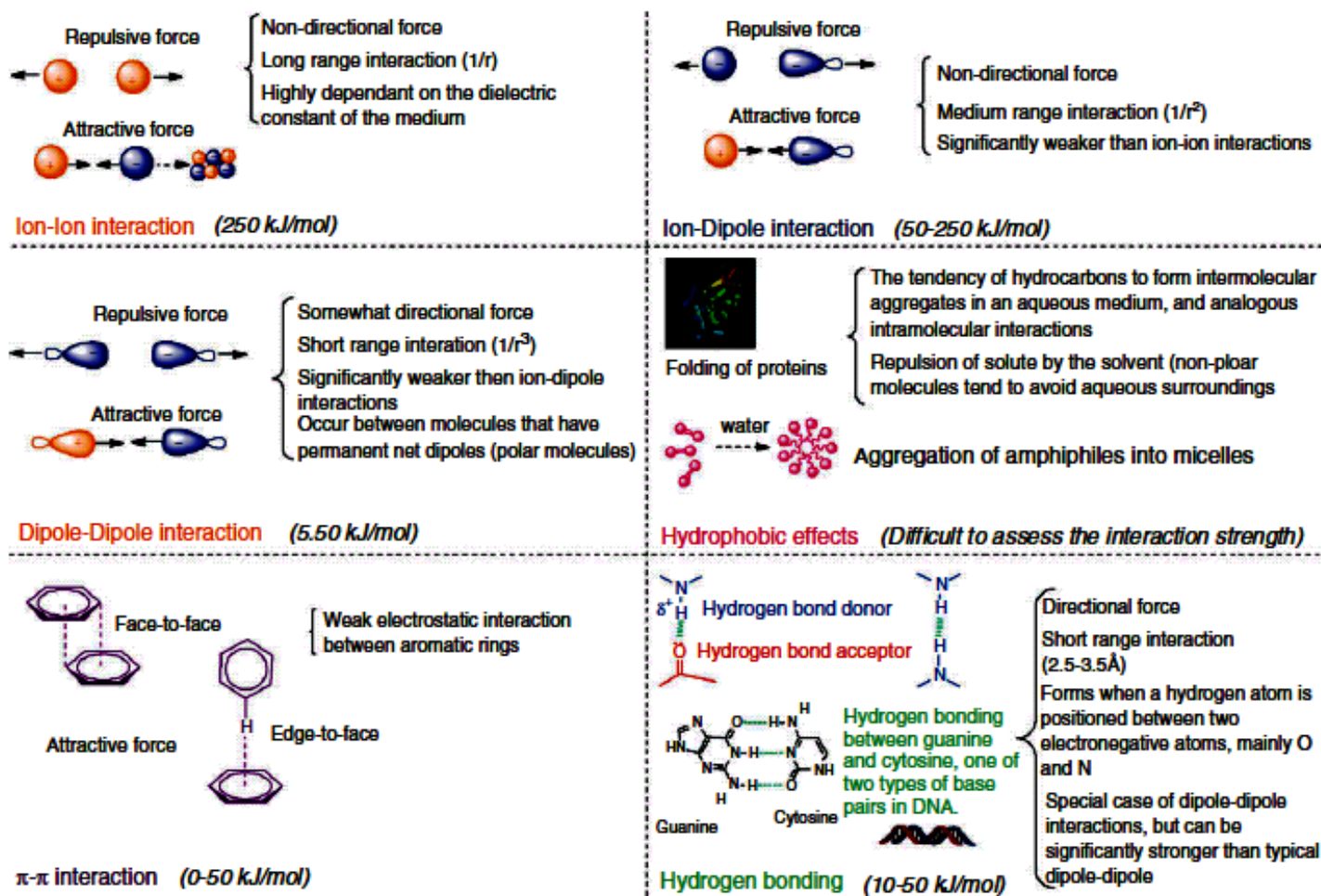
The hydrophobic interaction is a unique organizing force based on repulsion of solute by the solvent. Nonpolar molecules tend to avoid an aqueous surrounding.

#### 1.1.1.3. Aromatic Stacking ( $\pi$ - $\pi$ Stacking)

Aromatic stacking (also called  $\pi$ - $\pi$  stacking) refers to attractive interaction between aromatic rings when oriented face-to-face as in a stack of coins, being responsible for intramolecular stability.

#### 1.1.1.4. Hydrogen Bonding

Hydrogen bonding is a form of association between an electronegative atom and a hydrogen atom attached to a second, relatively electronegative atom. Hydrogen bonding (H-bonding) interactions is highly directional and can be of either short- or long-range nature. Hydrogen bonds may be intermolecular or intramolecular. The strength of single hydrogen bond depends mainly on the nature of donor or acceptor, although it is influenced to larger extent. Combining several hydrogen bonds in functional assembly strengthens the interaction and their spatial arrangement enhances its specificity.



**Fig. 1.1.** An illustration showing the noncovalent interactions involved in supramolecular chemistry and their strength. Reproduced from Mendes et al., 2013.

### 1.1.2. Supramolecular materials or building blocks

Self-assembly can be a simple and low cost bottom-up fabrication process to obtain functional supramolecular materials from pre-existing components (building blocks) involving a reduced number of steps (Whitesides et al., 2005). These building blocks can be atoms, small molecules or macromolecules, and be designed (chemical nature of the blocks, composition, length, and molecular architecture) to contain all the necessary information that

encodes their self-assembly for specific applications. A wide range of different molecules (**Fig. 1.2.**) can be used to form supramolecular nanostructures in a variety of different assembling conditions. The molecules must have the potential to form multiple noncovalent interactions in a given solvent. Broadly these molecules are classified as synthetic and biological building blocks. Synthetic block copolymers have been widely used for fabricating a variety of organized assemblies with distinct morphologies (e.g., micelles, vesicles, and tubes). Self-assembly of these supramolecular monomers relies on properties such as molecular dimension (including the relative volume fractions of the blocks), composition, solubility, stability, and stimulus responsive behaviour (Blanazs et al., 2009).

### 1.1.3. Classification of materials

#### 1.1.3.1. Polyelectrolytes

Polyelectrolytes are polymers bearing dissociated ionic groups; thus they have dual character of electrolytes and macromolecules (Forster et al., 1995; Radeva et al., 2001). Polyelectrolyte is the term used to classify macromolecules that have many charged or chargeable group when dissolved in polar solvents, predominantly water (Dautzenberg et al., 1994). The polyelectrolytes dissociate into a macroion and counterions in aqueous solution. One typical feature of polyelectrolytes is the extremely low activity coefficient of the counterion. If the charge density of the polyelectrolyte is high enough, a fraction of counterions is located in the vicinity or at the surface of the macroion (Manning et al., 1969). They can be classified into natural (e.g. DNA), modified natural (e.g. cellulose), and synthetic polymers (e.g. poly(diallyldimethylammonium chloride)). In terms of their charge, they can be divided into polycations, polyanions and polyampholytes. Depending on the charge density and acidity of the functional groups, they are classified as strong and weak polyelectrolytes. Strong polyelectrolytes have permanent charges and they are fully ionized

over the whole pH range in solution, whereas the degree of dissociation of the ionisable groups on weak polyelectrolytes is highly dependent on the pH.

Mixing a polycation solution and a polyanion solution leads to the formation of polyelectrolyte complexes (Tripathy et al., 2002; Kötz et al., 2007; Kabanov et al., 2003). This process is entropy-driven because of the release of counterions that are not restricted to the polymer backbone chain. The process is very fast and mainly controlled by counterion diffusion. In addition to electrostatic forces, inter-macromolecular interactions are also involved in polyelectrolyte complex formation such as hydrogen bonding, van der Waals forces, hydrophobic and dipole interactions. Polyelectrolytes form complexes not only with oppositely charged polyelectrolytes but also with oppositely charged surfactants.

#### 1.1.3.2. Surface active agents

Surfactants are amphiphilic molecules with unique tendency to adsorb at various interfaces. The term “amphiphile” indicates that surfactant molecule consists of two groups behaving differently in the solvents. Surfactants are compounds that consist of a hydrophobic (usually a long hydrocarbon chain) and a hydrophilic (ionic or polar group). Surfactants can be categorized in several ways. From the commercial point of view, they are often ranked according to their use as emulsifiers, foaming or wetting agents, dispersants, etc. (Myers et al., 1999). Surfactants were classified as anionic surfactants (e.g., sodium dodecyl sulfate), cationic surfactants (e.g., cetyl trimethylammonium bromide), zwitterionic surfactants (e.g., betaines) and non-ionic surfactants (e.g., Spans, Tweens). Numerous studies have demonstrated that surfactants self-assemble in aqueous solution into micellar, vesicle, and multilayer structures.

When surfactant is present in a solution at low concentration, its molecules are dissolved as individual species. As mentioned before, due to their amphiphilic structure they

tend to adsorb at the interfaces and reduce the surface free energy of a system. The surface tension decreases strongly with increasing concentration of surfactant molecules in the solution. The concentration at which micellization begins is known as the critical micelle concentration (CMC). Below CMC, surfactants are disassociated, while above the CMC, micelles and surfactant molecules coexist. Most micelles just above CMC are usually regarded as a spherical association of 50-100 surfactant molecules. The hydrocarbon chains gather inside to form the core of a micelle, while the shell of ionic or nonionic polar head groups is oriented towards the aqueous phase.

#### 1.1.3.3. Lipids

Lipids are the most important building blocks of cell membranes. Generally, they are composed of a hydrophilic head group and a hydrophobic tail region (Collier et al., 2001). Due to the large variability in the head group and tail chemistries, lipids are often categorized into polar and nonpolar. The hydrophobic nature and rigid structure of lipids creates a tendency of these molecules to aggregate into larger structures in water in which the position and orientation of the molecules is organized. In addition, the structural diversity of lipids (fatty acids, triglycerides, phospholipids, and cholesterol) with different polarities, charged groups and lengths allows the formation of dynamic (e.g., monolayers, bilayers) and compartmentalized (e.g., micelles, vesicles) structures in water, acting as barriers, within which isolated processes can occur.

#### 1.1.3.4. Nucleic acids

In biology, nucleic acids (DNA and RNA) are fundamental molecules of life as carriers of molecular information. DNA's base sequence stores and imparts instructions, while RNA's sequence plays the role of a messenger and a regulator of gene expression. As biological polymers, nucleic acids possess recognition capabilities and interesting chemical

properties which depend on their base sequence. Nucleic acids can be synthesized with a nearly infinite number of sequences (Li et al., 2011). The nucleobases present in DNA and RNA molecules can form hydrogen bonds and  $\pi$ - $\pi$  stacking interactions. These interactions can be engineered for the bottom up fabrication of a variety of nanostructures (Ko et al., 2010). DNA double helix is inherently a nanoscale object. Although being more chemically labile, RNA molecules have structural components that are very similar to DNA. In addition, most RNAs are single-stranded molecules with nanoscale motifs that mediate precise intra- and intermolecular interactions. Two strands of DNA with completely complementary sequences can bind to each other and form a fully base-paired duplex structure.

#### 1.1.3.5. Saccharides



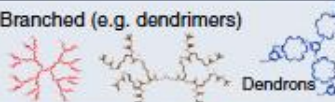

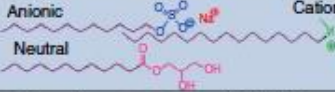







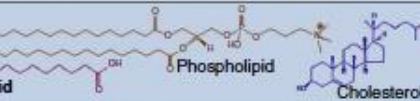
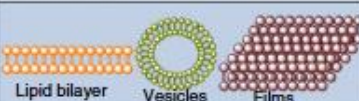


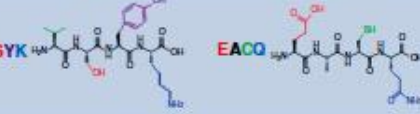
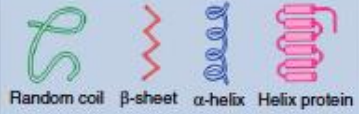
High-molecular weight saccharides (polysaccharides) are produced by a broad variety of plants and microorganisms with remarkable chemical (neutral, charged and linkage type) and structural diversity (linear or branched, random coil or helical conformation). Polysaccharides contain multiple OH groups capable of hydrogen bonding. In addition, carbohydrates play key roles in many molecular recognition processes (e.g., bacterial and viral infection, cancer metastasis, and inflammatory reactions) (Varki et al., 1993), are highly adaptable and can introduce densely charged templates into nanostructured assemblies (Capito et al., 2008).

#### 1.1.3.6. Peptides

Amino acids are naturally occurring molecules being the constituents of peptides and proteins. There are 20 natural (L-form) amino acids that are used by cells to synthesize peptides and proteins. With the exception of glycine (G), all amino acids are chiral and have the same basic structure, a central  $\alpha$  carbon atom to which a hydrogen atom, an amino group, a carboxyl group and side chain R group are attached. The nature of their side chain (charged,

polar, nonpolar, aliphatic and aromatic) contributes to their biochemical mode of action and dictates the conformation assumed by peptides and proteins. The aliphatic residues (Alanine, Isoleucine, Leucine, Methionine, Valine) provide a hydrophobic environment while amino acids with aromatic (Phenylalanine, Tryptophan, Tyrosine) side chains can be engaged in  $\pi$ - $\pi$  stacking. Neutral polar residues (Asparagine, Glutamine, Serine, Threonine) can be involved in the formation of hydrogen bonding through OH (Serine, Threonine) or CONH (Asparagine, Glutamine) groups. Basic (Histine, Lysine, Arginine) residues can be positively charged and acidic amino acids (Aspartic acid, Glutamic acid) can carry a negative charge. The presence of charged groups in these residues can be used to create electrostatic interactions that are important to drive the self-assembly process.



Building-Blocks		Supramolecular Assemblies	Applications
Synthetic	<b>Polymers</b> Linear (e.g. block-co-polymers) 		Nanoreactors; artificial organelles; nanocarriers drug delivery <sup>21, 22</sup>
	Branched (e.g. dendrimers) 		Nanocarriers for drug and gene delivery <sup>23-25</sup>
	<b>Surfactants</b> Anionic, Neutral, Cationic 		Drug and gene delivery systems; antimicrobial and antifungal activity <sup>26, 27</sup>
	<b>Others</b> Porphyrin, Rotaxane, Graphene 		Nanomedicine; drug delivery; hydrogels <sup>8, 28, 29</sup>
Biological	<b>Viruses</b> CPMV, λ phage, hHPBV 		Biomaterials; cell culture substrates <sup>30-33</sup>
	<b>Nucleic acids</b> RNA, DNA 		Therapeutics (vehicles for drug delivery); diagnostics (biosensing) <sup>11, 34, 35</sup>
	<b>Lipids</b> Fatty acid, Phospholipid, Cholesterol 		Nanoreactors; artificial organelles; controlled drug delivery <sup>19, 36-37</sup>
	<b>Saccharides</b> Amylose (helical), Cyclodextrin (cyclic) 		Drug delivery; biosensors <sup>38, 39</sup>
	<b>Peptides</b> VSYK, EACQ 		Hydrogel biomaterials; drug delivery; tissue engineering; 3D cell culture <sup>40-48</sup>

\*CPMV, cowpea mosaic virus; λ phage, lambda bacteriophage; hHPBV, human hepatitis B virus.

**Fig. 1.2.** Synthetic and biological building blocks used in supramolecular self-assembly and their potential biomedical applications. Reproduced from Mendes et al., 2013.

## **1.2. Drug delivery systems prepared through self-assembly**

Drug delivery deals with the design, synthesis and use of suitable materials for the safe and efficient delivery of drugs. The drug can be administered by various routes such as oral, intravenous, arterial, transdermal, nasal, subcutaneous, sublingual etc. in order to achieve a therapeutic effect. The problems associated with pharmaceutical drugs are low aqueous solubility, partial degradation in biological system and undesirable side effects by accumulation of non-targeted organs. Scientists from different disciplines are making considerable efforts to resolve these problems using efficient drug delivery systems. Efforts made in the direction include development of suitable biocompatible formulations with desired drug loading and release properties, long shelf-life, low toxicity and targeted delivery.

In recent years, research into nanostructured self-assembled systems has gained increased attention as they promise potential for drug delivery applications. The use of a variety of nanocarriers such as micelles, microemulsions, multilayer capsules, hydrogels, liposomes, niosomes, cubosomes formed by self-assembly approaches has drawn much attention for drug delivery applications due to their good pharmacological properties. These carriers have been found to be very effective in improving solubilization of drugs, enhancing drug targeting, reducing drug toxicity, controlling drug release rate, and in the protection against biochemical degradation.

Generally, the self-assembled structures formed by amphiphiles, polymers or lipids which have been explored extensively as drug delivery vehicles via different routes of administration. However, each of these carrier types has its own advantages and limitations. It is, therefore, very important to choose drug carriers in such a way that meets the requirements of the desired purpose. The properties (size and charge) of self-assembled carriers can be modified/controlled depending on the requirement for delivery purpose. These

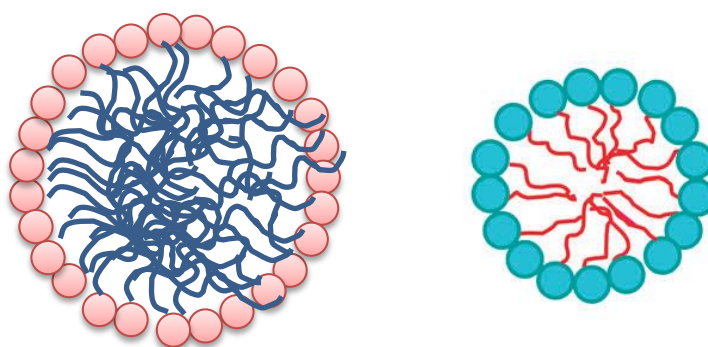
carriers can be made stimuli reactive, such as pH or temperature sensitive, and can even be used in targeted drug delivery by conjugating them with specific antibodies. Here, we will discuss structure, properties and drug delivery aspects of different types of self-assembled materials.

### 1.2.1. Micelles

Micelles are the simplest self-assembled structures formed by amphiphilic molecules such as surfactants, phospholipids, fatty acids, block copolymers etc. in certain solvents like water. The shape and size of the micelles depend on the surfactant concentration, pH, temperature and ionic strength of the solution. In recent years, micellar formulations have gained much attention in the field of drug delivery as they have several distinct features, which make them a promising candidate as drug delivery carrier. For example, the small size, narrow size distribution, simple preparation method and reproducibility are some of the important features of micellar delivery systems. The size, shape and charge of these carriers can also be modified depending on the requirement of the system. The hydrophobic drugs can be incorporated in the core of the micelles that is composed of hydrophobic part of the surfactant. The stability of the drug is also increased through micelle incorporation, thus protect the drug from enzymatic degradation and reduction of side effects.

Polyoxyethylene based nonionic surfactants have been extensively used in various oral and parenteral pharmaceutical formulations due to its compatibility and less toxic nature. The most commonly used non-ionic surfactants are Tween-80, cremophor EL, brij-35. They offer several advantages like less toxicity, less haemolytic and maintain almost physiological pH in solution form. They can be used as wetting agents, permeability enhancers, solubilisers and also as p-gp inhibitors.

In addition to surfactant micelles, polymeric micelles also considered as an ideal drug delivery carriers. Generally polymeric micelles are more stable than surfactant micelles because of its architecture, composition and low CMCs (Kim et al., 2010). Polymeric micelles have been explored almost all routes of drug delivery such as oral, parenteral, nasal and ocular to increase bioavailability and reduction of adverse effects. A number of poorly water-soluble drugs such as paclitaxel, indomethacin, amphotericinB, adriamycin, and dihydrotestosterone have been studied by incorporating into injectable formulations of polymeric micelles (Yu et al., 1998; Jeong et al., 1999; Allen et al., 2000). Recently, a lot of effort has been made to use stimuli responsive polymeric micelles (that respond to external stimuli such as pH, temperature etc.) for targeted drug delivery. There are several reports in which pH and temperature-responsive polymeric micelles have been demonstrated as a promising drug delivery vehicle.



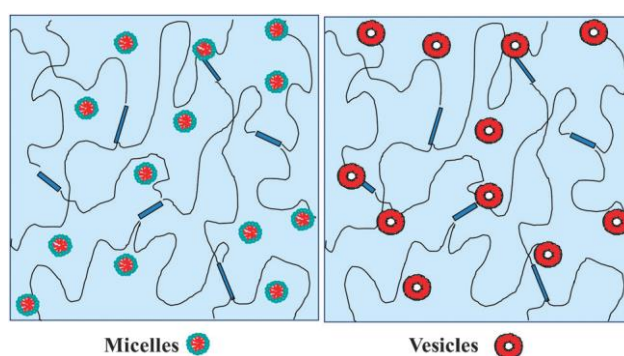
**Fig. 1.3.** Schematic representation of self-assembled micelles. Reproduced from Verma et al., 2013.

### 1.2.2. Hydrogels

Hydrogels are three-dimensional networks of cross-linked hydrophilic polymer chains, which are prepared by the entanglement of long fibrous polymeric structures into three-dimensional networks in water. The entanglement of fibrous structures can be made by various methods such as chemical cross-linking by covalent bonds, hydrogen bonding, van der Waals interactions or/and physical entanglements by photo polymerization or irradiated cross-linking of synthetic and natural polymers. Hydrogels can exhibit both solid-like and liquid-like properties, since they have the network of cross-linked polymers and the major constituent of hydrogel is water. These structures have the ability to entrap large amount of water and swell in water without dissolving. Their high water content makes them highly biocompatible. Hydrogels have been extensively studied and demonstrated to have great potential for various biomedical applications including tissue engineering, molecular imprinting, wound dressings materials and drug delivery.

Currently, hydrogels are being considered as a promising candidate for drug delivery applications. The encapsulation of hydrophilic drugs can be easily achieved in hydrogels, either by mixing the drug with the monomers followed by polymerization, or by swelling the gel in a drug containing aqueous medium. Hydrogels can also act as reservoir for various other self-assembled carriers like micelles and vesicles (Dowling et al., 2009). **Fig. 1.4** shows a schematic illustration of the vesicle or micelle trapped hydrogels that can be prepared via a self-assembly approach. A variety of such nanostructure trapped hydrogels can be explored for drug delivery applications, as they offer the advantage of encapsulating both hydrophilic and hydrophobic ingredients. Hydrogels can protect the drug from unfavourable environments such as the presence of enzymes and low pH in the stomach. Hydrogels are formed by weak interactions, so they show strong responses under the influence of external stimuli. There are several studies in which physical and chemical stimuli have been applied in

the hydrogel systems to induce various responses. The physical stimuli include temperature, electric fields, solvent composition, light, pressure, sound and magnetic fields, while the chemical or biochemical stimuli include pH, ions and specific molecular recognition events (Satarkar et al., 2008). A pH/temperature sensitive pentablock copolymer of poly-(b-amino ester)-poly( $\epsilon$ -caprolactone)-poly(ethylene glycol)-poly- ( $\epsilon$ -caprolactone)-poly(b-amino ester) hydrogel has been studied as a sustained injectable insulin delivery system on male Sprague-Dawley rats (Huynh et al., 2009).



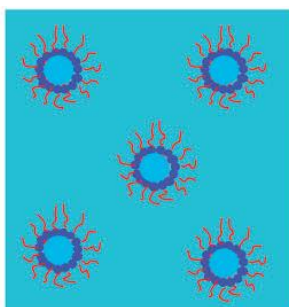
**Fig. 1.4.** Illustration of self-assembled structures (micelles or vesicles) trapped in hydrogels. Reproduced from Verma et al., 2013.

### 1.2.3. Microemulsions

Microemulsions are another class of self-assembled structures, which have been extensively employed for drug delivery applications. Microemulsions are thermodynamically stable colloidal dispersions of water and oil stabilized by an interfacial film of surfactant. In many cases a co-surfactant is used in combination with the surfactant as a stabilizer. Depending upon the microstructure, microemulsions can be categorized as oil-in-water (o/w), water-in-oil (w/o) and bicontinuous microemulsions. Microemulsions have attracted increasing attention as potential drug delivery systems due to several unique features such as high solubilization properties, long shelf-life, ease of preparation and administration. They can solubilize both hydrophilic and lipophilic drugs. Microemulsions have been used as drug

carriers in several routes of drug administration, viz. percutaneous, ocular, oral and parenteral.

Microemulsion formulations are promising delivery systems for oral formulations as they offer several advantages, such as enhanced bioavailability of poorly soluble drugs, which lead to a faster absorption of drug action, improved clinical potency and decreased drug toxicity over conventional oral formulations. A microemulsion formulation containing acyclovir showed an increase in bioavailability after oral administration when compared to commercially available tablets (Ghosh et al., 2006). Many examples of microemulsion based formulations are now in the market. For example a microemulsion based formulation of cyclosporin A by Novartis is marketed under the trade mark Neorals. This formulation gives more rapid absorption and increased bioavailability.



**Fig. 1.5.** Schematic representation of self-assembled micro-emulsion. Reproduced from Verma et al., 2013.

#### 1.2.4. Vesicles

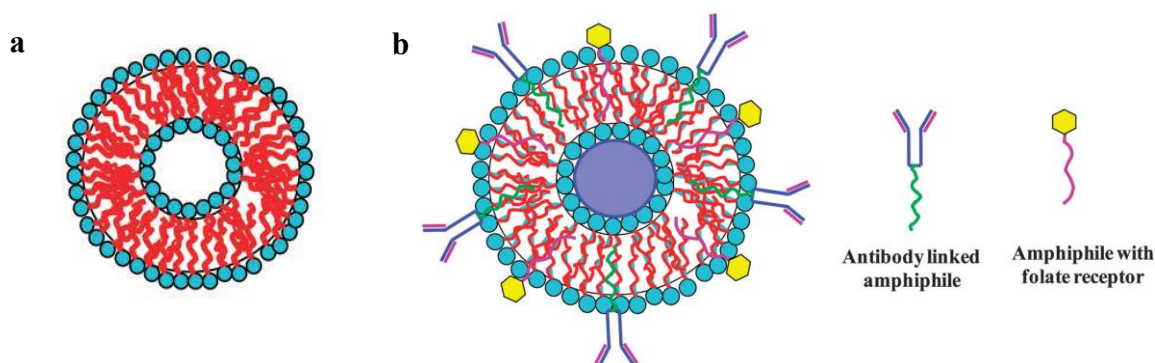
Vesicles are hollow spherical structures formed by the self-assembly of surfactants, lipids, or block copolymers in aqueous solution. They can be of varying size depending upon the length of surfactant chain and number of bilayers. Based on the number of bilayers they can be classified as large multilamellar vesicles (MLV), large unilamellar vesicles (ULV),

small unilamellar vesicles (SUV), oligolamellar vesicles (OLV) and multivesicular vesicles (MVV). In liposomes many concentric spherical bilayers of amphiphiles (mostly phospholipid) are present in which hydrophobic lipid bilayers are separated by water. There are several types of liposomes such as pH-sensitive liposomes, magnetic liposomes, niosomes, proniosomes, polyhedral niosomes etc.

Vesicles can be used as a vehicle for the administration of both hydrophilic as well as hydrophobic drugs as they have a hydrophilic reservoir, which can incorporate hydrophilic drugs and, at the same time, they have a hydrophobic wall, which protects the loaded molecules from the external solution. By tuning the permeability of this wall, the extent of loading and release of drugs from vesicles can be controlled. Multilamellar vesicles (MLV's) of a biodegradable surfactant PEG-8 Distearate (PEG8DS) have been prepared for encapsulation of sumatriptan (Redkar et al., 2007). The drug encapsulation efficiency was found to be very high (90%) and in-vitro drug release was rapid (10 min). Many drugs with liposomal delivery systems such as amphotericin B, cytarabine, daunorubicin, doxorubicin, morphine etc. have been approved and some are under clinical trials. Some of the commercial liposome based drugs available in the market include DAUNOXOME, DOXIL and AmBisomes.

Self-assembly can also be employed for interfacial functionalization of nanocarriers for specific targeting or targeted delivery. Recently, antibody functionalized surfactants have been reported for the immunotargeting of nonionic surfactant vesicles (Hooda et al., 2007). Using functionalized surfactants as the building blocks for self-assembled structures, diverse properties ranging from targeting to evasion of immune systems could be added to the carrier (**Fig. 1.6**). Vesicles formed of polypeptide containing amphiphilic block copolymers have received a great deal of attention due to their unique physicochemical and biological features (Tian et al., 2012; Maity et al., 2011).





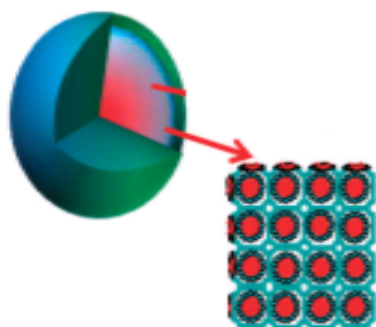
**Fig. 1.6.** Schematic representation of liposome vesicles (a) and liposomes with functionalised or covalently modified amphiphiles (b). Reproduced from Verma et al., 2013.

### 1.2.5. Cubosomes

Cubosomes are nanostructured particles of a bicontinuous cubic liquid crystalline phase. At very high concentrations, surfactants self-assemble in water to form very viscous thick fluids known as liquid crystals. Cubosomes are produced by high-energy dispersion of bulk cubic phase liquid crystals followed by colloidal stabilization using polymeric surfactants (Fong et al., 2010). Cubosomes possess the same microstructure as the parent cubic phase but have much larger specific surface area and their dispersions have much lower viscosity than the bulk cubic phase. In cubosomes, amphiphilic molecules form two distinct hydrophilic regions which are separated by a lipid bilayer. The main advantage of cubosomes is that they are stable at any dilution level due to the insolubility of the cubic liquid crystal phase which forms lipid in water. The commonly used surfactants for cubosome preparation are monoglyceride and glycerol monoolein.

Cubosomes have attracted significant interest in recent years as a drug delivery system due to unique characteristics such as biocompatible microstructure and capability for controlled release of both hydrophilic and hydrophobic drugs. For example, cubosome particles were produced by fragmenting a cubic crystalline phase of monoolein and water in

the presence of the stabilizer, poloxamer 407 to improve preocular retention and ocular bioavailability of dexamethasone (DEX) (Gan et al., 2010). Further the ability of nanostructured cubosomes formed of phytantriol (PHY) and glyceryl monooleate (GMO) has been evaluated to sustain the absorption of a poorly water soluble drug, cinnarizine (CZ) after oral administration to rats.



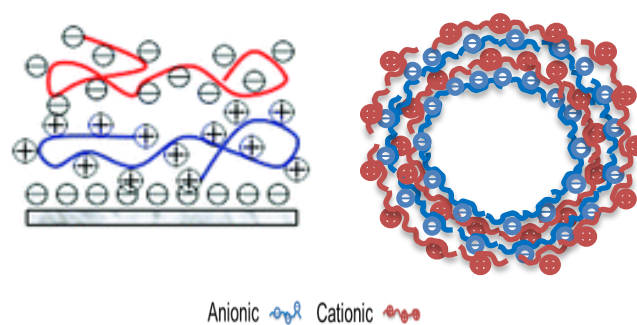
**Fig. 1.7.** Schematic representation of self-assembled cubosomes. Reproduced from Verma et al., 2013.

#### 1.2.6. Layer-by-layer assembled delivery carriers

Among the various self-assembly approaches, layer-by-layer (LbL) technique has gained increased interest for the fabrication of drug delivery carriers. The attractive features of LbL technique include low cost, simplicity and versatility (Ariga et al., 2007) made researchers to develop novel delivery carriers. LbL technique has been reported for the fabrication of multilayer thin films, surface coating of biomedical implants (Zelikin et al., 2010; de Villiers et al., 2011; Manna et al., 2010) and LbL microcapsules for encapsulation and sustained release of therapeutics (Trojer et al., 2014; Trojer et al., 2013).

The LbL technique was first developed by Decher and co-workers in the early 1990s for the preparation of thin films on planar substrate (Decher et al., 1992; Decher, 1997) based

on the pioneering work of Iler in 1966 (Iler, 1996). Generally, the process involves sequential adsorption of oppositely charged polyelectrolytes on a substrate with the assembly stabilized by electrostatic interaction. Since then, LbL films have attracted much attention because of their facile preparation and potential use in the development of functional devices, including biosensors. The approach is versatile in terms of the components of assembly and the type of interaction; not only polyelectrolytes but uncharged polymers, micelles (Bo et al., 2008), dendrimers (Khopade et al., 2002), nanoparticles (Mohanta et al., 2012; Mahanta et al., 2010) can be assembled via hydrogen bonding (Kharlampieva et al., 2009) or covalent bonding (Bergbreiter et al., 2009). Later, the LbL technique was extended to spherical and colloidal particles by Möhwald and coworkers for the preparation of hollow microcapsules by the LbL deposition of synthetic polyelectrolytes on the surface of microparticles, followed by dissolution of the core particles (Skorb and Möhwald, 2013). LbL deposition is a bottom-up nanofabrication technique that relies on the molecular interactions of materials, which is distinct from other methods for the preparation of polymer films and microcapsules. One of the advantages of LbL films is that the film thickness can be precisely tuned at the nanometer level by changing the number of deposited layers. It is also a merit of the LbL deposition protocol that the process for film preparation is carried out in aqueous media under mild conditions. In addition, one can use a wide variety of synthetic and biological materials for LbL deposition. Thus, the fine structure of LbL films and microcapsules can be tailored by a suitable choice of building block materials. Furthermore, systems for stimuli-sensitive drug release can be constructed if the materials are endowed with sensitivity to specific stimuli. External stimuli such as temperature, light, and electric and magnetic fields and internal stimuli including pH and biological ions and molecules are often used as the stimuli by which drug release is triggered (Delcea et al., 2011). In stimuli-sensitive drug delivery, required amounts of the drug can be released at the site of drug action in response to stimuli.



**Fig. 1.8.** Schematic representation of polyelectrolyte films and hollow capsules prepared by layer-by-layer assembly.

### 1.3. Basic principles of the layer-by-layer assembly

Layer-by-layer self-assembly is a simple and versatile technique for the formation of nanocoatings among other surface modification methods such as spin-coating, solution casting, thermal deposition and chemical self-assembly.

#### 1.3.1. Mechanism of self-assembly

The build-up of LbL multilayers is driven by the electrostatic attraction between the oppositely charged constituents (Iler et al., 1996). However, hydrogen bonding (Fu et al., 2002; Kharlampieva et al., 2005), hydrophobic interactions (Kotov et al., 1999) and van der Waals forces (Sato et al., 2005) may be exploited to assemble LbL systems or influence the stability, morphology and thickness of the films, particle/molecule depositions and permeation properties of the film (Decher et al., 1992; Hammond et al., 2000). Generally, LbL self-assembly proceeds as follows: (1) A charged substrate is immersed in a solution of an oppositely-charged colloid to adsorb the first monolayer, (2) a washing cycle follows to remove unbound material and preclude contamination of the subsequent oppositely-charged colloid, (3) in which the coated substrate is submerged to deposit a second layer and the

multilayered structure is formed (Lvov et al., 1999). Some LbL processes require no washing cycles thus shortens the duration of the assembly process (Bantchev et al., 2009).

The polyelectrolytes or colloids, which exhibit a high linear surface charge density, are utilized in excess to prime the substrate. Therefore, a non-stoichiometric excess of charge is absorbed after each step relative to the preceding layer (Ochs et al., 2010). This surplus of charge provides the step-wise mechanism for the reversal of the surface charge polarity, facilitating a favourable surface for the adsorption of the subsequent layer. Techniques, not reliant on intermolecular forces, i.e. covalent or click chemistry were developed to produce stable (Kinnane et al., 2009) or biodegradable (Lynn et al., 2006) multilayered structures. However, the principle of successive layering still applies.

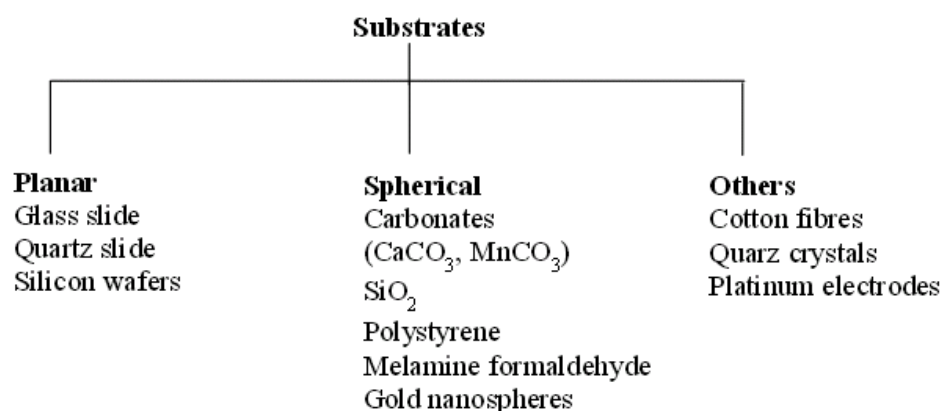
The LbL self-assembly methods have advantages compared to the more conventional coating methods, including (1) the simplicity of the LbL process and equipment, (2) its suitability to coating most surfaces, (3) the availability of an abundance of natural and synthetic colloids, (4) the flexible application to objects with irregular shapes and sizes, (5) the formation of stabilizing coats and (6) control over the required multilayer thickness (Bertrand et al., 2000; Becker et al., 2010; Johnston et al., 2005).

### 1.3.2. Substrates and coating materials

#### 1.3.2.1. Substrates

The primary requirement for layer-by-layer self-assembly is a suitable substrate which can hold as well as support the layer-by-layer assembly that is going to be organized on it. The important criterion for successful LbL adsorption is surface charge; however, charge can be induced to still facilitate LbL adsorption process (Caruso et al., 2000). Most commonly glass, quartz, silicon wafers, mica and gold-coated substrates are being used. Nanoparticles also utilized for LbL constructs are derived from stabilized colloidal dispersions of charged

silica, charged poly(styrene) spheres, metal oxides (Iler et al., 1966), polyoxometalates (Caruso et al., 1998; Caruso and Möhwald et al., 1999) and conducting liquid crystalline polymers. Surface charge and surface texture could also affect the adhesion properties. Pre-treatment of substrate with NaCl enhance the intimate contact and quality of coats (Nolte et al., 2009; Nolte et al., 2007). Layer-by-layer self-assembly can be instituted on a large number of substrates. Substrates are categorized broadly into planar, spherical (particulate) and other.



**Fig. 1.9.** Classification of substrates used in fabrication of layer-by-layer assembly.

### 1.3.2.2. Coating materials

#### 1.3.2.2.1. Polyelectrolytes

Polyelectrolytes are polymers, in which all or some of the monomers are charged. One can distinguish between two kinds of charged monomers (based on their chemical composition). Monomers that contain permanent charges e.g. the quaternary ammonium group, and monomers containing ionisable groups, e.g. primary amines and carboxylic acids that can dissociate in solution depending on the pH and ionic strength. The charge is then related to the degree of ionisation in solution (Kötz et al., 2001). The pH at which 50 % of the ionisable monomer groups are charged is given by the pKa of the ionisable group. Based on

charge polyelectrolytes are categorized into anionic and cationic polyelectrolytes. Polyelectrolytes are often referred to as weak or strong depending on the pKa of their monomer. Strong polyelectrolytes are completely charged over a broad range of pH values (~2-10), whereas weak polyelectrolytes are partially charged in this range. The polymer charge density largely affects the conformation, which can be altered by adjusting the solution ionic strength (screening of electrostatic repulsive forces) and for weak polyelectrolytes also by the pH. Polyelectrolytes are classified according to their origin. Synthetic polyelectrolytes (eg. poly(styrene sulfonate) (PSS), poly (dimethyl diallyl ammonium chloride) (PDDA)) and natural polyelectrolytes (eg. chitosan and sodium alginate).

The LBL technique is not only applicable for polyelectrolyte/ polyelectrolyte systems. Almost any type of charged species, including inorganic molecular clusters, nanoparticles (NPs), nanotubes, nanowires, nanoplates, organic dyes, dendrimers, porphyrins, biological polysaccharides, polypeptides, nucleic acids and DNA, proteins and viruses, can be successfully used as components to prepare LBL films. The universality of the LBL process has catalyzed the rapid development of biomedical applications of polyelectrolyte multilayers and related nanostructured organic–inorganic composites. This translates into an exceptionally wide variety of structural characteristics and thus, functional properties.

**Table 1.1.** List of polyelectrolytes used for layer-by-layer assembly.

	<b>Polyelectrolyte</b>	<b>pKa/PI</b>	<b>Molecular weight</b>
<b>Anionic polyelectrolytes</b>			
<b>Natural</b>	Nucleic acids (RNA and DNA)	-	-
	Proteins (BSA and EGF)	BSA:PI;4.5-4.7 EGF:PI: 4.5	BSA-66,500 EGF-6200
	Chondroitin sulfate	-	50,000-100,000
	Heparin	-	12,000-15,000
	Sodium alginate	3.4 - 4.4	70,000
	Dextran sulphate		500,000
<b>Synthetic</b>	Polyacrylic acid	4.5	450,000
	Poly(styrene sulfonate)	3.5	70,000
	Carboxy methyl cellulose	4.3	-
	Poly (methacrylic acid)	6.0	-
	Poly(vinyl sulfate)		-
<b>Cationic polyelectrolytes</b>			
<b>Natural</b>	Chitosan (CS)	6.5	200,000
	Gelatin	PI:5	-
<b>Synthetic</b>	Polyethylenimine	9.7	25000
	Poly(diallyldimethylammonium chloride)	-	150,000
	Poly(allylamine hydrochloride)	8.5	70,000
	Polylysine	10.5	-
	Poly(N-isopropyl acrylamide)	-	-

### 1.3.3. Influence of experimental parameters on LbL adsorption

The formation of polyelectrolyte layer-by-layer self-assembly depends on electrostatic interactions between substrate and subsequent polyelectrolyte layers. Along with electrostatic interactions other processing parameters play a significant role and are briefly discussed here:



#### 1.3.3.1. Coating material concentration

The concentration of coating material should be high enough for successful adsorption and to prevent depletion during layering (Decher, 1997). Concentration should exceed the minimum threshold concentration for attachment and to reverse charge polarity for each adsorbed layer. The threshold is dependent on solubility and charge density of coating material. Above the threshold, concentration was irrelevant to adsorption; however, result in an exponential increase in the thickness of the monolayers (Szarpak et al., 2008).

#### 1.3.3.2. Washing

In the process of LbL adsorption, coated substrate is washed after each polyelectrolyte adsorption to remove unbound polyelectrolytes and to prevent the cross-contamination of solutions (Hoogeveen et al., 1996). Washing solution should be compatible with polyelectrolytes used and should not damage the LbL construction. Mostly the layers formed with strong polyelectrolytes are strong and not influenced by washing solution. However, weak polyelectrolyte layers may be stripped off and limits successful LbL assembly (Linford et al., 1998).

#### 1.3.3.3. Drying

Alternate dipping of substrate in polyelectrolyte solutions generate moist environment, increase chain flexibility and ionization of polyelectrolyte leads to formation of thinner films (Bertrand et al., 2000). Hence, it is necessary to dry the substrate after each adsorption step. Drying should be done preferable under nitrogen streaming (Silva et al., 2008). Further drying rate and drying temperature are important experimental parameters that influence the effective assembly. For protein based polyelectrolytes structural rearrangements

may occur due to improper drying conditions. In contrary spontaneous drying under ambient temperature produce ordered films.

#### 1.3.3.4. Ion concentration and pH of the medium

In LbL process, electrostatic interactions between polyelectrolytes play important role for successful polyelectrolyte multilayer (PEM) growth. PEM film thickness can increase exponentially or linearly with each step, with linear growth taking place when the polyelectrolytes in the solution interact exclusively with the outer layer of the multilayer film (Laugel et al., 2006). Film thickness is mainly influenced by salt concentration or ion concentration and pH of the medium (Decher et al., 1997). Generally, an increase in ionic concentration results in an increase in film thickness due to polyelectrolyte charge compensation resulting in more globular rather than extended polyelectrolyte structure (Kolarik et al., 1999; Guzmán et al., 2009). Furthermore diffusion of polyelectrolyte chains into interior results in exponential increase in thickness. However, beyond threshold, with increase in salt concentration, all charges compensate and polyelectrolyte form turbid, coagulated dispersions (Bharadwaj et al., 2006; Buron et al., 2009). At these conditions successful multilayer formation will be difficult. A change in the pH of the solution will alter the dissociation of the polyelectrolytes and ions, which will further alter the successive adsorption process.

Similar to salt concentration, pH will also influence the exponential growth of films. A change in pH will change the charge density of weak polyelectrolytes leading to irregularities in linear growth in film formation (Chang et al., 2008; Bieker et al., 2010). Thickness of polyelectrolyte layers prepared by strong polyelectrolytes can be improved by adjusting salt concentration, whereas layers prepared by weak polyelectrolytes are improved by optimization of solution pH.

#### 1.3.3.5. Working medium

The working medium should enable the polyelectrolyte coating and PEM integrity. It is reported that polarity of working medium influence the efficiency of LbL process. Water soluble polyelectrolytes are mostly used as coating materials for effective layer-by-layer adsorption. Water, as working medium can ionize the water soluble polyelectrolytes, since the ionic interactions are important contributor for layer-by-layer assembly. Non-aqueous systems also investigated as working medium for an azo-polyelectrolyte in N,N-dimethylformamide (Tuo et al., 2005), PSS/PAH/formamide combinations (Kamineni et al., 2007) and PSS/PAH/chloroform systems (Hirsjärvi et al., 2006). Toluene is also reported as non-polar working medium by addition of surfactant. In non-polar solvents, dispersion forces and hydrogen bonding predominates to improve coating efficiency. This enables the assembly of substances that might not ionize or only ionize under harsh conditions. The interactions that are responsible for PEM integrity can therefore be strengthened or compromised by the environmental conditions resulting in assembly/disassembly of the films.

#### 1.3.4. Characterization of LbL assembly

There are several techniques available for characterization of layer-by-layer assembly, multilayer build-up, surface morphology; thickness and release of captured content from LbL assembly. Some of the more common methods are briefly discussed.

##### 1.3.4.1. UV-Visible spectroscopy

Layer-by-layer growth or build-up can be monitored by UV-visible spectroscopy that determines cumulative absorption attributed to stepwise deposition of UV-active polyelectrolytes (Picart et al., 2005; Decher et al., 1992). In the ultraviolet and visible (UV-Vis) region of the electromagnetic spectrum ( $\lambda = 200 - 800$  nm), most organic molecules absorb photons

and undergo electronic transitions. The absorption spectroscopy measures transitions from the ground state to the excited states of the molecules. The method is often used to quantitatively determine concentrations of an absorbing species in solution, following the Beer-Lambert law. The adsorption of polyelectrolytes during the film growth can be characterized by the UV-spectrophotometer. After the adsorption of each layer, the thin film is dissolved in a suitable solvent system and the absorbance is measured using UV-visible spectrophotometer. With increase in number of bilayers the absorbance of polyelectrolytes also increases linearly.

#### 1.3.4.2. Fourier transform Infrared (FTIR) spectroscopy

Sequential adsorption of polyelectrolytes on to the template can also be studied by FTIR spectroscopy. This method is used to determine concentration of an adsorbed material on substrate quantitatively. After adsorption of each layer, the template is directly attached to dynamic reflectance sample holder. Then the spectra were recorded between 4000–400  $\text{cm}^{-1}$  wavenumber using FTIR. With increase in number of bilayers the absorbance of desired wavenumber also increases linearly.

#### 1.3.4.3. Ellipsometry

Ellipsometry measures a change in polarization as light reflects or transmits from a material structure. The polarization change is represented as an amplitude ratio,  $\Psi$ , and the phase difference,  $\Delta$ . The measured response depends on optical properties and thickness of individual material. Thus, ellipsometry is commonly used to determine the layer thickness or adsorbed mass per layer during each step (Langereis et al., 2009; Harris et al., 2000). Ellipsometry is typically used for films whose thickness ranges from sub-nanometers to a few microns. As films become thicker than several tens of microns, interference oscillations become increasingly difficult to resolve, except with longer infrared wavelengths.

#### 1.3.4.4. Quartz crystal microbalance (QCM)

Quartz crystal microbalance (QCM) is an ultra-sensitive weighing device that measures a mass per unit area in the nanogram range. It uses the principle that a piezoelectric quartz crystal changes its oscillation frequency when mass is deposited or removed from the crystal surface. In the most common configuration, a thin (~200-400  $\mu\text{m}$ ) circular crystal disc is sandwiched between a pair of circular metal electrodes (usually gold). When a thin film is attached to the crystal the resonance frequency decreases. If the deposited film is thin and rigid the decrease in the frequency is proportional to the mass of the film. By collecting the resonance frequency of a quartz crystal, QCM technology can be used to characterise the formation of thin films (nm) such as proteins, polymers and cells onto surfaces, in liquid.

#### 1.3.4.5. Zeta-potential measurement

Particles in a colloidal suspension or emulsion are usually electrically charged. The amount of charges on the particle surface determines the stability of the colloids, and therefore it is an important particle characteristic. It can be measured by the electrophoretic mobility of the particles in suspension. Zeta potential indicates the potential stability of a colloidal system. Particles with a zeta potential above (30mV) generally have no tendency to aggregate due to the electrostatic repulsion to each other, and they are considered stable. Zeta potential is highly dependent on the pH value and the ion strength. Therefore, a zeta potential value needs to be measured at a known pH and ion strength. After adsorption of each polymeric layer, the spherical templates are dispersed in deionised water and zeta potential is measured. The zeta potential (positive or negative) depends on the polyelectrolyte charge (anionic or cationic).

The internal arrangement LbL assembly can be determined by X-ray reflectivity (Erokhina et al., 2008). The reflectogram intensities were converted to the thickness of the multilayers. Thickness of films is also measured using digital micrometer.

#### 1.3.4.6. Microscopy

There are several microscopic techniques available for the characterization of surface morphology and interior structure of LbL microcapsules and thin films. Normal optical microscope to high resolution scanning electron microscope, confocal laser scanning microscope, atomic force microscope and transmission electron microscope are widely being used by many researchers for characterization of various materials.

Scanning electron microscope (SEM) is a type of electron microscope that produces images of a sample by scanning it with a focused beam of electrons. The electrons interact with atoms in the sample, producing various signals that can be detected and that contain information about the sample surface topography and composition. Sample need to be dried overnight under vacuum to ensure complete removal of moisture and gold sputtered prior to imaging.

The surface texture and roughness of LbL assembly can be elucidated by atomic force microscopy (AFM) (Wang et al., 2008). AFM can aid studying the changes in wettability, contact angle and subsequently surface energy (Yoo et al., 1998). The AFM measures the forces acting between a fine tip and a sample. It consists of a piezocrystal that develops an electrical potential in response to mechanical pressure and the probe that is a cantilever with a fine tip at its end to scan the specimen surface. When the tip is brought into proximity of the sample surface, forces between the tip and the sample lead to a deflection of the cantilever. Typically, the deflection is measured using a laser spot reflected from the top surface of the cantilever into an array of photodiodes.

Confocal laser scanning microscopy (CLSM) is used to obtain high-resolution optical images. The key feature of confocal microscopy is its ability to acquire in-focus images from selected depths with a resolution of the fluorescence wavelength, a process known as optical sectioning through the specimen that have a thickness ranging up to 50  $\mu\text{m}$  or more. For opaque specimens, this is useful for surface profiling, while for non-opaque specimens, interior structures can be imaged. The stability of LbL assembly can be studied with CLSM, if fluorescently-labelled polyelectrolytes are assembled (Pastoriza-Santos et al., 2001; Sukhorukov et al., 2001). The method is limited to detectable particle size constraints. Release of fluorescently-labeled substances from LbL capsules and films also can be studied with CLSM (Müller et al., 2006). Multilayer thickness also scaled proportionally to the fluorescence intensity.

Transmission electron microscopy (TEM) is a microscopy technique in which a beam of electrons is transmitted through an ultra-thin specimen, interacting with the specimen as it passes through. An image is formed from the interaction of the electrons transmitted through the specimen; the image is magnified and focused onto an imaging device. The interior structure of specimen can be seen using TEM.

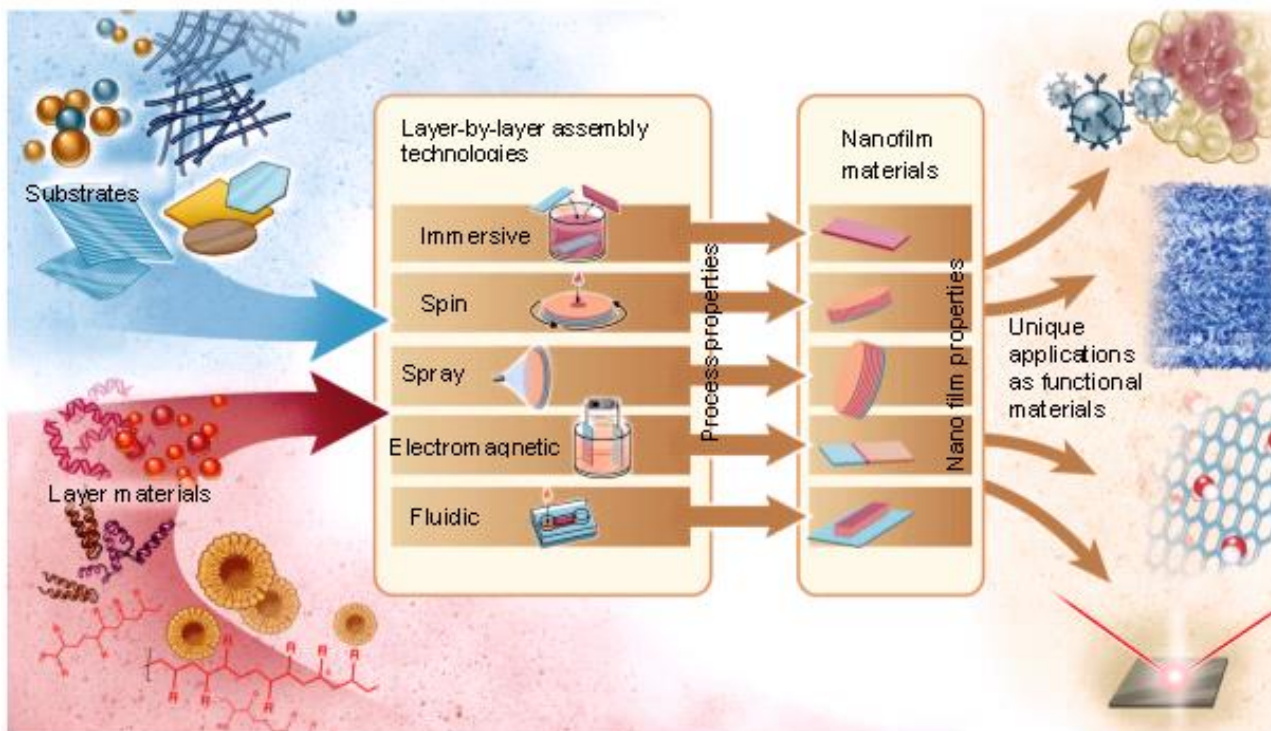
#### 1.4. Strategies for layer-by-layer assembly

Over the past few decades, layer-by-layer (LbL) assembly technique has been of considerable interest because of its ability to exert nanometer control over film thickness and its extensive choice of usable materials for coating planar and particulate substrates. Recent advances in LbL assembly technologies have explored different driving forces for the assembly process when compared with the diffusion-driven kinetics of classical LbL assembly, where a substrate is immersed in a polymer solution.

Examples of different assembly technologies that are now available include: dipping, dewetting, roll-to-roll, centrifugation, creaming, calculated-saturation, immobilization, spinning, high gravity, spraying, atomization, electrodeposition, magnetic assembly, electrocoupling, filtration, microfluidics and fluidized beds. These technologies can be condensed into five broad categories to which automation or robotics can also be applied—namely, (i) immersive, (ii) spin, (iii) spray, (iv) electromagnetic and (v) fluidic assembly. Many of these technologies are still new and are actively being explored, with research shedding light on how the deposition technologies and the underlying driving forces affect the formation, properties and performance of the films, as well as the ease, yield and scale of the processing. **(Fig.1.10)**

These assembly technologies affect both the process properties and the resultant material properties, and therefore careful choice of the assembly method can be crucial for successful application of the assembled films. Furthermore, two main themes can be identified for current developments in assembly technologies: The first is the move away from random diffusion-driven kinetics for layer deposition and the second is the advancement from manual assembly toward automated systems.





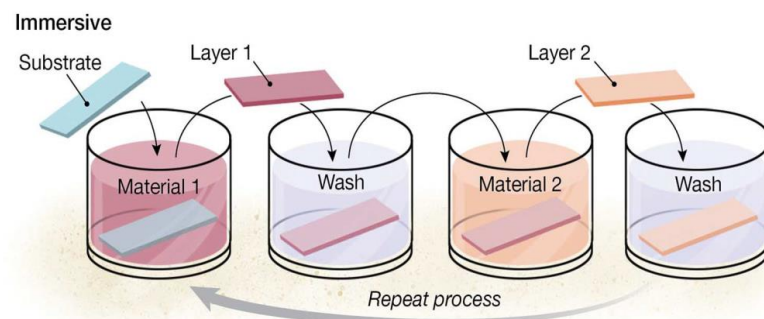
**Fig. 1.10.** Layer-by-layer assembly of nanofilms for preparing functional materials. The properties and performance of the resulting films depend on the substrate and layer material choices, as well as the assembly technology. Reproduced from Richardson et al., 2015.

#### 1.4.1. Immersive assembly

Immersive LbL assembly, sometimes referred to as dip assembly, is the most widely used method and reference standard for other technologies. Immersive assembly is typically performed by manually immersing substrate (mostly planar) into a solution of the desired material, followed by washing steps to remove unbound material (Lee et al., 2006; Decher et al., 1992; Dubas and Schlenoff, 1999). Particulate substrates can also be layered using immersion; however, the washing and deposition steps are generally broken up by centrifugation to pellet the particles (Caruso et al., 1998; Donath et al., 1998). Early studies on using particles for depositing planar multilayers noted that, theoretically, any material capable of having a surface charge (such as metals, non-metals, organics and inorganics) could be applied for growing multilayers if suitable conditions are used (Peiffre et al., 1981). Immersive assembly allows for more homogenous films when using either particle or polymer multilayers in comparison with non-LbL assembly technologies such as gas deposition and nucleation deposition, making LbL assembly widely used for thin-film formation.

Improvements in immersive assembly include speeding up the process by robotic immersion machines (Fou et al., 1996; Richardson et al., 2013). The colloids used for assembly in early studies required only 1 min of immersion for each adsorption step; however, for immersive assembly using polymers, the substrate is ideally immersed for ~15 min for sufficient layer deposition. To reduce the assembly time for polymers and to allow for the deposition of low-surface charge and/or small-contact area materials, solutions doped with organic solvents (e.g., dimethylformamide) can be used to eliminate the need for rinsing and drying steps through the process of dewetting (Shim et al., 2007).

The major driving force behind the development of immersive assembly technologies for particulate substrates is the attempt to avoid centrifugation, as it can lead to aggregation, is labour intensive, and is generally difficult to automate. A simple way to avoid centrifugation is to remove the need for washing steps. This can be achieved by adding exact amounts of polymer calculated to saturate the surface of the particulate substrates (Sukhorukov et al., 1998), rather than the high concentrations of excess polymer solution generally used. Initially, only two to three layers could be deposited before the particles start to aggregate, but more layers can be deposited by incrementally measuring the zeta potential during assembly. In summary, immersive assembly is considered to be a standard technique for other self-assembly techniques. The substrates of any shape and size can be layered using immersive technology. The films produced have an interpenetrated structure and form “fuzzy” nanoassemblies that are almost synonymous with LbL assembly (Decher, 1997). In recent days, there has been much improvement in using automated systems to reduce time and man power for making LbL assembly. For coating particulate substrates, there has also been considerable interest in technologies applicable to coat smaller, low-density particles (such as silica nanoparticles), which can be difficult to handle with the conventional centrifugation-based assembly.



**Fig. 1.11.** Layer-by-layer assembly using immersive technique. Reproduced from Richardson et al., 2015.

#### 1.4.2. Spin assembly

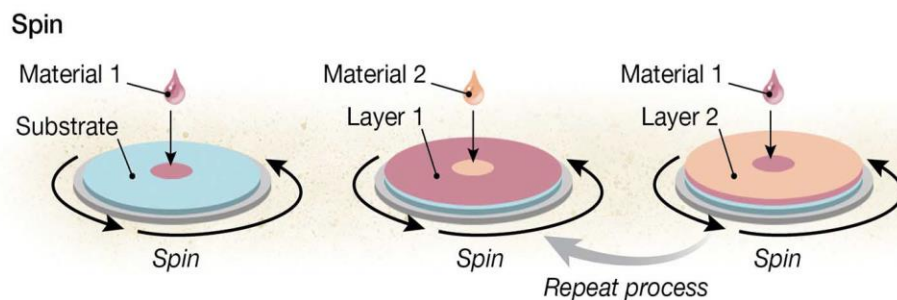
Layer-by-layer assembly using spin coating (spin assembly) utilizes the common coating technology of spinning a substrate to facilitate the deposition or adsorption of materials (Thomas, 1987). Moreover, drying a substrate after LbL assembly can be achieved through spinning (Hong et al., 1998). The majority of spin assembly is performed by either casting the solution onto a spinning substrate (Chiarelli et al., 2001) or casting the solution onto a stationary substrate (Cho et al., 2001).

Spin assembly results in more homogenous films compared with immersive assembly. This is because, assembly is driven by a collection of forces including electrostatic interactions (which cause the adsorption and rearrangement of polymers) and centrifugal, air shear and viscous forces (which cause desorption of weakly bound polymers and dehydration of the films) (Cho et al., 2001).

In a comparative study between automated immersive assembly and automated spin assembly, results showed the films prepared by immersive-assembly are thicker and rough, whereas films prepared by spinning resulted in thinner and smoother films (Seo et al., 2008). The spin-assembled films were transparent because of their distinct-layer stratification and the immersive-assembled films were opaque due to their inhomogeneous and interpenetrated layers. Upon spinning, centrifugal force pushes the layer material directly onto the substrate rather than across the substrate, hence the name “high gravity assembly” (Ma et al., 2012). This allows for improved film deposition and uniformity, especially at low polymer concentrations, because the rotation and increased turbulence lower the thicknesses of both the laminar layer and the diffusing layer around the substrate. The adsorption equilibrium can be reached at least five times faster than immersive assembly and is controllable by the spin speed. Furthermore, polymer combinations that grow exponentially using immersive

assembly also grow linearly using this technology. Similarly, the roughness is much lower (~2- to 10-fold) for LbL films assembled in this way (Jiang et al., 2014). Spin assembly typically produces substantially more organized films and multilayers than immersive assembly, which has made it a useful tool in preparing optical coatings with controllable and homogenous color and for preparing transparent films.

In summary, spin assembly uses rotating substrates to deposit layers and remove excess coating material. Spin assembly typically produces thinner, more organized and more stratified multilayers than does immersive assembly, and the process can be much faster (~30s). Furthermore, depositing multilayer films on non-flat surfaces, or even flat but rough surfaces, can be challenging due to the shear forces involved with film assembly. Nevertheless, the film and process properties arising from spin assembly, including smooth films assembled in a relatively short time, continue to make this method an attractive choice.



**Fig. 1.12.** Layer-by-layer assembly using spin assembly. Reproduced from Richardson et al., 2015.

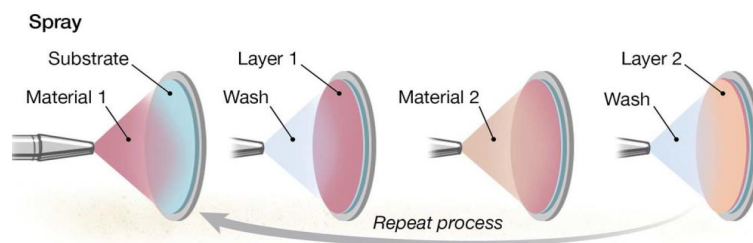
### 1.4.3. Spray assembly

Spray assembly is one of the assembly techniques where films are assembled by aerosolizing polymer solutions and sequentially spraying them onto substrates (Schlenoff et al., 2000). Spraying air has been used to dry films during LbL assembly to reduce contamination (Shim et al., 2005). Standard spray assembly is much faster (as quick as ~6 s per layer) than immersive assembly (Izquierdo et al., 2005). Vacuum can also be used to further speed up the process by minimizing the lag time between spraying and washing (Krogman et al., 2009). In spray assembly, the film properties such as the morphology, uniformity, chemical composition and membrane properties can be controlled in a similar way of immersive assembly technique. The film thickness is mainly influenced by polymer concentration, spray flow rate, spray duration, adsorption time, washing steps and flow direction (Merrill et al., 2009; Mulhearn et al., 2012; Alongi et al., 2013).

Spray assembly has also been combined with other technologies to improve the quality of layers and to automate the assembly process. For example, a disadvantage of spray LbL assembly is that the obtained films may not be homogeneous due to the effects of gravity draining, causing increased deposition in the vicinity of the solution drips and because of irregular patterns caused by the spray nozzles at certain distances (Alongi et al., 2013). To address this problem, rotating the substrate during spray assembly allows for the preparation of more homogeneous films and few seconds spray times for each layer (Krogman et al., 2007; Gittleston et al., 2012). By spraying onto the rotating substrates, a majority of the polymer added to the substrate is adsorbed. In comparison, the vast majority of polymer remains in the coating solutions after immersive assembly. Therefore, applicable concentrations roughly 10 to 50 times less than those required for immersive assembly can be used for spray assembly on rotating substrates (Gittleston et al., 2012).

A stand-alone spray assembly technology for coating particulate substrates uses surface acoustic waves of 1 to 10 nm in amplitude to atomize polymers and cargo (Qi et al., 2011). As the atomized droplets move through the air, the solvent evaporates and the polymer condenses into particle form, resulting in the first atomized solution becoming the template for subsequent coatings, with ~1000 carriers produced from each microliter of solution. The particles are dialyzed to remove excess polymer, added to a solution of oppositely charged polymer, and then re-atomized to coat the particles. This process can be repeated for multilayer assembly; however, the dialysis process increases the processing time of this technology to ~24 hours for each layer. Spray assembly has found use for a wide variety of applications because it can be used to coat industrial-scale substrates with relative ease and is not limited to planar substrates (Tang et al., 2013; Fukao et al., 2011; Krogman et al., 2013; Morton et al., 2013).

In summary, spray assembly produces multilayer films by aerosolizing coating solutions and spraying them onto the substrate. The resulting films are typically well organized with distinct layers. Spray assembly is a quick and easy method to coat large or nonplanar substrates, although immersive assembly remains the method of choice for coating complex 3D substrates. Spray assembly is one of the most highly relevant technologies for industrial applications, as it is already widely used in industry.



**Fig. 1.13.** Layer-by-layer assembly using spray assembly. Reproduced from Richardson et al., 2015.

#### 1.4.4. Electromagnetic assembly

Electromagnetic assembly is based on the use of an applied electric or magnetic field to effect layering, such as by coating electrodes in polymer solutions or by moving magnetic particulate substrates in and out of coating solutions (Sun et al., 2001; Hong et al., 2004). The former, commonly referred to as electrodeposition, is a well-established technology for coating materials using an applied voltage in electrolytic cells. In the standard electrodeposition setup, two electrodes are immersed in polymer solution and then an electric current is applied. The electrodes are then washed and placed into solution of an oppositely charged polymer; the polarities of the electrodes are reversed, and the process is repeated (Van Tassel et al., 2012). Electrodeposition can be used to rapidly assemble ions, polymers, and colloids in much less time than in immersive assembly (Sun et al., 2001).

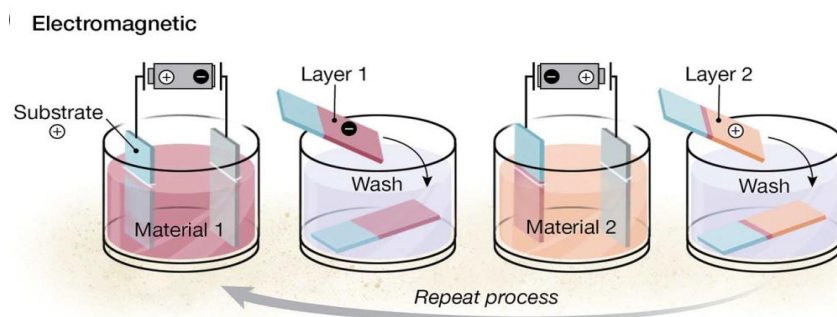
This technology results in films roughly twice the thickness of those resulting from centrifugation-based assembly. Electrodeposition can also use higher voltages, upwards of 30 V; however, the assembly process for immobilized particles can take as long as 15min per layer (Richardson et al., 2013). The thicknesses of the electrodeposited films are directly related to the voltage used during assembly, with the optimum voltage for achieving the thickest films depend on the pH of the polymer solution (Ko et al., 2011). Higher voltages can cause desorption of the film as the electrode (i.e., the substrate) begins to repel the previously deposited layer. Generally, pH values lower than the pKa (where Ka is the acid dissociation constant) of the polymers need lower voltages to reach peak thickness, and that peak thickness is also larger than the peak thickness at higher pH, closer to or above the pKa of the polymers.

Electrodeposition can also be achieved by using local effects at the electrodes, such as inducing redox reactions or changes in pH. The pH of the solution near the anode and



cathode changes markedly from bulk solution to lower and higher pH values, respectively (Wang et al., 2104). The low pH near the anode can induce polymer deposition. However, this pH-induced electrodeposition is fairly limited, as only a few bilayers can be deposited (using materials such as alginate and chitosan) because the layers become too thick (tens of micrometers) for the electric current to penetrate, resulting in no pH change and therefore no deposition.

In summary, electromagnetic assembly uses electric or magnetic fields, typically in the form of electrodes in polymer solutions or magnetic particulate substrates to deposit films. Electromagnetic assembly can exploit current-induced changes in pH or redox-reactions to affect film assembly, thus using a driving force substantially different from that of the other main assembly categories. Generally, electromagnetic-assembled films are thicker and more densely packed than films prepared using other LbL assembly methods. Electromagnetic assembly is still not as common as some of the other technologies, and even though it requires special equipment and expertise, it does offer a different approach to multilayer film assembly (e.g., through magnetic handling of substrates and materials or through electrically induced assembly), thereby providing alternative opportunities for assembling films.



**Fig. 1.14.** Layer-by-layer assembly using electromagnetic assembly. Reproduced from Richardson et al., 2015.

#### 1.4.5. Fluidic assembly

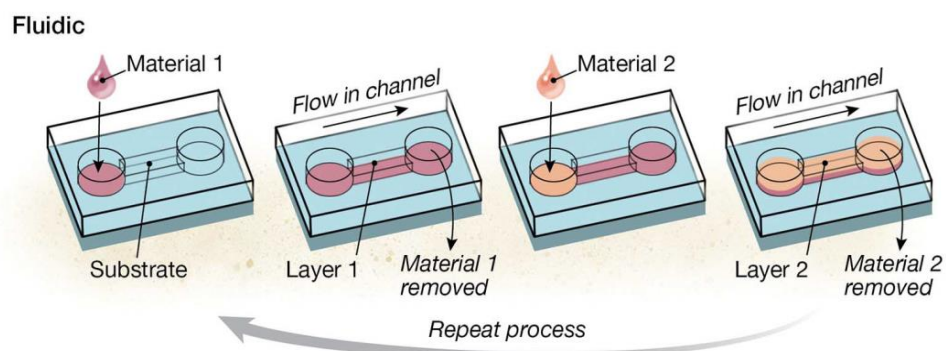
Fluidic assembly can be used to deposit multilayers with fluidic channels, both by coating the channel walls and by coating a substrate placed or immobilized in a fluidic channel (Wang et al., 2011). The general method involves using pressure or vacuum to sequentially move polymer and washing solutions through the channels, which can be fluidic components such as tubing or capillaries, or designed microfluidic networks (Raman et al., 2014; Madaboosi et al., 2012). Flow chamber– based QCM is a common fluidic assembly technology used for investigating thin-film properties and multilayer growth by providing crucial real-time information (Picart et al., 2001). Higher concentrations of polymer solution typically yield thicker films (Madaboosi et al., 2012), with the contact time rather than the flow rate as the crucial factor determining the amount of adsorbed polymer under flow (Kim et al., 2005).

However, fluidic assembly strongly resembles immersive assembly when polymer solutions are allowed to remain in static contact with the substrate for more than 10min (Katayama et al., 1998; Barker et al., 2000). Polymer and washing solutions loaded into channels with a pump or vacuum can deposit ~1.5-nm-thick layers in 5 to 10min (Reyes et al., 2004). Capillary forces can also be used to pull polymer solutions through microfluidic channels by placing droplets of solution at fluidic inlets, followed by spinning the substrate to remove the solution, allowing for ~1.2-nm-thick layers to be deposited in less than 2min (Jang et al., 2003).

This technology not only allows for the deposition of polymers but also for the deposition of larger cargo, such as gold nanoparticles or liposomes and produces films with nearly identical thickness to those prepared by standard centrifugation-based assembly. Fluidic assembly is not restricted to planar substrates and is a viable alternative for

centrifugation-free assembly on particulate substrates (Priest et al., 2008; Kantak et al., 2011; Matosevic et al., 2013). Many fluidic assembly approaches coat emulsions or liquid crystals, as these materials are well studied in the fluidics field.

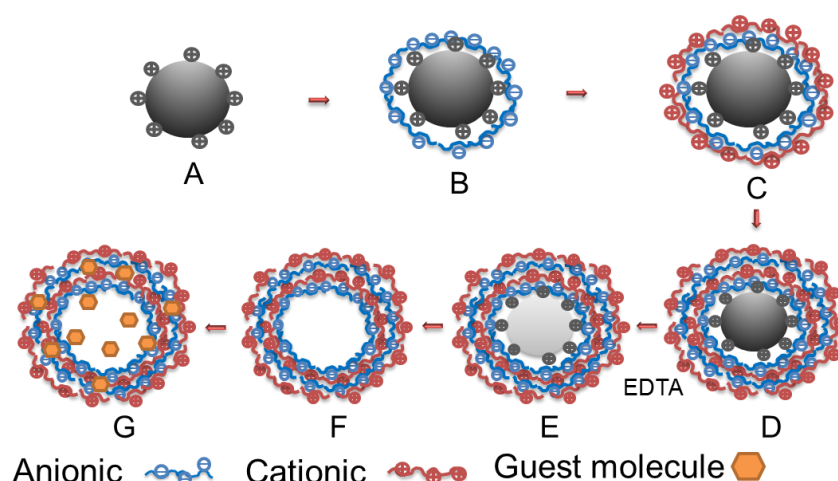
In summary, fluidic assembly provides the means to assemble multilayers on surfaces not easily accessible to other methods (e.g., inside capillaries), provides new ways for region-specific patterning (e.g., by masking a surface with a fluidic channel), and increases the industrial capacity of multilayer assemblies (e.g., through parallelization of film assembly and decrease of reagent consumption). Although the specialized equipment and expertise required to set up (micro) fluidic systems can complicate the use of fluidic assembly, these advantages make it attractive for many applications.



**Fig. 1.15.** Layer-by-layer assembly using fluidic assembly. Reproduced from Richardson et al., 2015.

## 1.5. Layer-by-layer self-assembled micro- and nanocapsules

The layer-by-layer technique was first applied to planar films. Later, it was extended to spherical and colloidal particles by Möhwald and coworkers for the preparation of micro/nano capsules (Skorb and Möhwald, 2013). Polyelectrolyte micro and nanocapsules are generally prepared by LbL adsorption of oppositely charged polyelectrolytes onto sacrificial template of size ranging from 0.1 to 10  $\mu\text{m}$  and subsequent dissolution of core results hollow capsules. The prepared hollow micro/nano capsules can be further used for drug loading or encapsulation (Decher, 1997; Sukhorukov et al., 1998). Schematic representation of hollow LbL micro/nano capsules preparation showed in **Fig. 1.16**.



**Fig. 1.16.** Schematic representation of layer-by-layer micro/nano capsules preparation.

Generally, there are three main approaches for the preparation of micro/nano capsules. The first approach involves the LbL polyelectrolyte coating of drug particle itself (Qiu et al., 2001). The second approach is the preparation of hollow capsules by adsorption of polyelectrolyte multilayers on soluble templates. The prepared hollow capsules will be permeabilized by changing the pH and/or solvent polarity to allow the diffusion drug molecules into the capsules (Antipov and Sukhorukov, 2004; Antipov et al., 2003). Finally, the third approach involves use of porous inorganic templates preloaded with therapeutic

agents before being coated with polyelectrolytes (Sukhorukov et al., 2004; Wang et al., 2007). Their dissolution results diffusion of small molecular weight ions while the other molecules remain trapped in the capsules.

The polyelectrolytes poly(styrene sulfonate) / poly(allylamine hydrochloride) (PSS/PAH) combination is considered to be a very popular polyelectrolyte pair for fabrication of hollow polyelectrolyte microcapsules. Many researchers have already developed and proved that the preparation of PSS/PAH LbL microcapsules is reproducible and did not show any sign of aggregation or decomposition of capsule upon removal of the core template. Also, the LbL MC prepared by this combination showed good physicochemical and mechanical properties (Antipov and Sukhorukov, 2004; Gao et al., 2001; Gao et al., 2001).

Initially hollow capsules were prepared using organic templates including cross-linked melamine formaldehyde (MF) and polystyrene (PS) and dissolved in organic solvents (DMF) and acidic solutions (0.1M HCl) after deposition of polyelectrolyte multilayers. The main drawback during the core removal is the integrity of the capsule wall. It is already reported that organic solvents create pores in capsule wall and allow template to diffuse outwardly from the capsules. However, the removal of MF templates is more difficult as it is reported that MF stay complexed to the capsule wall and interior of capsule even after prolonged incubation in an acidic environment may cause toxicity. Hence, the use of MF particles became less frequent. In case of polystyrene, dissolution in organic solvents creates an osmotic pressure which may destroy the microcapsule shell (Gao et al., 2002; Gao et al., 2001; Dong et al., 2005; Dejugnat and Sukhorukov, 2004).

To overcome the problems associated with core dissolution and integrity of capsule wall, use of inorganic carbonates ( $\text{CaCO}_3$ ,  $\text{MnCO}_3$  and  $\text{CdCO}_3$ ) have introduced recently as a

template for LbL hollow capsule preparation (Antipov et al., 2003; Petrov et al., 2005; Sukhorukov et al., 2004; Volodkin et al., 2004). The preparation of CaCO<sub>3</sub> microparticles involves simple mixing of calcium chloride and sodium carbonate and further used for LbL polyelectrolyte adsorption. The CaCO<sub>3</sub> core particles were easily dissolved in EDTA solution. The major advantage of inorganic templates is the low molecular weight of the ions. Polyelectrolyte shells commonly allow molecules with less molecular weight (< 5kDa) (Sukhorukov et al., 1999), so capsules would not undergo osmotic stress during dissolution of inorganic templates.

#### 1.5.1. Drug delivery applications of polyelectrolyte microcapsules

Polyelectrolyte microcapsules have wide variety of applications in different fields. They can be used as microreactors for the synthesis (Shchukin and Sukhorukov, 2004), sensors (Zhu and McShane, 2005) and in separation (Shchukin and Sukhorukov, 2003) of materials. In recent days the potential application of LbL capsules in drug delivery is increased significantly. The important advantage of LbL capsules is their able to load variety of molecules and can control the release (Ai et al., 2003). An interesting feature of these polyelectrolyte multilayer capsules is response to external stimuli like pH, temperature, light, ultra sound, magnetic field, solvent polarity, glucose levels and electrochemical potential.

##### 1.5.1.1. pH responsive polyelectrolyte capsules

Polyelectrolyte capsules made of weak polyelectrolytes are generally responsive to change in the pH of the environment. This change results in decrease of charge density of the LbL assembly and leads to increase in permeability when the pH of the surrounding environment containing polyelectrolytes is close to their pKa. For example a weak polyelectrolyte, PAH (pKa of 8.7) commonly used in fabrication of LbL capsules when complexed with PSS the pKa changes to 10.7 reported by Petrov et al. (Petrov et al., 2003)

When surrounding pH becomes higher (incase of polybase) or lower (incase of poly acid) than the pKa, the polyelectrolyte become uncharged or reduction in charge density results swelling and disassembles the capsules. Antipov et al. also observed that polyelectrolyte microcapsules prepared with PSS/PAH clearly showed the pores present in capsules treated with an acidic solution, whereas the capsules treated with an alkaline solution are intact (Antipov et al., 2002). The pH dependent permeability of the capsules to high molecular weight substance, FITC-dextran studies showed permeability at acidic pH and impermeable at alkaline regions (Sukhorukov et al., 2001).

A pharmaceutical application of pH responsive capsules is delivery of encapsulated drugs or therapeutic agents in locations with mild acidic environments. A lower pH conditions generally found in extracellular matrix of tumours, inflammatory and ischemic regions, intracellular vesicles like endosomes, lysosomes and secretory granules (Galvin, P., et al., 2012). In addition, accumulation of nanocapsules in tumor tissue is enhanced by enhanced permeability and retention effect (EPR) (Maeda, 2001).

#### 1.5.1.2. Light responsive polyelectrolyte capsules

Generally, release of encapsulated therapeutics from capsules by light response is related to chromophore embedded in non-absorbing polyelectrolyte. When light irradiates, the chromophore gets heated and leads to increase in permeability of capsule shell or its rupture (Vogel et al., 2003). The primary requirement for the use of light responsive capsules is not to cause any damage or destruction to the encapsulated drug and surrounding environment due to light illumination. The first report on optically sensitive polyelectrolyte microcapsules was made by Tao et al. They reported on the use of the organic dyes like azo dye Congo red as absorbers for light responsive polyelectrolyte capsules (Tao et al., 2004). Irradiation of such polyelectrolyte microcapsules with visible light (for 120 min) slightly

distorted the polyelectrolyte multilayers, enhancing their permeability for fluorescently labelled dextrans with a molecular weight of up to 464 kDa.

The best region in the electromagnetic spectrum is in between 780 and 900 nm, where no chief chromophore absorbance is observed (Vogel et al., 2003). The absorption properties of the capsule can be controlled by selecting size and the substrates of the nanomembrane, which regulates heat production and response. The Caruso et al., first time reported the release of encapsulated macromolecule from capsules functionalized with gold nanoparticles upon irradiation of IR light (Caruso et al., 1998). When IR light irradiates, the gold nanoparticles absorb the energy and convert into heat, which disturbs the integrity of the capsules (Angelatos et al., 2005; Radt et al., 2004; Skirtach et al., 2005). A novel type of optical responsive capsules has been demonstrated by Wang et al. by encapsulation of photosensitizers to induce cell death for the treatment of cancer and viral infections by generation of singlet oxygen upon exposure to light (Wang et al., 2007).

#### 1.5.1.3. Magnetic responsive polyelectrolyte capsules

The incorporation of magnetic responsive materials like  $\text{Fe}_3\text{O}_4$  into layer-by-layer assembly is the common way to achieve magnetic response. Navigation of LbL nanocapsules by means of magnetic field is a promising technique to achieve controlled release and targeted delivery of therapeutics of interest. Caruso et al., first time reported the preparation of magnetic polyelectrolyte capsules using polystyrene beads alternatively coated with negatively charged  $\text{Fe}_3\text{O}_4$  nanoparticles and positively charged PAH (Caruso, F., et al., 1999). Different strategies were developed for the preparation of magnetic responsive capsules such as hollow magnetic capsule after dissolution of core (Caruso et al., 2000) and incorporation of magnetic nanoparticles in pH dependent polyelectrolytes (Antipov et al., 2002). In the



latter example, the  $\text{Fe}_3\text{O}_4$  nanoparticles ( $< 10\text{nm}$ ) could diffuse/permeable through the PAH/PSS polyelectrolyte membrane at pH 4.5 and reach the interior of the capsule shell.

The interesting feature of magnetic responsive capsules is the ability to respond upon applying an oscillating magnetic field, which disturbs the structure of the polyelectrolyte multilayers and, consequently, allows the diffusion of therapeutic agents through the capsule wall. In-vitro experiments using  $\text{Fe}_3\text{O}_4$  impregnated PSS/PAH capsules targeted on breast cancer cells showed that a high level of cellular internalization and release of payload when the capsules placed under magnetic field (Zebli et al., 2005). Hu et al. also observed the rupture of  $\text{Fe}_3\text{O}_4$ /PAH capsules leading to the release of FITC-dextran under high frequency magnetic field (Hu et al., 2008). The release mechanism is related to the local heating and stress induced by the magnetic capsules on exposure to magnetic field results in relaxation of capsule membrane. It is important to note that the magnetic particles or capsules can be used in magnetic resonance imaging (MRI) for drug delivery tracking in-vivo and visualization of contrast agents (Ai et al., 2011).

#### 1.5.1.4. Electrochemical delivery from polyelectrolyte capsules

Graf and co-workers recently reported the use of physical stimuli responsive polyelectrolyte capsules to achieve controlled delivery. Using electrochemical stimuli they delivered a dye, calcein which was previously loaded in liposomes embedded in sandwich of polyelectrolyte multilayers. This kind of delivery techniques can be used for surface mediated drug delivery or for realizing intelligent cell cultures (Graf et al., 2012).

#### 1.5.1.5. Ultrasound responsive polyelectrolyte capsules

Ultrasound technique is widely used in therapy and diagnostics of several diseases. It has also been investigated for biomedical applications, improving drug uptake, anti-

inflammatory treatment and imaging. Therefore this technique has great potential in controlled delivery of drugs from polyelectrolyte capsules. The major challenge is to optimize the ultra sound frequency to respond the polyelectrolyte capsules without causing any damage to the living organisms. When polyelectrolyte capsules are subjected to ultrasound, a morphological change of the capsule wall may occur due to the creation of shear forces between the successive fluid layers, resulting in the disruption of the capsule membrane and release of encapsulated species. Mason et al. reported the release of protein from polymer and gold capsule upon exposure to ultrasound frequency (850 kHz and 1-3 W) (Pavlov et al., 2011).

#### 1.5.1.6. Glucose responsive polyelectrolyte capsules

Glucose responsive polyelectrolyte capsules have great potential in delivery of insulin to treat diabetes mellitus. These glucose responsive capsules release the insulin when the glucose levels in the body exceed a normal value. Brown et al. fabricated and encapsulated glucose oxidase in polyelectrolyte capsules. They expected that the capsules to be glucose sensitive because the oxidation of glucose by glucose oxidase which is already loaded in capsules leads to formation of glucuronic acid. The formed acid may cause decrease the pH at the surface of the capsules and modify the permeability of capsules (Brown et al., 2005).

#### 1.5.1.7. Degradable polyelectrolyte microcapsules

Biodegradable polyelectrolyte capsules are best choice over non-biodegradable ones for drug delivery and other biomedical applications. There are several reports on biodegradable LbL films, for example degradable polycations (poly- $\beta$ -aminoesters) was used to make LbL films for the controlled release of small drug molecules and DNA. (Lynn et al. 2000). Mohwald and group first time reported the preparation of biodegradable polyelectrolyte capsules and covered with lipid bilayer to make impermeable to low

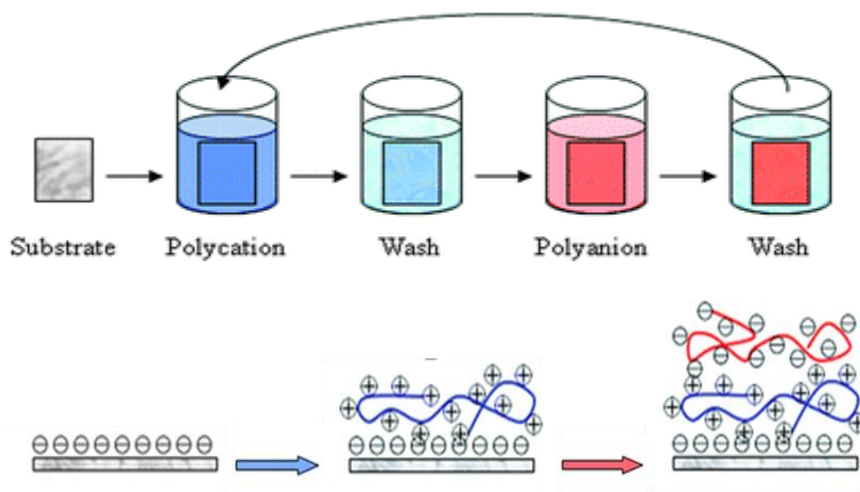
molecular weight carboxy fluorescein. In presence of phospholipase A2, the lipid bilayer was degraded and created pores and capsules became permeable to carboxy fluorescein (Mohwald et al., 2003).

#### 1.5.1.8. Redox responsive polyelectrolyte capsules

Redox sensitive polyelectrolytes containing a disulfide linkage in their backbone is a key factor for their redox responsiveness. In recent days researchers are focusing on intracellular delivery of various macromolecules including plasmid DNA, antisense oligonucleotides and small interfering RNAs using redox sensitive technique (Saito et al., 2003). The mechanism is attributed to the redox responsiveness in which, the high redox-potential inside cells would trigger or enhance the intracellular release of encapsulated molecules from pharmaceutical carriers containing disulfide linkages.

Haynie et al. recently reported the redox sensitive polyelectrolyte microcapsules made of anionic and cationic polypeptides containing cysteine groups (Haynie et al., 2005). Upon cross-linking of the cysteine's thiol groups (leading to disulfide bonds), the prepared capsules were found to be stable at both neutral and acidic pH. However after reduction of disulphide bonds, the microcapsules disassembled at a pH lower than the pKa of the anionic polypeptides. They reported that to achieve redox triggered disassembly of polyelectrolyte microcapsules, still acidic conditions are necessary.

## 1.6. Layer-by-layer self-assembled thin films



**Fig. 1.17.** Schematic representation of layer-by-layer thin film formation.

Biocompatible and biodegradable materials are appropriate for drug delivery are usually fabricated by self-assembly and related processes (Ariga et al., 2011). In many cases, bio-membrane like thin or ultrathin films in flat, curved and shell structures are used as self-assembled materials for drug delivery. Various methodologies for ultrathin film preparation have been widely used, such as the Langmuir--Blodgett (LB) technique (Mori et al., 2010), the self-assembled monolayer (SAM) method (Vericat et al., 2010) and the layer-by-layer (LbL) adsorption technique (Ariga et al., 2010).

If one looks specifically to the use in drug delivery applications, the number of research examples based on the LbL technique is much larger than for the other two formation techniques. This is a logical consequence of the freedom in material selection and flexibility in structural design offered by the LbL approach, as these characteristics are well suited to the demands on fabrication of drug delivery materials that require rather complicated design in their components and structures. In addition, the apparatus required for

the LbL procedure are relatively simple and inexpensive, which further supports the viability of the approach for practical application by enabling rapid prototyping and scale-up for commercialization. To understand this technique and its potential, it is worthwhile considering the history of developments that have led to the current state of the art. Sometime after the suggestive report by Iler (Iler, 1966), the LbL assembly was first experimentally realized and established by Decher and Hong (Decher et al., 1991). Several years later, a powerful strategy for the application of LbL to coating colloids and subsequent shell formation was invented (Caruso et al., 1998).

As exemplified in the LbL assemblies between cationic and anionic polyelectrolytes, adsorption of the cationic polyelectrolyte at the negatively charged surface of a solid support usually causes over-adsorption, resulting in surface charge reversal under appropriate conditions. This yields a self-limiting and highly repeatable process. Subsequent adsorption of anionic polyelectrolyte again reverses the surface charge so that alternation of the surface charge permits continuous fabrication of the layered structure. This process can also be applied to assemblies between cationic polyelectrolyte and anionic particles such as protein molecules. It is noteworthy, however, that the driving force of self-assembly is not limited to electrostatic interaction. Various interactions including hydrogen bonding (Stockton et al., 1997) and bio-specific interaction (Lvov et al., 1995) can be used, which expands further the options for materials and deposition conditions for film construction and also yields different and useful film properties.

In addition, there is a vast choice of available materials, including biological substances such as proteins (Lvov et al., 1995), nucleic acids (Shchukin et al., 2004), saccharides (Lvov et al., 1998) and virus particles (Lvov et al., 1994) as well as various organic polymers (Fujii et al., 2010), molecular assemblies (Ariga et al., 1997) and inorganic substances (Honma et al., 2010) for the LbL assembly. As one can imagine from the simple

procedure of the LbL assembly, the assembling procedure can be performed in mild aqueous medium and does not require chemically harsh conditions.

In addition, the LbL structures are less densely packed than those of LB films (Okahata et al., 1989), which is advantageous for diffusion driven release of drugs through the films (Onda et al., 1999). As exemplified in nanofilm reactors (Onda et al., 1996) with enzymatic LbL structures, biomolecules softly fixed in the LbL films are usually more stabilized against external disturbances and show increased duration of activity. With these characteristics of the LbL technique established, LbL assemblies have recently undergone extensive research for drug delivery applications (Becker et al., 2010). Capsule-type LbL assemblies have been of particular interest, because of their potential for targeted delivery in the body. In contrast, film-type LbL assemblies cannot generally travel through the body, but they can be a very powerful methodology for coating of biomedical apparatus that need sustained release of drugs (e.g., implanted devices such as stents).

#### 1.6.1. Layer-by-layer films for biological applications

Before describing specific drug delivery applications, recent research examples of LbL film fabrication which have significant value for biomedical applications are briefly summarized. Khutoryanskaya and co-workers prepared LbL assembly of inter polymer complexes formed by poly(acrylic acid) and methylcellulose (Khutoryanskaya et al., 2010) on silanized glass slide. Thermal treatment of the films promoted crosslinking of polymers, resulting in non-detachable ultrathin hydrogels that showed pH-dependent swelling properties. Specifically, they observed minimal water uptake at  $\text{pH} < 6$ , compared with a dramatic volume increase at higher pH and the usual dependence on sample thickness.

Carlmark and co-workers synthesized thermos-responsive block polymers from N-isopropylacrylamide and (3-acrylamidopropyl) trimethylammonium chloride and assembled

the synthetic polymers with nano-fibrillated cellulose in layer-by-layer fashion (Utsel et al., 2010). Cellulose is a renewable, fibrillar nanomaterial with interesting strength and biocompatibility properties, and the composite films obtained have potential for coatings in bio-related applications, including sensors, filters, membranes and drug delivery systems. Bulwan et al. reported the preparation of stable single-component multilayered films of chitosan by means of the LbL technique, using two water soluble chitosan derivatives: polycationic and polyanionic forms (Bulwan et al., 2009). As chitosan derivatives have been reported to possess excellent biocompatibility and bacteriostatic properties, these LbL films could be useful for many kinds of biomedical and environmental protection applications.

Kim et al. synthesized star polymers with oppositely charged arm structures, poly[2-(dimethylamino)ethylmethacrylate] star polymer and poly(acrylic acid) star polymer, with crosslinked cores (Kim et al., 2009). These polymers were assembled by the LbL assembly to form non-uniform and porous structures owing to their architecture and high molecular mass as compared with conventional linear polyelectrolytes. The prepared films showed extensive structural reorganization on post-treatment with different pH conditions owing to the highly pH-sensitive nature of star polymers. The interesting architectures and high degree of functionalities of these star polymers would lead to potential applications such as vehicles for drug delivery. Buck and Lynn used an approach of the LbL assembly for the preparation of semipermeable membranes (Buck et al., 2010). It is based on the rapid reaction of azlactone-functionalized polymers with polymers containing primary amine functionality. Freely suspended and mechanically robust semipermeable membranes that span across the open ends of pores and orifices with dimensions in the order of tens of micrometers to several millimeters can be obtained. This approach is especially suited to the fabrication of suspended membranes within the channels of microfluidic devices or the open ends of

micropipettes, which is expected to find use in biomedical separation, sensing and drug delivery.

As a DNA-related example, Cai and co-workers prepared gene-functionalized LbL films composed of chitosan and plasmid DNA on a titanium surface that were used to investigate the surface-mediated in situ differentiation of mesenchymal stem cells (Hu et al., 2009). Functional genes were released in a sustained manner during the degradation of the LbL structures. The released genes positively stimulated the adhered mesenchymal stem cells for 2 weeks, as reflected by gene expression and protein production. This type of system has great potential in applications such as the development of gene-stimulating biomaterials and implant technology.

#### 1.6.2. Layer-by-layer films for delivery of small drugs

LbL films have been explored for the delivery of various small molecules for biomedical applications. Controlled release and high drug payload are particularly important for small molecule delivery. Sun and co-workers proposed a facile way to incorporate ibuprofen in surgical sutures by the LbL deposition of chemically crosslinked poly(allylamine hydrochloride) and dextran with hyaluronic acid (Wang et al., 2009) for wound healing applications. The prepared sutures showed sustained release of ibuprofen with retained mechanical properties. The release kinetics can be controlled by LbL process and parameters.

Hu and Ji developed LbL films of sulfonated hyper branched polyether with chitosan as nanoreservoirs for hydrophobic guest molecules (Hu, 2010). A coating with potential anticoagulation and antibacterial activity, and local release of the hydrophobic drug Probucal was investigated. Probucal is known to have powerful antioxidant properties and can prevent



restenosis after coronary angioplasty. This strategy could lead to a multifunctional coating capable of anticoagulant and antibacterial activity, and local drug delivery.

Dubas and co-workers investigated loading of curcumin into polyelectrolyte multilayer films (Dubas and Schlenoff, 1999; Kittitheeranun et al., 2010). Curcumin has already been used in the treatment of wound healing and cancer. Their results suggest that LbL thin films are a promising matrix for incorporating curcumin, especially for drug delivery applications.

Hammond and co-workers reported on LbL films for small molecule delivery capable of hydrolytic top-down film degradation, linear release profiles and programmable release kinetics through facile aqueous manufacturing (Smith et al., 2009). The LbL films were assembled with poly(b-amino esters) as the degradable polycations and poly(carboxymethyl- $\beta$ -cyclodextrin) complexed with a small molecule as the anionic supramolecular complex. Charged cyclodextrin polymers are essential for the accommodation of cyclodextrin-drug complexes in stable fashion. These surface-eroding films are capable of drug release from within the cyclodextrin carrier without altering drug activity.

Hammond and co-workers expect that this strategy would lead to the development of nanomedicine coatings for applications in personalized medicine, transdermal delivery, medical devices, nanoparticulate carriers and prosthetic implants. The same research group further investigated hydrophobic effects of polyelectrolytes on destabilization and release dynamics of degradable LbL films (Smith et al., 2009), which are determined by a complex balance between hydrophobic composition, charge density and stability of electrostatic ion pairs. The data obtained showed a correlation between the octanol/ water partition coefficient and sustained release profiles that can be useful in designing custom drug delivery coatings.

Other drug delivery systems have targeted release profiles that vary with environmental stimuli, such as pH or temperature changes.

For example, Anzai and co-workers prepared LbL films containing insulin and demonstrated the pH-triggered release of insulin (Yoshida et al., 2010). The insulin-containing LbL films were assembled through alternate adsorption of insulin and poly(vinyl sulfate), poly(acrylic acid), or dextran sulfate in acidic solutions.

Finally, research to exploit the multilayer and inherently composite nature of LbL films to incorporate multiple drugs for coordinated release has also been initiated. Hammond and co-workers proposed a multiagent-delivery nanolayer that would make possible the co-delivery of different types of drug, such as charged macromolecules and uncharged, small hydrophobic drugs from a single LbL film (Kim et al., 2009). Release of both therapeutic polysaccharides (heparin and dextran sulfate) and hydrophobic drugs (diclofenac and paclitaxel) under physiological conditions was through the hydrolytic degradation of a poly( $\beta$ -amino ester) as the assembling film component.

### 1.6.3. Layer-by-layer films for delivery of macromolecules (biomolecules)

Drugs for biomedical applications are not limited to low molecular-mass analogues. Biomolecules including DNA, RNA, poly/oligopeptides and proteins often have more important roles. For example, localized intracellular controlled release of nucleic acid therapeutics would be an effective route to overcome the extracellular barriers that plague gene therapy. Reineke and co-workers demonstrated the LbL assembly for in-vitro controlled release of plasmid DNA where cationic poly(L-tartaramidopentaethylenetetramine) and anionic plasmid DNA were used as assembling components (Taori et al., 2009).

Interaction between zirconium and phosphate is also known as an effective interaction that can be exploited to construct layered films comprising nucleic acids. Wang et al. prepared assembled multilayer films through coordination/electrostatic interactions between inorganic zirconium ion ( $Zr^{4+}$ ) and phosphate groups in the backbone of the DNA chain (Wang et al., 2009). LbL films were demonstrated using plasmid DNA to sustain the consecutive release of DNA and retain transcriptional activity. This strategy could be extended to other targets, from polynucleotides to other negatively charged biomolecules. Other stimulation methods have been developed, as well, including the work of Volodkin et al. to demonstrate light-triggered delivery of DNA from designed LbL assemblies comprising gold nanoparticles, microcapsules and DNA (Volodkin et al., 2009).

Blacklock et al. reported modulation of DNA release from LbL films by utilizing both condensed and uncondensed DNA in different layers (Blacklock et al., 2010). Polyplex layers induced faster DNA delivery in its condensed and non-aggregated state as released form. In contrast, the naked DNA layer showed slower DNA delivery, where the released DNA was more likely to be in an uncondensed aggregated state.

For improvement of transfection efficiency of small interfering RNAs (siRNAs), Fujimoto et al. fabricated LbL films of siRNA and cationic polymers, the branched or linear form of poly(ethyleneimine) (Fujimoto et al., 2010). Similarly, Chan and co-workers proposed a multilayer-mediated forward method for patterned siRNA transfection (Mehrotra et al., 2009). In this case, they used pH-responsive LbL films as the delivery platform, where a microcontact printing technique was applied to pattern nanoparticles of transfection reagent-siRNA complexes onto degradable multilayers. The proposed method provides an efficient and simple approach to spatially controlled siRNA delivery.

Delivery of peptides and proteins are also important targets for research in the corresponding fields. For example, antimicrobial resistance to avoid biofilm-related implant failure is important for the treatment of flesh wounds as well as the functionalization of bandages, medical devices and implant materials. For this purpose, Shukla et al. studied the incorporation and release of an antimicrobial peptide, ponicin G1, from hydrolytically degradable LbL assembled thin films (Shukla et al., 2010). It was found that the film composition – in particular, the polyanion used -- strongly influences the film growth and degradation properties as well as the incorporation and release properties of ponicin G1.

Wang and Ji fabricated LbL films of poly(L-lysine) and hyaluronic acid at controlled pH conditions to induce exponential growth of the multilayer (Wang and Ji, 2009). These exponential growth LbL films were utilized as reservoirs for loading a trans-activating transcriptional factor peptide. As compared with the direct LbL assembly of the trans-activating transcriptional factor peptide and hyaluronic acid, greater amounts of the peptides could be loaded within the film via the post-diffusion of trans-activating transcriptional factor peptide into the pH-amplified exponential growth multilayer. The post diffusion of oligopeptide within an exponential growth multilayer can serve as an effective approach for localized transport of the peptides into cells.

Mehrotra et al. reported time-controlled protein release from LbL films assembled on agarose hydrogel (Mehrotra et al., 2010), where the proteins such as lysozyme were incorporated within the degradable LbL multilayer coatings. The protein was loaded subsequent to the agarose hydrogel fabrication rather than pre-loaded directly into the hydrogel, avoiding the caustic conditions used in the templated agarose scaffold fabrication. A variety of proteins can be applied in film degradation based controlled release without the concern or constraints that may be imposed by potential interactions between the drug and

hydrogel. This approach does not require any specific chemical alterations to the LbL components.

#### 1.6.4. Layer-by-layer hybrid films for drug delivery

One of the most outstanding features of the LbL technique is the wide choice of layering components, which is advantageous for fabrication of hybrid structures comprising virtually any combination of materials. Hybridization of the LbL assemblies with inorganic and/or organic materials often induces significant enhancement of the whole LbL system. As an attractive strategy of organic/inorganic hybrid LbL films, Mohammed and McShane reported fabrication of multicomponent patterned films comprising polymer/ nanoparticle multilayers using conventional lithography and LbL assembly (Mohammed et al., 2008).

The concept of hybrid LbL films is also used for drug delivery applications. Polyoxometalate is a promising antitumor drug that has a very strong interaction with carbon nanotube surfaces. Zhao et al fabricated LbL films of polyoxometalate modified single-walled carbon nanotubes with chitosan for sustained release of polyoxometalate (Zhao et al., 2009). For better cytotoxic properties, positively charged chitosan was used to complex with negatively charged polyoxometalate-nanotube complex; because of the enzyme responsiveness and biodegradability of chitosan, these LbL-assembled films could find use as implantable drug release systems. Hybrid LbL assemblies with mesoporous materials have also gained recent attention (Ariga et al., 2009). Some of these have been used for biological applications, including drug delivery and sensing (Wang et al., 2010). Cai and co-workers assembled LbL films of chitosan/gelatin pairs where mesoporous silica nanoparticles loaded with beta-estradiol are embedded for a nanoreservoir type drug delivery system onto titanium substrates (Hu et al., 2010). beta-Estradiol release is responsible for regulating the growth of

both osteoblasts and osteoclasts and, as such, the fabricated nanoreservoir structures displayed potential to maintain bone homeostasis.

Thus, similar hybrid systems may find wide applications in implant technology and regenerative medicine. Tao and co-workers fabricated mesoporous silica nanotubes coated with LbL films for pH-controlled drug release (Yang et al., 2010). The effect of pH on the interaction between polyelectrolyte multilayers as well as between hybrid composites and drug molecules alters the drug release process. The pH-responsive hybrid composites are potentially applicable for local drug delivery and cancer therapy.

Halloysite is an aluminosilicate inorganic clay widely used in hybrid systems. Halloysite microtubules have potential to encapsulate many types of material, including highly water-soluble and lipophilic materials, by exploiting either solvent replacement of bound water or chemical surface treatments. Delivery of the active reagents such as tetracycline HCl, khelline and nicotinamide adenine dinucleotide was successfully demonstrated. In their separate research, Lvov and co-workers demonstrated use of halloysite nanotubules for the entrapment, storage and subsequent release of three drugs: nifedipine (anti-anginal), furosemide (anti-hypertension and diuretic) and dexamethasone (synthetic corticosteroid) (Veerabadran et al., 2007).

## 1.7. Objectives

Layer-by-layer (LbL) assembly technique has gained increased potential in fabrication of various novel drug delivery carriers including layer-by-layer microcapsules (LbL-MC) and layer-by-layer thin films. Little is known about the influence of various physico-chemical properties of drugs on encapsulation and release in LbL-MC. We have selected molecules with different molecular charge, molecular weight, pKa and method of preparation and studied their influence on LbL-MC encapsulation. Delivery of therapeutic agents using layer-by-layer thin films is an attractive carrier system for topical application. There are few reports available for the combination or dual delivery of therapeutic agents. Towards this, we have selected two macromolecules including siRNA and EGF (epidermal growth factor) for loading in LbL thin films and performed in-vivo studies for their suitability for topical application.

The overall objective of the study is to develop LbL assembled polymeric carriers for the delivery of small and macro molecule therapeutics. The LbL technique was used for the preparation of layer-by-layer microcapsules (LbL-MC) and layer-by-layer thin films for systemic and topical drug delivery applications, respectively.

**Objective I.** Fabrication and characterization of LbL-MC for encapsulation of small model molecules.

Specific aims:

- (i) To study the influence of incubation time, pH, solute concentration and sodium chloride concentration on encapsulation of small molecules in LbL-MC.
- (ii) To study the influence of molecular charge of actives on encapsulation in LbL-MC.

- (iii) To study the cytotoxicity of anti-cancer drug imatinib loaded LbL-MC and blank LbL-MC.
- (iv) To study the biodistribution of imatinib loaded LbL-MC before and after PEGylation.

**Objective II.** Encapsulation of model protein bovine serum albumin (BSA) in LbL-MC.

Specific aims:

- (i) To study the encapsulation efficiency of bovine serum albumin in LbL-MC using co-precipitation and adsorption methods.
- (ii) To study the influence of pH on release of BSA from LbL-MC.
- (iii) To study the stability of BSA encapsulated in LbL-MC in the presence of proteases.

**Objective III.** Fabrication and characterization of LbL thin films to deliver model small molecule pirfenidone.

Specific aims:

- (i) To study the physical and mechanical properties of chitosan and sodium alginate LbL thin films.
- (ii) To study the antimicrobial activity and cyto-compatibility of LbL thin films.
- (iii) To study the effect of anti-fibrotic drug pirfenidone on excisional wound healing.



**Objective IV.** Co-delivery of epidermal growth factor (EGF) and TGF-beta siRNA using LbL thin films.

Specific aims:

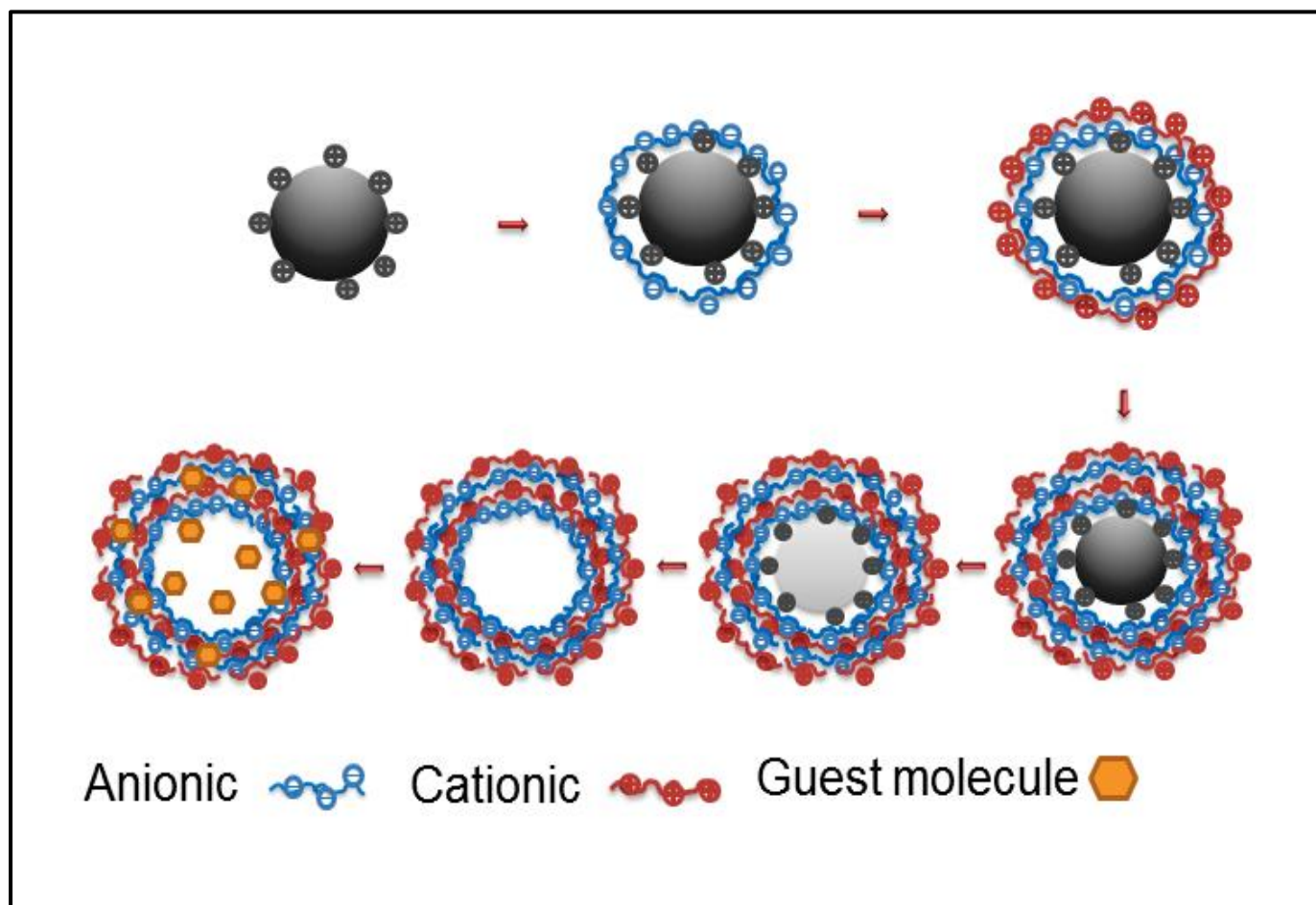
- (i) To entrap and characterize EGF and siRNA within LbL thin films.
- (ii) To study the effect of EGF and TGF-beta siRNA loaded LbL thin films on excisional wound healing.

# Chapter 2

## Layer-by-layer microcapsules for small molecule delivery

---

## Graphical Abstract



Schematic representation of preparation of layer-by-layer microcapsules for encapsulation of small molecules.

## 2.1. INTRODUCTION

Self-assembly of polymers is an important phenomenon used to prepare a better carrier system to deliver drug molecules (Kotz et al., 2001). Polyanions and polycations are used to prepare self-assembled nano- and microstructures for various applications (Kotz et al., 2001; Ariga et al., 2008). Self-assembly controlled through layer-by-layer (LbL) strategy has attracted from preparation of delivery systems to smart sensors (Loh et al., 2007; Hammond, 2011; Johnston et al., 2006; Yang et al., 2006). Since the initial reports from Decher and colleagues, there has been a tremendous increase in the number of publications reporting varied prospects of self-assembly through LbL strategy (Decher et al., 1992; Decher, 1997). Sequential adsorption of polyions on to a template with primarily electrostatic attractive interactions involves LbL self-assembly (Schonhoff, 2003). It was found that hydrogen bonds (Clark & Hammond, 2000; Fu et al., 2002; Kharlampieva et al., 2005), hydrophobic interactions (Kotov, 1999) and weaker van der Waal's interactions (Sato & Sano, 2005) are also possible between the polyelectrolytes. Adsorption on a planar template results in LbL assembled film (Decher et al., 1992; Kleinfeld & Ferguson, 1994) whereas a colloidal template results in nano- and microcapsule (Peyratout & Dahne, 2004; Tong et al., 2012). Upon adsorption of a desirable number of layers, core template is disintegrated to obtain core-shell capsular structure (Ibarz et al., 2002). Layer-by-layer assembly has been shown to have better control over the size, shell thickness, factors influencing the encapsulation of molecules, controlled release, stimuli responsive release and stability of encapsulated molecules (Peyratout & Dahne, 2004; Tong et al., 2012).

The advantages of LbL self-assembly have led to studies where drug molecules have been micronized and coated with polymers by LbL approach (Pargaonkar et al., 2005; De Villiers et al., 2011). Studies showed that controlled release is achieved depending upon the number of

layers of polymers (Ai et al., 2003). Alternatively, studies have been performed to encapsulate drug molecules into preformed LbL-MC. Influence of incubation time, temperature, solute concentration, salt concentration, number of polymer layers on encapsulation efficiency has been studied (Zhao et al., 2006). Primarily, the studies were performed on hydrophilic and lipophilic molecules. It has been shown that encapsulation efficiency increased with molecular concentration and in presence of NaCl (Zhao et al., 2006). However, it is important to understand the influence of molecular size, partition coefficient ( $\log P$ ), charge, hydrogen bonding on the entrapment of small molecules inside LbL-MC. Further, the release characteristics of entrapped molecules in correlation to the nature of molecular interactions with the polymeric shell in LbL-MC have to be studied.

The objective of this study is to understand the influence of various physical and chemical properties of small molecules on encapsulation and release in LbL-MC. Poly(ethylene imine) (PEI) and poly(styrene sulfonate) (PSS) were used to prepare LbL-MC. Six model molecules with varying molecular weight, charge, aqueous solubility, and dissociation constant have been studied (Table 2.1). Structure of molecules studied was shown in Fig. 2.1. Influence of LbL-MC on cell viability was studied in murine melanoma B16F10 cells. Further, biodistribution of a model molecule before and after encapsulation in LbL-MC was studied in BALB/c mice. As the LbL-MC is susceptible to clearance from reticulo-endothelial system, LbL-MC was PEGylated. Biodistribution of PEGylated LbL-MC was studied.

## 2.2. MATERIALS AND METHODS

Poly(styrene-4-sulphonic acid) (PSS, MW: 70kDa), branched polyethylene imine (PEI, MW: 25kDa), ethylene diamine tetra acetic acid (EDTA), rhodamine B base (RA), estradiol (ES), ascorbic acid (AA), imatinib mesylate (IM), indomethacin (IDM), 5-fluorouracil (5-FU), acetonitrile, methanol, dimethylsulfoxide (DMSO), chloroform, methoxy polyethylene glycol (mPEG; MW: 5000Da), 3-(4,5-dimethyl-2-thiazolyl)-2,5-diphenyl-2H-tetrazolium bromide (MTT) and components for buffer preparation were purchased from Sigma-Aldrich Chemical Company (Bengaluru, India). All the chemicals were used without further purification. Milli-Q (Millipore, USA) water was used for all the experiments.

### 2.2.1. Preparation of LbL-MC

LbL-MC was prepared on  $\text{CaCO}_3$  sacrificial template. In step one,  $\text{CaCO}_3$  microparticles were incubated with PSS (1mg/mL, pH 4, 0.5M NaCl) for 15 minutes followed by centrifugation and three washing cycles. In step two, PSS coated microparticles were incubated with PEI (1mg/mL, pH 9) for 15min followed by centrifugation and three washing cycles. The above two steps were repeated five more times to produce twelve alternative layers of PSS and PEI. Later,  $\text{CaCO}_3$  core was disintegrated by addition of sodium EDTA (0.2M) resulting in hollow microcapsules. Samples were lyophilized and stored for further studies.

### 2.2.2. Encapsulation of model molecules in LbL-MC

For drug encapsulation experiments, we have selected six model molecules, including anionic (AA and IDM), cationic (RA and IM) and neutral (5-FU and ES) molecules. Lyophilized LbL-MC (2mg) was dispersed in 1mL solution of respective molecule. Factors that affect the

encapsulation, including incubation time, solute concentration, pH and ionic strength were studied. To study the influence of solute concentration, a range of 0.5-5mg/mL concentration was used. To study the influence of loading time on encapsulation, LbL-MC was incubated in 1mg/mL or 0.5mg/mL (in case of RA) for 0.5-4h. To study the influence of pH, LbL-MC was incubated in 1mg/mL or 0.5mg/mL (in case of RA) with pH range of 2-10. To study the influence of salt concentration on encapsulation, LbL-MC was incubated in optimized solute concentration containing 0.1-0.5M NaCl. After being incubated in various conditions, the drug loaded LbL-MC was centrifuged (10000rpm, 10 minutes) and supernatant was collected for UV-Visible spectroscopic analysis at respective wavelengths. The encapsulation efficiency was calculated using Eq. (1).

$$\text{Encapsulation efficiency} = \frac{\text{mass of molecule in LbL-MC}}{\text{total mass of molecule}} \quad \text{--- (1)}$$

### 2.2.3. PEGylation of LbL-MC

Methoxy polyethylene glycol (mPEG) was activated to mPEG aldehyde by dissolving 1g of mPEG in 1:9 mixture of chloroform and dimethyl sulfoxide (DMSO). Acetic anhydride was added drop wise to above solution and incubated for 24h. Later, mPEG-CHO was added to 2.5g of PEI dissolved in deionized water. pH was adjusted to 9.0 with the addition of 0.2M NaOH. After two hours of stirring, 1mL of NaBH<sub>4</sub> aqueous solution was added. The reaction was performed for 24h. Then, free PEG was separated by dialysis (MWCO: 12kDa) for 24h (Petersen et al., 2002). The samples were freeze dried and characterized using <sup>1</sup>H NMR , FTIR and DSC. PEGylated LbL-MC (LbL-MC-PEG) was prepared similar to preparation of LbL-MC, except

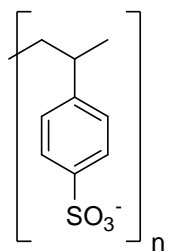
that twelfth layer was adsorbed with PEI-PEG copolymer. Later, IM was encapsulated into LbL-MC-PEG to perform biodistribution studies.

**Table 2.1.** Physico-chemical properties of polymers and model small molecules used in the present study.

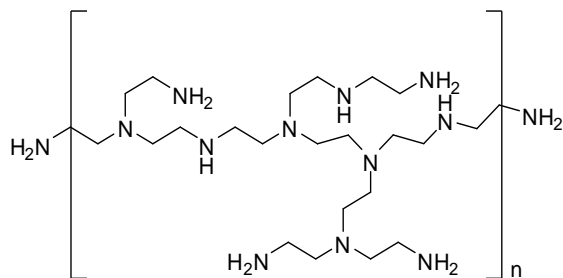
<b>Name</b>	<b>log P</b>	<b>pK<sub>a</sub></b>	<b>Molecular Weight (Da)</b>	<b>Charge</b>	<b>H-bond donors</b>	<b>H-bond acceptors</b>
<b>Poly (styrene-4-sulphonic acid)</b>	-	3.5	70000	Anionic	-	-
<b>Poly ethyleneimine</b>	-	9.7	25000	Cationic	-	-
<b>Ascorbic acid</b>	-1.85	4.10, 11.6	176.1	Anionic	3	5
<b>Indomethacin</b>	4.26	4.5	357.8	Anionic	0	2
<b>Imatinib mesylate</b>	3.69	1.52 - 8.07	589.7	Cationic	2	4
<b>Rhodamine b</b>	5.87	8.1	442.6	Cationic	0	1
<b>Estradiol</b>	4	10.7	272.4	Neutral	2	2
<b>5-Fluorouracil</b>	-0.89	8	130.1	Neutral	2	2

Log P values and hydrogen bond (H-bond) donors/acceptors were determined using Schrodinger molecular modeling software. Predicted log P values showed good correlation with reported values.

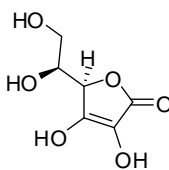




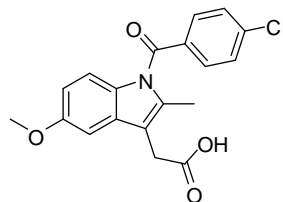
Poly(styrene-4-sulphonic acid)



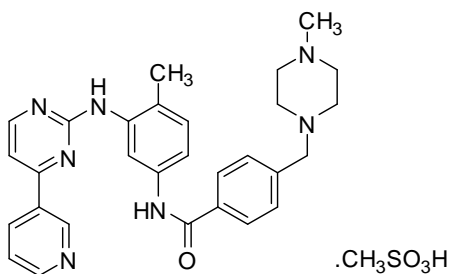
Polyethylenimine (branched)



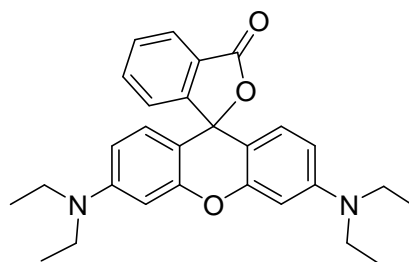
Ascorbic acid



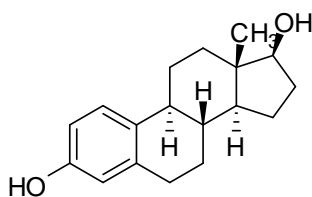
Indomethacin



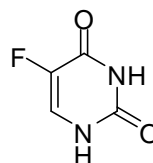
Imatinib mesylate



Rhodamine B base



Estradiol



5-Fluorouracil

**Fig. 2.1.** Structure of polymers and model small molecules used in the present study.

#### 2.2.4. Particle size and zeta-potential measurement

The particle size and surface morphology of CaCO<sub>3</sub>, LbL-MC was characterized using scanning electron microscope (Sirion-100, FEI, USA) operated at 3keV. Samples of CaCO<sub>3</sub> and LbL-MC were dried over copper plates and sputter coated with gold before analysis. Further light microscope was used to observe the LbL-MC suspended in an aqueous vehicle. Particle size from dynamic laser scattering and  $\zeta$ -potential after adsorption of each polymeric layer were determined by zetasizer (Nano ZS, Malvern, UK).  $\zeta$ -potential was measured from lyophilized samples redispersed in deionized water.

#### 2.2.5. Fourier transform Infrared (FTIR) spectroscopy

Sequential adsorption of polymers on to the CaCO<sub>3</sub> template was studied by FTIR spectroscopy (Jasco FTIR Spectrometer, USA). Spectra were recorded for lyophilized samples of free CaCO<sub>3</sub> particles and after adsorption of each polymeric layer. Further, FTIR was also used to characterize the encapsulation of model molecules in LbL-MC. In both the cases, samples (2mg) were mixed with potassium bromide at 1:1 ratio before analyses. Spectra were recorded within the range of 4000–400cm<sup>-1</sup> at a spectral resolution of 2cm<sup>-1</sup> in a dynamic reflectance sample holder.

#### 2.2.6. Differential Scanning Calorimetry (DSC)

Differential Scanning Calorimeter (DSC 60, Shimadzu, Japan) was used to study the thermal transitions of lyophilized CaCO<sub>3</sub> microparticles and LbL-MC. Further, DSC was also performed to study the encapsulation of model molecules inside LbL-MC. Sample of 2mg was

placed in aluminum pan and sealed with a lid using a press. Thermograms were recorded at a heating rate of 10°C per minute from ambient temperature up to 500°C.

#### 2.2.7. In-vitro release studies

In-vitro release of encapsulated model molecules was performed using dialysis membrane method. Samples (2mg) of free model molecules and LbL-MC encapsulated molecules were dispersed in 1mL PBS and dialyzed in regenerated cellulose membrane (Spectrum labs, USA) with molecular weight cutoff of 12kDa. Dialysis was performed against PBS at pH 7.4 and 37°C temperature in water bath. In case of ES and IDM samples, dialysis medium contained 0.5% tween 80 to maintain the concentration gradient for release. Samples of 1mL were withdrawn at predetermined time points, including 0.5, 1, 2, 4, 8, 12, 18, 24, 36, 48, 72, 96, 120, 180, 240h and were replaced with fresh PBS maintained at 37°C. Then, samples were analyzed using UV-Visible spectrophotometer (Jasco, USA) at 265, 320, 256, 553, 280 and 265nm wavelength for AA, IDM, IM, RA, ES and 5-FU respectively. Cumulative release of molecules was analyzed by fitting into release kinetic models and presented under the result's section.

#### 2.2.8. Cell viability studies

Cell viability in presence of LbL-MC was studied in B16F10 murine melanoma cells. Cells were grown in DMEM supplemented with 10% FBS, and 1% penicillin/streptomycin solution and incubated at 37°C and 5% CO<sub>2</sub>. Cells ( $5 \times 10^4$ ) were seeded in 96 well plates 24h before incubation with formulations. Cells were treated with LbL-MC-IM and free IM solution for 48h. Later, cell viability was determined using MTT assay with absorbance of DMSO

solubilized formazan measured at 595nm wavelength (Vector III, Perkin Elmer, USA). IM acts as tyrosine kinase inhibitor and is indicated for multiple types of cancers, including chronic myelogenous leukemia (CML). Therefore, IM encapsulated LbL-MC was used to perform the cell viability studies.

#### 2.2.9. In-vivo biodistribution studies

Animal experiments were performed after approval from the Institutional animal ethics committee (IAEC). Male BALB/c mice were purchased from local supplier and housed in clean room with 12h light/dark cycle with at-will food and water availability. After one week of acclimatization, 7-8 week-old mice were segregated randomly into four groups. Later, mice were administered with 200 $\mu$ L of formulation, including saline, LbL-MC, LbL-MC-IM and LbL-MC-PEG-IM through the tail vein. All the formulations were titrated to have IM dose of 12.5mg/kg body weight for administration. Mice were killed using excess ether anesthesia 1.5h after administration of formulation. Then, blood sample was collected in sodium citrate (3.8% w/v) at 9:1 ratio and organs of heart, liver, lung, kidney and spleen were harvested. Tissue samples were weighted and stored at -20°C for further analysis. To extract IM from blood samples, plasma was separated and equal volume of acetonitrile was added. For tissue samples, IM was extracted after homogenization in ice bath with addition of acetonitrile. Later, homogenized samples were centrifuged at 10000rpm and supernatant was collected. HPLC (Shimadzu, Japan) separation of the collected samples was performed by injecting 50 $\mu$ L into reverse phase C8 column with mobile phase containing methanol: water (60: 40v/v) and triethanolamine (1% v/v) at pH 10.5. Separation was performed at a flow rate of 1mL/minute where IM was analyzed at 254nm wavelength using UV detector (Bende et al., 2010).

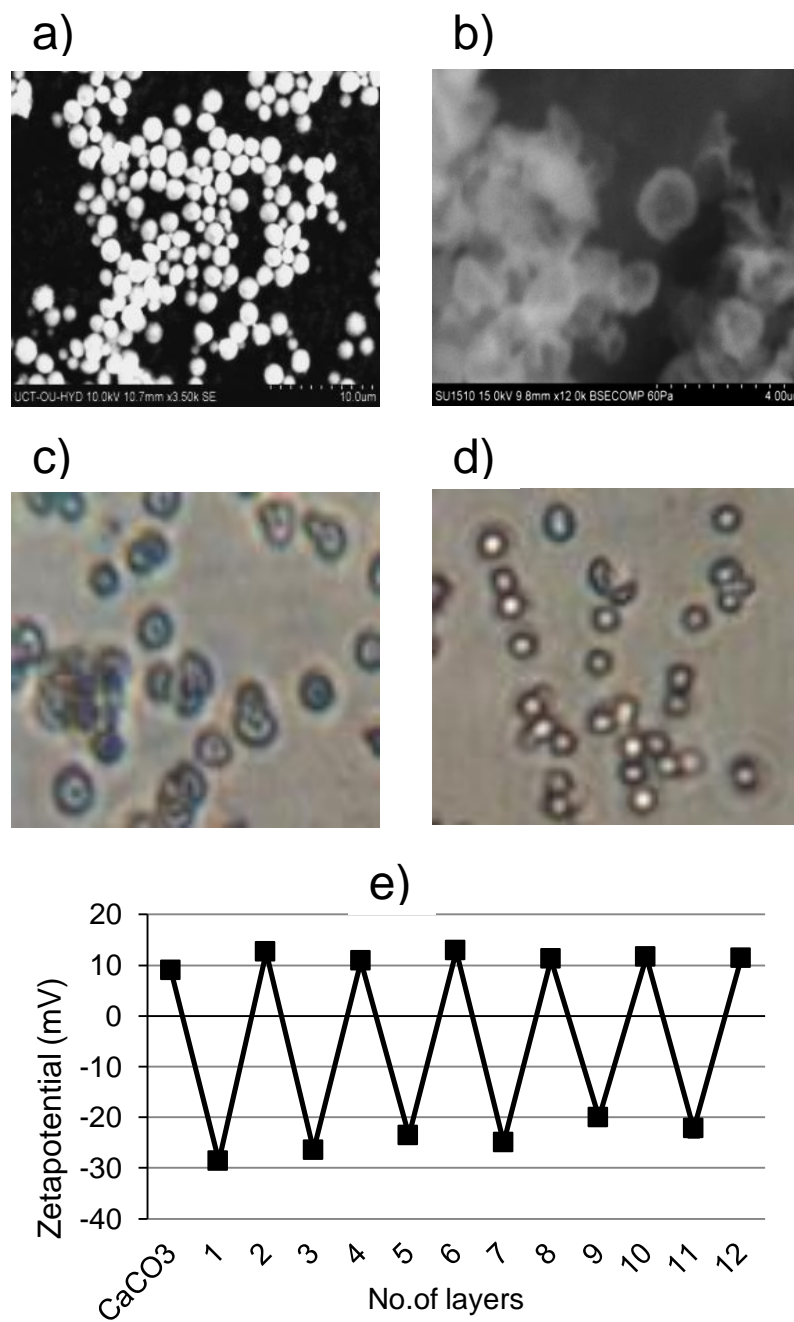
### 2.2.10. Statistical Analysis

All the results were presented as mean  $\pm$  standard deviation. Significance between groups was determined by Student's t-test (Graphpad Prism, USA) where  $P < 0.05$  was considered to be significant.

## 2.3. RESULTS

### 2.3.1. Formation of LbL-MC

Fig. 2.2 showed the morphological and size characterization of  $\text{CaCO}_3$  template particles and LbL-MC. SEM images showed that  $\text{CaCO}_3$  particles were spherical in shape (Fig. 2.2a); while LbL-MC was shown to be hollow and collapsed (Fig. 2.2b). Light microscope images showed LbL-MC before and after disintegration of core  $\text{CaCO}_3$  (Fig. 2.2c, 2.2d). The average particle size of LbL-MC with  $\text{CaCO}_3$  core was found to be  $2.8 \pm 0.3 \mu\text{m}$ . After disintegration of  $\text{CaCO}_3$  core using EDTA, particle size increased to  $3.0 \pm 0.4 \mu\text{m}$ . Fig. 2.2e showed  $\zeta$ -potential values for free  $\text{CaCO}_3$  and after sequential adsorption of charged polymer. It was found that free  $\text{CaCO}_3$  particles have positive charge at  $8.9 \pm 0.3 \text{mV}$ , which was decreased to  $-28.7 \pm 0.5 \text{mV}$  upon adsorption of anionic PSS. Further, adsorption of cationic PEI and anionic PSS increased and decreased the  $\zeta$ -potential sequentially. Zeta-potential of final LbL-MC with twelve layers was  $11.2 \pm 0.9 \text{mV}$ .



**Fig. 2.2.** Characterization of LbL-MC. Scanning electron micrographs of CaCO<sub>3</sub> (a) blank LbL-MC (b), light microscopic images of LbL-MC before (c) and after disintegration (d) of CaCO<sub>3</sub>. (e) represents  $\zeta$ -potential (mean  $\pm$  SD) obtained for CaCO<sub>3</sub> and sequential layers of polymers.

FTIR spectroscopic studies were performed to determine the interaction between the layered polymers. Fig. 2.3a showed the FTIR spectra for free CaCO<sub>3</sub>, PEI, PSS and after adsorption of successive layers. The characteristic peaks of free CaCO<sub>3</sub> at 1755cm<sup>-1</sup> and 2511cm<sup>-1</sup> are attributed to C=O stretch and carbonate (C-O) stretch respectively. The characteristic peaks for PSS at 1044cm<sup>-1</sup> and 1192cm<sup>-1</sup> are attributed to S=O symmetric and asymmetric stretch respectively. Similarly, for PEI, the characteristic peaks were found at 1296cm<sup>-1</sup> for C-N stretch, 1593cm<sup>-1</sup> and 1662cm<sup>-1</sup> for N-H bending and 3544cm<sup>-1</sup> for N-H stretch. It was found from FTIR spectroscopic studies that PSS and PEI adsorbed on to CaCO<sub>3</sub> template as showed by a shift in characteristic peaks (Fig. 2.3a). After disintegration of CaCO<sub>3</sub> core, C=O stretch and C-O stretch were not observed.

Further, DSC studies were performed to understand the thermal transitions of microcapsules upon adsorption of charged polymers. Results from DSC studies showed characteristic glass transition (T<sub>g</sub>) at 72.8°C, melting endotherm (T<sub>m</sub>) at 206.8°C and decomposition at 465°C for PSS (Fig. 2.4a). For PEI, the melting endotherm (T<sub>m</sub>) was observed at 81.6°C. Free CaCO<sub>3</sub> did not show any endotherm up to 500°C (Fig. 2.4a). DSC studies for LbL-MC showed that T<sub>g</sub> for PSS and T<sub>m</sub> for PEI shifted to 86.3°C. Similarly, Fig. 2.4a also showed that T<sub>m</sub> and decomposition temperature of PSS were shifted to 222.5°C and 463.2°C respectively.

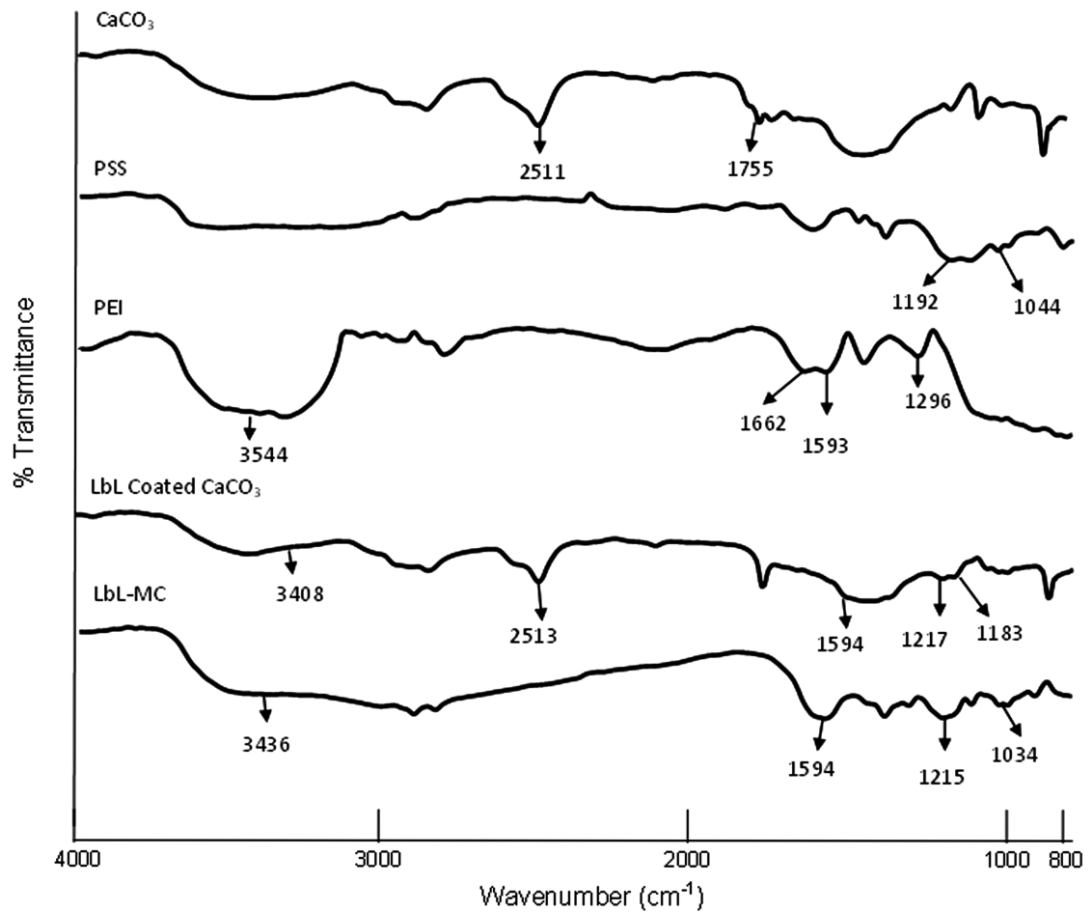
### 2.3.2. Encapsulation of model molecules in LbL-MC

Encapsulation of model molecules into LbL-MC was studied using FTIR spectroscopy and DSC thermograms. Fig. 2.3b showed FTIR spectra of free molecules and after encapsulation in LbL-MC. The characteristic peaks of AA (1313cm<sup>-1</sup> C-H stretch, 1653cm<sup>-1</sup> C=C stretch, 1753cm<sup>-1</sup>

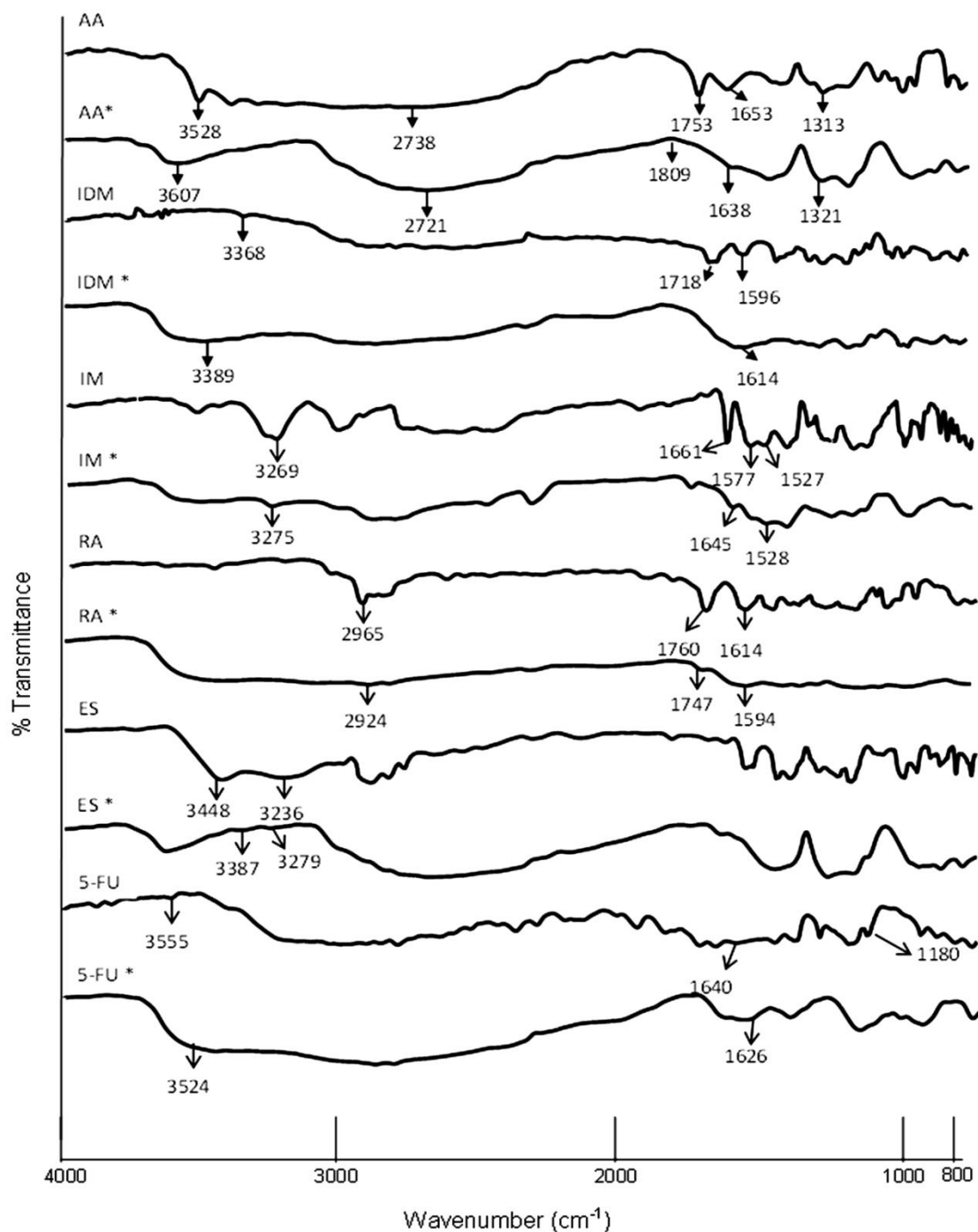
C=O stretch and  $3528\text{cm}^{-1}$ ,  $2738\text{cm}^{-1}$  O-H stretch); IDM ( $1596\text{cm}^{-1}$  C=N stretch,  $1718\text{cm}^{-1}$  C=O stretch and  $3368\text{cm}^{-1}$  O-H stretch); IM ( $1527\text{cm}^{-1}$ ,  $1577\text{cm}^{-1}$  C=C stretch,  $1661\text{cm}^{-1}$  C=O stretch and  $3269\text{cm}^{-1}$  N-H stretch); RA ( $1614\text{cm}^{-1}$  C=N stretch,  $1760\text{cm}^{-1}$  C=O stretch and  $2965\text{cm}^{-1}$  O-H stretch); ES ( $3236\text{cm}^{-1}$  and  $3448\text{cm}^{-1}$  O-H stretch); and 5-FU ( $1180\text{cm}^{-1}$  C-O stretch,  $1640\text{cm}^{-1}$  N-H bending and  $3555\text{cm}^{-1}$  N-H stretch) were found. After encapsulation into LbL-MC, respective peaks were observed along with spectral peaks of charged polymers (Fig. 2.3b). Results from DSC thermograms showed a  $T_m$  for the model molecules studied (Fig. 2.4b). These studies qualitatively confirmed the encapsulation of model molecules in LbL-MC.

Quantitative characterization through encapsulation efficiency (EE) of molecule into LbL-MC was determined by UV-Visible spectroscopy. Table 2.2 showed the factors optimized to study the EE of model molecules into LbL-MC. Fig. 2.5a showed the optimization of incubation time on encapsulation of molecules. EE increased initially with the increase in incubation time from 1–2h and remained same for a further increase in incubation time up to 4h. Incubation time of 1h was found to be desirable for molecules, including RA, ES and 5-FU and 2h was optimal for IDM, AA and IM samples (Table 2.2). Further studies to optimize solute concentration on EE were performed at respective equilibrium incubation time. Fig. 2.5b showed EE of model molecules into LbL-MC at different concentrations. All the molecules showed a linear increase in EE with concentration. The correlation coefficient for regression analysis was found to be between 0.89-0.99 for all the molecules (Fig. 2.5b). For further studies, 1mg/mL concentration was selected as optimal concentration for all the molecules except for RA. As 1mg/mL concentration of RA is not stable 0.5mg/mL was studied (Table 2.2).

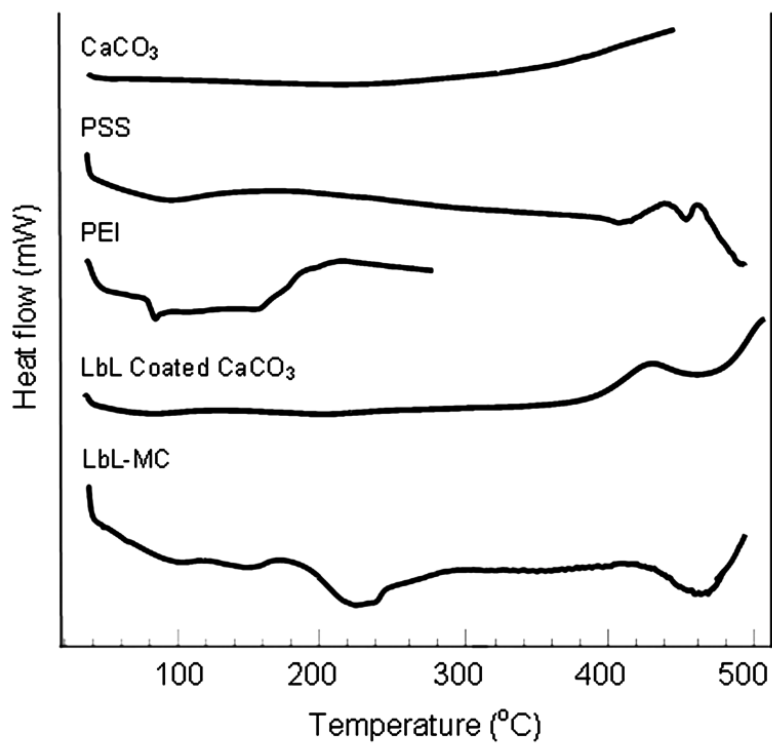




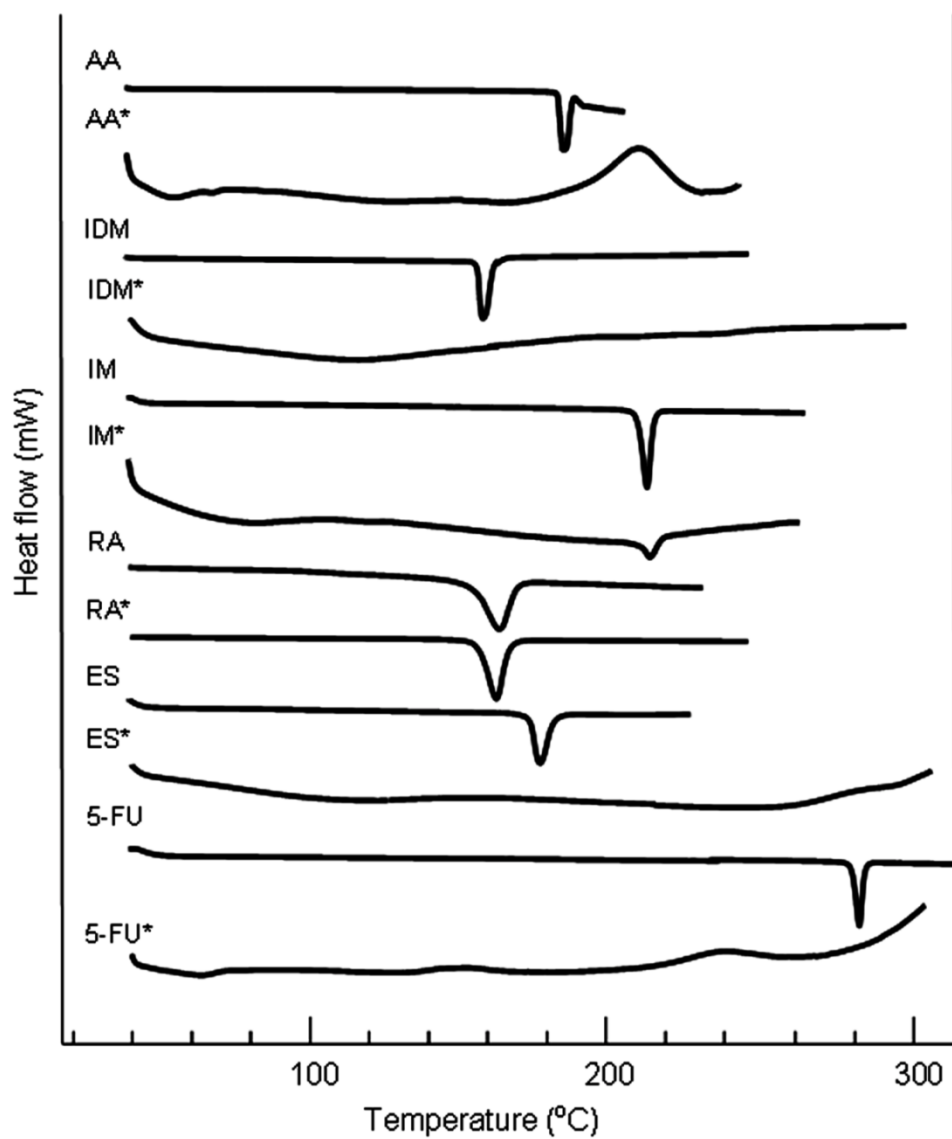
**Fig. 2.3a.** Characterization of LbL-MC. FTIR spectra of CaCO<sub>3</sub>, PSS, PEI, LbL coated CaCO<sub>3</sub> and LbL-MC.



**Fig. 2.3b.** Characterization of LbL-MC. FTIR spectra of free and LbL-MC encapsulated model molecule. Characteristic peaks for respective molecules were denoted on the spectra. \* indicates molecule encapsulated in LbL-MC.



**Fig. 2.4a.** DSC thermograms of CaCO<sub>3</sub>, PSS, PEI, LbL coated CaCO<sub>3</sub> and LbL-MC.



**Fig. 2.4b.** DSC thermograms of free and LbL-MC encapsulated model molecule. \*indicates molecule encapsulated in LbL-MC.

Later, influence of pH on the EE of molecules was analyzed varying the pH from 2-10. Results from pH optimization were shown in Fig. 2.5c. It was found that for acidic molecules of AA and IDM, the increase in pH from 2 to 6 increased the EE from  $5.2 \pm 1.3$  and  $0.5 \pm 0.4$  to  $25.0 \pm 0.7$  and  $2.5 \pm 1.1$  respectively. Additionally, increase in pH up to 10 did not further increase in EE (Fig. 2.5c). In case of basic molecules of IM and RA, increase in pH from 2 to 6 increased EE from  $22.8 \pm 3.1$  and  $10.1 \pm 1.9$  to  $58.4 \pm 4.5$  and  $30.4 \pm 3.6$  respectively. Similar to acidic molecules, RA also did not show any further increase in EE with the increase in pH from 6 to 8. EE of IM at pH 8 and 10 was not studied as it was not soluble in those pH conditions. Similarly, Fig. 2.5c also showed that increase in pH from 2 to 8 increased the EE of neutral molecules of ES and 5-FU from  $2.0 \pm 0.2$  and  $1.6 \pm 0.1$  to  $6.7 \pm 0.1$  and  $2.9 \pm 0.6$  respectively. pH of 6 was further used to study the influence of salt concentration on EE.

Effect of salt concentration was studied for AA, 5-FU and RA. IM precipitated out with the addition of NaCl. Ethanol: water (80: 20) was used as solvent for IDM and ES in which NaCl was not soluble. Fig. 2.5d showed that AA and 5-FU increased EE with the increase in NaCl concentration compared to the absence of NaCl. RA did not showed any difference before and after addition of NaCl. Overall, the greatest encapsulation found for AA, IDM, IM, RA, ES and 5-FU was  $50.4 \pm 1.9$ ,  $10.9 \pm 1.9$ ,  $73.8 \pm 2.0$ ,  $56.4 \pm 0.8$ ,  $5.9 \pm 0.2$  and  $3.3 \pm 1.2$  respectively (Fig. 2.5).

### 2.3.3. In-vitro release of model molecules from LbL-MC

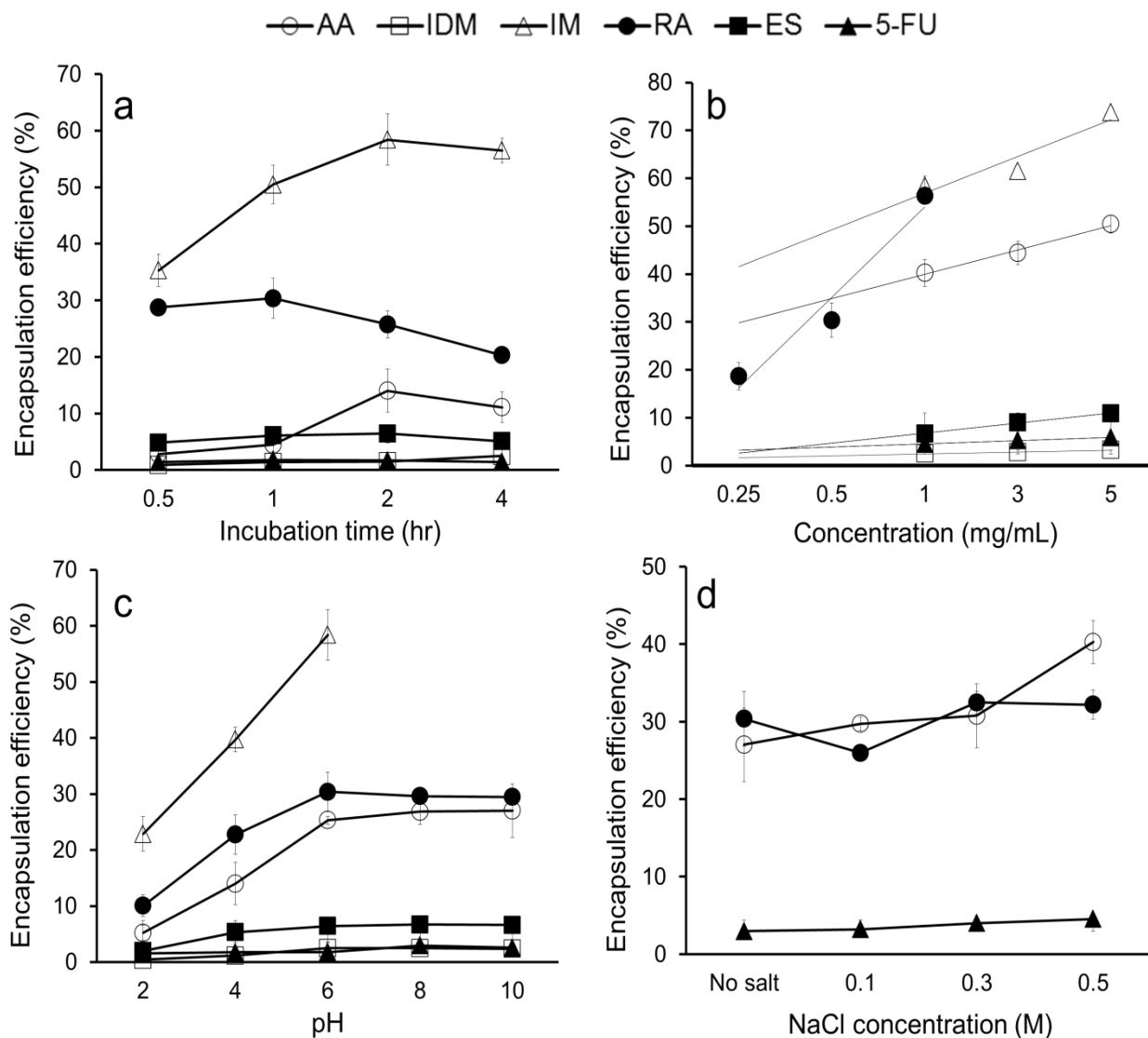
Results from in-vitro release studies were shown in Fig. 2.6. Cumulative release of molecules from LbL-MC was compared to diffusion of the free molecule through dialysis membrane. All the model molecules studied freely diffused through the dialysis membrane, and 100% release was achieved with in 4h (Fig. 2.6a). Molecules encapsulated in LbL-MC released

slowly compared to free molecules. It was found that IDM, ES and 5-FU encapsulated in LbL-MC showed 100% cumulative release in 2h, 4h and 2h respectively. For AA, IM and RA 100% cumulative release were achieved in 120h, 240h and 144h respectively (Fig. 2.6b).

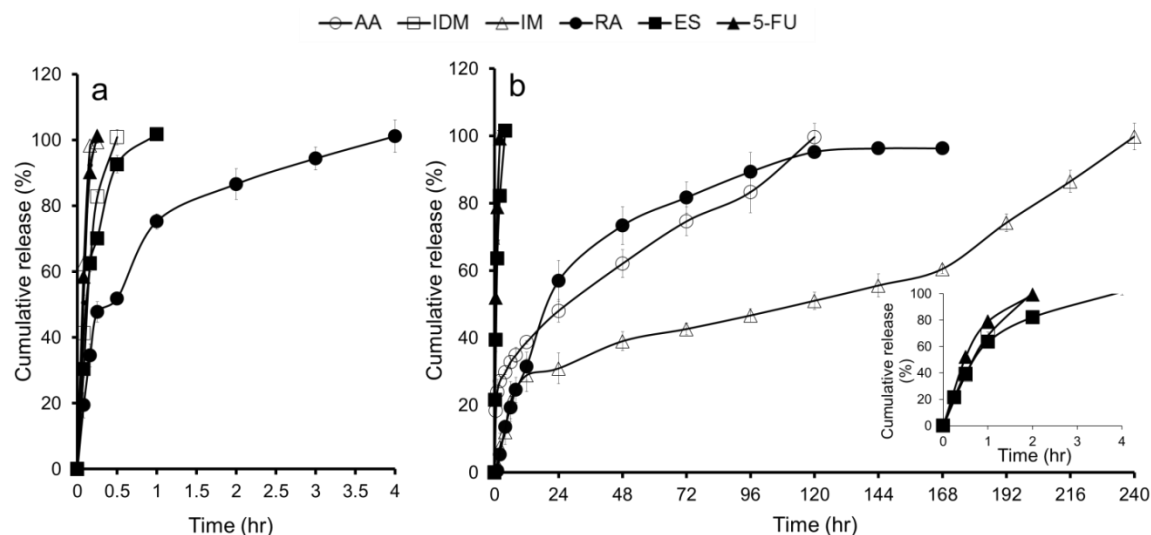
**Table 2.2.** Optimized parameters for entrapment of molecules in LbL-MC.

<b>Model molecule</b>	<b>Incubation time (h)</b>	<b>Molecular concentration (mg/mL)</b>	<b>pH</b>	<b>NaCl concentration (M)</b>
<b>Ascorbic acid</b>	2	1	6	0.5
<b>Indomethacin</b>	2	1	6	NA
<b>Imatinib mesylate</b>	2	1	6	NA
<b>Rhodamine b</b>	1	0.5	6	0.3
<b>Estradiol</b>	1	1	8	NA
<b>5-Fluorouracil</b>	1	1	6	0.5

NA: not analyzed.



**Fig. 2.5.** Factors influencing encapsulation of molecules into LbL-MC. Encapsulation efficiency as a function of incubation time (a); molecular concentration (b); pH (c); NaCl concentration (d). The correlation coefficient from regression analysis for concentration vs. encapsulation efficiency of molecules was, AA: 0.989; IDM: 0.968; IM: 0.894; RA: 0.954; ES: 0.997; 5-FU: 0.997. Data was represented as mean ( $n=3$ )  $\pm$  SD.



**Fig. 2.6.** In-vitro cumulative release profiles of (a) neat solutions and (b) molecules encapsulated in LbL-MC. Release studies were performed in PBS (pH 7.4) at 37°C. Inset in (b) represents cumulative release up to 4h for IDM, ES and 5-FU. Data was presented as mean (n=3)  $\pm$  SD.

**Table 2.3.** Correlation coefficients from regression analysis after model fitting of the release profiles for model molecules.

Model molecule	Zero order	First order	Baker-Lonsdale	Korsmeyer-Peppas	n-value*
AA	0.866	0.973	0.994	0.974	0.274
IDM	0.955	0.992	0.978	0.988	0.695
IM	0.930	0.563	0.691	0.928	0.569
RA	0.917	0.958	0.986	0.987	0.299
ES	0.819	0.992	0.993	0.949	0.549
5-FU	0.859	0.998	0.980	0.973	0.467

\*‘n’ is the diffusional exponent from Korsmeyer-Peppas model fitting as reported in results section.



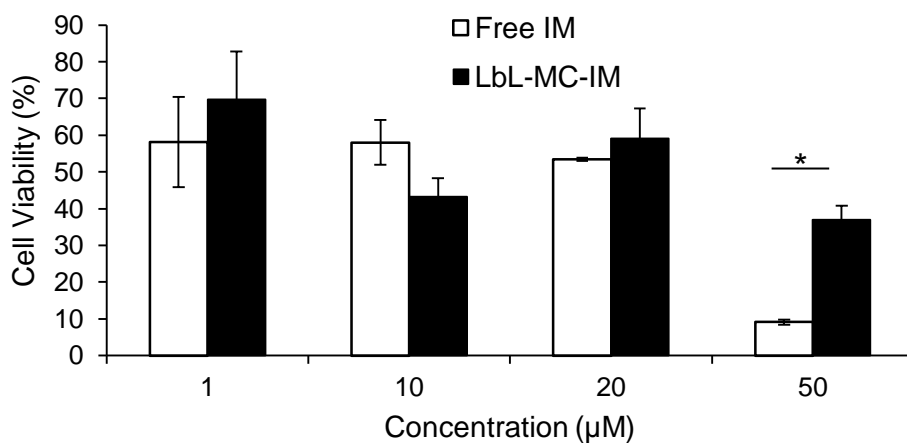
**Table 2.4.** Physical constants from Freundlich adsorption isotherm.

Model molecule	n	K (mL/mg)	Correlation coefficient
Ascorbic acid	0.883	0.199	0.998
Indomethacin	0.864	0.012	0.997
Imatinib mesylate	0.886	0.286	0.995
Rhodamine b	0.557	0.276	0.999
Estradiol	0.772	0.033	0.999
5-Fluorouracil	0.865	0.023	0.999

Values were calculated from amount of solute loaded after incubation at different concentrations and using the Eq. (6) provided in the discussion section.

#### 2.3.4. Cell viability in the presence of LbL-MC

Fig. 2.7 showed the percentage cell viability as determined by MTT assay after 48h incubation with different concentrations of IM. It was found that free IM showed decreased cell viability with the increase in concentration from 1 $\mu$ M to 50 $\mu$ M. IM encapsulated LbL-MC also showed a similar decrease with the increase in concentration from 1 $\mu$ M to 50 $\mu$ M. However, at 50 $\mu$ M concentration free IM significantly ( $P < 0.05$ ) decreased cell viability to  $9.1 \pm 0.8\%$  compared with  $36.9 \pm 3.9\%$  after LbL-MC-IM treatment.

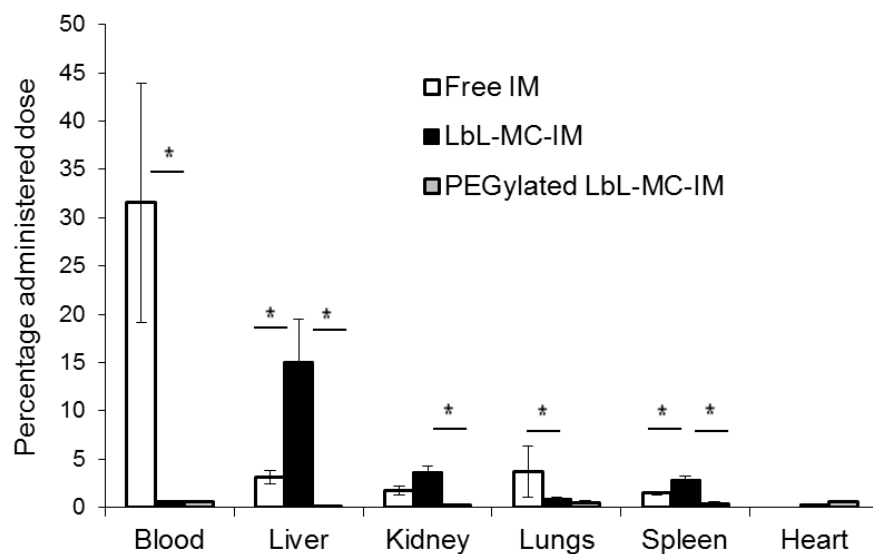


**Fig. 2.7.** B16F10 cell viability after incubation with free IM and IM encapsulated LbL-MC.

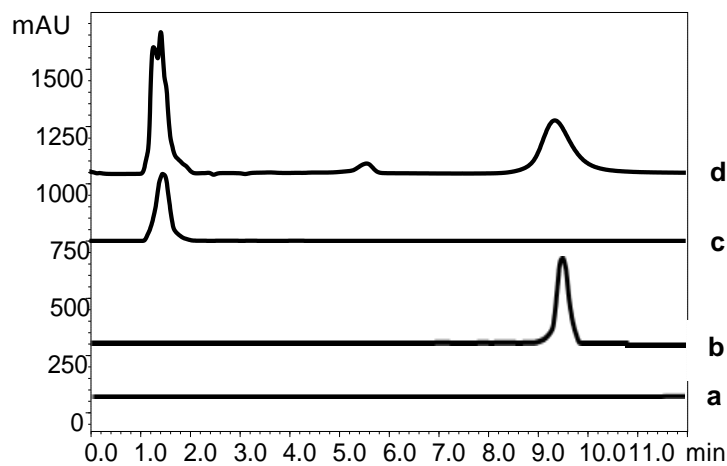
### 2.3.5. Biodistribution of LbL-MC

Fig. 2.8 showed the in-vivo biodistribution of different formulations in male BALB/c mice. In control mice, saline administration did not show any peak at retention time of 9.5 minutes (Fig. 2.9). Free IM solution showed 29% of administered dose in the blood sample while, liver, lungs and spleen showed 2.9%, 3.4% and 1.3% respectively of administered dose. In contrast, IM was found to distribute significantly ( $P < 0.05$ ) more into liver (13.8%) and spleen (2.6%) after administration with LbL-MC (Fig. 2.8). LbL-MC decreased the blood distribution of IM to 0.6% of administered dose.

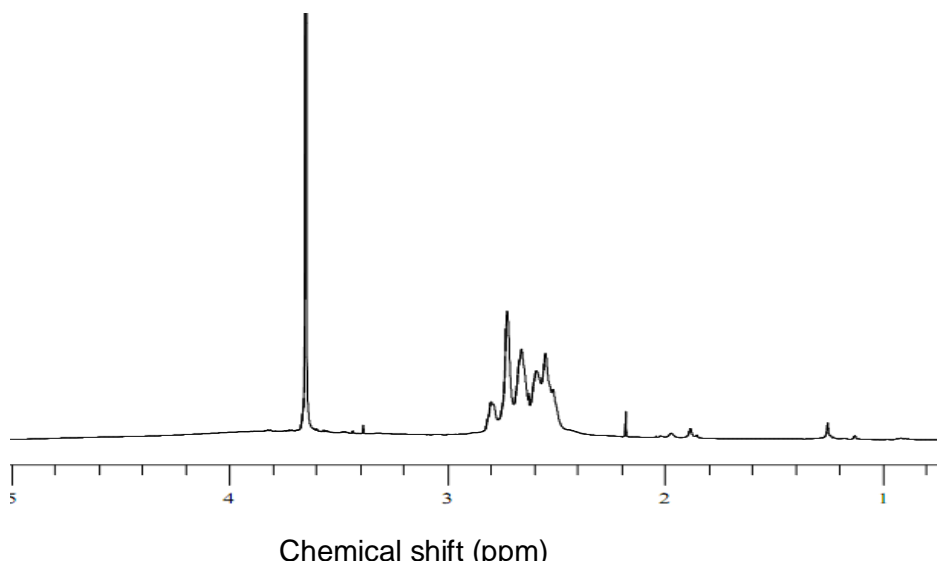
PEGylation of LbL-MC was performed to overcome the uptake by liver and spleen. PEGylated PEI characterized by NMR showed a peak at 3.6ppm associated with PEG (-CH<sub>2</sub>-CH<sub>2</sub>-O-) and a peak at 2.6ppm associated with PEI (-CH<sub>2</sub>-CH<sub>2</sub>-NH<sub>2</sub>-) (Fig. 2.10). PEGylated LbL-MC decreased the  $\zeta$ -potential to  $4.4 \pm 0.2$  mV and did not alter the size. The characterization of PEGylated LbL-MC by DSC and FTIR were shown in Fig. 2.11 and 2.12. It was found that IM from PEGylated LbL-MC decreased the liver and spleen accumulation to 0.03% and 0.3% of administered dose respectively (Fig. 2.8). However, the overall recovery of IM was less after administration with PEGylated LbL-MC because of reduced release of IM.



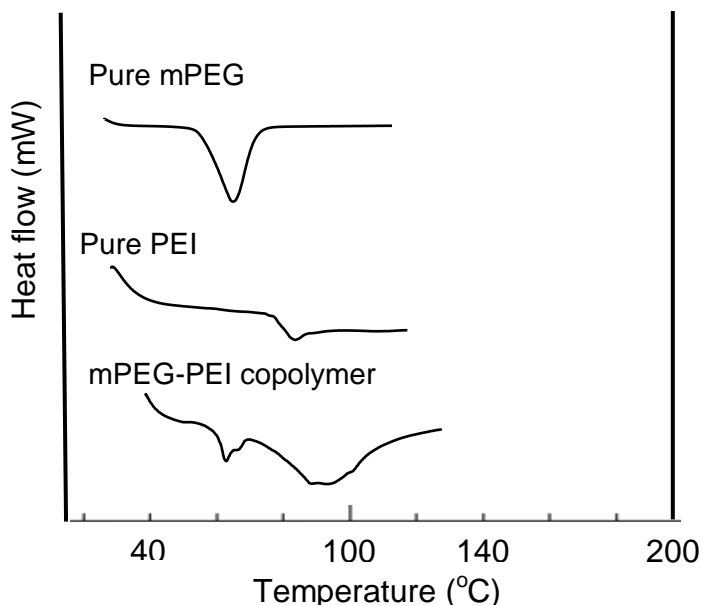
**Fig. 2.8.** Biodistribution of free IM, IM encapsulated LbL-MC and IM encapsulated in PEGylated LbL-MC after intravenous administration in BALB/c mice. Data was presented as mean (n=4)  $\pm$  SD. \* represents significance between groups at P<0.05.



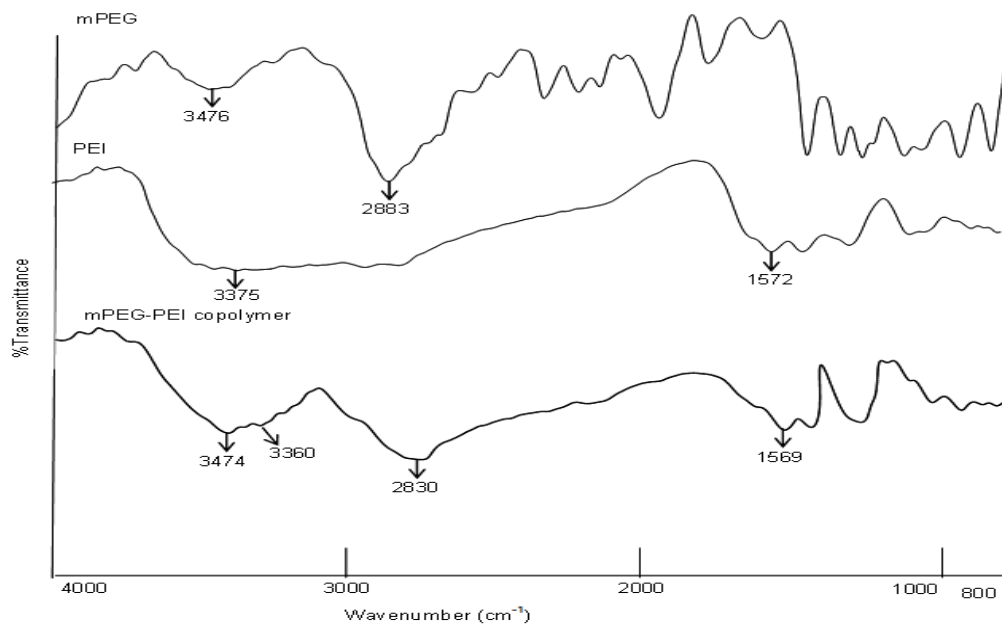
**Fig. 2.9.** Representative HPLC chromatograms of deionized water (a), IM in deionized water (b), mouse plasma sample (c), IM in mouse plasma sample (d). IM was analysed by UV-detector at 285nm.



**Fig. 2.10.**  $^1\text{H}$  NMR spectrum of mPEG-PEI copolymer.  $^1\text{H}$ -NMR (Bruker 400MHz, USA) spectroscopy was performed for PEI (25kDa), PEG (5kDa) and PEGylated-PEI to elucidate the synthesis of mPEG-PEI copolymer. The peak at 3.6ppm is associated with PEG ( $-\text{CH}_2-\text{CH}_2-\text{O}-$ ) and peak at 2.6ppm is associated with PEI ( $-\text{CH}_2-\text{CH}_2-\text{NH}_2-$ )



**Fig. 2.11.** DSC thermograms of mPEG, PEI and mPEG-PEI copolymer. Samples (2mg) were heated at  $10^\circ\text{C}/\text{min}$ . DSC results showed characteristic melting endotherms of mPEG and PEI at  $63^\circ\text{C}$  and  $81.6^\circ\text{C}$  respectively. In mPEG-PEI copolymer the melting peaks of both PEG and PEI were observed at  $61.2$  and  $81.58$  respectively.



**Fig. 2.12.** FTIR spectra of mPEG, PEI and mPEG-PEI copolymer. Neat mPEG showed characteristic peaks at  $3476\text{cm}^{-1}$  and  $2883\text{cm}^{-1}$  corresponds to stretches of O-H and C-H. Similarly, for PEI characteristic peaks were found to be at  $3375\text{cm}^{-1}$  and  $1572\text{cm}^{-1}$  corresponding to N-H and C-N stretch respectively. The characteristic peaks of PEI at  $3360\text{cm}^{-1}$ ,  $1569\text{cm}^{-1}$  and mPEG at  $3474\text{cm}^{-1}$ ,  $2830\text{cm}^{-1}$  were found in mPEG-PEI copolymer.

## 2.4. DISCUSSION

Molecular interactions among the polymers in LbL-MC reduce the polarity with regions of hydrophobicity resulting in their decreased solubility (Smith et al., 2009). As charge density is an important factor for electrostatic interactions and formation of LbL-MC, pH and  $pK_a$  of polymer needed to be optimized (Krasemann & Tieke, 2000; Mak et al., 2008). In the present study, pH of the polymeric solution was maintained at  $pK_a$  of respective polymers resulting in fifty percent ionization. Further as the polymers used in the study, PEI ( $pK_a$  9) and PSS ( $pK_a$  3.5) are strong electrolytes charged at a wide range of pH, LbL-MC formed were stable (Mak et al., 2008). Results from  $\zeta$ -potential, FTIR and DSC studies have confirmed the sequential adsorption of

polyelectrolyte layers. These were in correlation to studies performed with similar polymers and other charged polymers (Mak et al., 2008).

LbL-MC has been studied for encapsulation efficiency (EE) of small model molecules, including 5-FU (Yan et al., 2011), perylene (Manna & Patil, 2009), curcumin (Manju & Sreenivasan, 2011), ciprofloxacin hydrochloride (Mao et al., 2005), doxorubicin (Tao et al., 2007; Liu et al., 2010) and daunorubicin (Han et al., 2008). Further, fluorescent dyes including rhodamine (Manna & Patil, 2009; Liu et al., 2005) and fluorescein (Ibarz et al., 2002) have also been studied for their encapsulation in LbL-MC. The present study chose different molecules based on their varied physical and chemical properties with an intention to understand the nature of interactions which are important to their encapsulation. In general, the spatial location of a small molecule within LbL-MC could be trapped within the lumen of capsule core and/or adsorbed to polymeric layers of capsule shell (Manna & Patil, 2009; Liu et al., 2005). The diffusion of a molecule through the nano-pores of shell into the core of the capsule depends on concentration gradient, molecular size and partition coefficient. Therefore, increase in solute concentration resulted in greater encapsulation. Studies from nuclear magnetic resonance spectroscopy (NMR) showed that LbL-MC of PSS/PAH polyelectrolytes bear nano-sized pores ranging from 0.6 – 1nm (Chávez and Schönhoff, 2007). In contrast to other reports, it was found that number of layers would not significantly alter the pore size distribution (Chávez and Schönhoff, 2007). LbL-MC was reported showing permselectivity based on the molecular size of solute for encapsulation (Gleb et al., 1999). In the present investigation, the range of molecular weight for molecules studied was 130-590Da. No correlation was observed between molecular size and EE. A plausible reason is that small molecule permeated into the aqueous core of LbL-MC and adsorbed to polymeric shell of LbL-MC, both considered to be

encapsulated. Further, as the polymeric shell of LbL-MC is considered to be less polar, molecule solubilized in the incubation medium has to partition across the shell into the core. The reported log P values showed in Table 2.1 suggested that molecules with greater log P value presented in an aqueous medium would partition well. On the other hand, IDM and ES with poor aqueous solubility were presented in ethanol: water (80: 20) as a vehicle. Therefore, IDM and ES showed less EE.

Alternatively, factors influencing the adsorption of small molecules in a polymeric shell of LbL-MC are i) charge, dependent on  $pK_a$  and pH; ii) affinity, dependent on nature of molecular interactions between small molecule and LbL-MC, including electrostatic interactions, hydrophobic interactions and hydrogen bonds. The outer layer in our LbL-MC was PEI resulting in positive surface charge with  $\zeta$ -potential of 11mV. It is expected that PEI is positively charged in acidic pH, and show reduced charge density in neutral and basic pH (Mak et al., 2008). Acidic molecules, AA and IDM have  $pK_a$  values of 4.1 and 11.6, and 4.5 respectively, where the hydroxyl group at C3 position of AA and carboxyl group of IDM dissociate. Therefore, increase in pH from 2-6 increased the dissociation for greater attractive electrostatic interaction with PEI in LbL-MC. However, further increase in pH from 6-10 did not increase the EE. Increase in pH results in deprotonation of amine in PEI leading to decreased charge density. Further, at higher pH conditions, AA was reported undergoing dehydrogenation at C2 and C3 positions to form L-dehydroascorbic acid (Gallarate et al., 1999). On the other hand, stability of AA was found to be increased in presence of counter ions (Gallarate et al., 1999). In the present study, encapsulation of AA increased by 25% in presence of 0.5M NaCl compared to EE in no salt medium.

Charged molecules, including IM showed greater EE in LbL-MC through electrostatic interactions (Cingolani et al., 2010). EE did not depend on the nature of charge of molecule.

However, indomethacin which is anionic with  $pK_a$  of 4.26 showed poor EE. Apart from electrostatic attractive interactions, hydrogen bonding and hydrophobic interactions were reported being important. In the present study, molecules with fewer numbers of hydrogen bond donors and acceptors, including IDM, 5-FU and ES showed poor EE. On the other hand, RA with only one hydrogen bond acceptor showed greater encapsulation. RA was found to show hydrophobic interaction with PSS through  $\pi$ - $\pi$  interactions associated with carbon ring structures (Moreno-Villoslada et al., 2006). To validate the adsorption of molecules to polymers in LbL-MC, Freundlich adsorption coefficients were calculated. It is assumed that LbL-MC surface is heterogeneous with varied adsorption efficiencies. Freundlich adsorption isotherms can be described from Eq. (6),

$$Q=KC^{1/n} \quad \text{--- (6)}$$

Where, “C” is the equilibrium concentration of solute, “Q” is the mass of solute adsorbed per unit weight of adsorbent (LbL-MC), “K” and “1/n” are physical constants, which represent adsorption capacity and adsorption intensity. In other words, “K” represents the force of adsorption and the value of “n” would range between 0-1 (Krishna and Bhattacharyya, 2005). Table 2.4 showed the adsorption constants for respective molecules. All the molecules showed a good fit with Freundlich adsorption equation. In addition, “n” value was found between 0.5-1 suggesting positive adsorption between the molecules and LbL-MC. The model molecules which showed greater EE, IM, RA and AA had “K” values over an order of magnitude more compared to 5-FU, ES and IDM.

Though the present studies did not delineate the mass of the molecule present in the luminal core and/or adsorbed on the polymeric shell, release profiles of molecules provide useful information. A molecule smaller than the pores in shell and present in the luminal core of LbL-



MC can freely diffuse out (Liu and Bruening, 2004). Alternatively, molecules adsorbed to polymeric shell through various molecular interactions show controlled release profile (Pargaonkar et al., 2005). For example, AA showed an initial burst release with 18% of the encapsulated molecule released within 30 minutes. This was followed by diffusion controlled release modeled by Baker-Lonsdale. Other molecules with lesser molecular weight (<300Da), 5-FU and ES also showed a uniform cumulative release with diffusion as rate limiting step. Similar results were shown for 5-FU release from LbL-MC made of poly-L-glycolic acid – chitosan characterized by Baker-Lonsdale model (Yan et al., 2011). In case of molecules with greater molecular weight (>300Da) and multiple possibilities of molecular interactions, IM and RA showed distinct stages in cumulative release profiles. Model fitting of release profiles showed a non-diffusional controlled release for these molecules. Zero-order release was achieved where swelling followed by dissolution or erosion of superficial layers could be possible. Similar bimodal release profile was previously shown for doxorubicin and daunorubicin from PAH/PSS LbL-MC (Zhao et al., 2006). Initial 180 minutes showed diffusion controlled release of molecules followed by much slower non-diffusional release kinetics (Zhao et al., 2006). Further, controlled release of rhodamine from PSS-PAH and SDS micelle-chitosan pair LbL-MC was attributed to ionic interactions (Manna & Patil, 2009). When two charged molecules of rhodamine and daunorubicin were compared, release was slower for rhodamine attributed to additional hydrophobic interactions (Liu et al., 2005). However further studies are required to confirm the mechanism for non-diffusional release kinetics.

In-vitro cell culture studies provide the influence of LbL-MC on the cell viability in presence of a model molecule. IM encapsulated LbL-MC was used to perform the cell viability studies in murine melanoma B16F10 cells because of anti-cancer activity of IM (Jiang et al.,

2008). While, both free IM and LbL-MC-IM showed concentration dependent decrease in cell viability, free IM was found to be more potent. This could be because of slow release of IM from LbL-MC and binding to serum proteins. As PEI is known for cytotoxicity, free PEI dissociated from LbL-MC could show cytotoxicity. Further studies are required to understand dissociation of polymers in LbL-MC.

It is important to understand the in-vivo behavior of delivery systems (Morton et al., 2013). Carrier systems with more than one micrometer size are known to be taken up by reticulo-endothelial system. Therefore, LbL-MC particles held an advantage of targeting liver and spleen (Morton et al., 2013). However for controlled release of an encapsulated molecule, it is required to escape the reticulo-endothelial system and prolong the blood circulation time. PEGylation of LbL-MC provided advantages of escaping the reticulo-endothelial system. Further studies are required to study the pharmacokinetics of LbL-MC encapsulated molecules. Overall, the present studies support the ability of LbL-MC to deliver small molecules for in-vitro and in-vivo applications.

## **2.5. CONCLUSION**

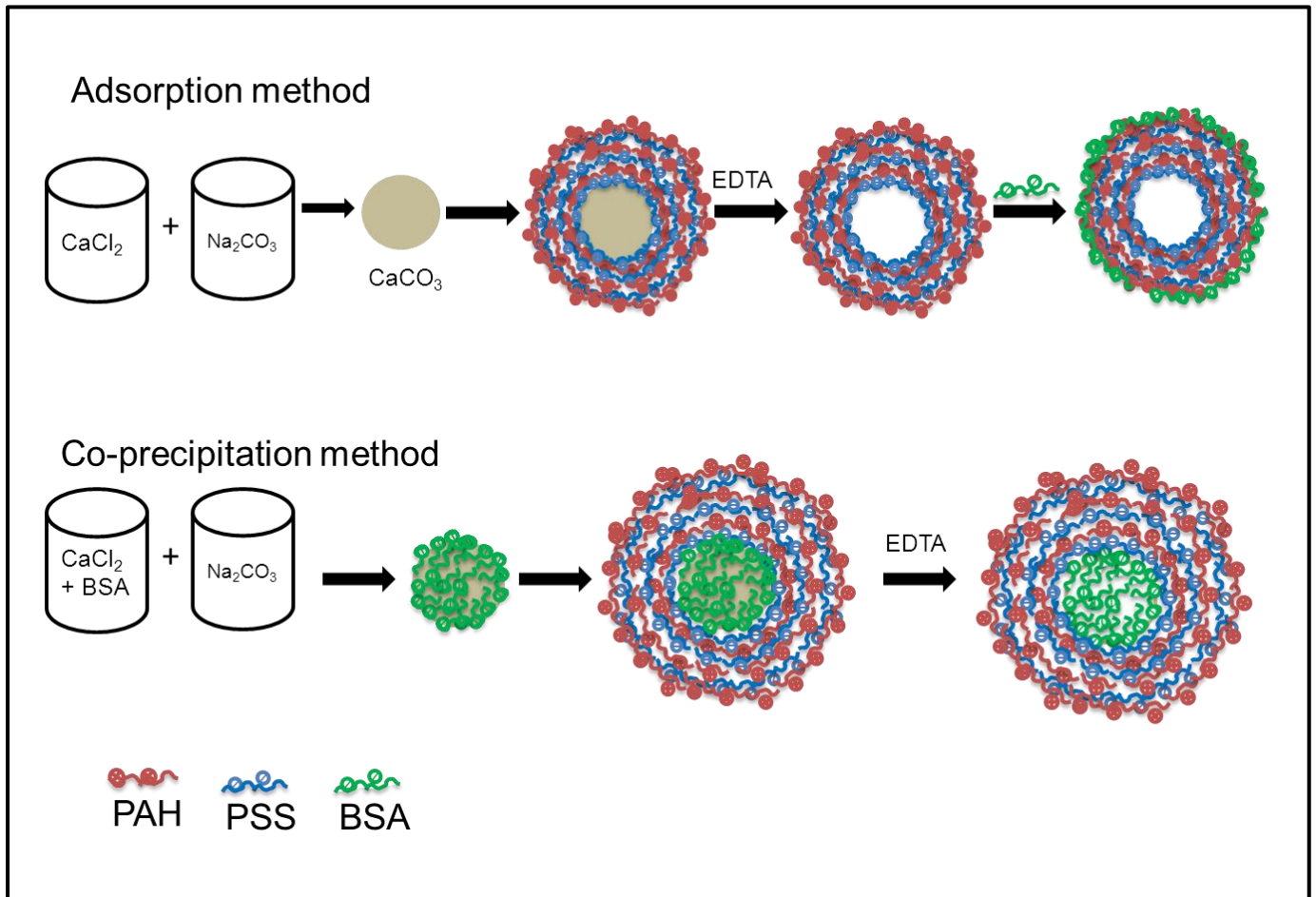
The results from the present study conclude that physical and chemical properties of small molecules play an important role in their encapsulation in LbL-MC. Molecular interactions between polymeric shell and small molecules, including electrostatic interaction, hydrogen bond and hydrophobic interactions enhance the adsorption of molecules. pH for ionic molecules and solubility for hydrophobic molecules are important factors to be optimized. Controlled release of small molecules from LbL-MC can be achieved. LbL-MC can further be developed to target liver and spleen or increase the blood circulation through PEGylation.

# Chapter 3

## Layer-by-layer microcapsules for protein delivery

---

## Graphical abstract



Schematic representation of different strategies for encapsulation of protein in LbL-MC.

### 3.1. INTRODUCTION

Over the past decade there have been many protein-based therapeutics approved for clinical use (Chalker JM., 2013). These include enzymes, clotting factors, insulin, monoclonal antibodies, immune-modulatory agents among others (Carter PJ., 2011; Caravella et al., 2010). However, the major limitation for clinical development of protein-based therapeutics is lack of efficient delivery system. Proteins are liable to degradation through widely present proteases (Caravella et al., 2010). Of the many carrier systems being studied to enhance the stability and efficiency of protein products, self-assembly through layer-by-layer particle technology has shown promise (Petrov et al., 2005; Yuri et al., 2001; Anandhakumar et al., 2010; De Temmerman et al., 2011). Self-assembled layer-by-layer microcapsules (LbL-MC) have been developed to study their deliverability of small molecules, proteins and nucleic acid based therapeutics (Sukhorukov et al., 2004; Lensen et al., 2008; Salloum et al., 2004).

In general, it was found that LbL-MC were able to encapsulate proteins/peptides and also increase their stability manifested by protection against proteolytic enzymes (Karamitros et al., 2013). However, encapsulation efficiency of protein in LbL-MC was found to be limited (Petrov et al., 2005). Different strategies were investigated to encapsulate model proteins such as bovine serum albumin (BSA) (Petrov et al., 2005),  $\alpha$ -chymotrypsin (Balabushevitch et al., 2001), lysozyme (Petrov et al., 2005), urease (Yuri et al., 2001), insulin (Fan et al., 2006) glucose oxidase (Onda et al., 1996) in LbL-MC. Majority of them studied adsorption of protein onto pre-formed LbL-MC (Hammond et al., 2012; Beyer et al., 2012). Furthermore, encapsulation of model protein by adsorbing onto sacrificial core, which was disintegrated after layering of polymers (Shen et al., 2013; Kazakova et al., 2013; Dam et al., 2013; Christophe et al., 2004; Peyratout et al., 2004; Tong et al., 2012). Moreover, different factors which could influence encapsulation efficiency of protein have been

optimized. These include protein concentration, salt concentration, pH and incubation time. In this study, we investigated the encapsulation of BSA in LbL-MC after co-precipitation with calcium carbonate core and physical adsorption onto preformed LbL-MC. We hypothesize that co-precipitation could lead to better encapsulation efficiency compared with physical adsorption technique. In this study, cationic polyallylamine hydrochloride (PAH) and anionic polystyrene sulfonate (PSS) were used to prepare LbL-MC. Therefore, influence of pH on encapsulation of BSA was studied. Moreover, influence of pH on release behavior of BSA from LbL-MC was studied.

### **3.2. MATERIALS AND METHODS**

Poly(styrene-4-sulphonic acid) (PSS, MW: 70kDa), polyallyl amine hydrochloride (PAH, MW: 58kDa), Bovine serum albumin (BSA), calcium chloride ( $\text{CaCl}_2$ ), sodium carbonate anhydrous ( $\text{Na}_2\text{CO}_3$ ), sodium chloride, disodium ethylenediamine tetraacetic acid dihydrate (EDTA), potassium chloride, di-sodium hydrogen orthophosphate anhydrous, potassium di-hydrogen orthophosphate, citric acid anhydrous, sodium citrate dihydrate, tris base, sodium azide, sodium hydroxide and hydrochloric acid were purchased from Sigma Aldrich Chemical Company (Bengaluru, India). All the chemicals were used without further purification. Milli-Q (Millipore, USA) water was used for all the experiments.

#### **3.2.1. Preparation of the LbL-MC**

The LbL-MC were prepared on calcium carbonate ( $\text{CaCO}_3$ ) sacrificial templates. The preparation of  $\text{CaCO}_3$  microparticles was as follows; briefly, 0.33M  $\text{CaCl}_2$  solution was added to 0.33M  $\text{Na}_2\text{CO}_3$  solution under vigorous stirring at 8000 rpm for 1h. The  $\text{CaCO}_3$  microparticles thus formed were centrifuged and dried at  $100^\circ\text{C}$  for 24h and used for layer-

by-layer adsorption of polymers. LbL-MC were prepared in a two-step process. In step one,  $\text{CaCO}_3$  microparticles were incubated with PSS (1mg/mL, pH 6.5, 0.5 M NaCl) for 15 minutes followed by centrifugation (10000 rpm, 10 minutes). The unbound PSS polymer was removed by washing with water. In step two, PSS coated microparticles were incubated with PAH (1mg/mL, pH 6.5, 0.5M NaCl) for 15 minutes followed by centrifugation (10000 rpm, 10 minutes). The unbound PAH polymer was removed by washing with water. The above two steps were repeated two more times to produce six alternative layers of PSS and PAH on  $\text{CaCO}_3$  microparticles. Later,  $\text{CaCO}_3$  core was disintegrated by addition of sodium EDTA (0.2M) resulting in hollow microcapsules. LbL-MC were lyophilized (Scanvac-cool safe™, Labogene, Denmark) and used for encapsulation of BSA by adsorption method.

### 3.2.2. Encapsulation of BSA in the LbL-MC by adsorption method

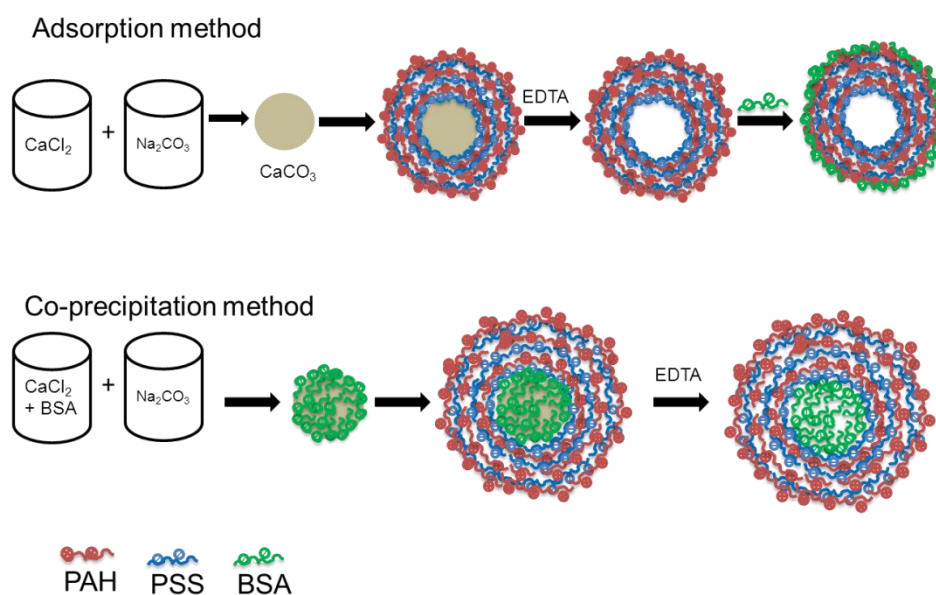
Figure 3.1 shows the schematic for encapsulation of BSA in the LbL-MC through adsorption method. For encapsulation of BSA by adsorption method, lyophilized LbL-MC (2mg) were dispersed in 1mL of 1mg/mL BSA solution. Factors that affect the encapsulation, including pH and NaCl concentration were studied. To study the influence of pH, LbL-MC was incubated in 1mg/mL of BSA for 1h at pH range of 2-9. The influence of salt concentration on encapsulation was studied by incubating LbL-MC in optimized BSA concentration containing 0.05-0.5M NaCl. After incubation in different conditions, the BSA loaded LbL-MC were centrifuged at 10,000 rpm for 10min. The supernatant was collected and analyzed by UV-visible spectrophotometer (V-650, Jasco, USA) at 280nm. The concentration of BSA in supernatant was determined from standard calibration curve (0.001 to 0.2mg/mL) with correlation coefficient of 0.999. Encapsulation efficiency of BSA was calculated using Eq. (7).

$$\text{Encapsulation efficiency (\%)} = \frac{\text{amount of BSA in LbL-MC}}{\text{total amount of BSA}} * 100 \quad (7)$$

### 3.2.3. Encapsulation of BSA in the LbL-MC by co-precipitation method

Figure 3.1 shows the schematic for encapsulation of BSA in LbL-MC through co-precipitation method. In co-precipitation method, BSA encapsulated  $\text{CaCO}_3$  microparticles were used as template for layer-by-layer adsorption of charged polymers. BSA encapsulated  $\text{CaCO}_3$  microparticles were prepared by mixing 0.33M  $\text{CaCl}_2$  solution containing BSA (1 mg/mL; pH 6) with 0.33M  $\text{Na}_2\text{CO}_3$  solution under vigorous stirring at 8000 rpm for 1h. LbL-MC were prepared in a two-step process as mentioned above. In step one, BSA encapsulated  $\text{CaCO}_3$  particles were incubated with PSS (1mg/mL, pH 6.5, 0.5M NaCl) for 15 minutes followed by centrifugation (10000 rpm, 10 minutes). The unbound PSS polymer was removed by washing cycle with water. In step two, PSS coated BSA encapsulated microparticles were incubated with PAH (1mg/mL, pH 6.5, 0.5M NaCl) for 15 minutes followed by centrifugation (10000 rpm, 10 minutes). The unbound PAH polymer was removed by washing with water. The above two steps were repeated two more times to produce six alternative layers of PSS and PAH on BSA encapsulated  $\text{CaCO}_3$  microparticles. BSA encapsulated LbL-MC were obtained upon disintegration of  $\text{CaCO}_3$  core by sodium EDTA (0.2M). After disintegration, the formed LbL-MC were separated by centrifugation (10000 rpm, 10 minutes) and supernatant was collected for BSA quantification. The concentration of BSA in supernatant collected in above steps was determined from standard calibration curve (0.001 to 0.2mg/mL) with correlation coefficient of 0.999. The encapsulation efficiency of BSA was calculated using Eq. (7).





**Fig. 3.1.** Schematic of BSA encapsulation in LbL-MC through adsorption and co-precipitation methods.

#### 3.2.4. Particle size and zeta-potential measurement

The surface morphology of LbL-MC was characterized using scanning electron microscope (JEOL, Akishima, Tokyo, Japan). The lyophilized LbL-MC were analyzed by directly mounting the sample on copper plate. An voltage of 20kV was applied during operation. The images were analyzed using SmartSEM version 5.05 software.

The particle size and zeta-potential after adsorption of each polymeric layer were determined by zetasizer (Nano ZS, Malvern, UK). For the particle size analysis, samples were dispersed in deionized water. Sample was maintained at 25°C during analysis. For zeta-potential analysis, samples were dispersed in deionized water and 0.75mL of sample solution was injected into clear folded capillary cell (DTS1060). Zeta-potential measurement was carried out at 25°C using smoluchowski model in automatic mode.

### 3.2.5. Fourier transform Infrared (FTIR) spectroscopy

Sequential adsorption of polymers on to CaCO<sub>3</sub> template was studied by Fourier transform infrared spectrometer (FT/IR-4200, Jasco, USA). Spectra were recorded for lyophilized samples of free CaCO<sub>3</sub> particles and after adsorption of each polymer layer. Furthermore, FTIR was also used to characterize the encapsulation of BSA in LbL-MC. In both the cases, samples (2mg) were mixed with potassium bromide at 1:1 ratio before analysis. Spectra were recorded within the range of 4000–400cm<sup>-1</sup> at a spectral resolution of 2cm<sup>-1</sup> in a dynamic reflectance sample holder.

### 3.2.6. Differential Scanning Calorimetry (DSC)

Differential Scanning Calorimeter (DSC-60, Shimadzu, Japan) was used to study the thermal transitions of lyophilized CaCO<sub>3</sub> microparticles and LbL-MC. Further, DSC was also performed to study the encapsulation of BSA in LbL-MC. Sample of 2mg was placed in an aluminum pan and sealed with a lid using a press. Thermograms were recorded at a heating rate of 10°C per minute from ambient temperature up to 500°C.

### 3.2.7. In-vitro release of BSA from the LbL-MC

In-vitro release studies of BSA from LbL-MC, formed by adsorption and co-precipitation methods were performed using cellulose ester dialysis membrane (molecular weight cutoff of 100-300kDa, Spectrum labs, USA). Release studies were performed in three different buffers including citrate buffer (pH 4.0), phosphate buffered saline (PBS, pH 7.4) and Tris buffer (pH 9.0). In co-precipitation method, LbL-MC (3mg) were dispersed in 1mL of respective buffer and transferred to dialysis membrane. The dialysis bag was immersed in

respective dissolution media (50mL). In adsorption method, LbL-MC (2mg) were dispersed in 1mL of respective buffers and volume of dissolution media used was 10mL. In-vitro release of equivalent concentrations of free BSA was also performed. The dialysis was performed in a orbital shaking incubator maintained at 37°C and 100 rpm. Samples of 1mL were withdrawn at predetermined time intervals, including 0.5, 1, 2, 4, 8, 12, 18, 24, 36, 48, 72, 96, 120h. Samples withdrawn were replaced with fresh media maintained at 37°C. Samples were analyzed using UV-Visible spectrophotometer (V-650, Jasco, USA) at 280nm. The amount of BSA released was determined using standard calibration curves constructed in respective buffers. Standard calibration curves were constructed with a BSA concentration range of 0.001 to 0.2mg/mL and having a correlation coefficient of 0.999.

### 3.2.8. Stability of BSA encapsulated in LbL-MC in the presence of trypsin

To study the integrity of BSA encapsulated in LbL-MC through co-precipitation and adsorption methods, sodium dodecyl sulfate-polyacrylamide gel electrophoresis (SDS-PAGE) was performed. This method involves the partial proteolysis of BSA in LbL-MC by protease enzyme trypsin (Takahata et al., 1998). BSA (200µg equivalent) encapsulated LbL-MC were suspended in 3.2mg/mL of trypsin dissolved in phosphate buffered saline (pH 7.4) for 2h at 37°C. After incubation, the LbL-MC were centrifuged (10000 rpm, 10 minutes) and the supernatant was collected. Further, sedimented LbL-MC were dissolved in 0.1N NaOH to extract remaining BSA. Later, trypsin was inactivated by heating samples at 100°C for 3 minutes followed by acidification with 0.1N HCl. The samples, supernatant and NaOH dissolved samples were mixed with 4x sample buffer containing SDS. Free BSA, BSA treated with trypsin and untrypsinized LbL-MC prepared by adsorption and co-precipitation methods were used as controls. Samples (10µl) were loaded in polyacrylamide gel (5%

stacking gel; 15% resolving gel) of 0.75mm thickness. Electrophoresis was performed in vertical gel electrophoresis unit (Hoefer Inc. USA) at 100V for 2h. Later, bands were visualized after 30 minute staining using coomassie blue.

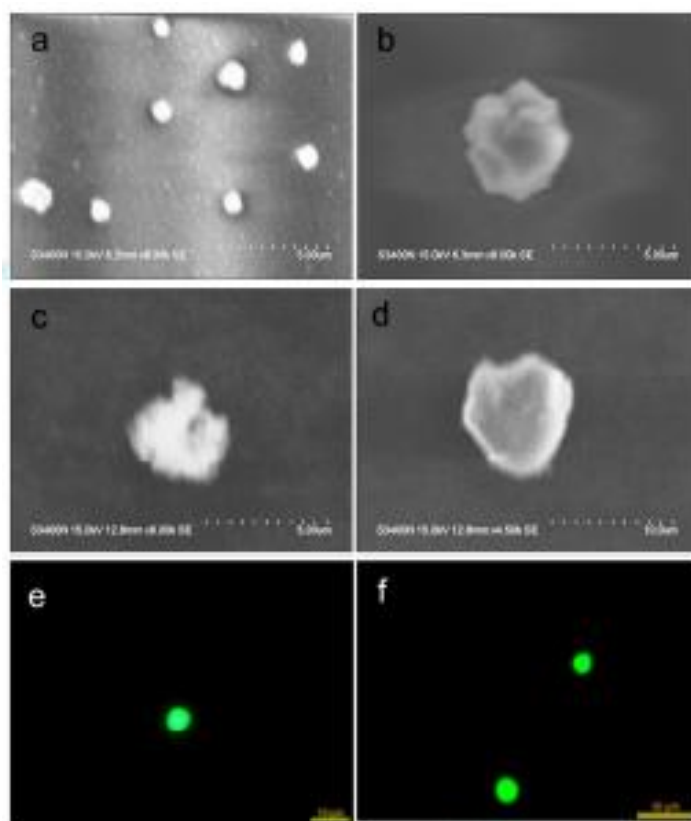
### 3.2.9. Statistical Analysis

All the results were presented as mean  $\pm$  standard deviation. Significance between groups was determined by Student's t-test (Graphpad Prism, USA) where  $P < 0.05$  was considered to be significant.

## 3.3. RESULTS

### 3.3.1. Preparation and characterization of LbL-MC

Figure 3.2 shows scanning electron micrographs of  $\text{CaCO}_3$ , BSA co-precipitated in  $\text{CaCO}_3$ , free LbL-MC and BSA loaded LbL-MC through co-precipitation (Figure 3.2). SEM studies showed that all the particles were less than 5  $\mu\text{m}$  in size. The average particle size of free  $\text{CaCO}_3$  microparticles studied using dynamic light scattering was found to be  $1.6 \pm 0.2 \mu\text{m}$  (Table 3.1). The particle size increased to  $3.1 \pm 0.4 \mu\text{m}$  for  $\text{CaCO}_3$  co-precipitated with BSA. Furthermore, the particle size increased to  $2.4 \pm 0.1 \mu\text{m}$  after adsorption of three bilayers of polymers on  $\text{CaCO}_3$ . Disintegration of  $\text{CaCO}_3$  to achieve hollow LbL-MC decreased the size to  $2.0 \pm 0.6 \mu\text{m}$ . In case of LbL-MC prepared through co-precipitation method, the average particle size was  $3.4 \pm 0.8 \mu\text{m}$  (Table 3.1). Figure 3.2 also shows the fluorescence images of FITC-BSA encapsulated in LbL-MC through co-precipitation and adsorption methods.



**Fig. 3.2.** Scanning electron micrographs of free  $\text{CaCO}_3$  (a),  $\text{CaCO}_3$  co-precipitated BSA (b), free LbL-MC (c), BSA encapsulated LbL-MC through co-precipitation (d). Fluorescence micrographs of FITC labelled BSA encapsulated in LbL-MC through co-precipitation (e) and adsorption (f) methods. Images are representative of at least three different experiments. Scale bar on SEM images represents  $5\mu\text{m}$  and scale bar on fluorescence images represents  $10\mu\text{m}$ .

Table 3.1 showed the zeta-potential as analyzed by zetasizer. Zeta-potential for free CaCO<sub>3</sub> was found to be 15.0±1.9 mV. Zeta-potential was reduced to (-)32.0±1.5 mV when CaCO<sub>3</sub> was co-precipitated with BSA. It was found that zeta-potential increased and decreased with the adsorption of PAH and PSS, respectively. After disintegration of CaCO<sub>3</sub>, zeta-potential of LbL-MC was found to be 8.1±1.9 mV. In case of LbL-MC containing BSA prepared through co-precipitation method, zeta-potential was (-)7.4±0.7 mV.

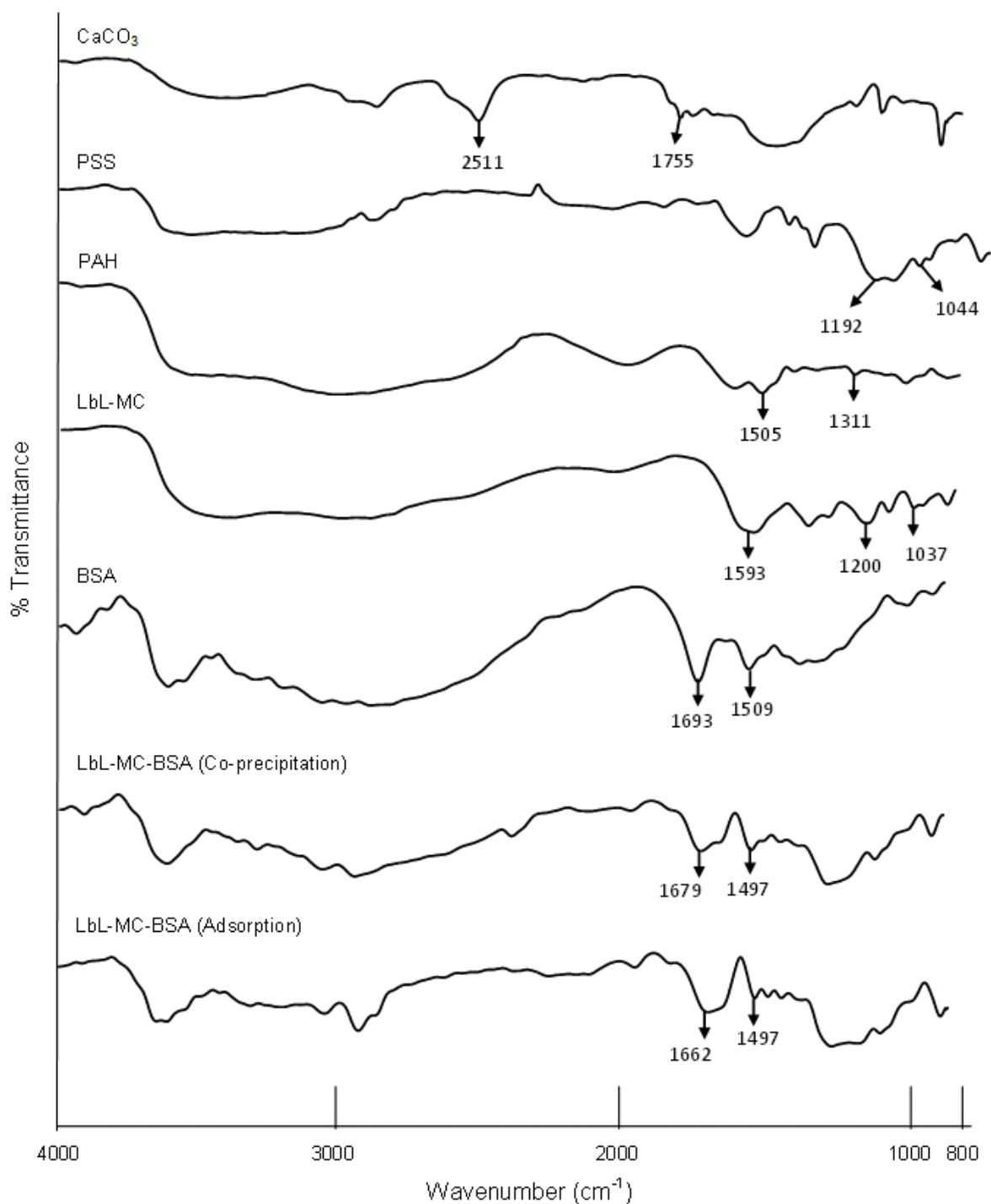
**Table 3.1** Particle size and zeta-potential measurement of BSA encapsulated LbL-MC.

Parameters	Stage	Adsorption method	Co-precipitation method
<b>Zeta potential (mV)</b>	CaCO <sub>3</sub>	15.0±1.9	Not applicable
	BSA CaCO <sub>3</sub>	Not applicable	-32.0±1.5
	PSS (1 <sup>st</sup> Layer)	-21.2±1.1	-25.4±1.0
	PAH (2 <sup>nd</sup> Layer)	7.0±1.5	-2.5±0.7
	PSS (3 <sup>rd</sup> Layer)	-14.6±0.6	-30.1±0.6
	PAH(4 <sup>th</sup> Layer)	5.1±1.5	-3.3±0.2
	PSS (5 <sup>th</sup> Layer)	-16.5±1.1	-33.4±1.2
	PAH(6 <sup>th</sup> Layer)	8.1±1.9	-7.4±0.7
	LbL MC-BSA	-5.7±1.0	-7.4±0.7
<b>Size (µm) *</b>	CaCO <sub>3</sub>	1.6±0.2 (0.44±0.21)	Not applicable
	BSA CaCO <sub>3</sub>	Not applicable	3.1±0.4 (0.43±0.15)
	CaCO <sub>3</sub> core with 6 layers	2.4±0.1 (0.65±0.31)	3.5±0.7 (0.73±0.44)
	LbL MC	2.0±0.6 (0.39±0.26)	3.4±0.8 (0.45±0.13)

Data is presented as mean ± standard deviation (n=3). \*Values in parentheses represent polydispersity index (PDI) ± standard deviation (n=3).

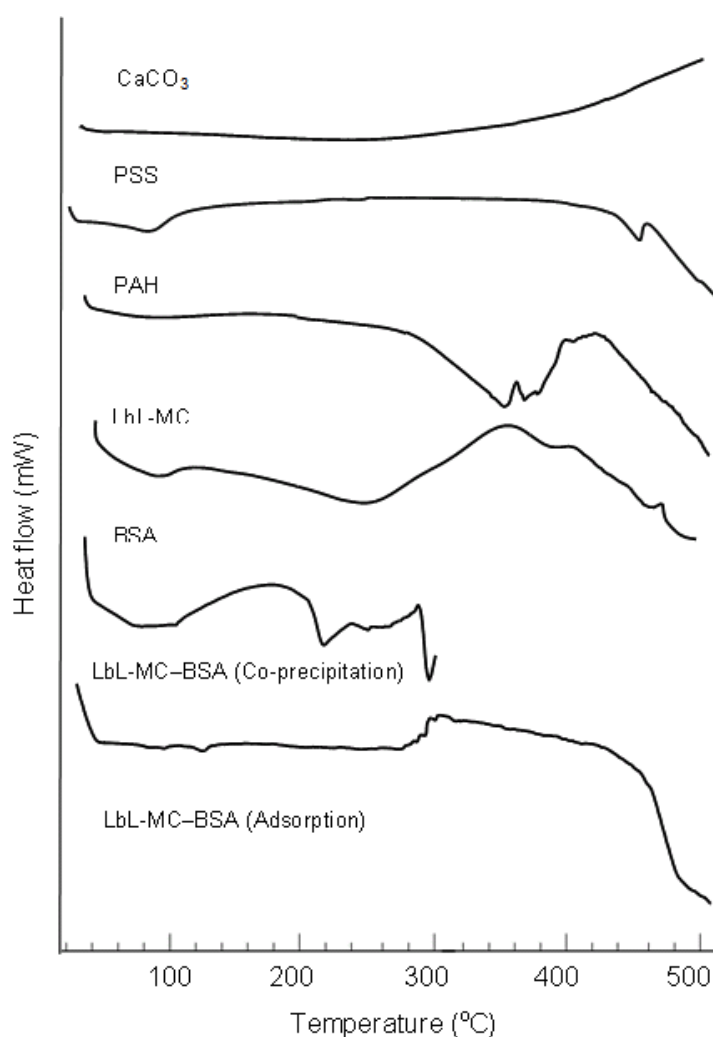
FTIR spectroscopic studies were performed to determine the interaction between the layered polymers. Figure 3.3 shows the FTIR spectra of free CaCO<sub>3</sub>, PAH, PSS, CaCO<sub>3</sub> layered with PSS and PAH alternatively. Figure 3.3 also shows the free LbL-MC after CaCO<sub>3</sub> disintegration. It was observed that the characteristic wave numbers of respective polymers shifted upon layering onto CaCO<sub>3</sub>. In case of PAH, characteristic wavenumber for N-H deformation at 1505 cm<sup>-1</sup> was shifted to 1593 cm<sup>-1</sup>. In PSS, wavenumbers of 1044 cm<sup>-1</sup> for

S=O symmetric;  $1192\text{ cm}^{-1}$  for S=O asymmetric stretch were shifted to  $1037\text{ cm}^{-1}$  and  $1200\text{ cm}^{-1}$  respectively.



**Fig. 3.3.** FTIR spectra of neat  $\text{CaCO}_3$ , neat PSS, neat PAH, blank LbL- MC, BSA and BSA encapsulated in LbL-MC prepared by co-precipitation and adsorption method.

Studies using DSC showed characteristic glass transition ( $T_g$ ) at 72.8°C, melting endotherm ( $T_m$ ) at 206.8°C and decomposition at 465°C for PSS (Fig. 3.4). For PAH,  $T_g$  was observed at 91.46°C and  $T_m$  was observed at 347.9°C. Free  $\text{CaCO}_3$  did not show any endotherm up to 500°C. DSC studies for LbL-MC showed shift in  $T_g$  for both PSS and PAH to 86.3°C and shift in  $T_m$  and decomposition temperature of PSS to 232.3°C and 462.2°C respectively. Similarly  $T_m$  of PAH was also shifted to 379.5°C.



**Fig. 3.4.** DSC thermograms of neat  $\text{CaCO}_3$ , neat PSS, neat PAH, blank LbL- MC, BSA and BSA encapsulated in LbL-MC prepared by co-precipitation and adsorption method.

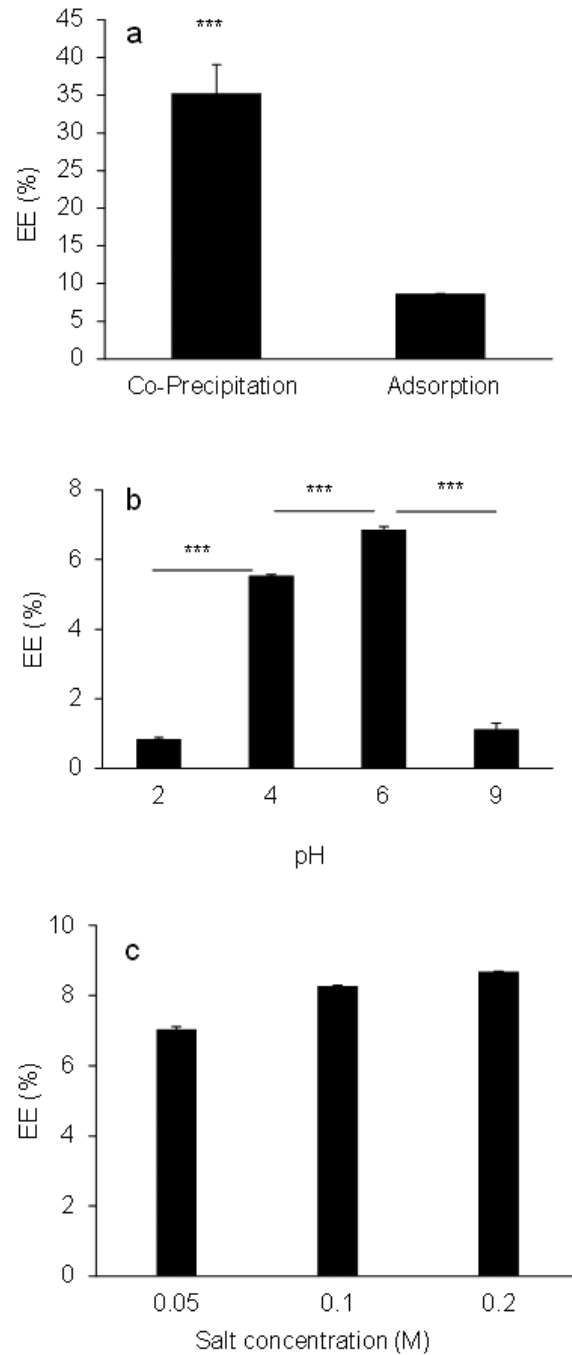


### 3.3.2. Encapsulation of the BSA in LbL-MC

Encapsulation of the BSA in LbL-MC was characterized using FTIR and DSC. Results from FTIR studies showed presence of characteristic peaks for BSA after encapsulation in LbL-MC (Fig. 3.3). In co-precipitation method, the peaks were found at wavenumbers of  $1497\text{cm}^{-1}$ ,  $1679\text{cm}^{-1}$  for amide-1 region;  $3284\text{cm}^{-1}$  for N-H stretch. Similarly, after BSA loading through adsorption method, the peaks were identified at wavenumbers of  $1497\text{cm}^{-1}$ ,  $1662\text{cm}^{-1}$  for amide-1 region;  $3308\text{cm}^{-1}$  for N-H stretch. Results from DSC studies showed glass transition ( $T_g$ ) and melting temperature ( $T_m$ ) for BSA at  $76.4^\circ\text{C}$  and  $216.1^\circ\text{C}$  respectively (Fig. 3.4). After co-precipitation, the  $T_g$  and  $T_m$  of BSA were shifted to  $105.2^\circ\text{C}$  and  $266.4^\circ\text{C}$  respectively (Fig. 3.4). Similarly, BSA encapsulated in LbL-MC through adsorption method showed  $T_g$  and  $T_m$  at  $148.3^\circ\text{C}$  and  $233.6^\circ\text{C}$  respectively.

Encapsulation efficiency of BSA in LbL-MC was determined through UV absorption spectroscopy. Encapsulation efficiency of BSA in LbL-MC obtained through co-precipitation method was found to be  $35.26\pm 3.81\%$  (Fig. 3.5a). For BSA encapsulated through adsorption method, influence of pH and salt concentration were studied. In general, adsorption method resulted in significantly ( $p<0.05$ ) less encapsulation compared to co-precipitation method. The greatest encapsulation efficiency obtained from adsorption method was  $8.7\pm 0.02\%$ . Incubation time of 1h showed greater encapsulation. Encapsulation efficiency was found to be  $0.85\pm 0.04\%$ ,  $5.54\pm 0.04\%$ ,  $6.86\pm 0.08\%$  and  $1.13\pm 0.17\%$  after BSA incubation at pH 2, 4, 6 and 9, respectively (Fig. 3.5b). To understand the influence of pH on adsorption of BSA, zeta-potential of free BSA and free LbL-MC was determined at pH 2, 4, 6 and 8 (Table 2). The zeta-potential of free LbL-MC decreased from  $38.7\pm 1.76\text{ mV}$  at pH 2 to  $18.1\pm 0.51\text{ mV}$  at pH 9. Similarly the zeta-potential of free BSA was found to be  $30.3\pm 1.93$ ,  $-9.9\pm 1.56$ ,  $-18.3\pm 3.32$ , and  $-26.0\pm 0.89\text{ mV}$  at pH 2, 4, 6 and 9 respectively. Further studies were performed at pH 6. NaCl concentration also influenced the BSA encapsulation in LbL-MC.

At lower NaCl concentration (0.05 – 0.2M), encapsulation efficiency was between  $7.0\pm 0.07\%$  to  $8.7\pm 0.02\%$ . Further increase in NaCl concentration to 0.3 and 0.5M decreased the encapsulation efficiency to  $4.6\pm 0.03\%$  and  $4.2\pm 0.15\%$  (Fig. 3.5c).



**Fig. 3.5.** Encapsulation of BSA in LbL-MC. Influence of encapsulation technique (a), pH on BSA adsorption (b) and NaCl concentration on BSA adsorption (c). Results are presented as mean  $\pm$  standard deviation (n=3). \*\*\* represents that the values are significantly different at  $p < 0.001$ .

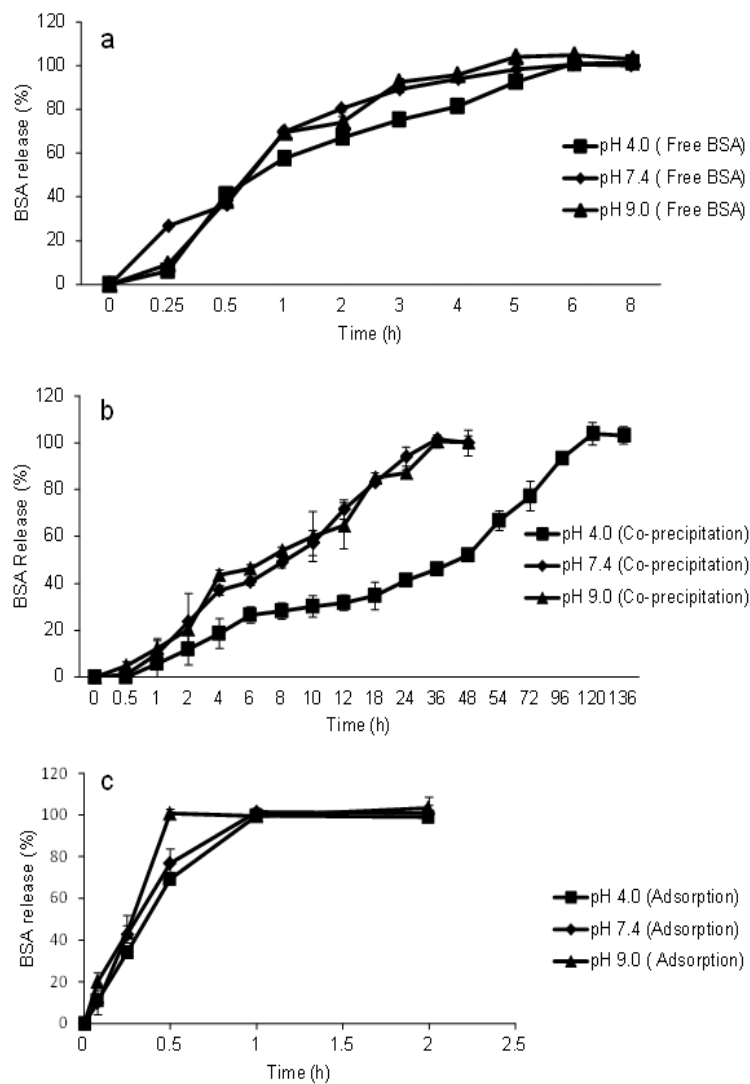
**Table 3.2.** Zeta-potential measurements of free BSA and free LbL-MC at different pH conditions and NaCl concentrations.

pH	Zeta-potential (mV)	
	Free BSA	Free LbL-MC
2	30.3 ± 1.93	38.7 ± 1.76
4	-9.9 ± 1.56	28.7 ± 0.26
6	-18.3 ± 3.32	26.4 ± 0.42
9	-26.0 ± 0.89	18.1 ± 0.51
<b>NaCl concentration (M)*</b>		
0	-17.17 ± 2.73	Not applicable
0.05	-8.34 ± 1.03	Not applicable
0.1	-6.45 ± 0.66	Not applicable
0.2	-6.49 ± 0.91	Not applicable

\* Zeta-potential of free BSA at different NaCl concentrations is obtained at pH 6.

### 3.3.3. In-vitro release of BSA from LbL-MC

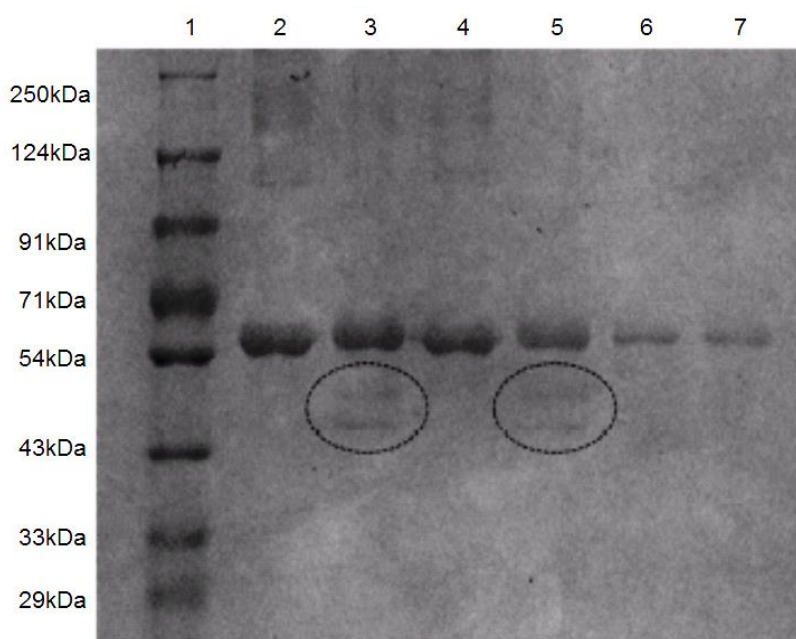
Figure 3.6a shows the diffusion of free BSA through the dialysis membrane at different pH conditions. It was found that there was no significant difference in BSA diffusion across the membrane at different pH, 4, 7 and 9. Figure 3.6b shows release of BSA encapsulated through co-precipitation method from LbL-MC. At pH 4, BSA release was controlled, where 100% release was achieved after 120h. At pH 7.4 and 9, 100% of BSA was released within 36h. Figure 3.6c shows the BSA release from LbL-MC encapsulated through adsorption method. It was found that 100% of BSA released within 1h at all the pH conditions. Therefore, BSA encapsulated through adsorption methods showed burst release, while BSA encapsulate through co-precipitation method showed controlled release.



**Fig. 3.6.** In-vitro cumulative release profiles of free BSA solutions (a); BSA encapsulated in LbL-MC prepared by co-precipitation method (b) and adsorption method (c). Release studies were performed in different buffers including citrate (pH 4), phosphate buffered saline (pH 7.4) and tris buffer (pH 9) at 37°C. Results are presented as mean  $\pm$  standard deviation (n=3).

### 3.3.4. Stability of BSA encapsulated in LbL-MC in the presence of trypsin

Figure 3.7 shows the integrity of BSA encapsulated in LbL-MC by adsorption and co-precipitation methods. Free BSA without trypsin treatment showed a single band between 47 and 73 kDa. In case of trypsin treatment, BSA was degraded to show a band between 38 and 47kDa. BSA encapsulated in LbL-MC through co-precipitation method showed lesser degradation (lanes 6 and 7, Fig. 3.7) compared with adsorption method (lanes 4 and 5, Fig. 3.7).



**Fig. 3.7.** Stability of BSA encapsulated in LbL-MC in presence of trypsin determined using SDS-PAGE. Lane 1, protein molecular weight marker; lane 2, free BSA; lane 3, free BSA after treatment with trypsin; lane 4, BSA encapsulated in LbL-MC by adsorption method and before treatment with trypsin; lane 5, BSA encapsulated in LbL-MC by adsorption method and after treatment with trypsin; lane 6, BSA encapsulated in LbL-MC by co-precipitation method before treatment with trypsin; lane 7, BSA encapsulated in LbL-MC by co-precipitation after treatment with trypsin. The dotted circle shows degradation bands of BSA after trypsin treatment. Image is representative of three different experiments.

### 3.4. DISCUSSION

Development of a responsive carrier system is one of the potential applications of LbL-MC (Cranford et al., 2010; Gao et al., 2001; Koker et al., 2011; Shu et al., 2010). Polyelectrolytes with varied degree of dissociation are attractive candidates for development of pH-sensitive carriers (Pechenkin et al., 2012). The combination of PSS and PAH based LbL-MC have been widely studied for pH dependant encapsulation and release behavior of small molecules (Pechenkin et al., 2012; Sato et al., 2011). Furthermore, model protein BSA has also been studied for its encapsulation in LbL-MC. Sukharokov's group has performed studies to enhance the poor encapsulation efficiency of BSA in LbL-MC. BSA encapsulation in LbL-MC was compared between adsorption on preformed LbL-MC and polymer layering after adsorption of BSA onto  $\text{CaCO}_3$  template (Petrov et al., 2005). In this study, we have compared the adsorption method with co-precipitation method, where BSA was co-precipitated with growing  $\text{CaCO}_3$  microparticles.

The sequential adsorption of polyelectrolytes onto  $\text{CaCO}_3$  microparticle templates was confirmed by zeta-potential measurements, FTIR spectra and DSC thermograms. Our results were in agreement with previous reports. Further, BSA adsorption on pre-formed PSS/PAH LbL-MC was confirmed by changes in zeta-potential, shift in characteristic vibrational stretching and melting temperature measured using FTIR and DSC respectively. pH was found to be an important factor which influences the encapsulation of BSA. Earlier reports showed 8% encapsulation efficiency after physical adsorption method which was similar to that showed in this study (Petrov et al., 2005). It was reported that BSA interacts with outer PAH layer through electrostatic interactions. The anionic side of the coiled BSA interacts with outer PAH layer. Furthermore, as the concentration of the BSA is increased, it was showed that BSA forms a multilayer over LbL-MC, where PAH penetrates the BSA

layers and/or oppositely charged sides of BSA will electrostatically interact to form multilayers (Ladam et al., 2000; Ladam et al., 2002).

As charge density is an important factor in encapsulation, pH and salt concentration needed to be optimized (Georgieva et al., 2005; Yang et al., 2002). The  $pK_a$  of PSS and PAH were reported to be 3.5 and 8.5 respectively (Mak et al., 2008). Furthermore, the isoelectric point of BSA is 4.7 (Peng et al., 2004). At acidic pH of 4, the charge density of both PSS and PAH is higher leading to greater interaction. This was found to decrease the size of pores present in the polymeric shell (Balabushevitch et al., 2001; Glinel et al., 2007). On the other hand, at pH 9, PAH is only partially charged with lesser electrostatic interactions (Balabushevitch et al., 2001). This was showed to lead to larger pores and swelling of polymeric shell (Glinel et al., 2007)). Therefore increase in pH has resulted in greater encapsulation of BSA in LbL-MC. Furthermore, NaCl is suggested to interact with the polyelectrolytes and reduce the interactions among them (Gao et al., 2003; Steitz et al., 2001). This is found alter the encapsulation efficiency of BSA in LbL-MC.

In case of co-precipitation method, BSA was captured into growing calcium carbonate particles. Co-precipitated BSA decreased the zeta-potential of  $\text{CaCO}_3$  particles. Co-precipitation showed 4-fold increase in BSA loading in LbL-MC compared to adsorption method. Entrapment of molecules in the growing  $\text{CaCO}_3$  has been previously reported for small molecules including curcumin and etoposide, (Peng et al., 2013) and proteins such as urease, L-asparaginase,  $\alpha$ -chymotrypsin and lysozyme (Yuri et al., 2001; Balabushevitch et al., 2001; Peng et al., 2004).

As the pH has influenced the encapsulation efficiency of BSA in PSS/PAH LbL-MC, it is expected that release of BSA will be pH dependent. At neutral and basic pH conditions of 7.4 and 9, co-precipitated and adsorbed BSA release characteristics were similar to free BSA diffusion through dialysis membrane. At acidic pH, however, the BSA release was

controlled. This is again attributed to the increased charge density in layering polymers leading to decreased porosity (Mak et al., 2008; Peng et al., 2004; Glinel et al., 2007). Furthermore, the integrity of BSA encapsulated in LbL-MC prepared by co-precipitation and adsorption methods was determined by SDS-PAGE. Co-precipitation of BSA in LbL-MC was more resistant to proteolysis by trypsin compared with adsorbed BSA. This is attributed to greater exposure of adsorbed BSA to trypsin compared to co-precipitated BSA. Similar results were reported, where L-asparaginase encapsulated in dextran sulfate and polyarginine based LbL microcapsules was resistant to proteolytic degradation from trypsin (Karamitros CS et al., 2013). Furthermore, BSA was found to be intact in LbL-MC in the absence of trypsin. This confirms that BSA was not degraded during encapsulation in LbL-MC. Overall, PSS/PAH LbL-MC can be developed as pH sensitive, protective carriers for delivery of protein therapeutics.

### **3.5. CONCLUSION**

This study showed that greater encapsulation efficiency of model protein BSA in LbL-MC can be achieved through co-precipitation in  $\text{CaCO}_3$  compared with adsorption on preformed LbL-MC. The encapsulation efficiency through adsorption method is influenced by pH and salt concentration. Further, PSS/PAH LbL-MC can be developed as pH-responsive carriers for controlled release of protein therapeutics.

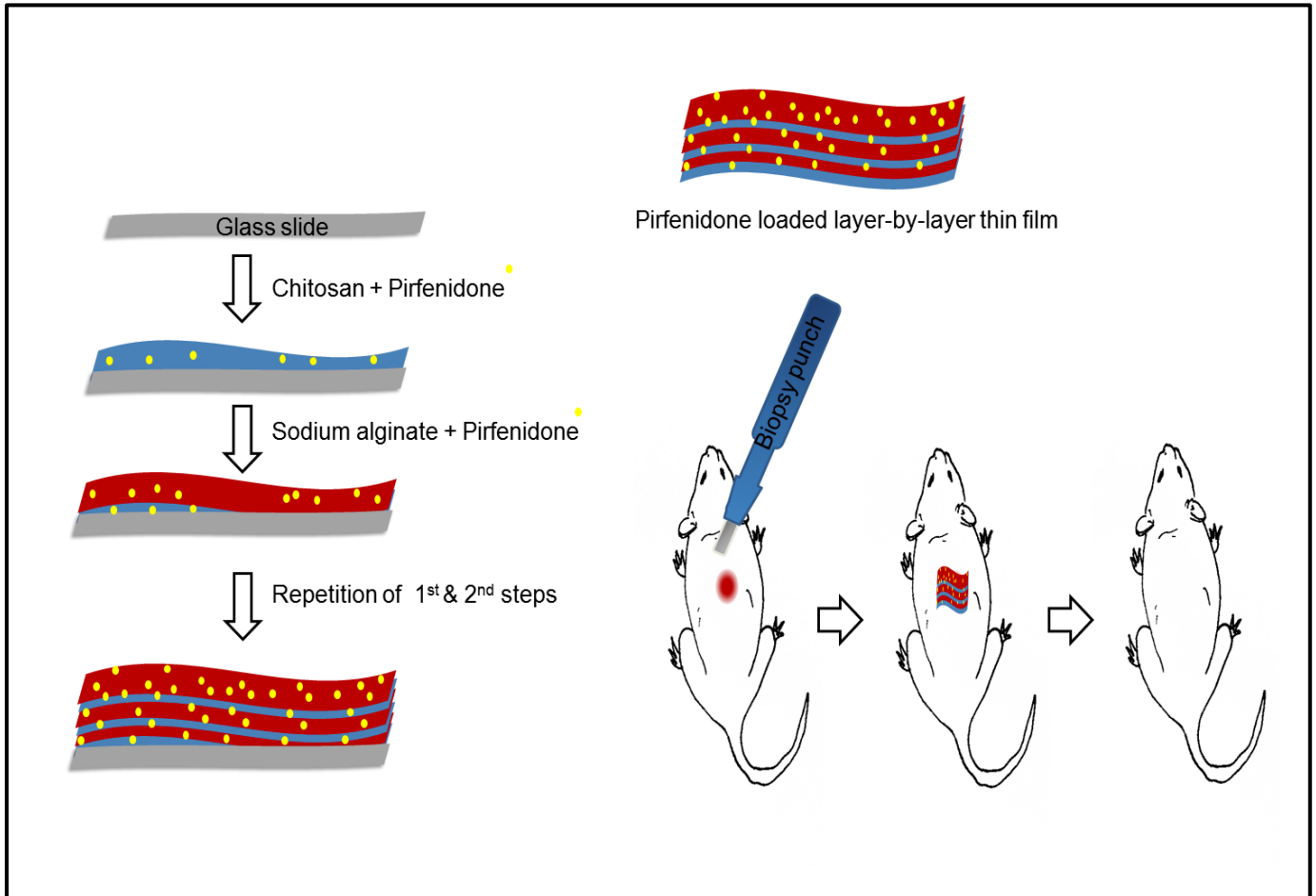


# Chapter 4

## Layer-by-layer thin films for small molecule delivery

---

## Graphical abstract



Schematic representation of pirfenidone loaded layer-by-layer thin film fabrication for excisional wound application.

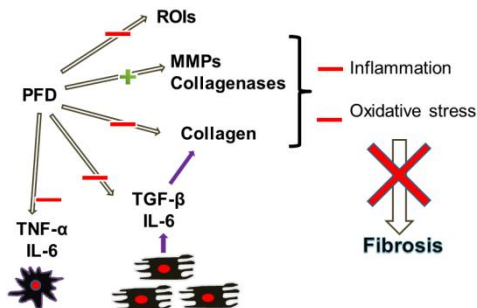
## 4.1. INTRODUCTION

Layer-by-layer technique involves the sequential adsorption of oppositely charged polyelectrolytes on a planar template would result in the formation of a thin film. These LbL thin films are especially attractive for the topical application of therapeutic and cosmetic agents. Some of the advantages of LbL thin films for topical application include potential for entrapment and release of actives in a controlled manner, adhesiveness to skin tissue, ease of application, enhanced user compliance because of the thin and transparent property, use of non-irritating and biodegradable polymers, ease of dose termination and delamination of the film after usage (Thu et al., 2012). These properties would allow application of the LbL thin films on dermal injuries to provide barrier protection and the release of entrapped drugs at the injury site for an accelerated wound healing. Furthermore, incorporation of a bioadhesive polymer such as chitosan will improve the film adhesion to skin tissue.

Dermal injuries are commonly caused by the accidental cuts, burns, diabetic ulcers among others (Falanga, 2005; Aarabi et al., 2007; Albertini et al., 2013). These dermal wounds often result in the scar tissue formation attributed to excessive production of the extracellular matrix components including collagen (Wynn, 2008). TGF-beta is a pro-inflammatory cytokine which is over-expressed at the site of tissue injury (Kryger et al., 2007). TGF-beta induces the proliferation of fibroblast cells leading to excess production of collagen (Hong et al., 2008). Previous reports showed that the inhibition of TGF-beta controlled wound healing process, resulted in a lesser scar tissue formation (Shah et al., 1992).

The pirfenidone (PFD) is a novel anti-fibrotic and anti-inflammatory agent approved by US-FDA for the treatment of idiopathic pulmonary fibrosis (Taniguchi et al., 2010). Pirfenidone

is chemically as (5-methyl-1-phenylpyridin-2[H-1]-one). It has also been studied for its efficacy in the hepatic and renal fibrosis (García et al., 2002; Cho & Kopp, 2010). A number of cell-based studies have shown that pirfenidone reduces fibroblast proliferation, inhibits TGF-beta stimulated collagen production and reduces the production of fibro genic mediators such as TGF-beta (Iyer et al., 1999; Tada et al., 2001). Pirfenidone has also been shown to reduce production of inflammatory mediators such as TNF- $\alpha$  and IL-1 $\beta$  (Hale et al., 2002). Furthermore, the PFD loaded nanoparticles were used to improve the corneal wound healing after an alkali induced injury in a rabbit model (Chowdhury et al., 2013). The anti-fibrotic and anti-inflammatory properties of PFD have been majorly attributed to its anti-TGF-beta and anti-TNF-alpha activity (Nakazato et al., 2001; Yang et al., 2013). Here we have hypothesized that the PFD would enhance the wound healing after dermal injury with a reduced scar tissue formation. To the best of our knowledge, we were the first to report the application of PFD in dermal wound management. PFD was entrapped in the LbL thin film prepared using biodegradable chitosan and sodium alginate. These films were applied on an incisional dermal injury mouse model to study the wound contraction, total protein and collagen content. A commercially available povidone-iodine gel was used as control treatment.



**Fig. 4.1.** Molecular mechanisms of pirfenidone in reduction of fibrosis (‘plus sign’ indicates the mechanisms promoted by pirfenidone; ‘minus sign’ indicates the mechanisms that are inhibited by this drug).

## 4.2. MATERIALS AND METHODS

Chitosan (75-85% deacetylated, MW: 100-300 kDa), sodium alginate (MW: 80 kDa), pirfenidone (PFD), DAPI, Triton X-100, TRI reagent, isopropanol, sodium dodecyl sulfate (SDS), hydroxyproline, hydrogen peroxide, sodium chloride, disodium hydrogen orthophosphate, potassium dihydrogen orthophosphate, sodium citrate, hydrochloric acid, sodium hydroxide, sulphuric acid, potassium bromide, ketamine, xylazine, HPLC grade acetonitrile and ammonium acetate were purchased from Sigma-Aldrich Chemical Company (Bengaluru, India). Primary antibody  $\beta$ -Actin mouse monoclonal IgG, Horse radish peroxidase–conjugated (HRP) goat anti-mouse IgG were purchased from Santa Cruz Biotechnology, USA. Anti-human/mouse TGF-beta functional grade purified was purchased from eBioscience, USA. Dulbecco's modified Eagle's medium (DMEM), Dulbecco's phosphate buffered saline, fetal bovine serum (FBS), penicillin, streptomycin and trypsin were purchased from Himedia labs (Mumbai, India). All the chemicals were used without further purification. Milli-Q (Millipore, USA) water with 18.2 M $\Omega$  resistivity was used for all the experiments.

### 4.2.1. Preparation of the layer-by-layer thin film

The LbL thin film was prepared on a glass slide template in a two-step process. In step one, cationic polymer, chitosan (5mg/ml, pH 5, 0.1M NaCl) was spiked on to the glass slide. After 15min, unadsorbed chitosan was decanted and the glass slide was washed thrice with water. In step two, sodium alginate (5mg/ml, pH 4, 0.1M NaCl) was spiked on to the chitosan coated glass slide. After 15min, unadsorbed polymer was decanted and the glass slide was washed with water. The above two steps were repeated fourteen more times to produce a fifteen

bilayered chitosan-alginate LbL thin film. Later, the film was delaminated from the template by dipping in 0.1N NaOH for 2min and carefully delaminated film was stored in a closed container.

#### 4.2.2. Preparation of the PFD loaded layer-by-layer thin film

The PFD loaded LbL thin film was prepared after the addition of PFD (5mg/ml) to the chitosan and alginate solution. This PFD/polymer mixture was used for the alternative layering to prepare the PFD loaded LbL thin film.

#### 4.2.3. Preparation of PFD ointment

PFD ointment was prepared by heat and mechanical incorporation method described in the USPXXII. A hydrophilic ointment base was prepared using PEG MW 400 and 4000, after heating at 60°C PFD (2%) solution was added slowly to the PEG ointment base under continuous stirring for 10min. The solution was congealed with continuous agitation until it formed an ointment.

#### 4.2.4. Characterization of the LbL thin film and PFD loading efficiency

The adsorption of polymers during the film growth was characterized by the UV-spectrophotometer and FTIR. After the adsorption of each bilayer, the thin film was dissolved in 0.1N NaOH. Samples were then sonicated and filtered through a 0.45 $\mu$ m pore size membrane

filter. Later the absorbance was recorded using UV-visible spectrophotometer (SpectraMax M4, Molecular Devices Inc., USA) at 220nm wavelength.

The sequential adsorption of polymers on to a glass template was studied by FTIR spectroscopy (FT/IR-4200, Jasco Inc., USA). Spectra were recorded for the neat chitosan, sodium alginate, blank LbL thin film and PFD loaded LbL thin film. The sample film (2mg) was mixed with potassium bromide at a 1:1 ratio before analysis. Then the spectra were recorded between 4000–400  $\text{cm}^{-1}$  wavenumber at a spectral resolution of 2  $\text{cm}^{-1}$  in a dynamic reflectance sample holder.

Differential scanning calorimeter (DSC 60, Shimadzu, Japan) was used to study the thermal transitions of the neat chitosan, sodium alginate and blank LbL thin film. Furthermore, DSC was also performed to study the encapsulation of PFD in the LbL thin film. The sample film (2mg) was placed in an aluminum pan and was sealed with a lid using a press. Then the thermograms were recorded at a heating rate of 10°C per minute from ambient temperature up to 500°C.

The PFD loading efficiency was determined by suspending the LbL thin film (1  $\text{cm}^2$  area) in 2ml water while sonication for 5min. Later, the samples were filtered using a 0.22 $\mu\text{m}$  pore size syringe filter and was analyzed using HPLC (LC-20AD, Shimadzu, Japan). The chromatographic separation of PFD (50 $\mu\text{l}$  injection volume) was achieved on an end capped Luna C8 analytical column (150  $\times$  4.6mm i.d., 5  $\mu\text{m}$ ), at a flow-rate of 1 ml/min and maintained at 40°C. The mobile phase consisted of acetonitrile and 10 mM ammonium acetate, pH 6.6 (30:70 v/v). The PFD concentration in the samples was determined after recording the absorbance at 310nm wavelength and comparing with the standard curve (50-500ng/ml concentration range,  $R^2 = 0.999$ ). The PFD loading efficiency was calculated using Equation (8).

$$\text{Loading efficiency} = \frac{\text{Amount of PFD in LbL thin film}}{\text{Surface area of LbL thin film}} \times 100 \quad (8)$$

#### 4.2.4.1. Physical characterization of the LbL thin films

(a) *Thickness*: The thickness of LbL thin films was measured using a digital micrometer (Baker Gauges India Pvt. Ltd., Mumbai, India). The thickness was measured at least on three different locations of a film and for at least three different films.

(b) *Scanning electron microscopy*: The surface morphology of the LbL thin film was characterized using the scanning electron microscope (JEOL, Tokyo, Japan). A free standing LbL thin film was directly mounted on a copper plate and the image was acquired after the application of 20 kV voltage.

(c) *Porosity*: Porosity of the LbL thin film was evaluated by alcohol displacement method. Briefly, small piece ( $1 \times 1 \text{ cm}^2$ ) of pre-weighed film was immersed in alcohol. After 24h the film was taken out and the final weight was noted. Porosity was calculated by the following formula (Sudheesh Kumar et al., 2013)

$$\text{Porosity (\%)} = \frac{(W_2 - W_1)}{\rho V_1} \times 100 \quad (9)$$

Where  $W_1$  and  $W_2$  indicate the weight of the polymer film before and after alcohol immersion, respectively, and  $V_1$  is the volume before immersion,  $\rho$  is a constant of the alcohol density. Results were presented as an average of three experiments.

(d) *Swelling ratio*: The swelling ratio of LbL thin film was determined after immersion of film samples in phosphate buffered saline (PBS, pH 7.4) at room temperature for 24h. The weight of films samples was recorded before (dry weight,  $W_d$ ) and after (wet weight,  $W_w$ )



immersion in PBS. Swelling ratio was calculated using the Equation (10) (Sudheesh Kumar et al., 2013)

$$\text{Degree of swelling (DS)} = \frac{(W_w - W_d)}{W_d} \times 100 \quad (10)$$

#### 4.2.4.2. Mechanical properties of LbL thin films

Mechanical properties of films were evaluated by Texture Analyzer (TAXT plus, Stable Microsystems, UK; maximum load 5kg).

(a) *Burst Strength*: Film burst strength is the force required to break or rupture the film, which is an indicator of the flexibility of the film. Burst strength of the film was studied using film support rig, which was fitted to a heavy duty platform and the probe (3mm cylindrical stainless steel) was connected to a 5kg load cell. The test was performed at a probe speed of 1 mm/s and an acquisition rate of 500 points/s. The force applied increases until the film bursts and the peak force was recorded as film burst strength. The displacement of film was the distance to burst, which is an indication of flexibility of the LbL thin film.

(b) *Tensile Strength*: Tensile strength of a film is an indicator of toughness of film. Tensile strength of the film was determined with tensile grips (A/TG). The test film was fixed to the upper tensile grip and load cell was tared to zero weight. Upper tensile grip was moved to the preset distance of 25mm and the test film was securely clamped to lower grip. The tensile force was gradually applied on the test film till the film broke. The parameters maintained were 1mm/s pretest speed, 1mm/s test speed, in distance target mode.

$$\text{Tensile strength} = \frac{F_{max}}{A_{film}} \quad (11)$$

where “ $F_{\max}$ ” is the maximum force at breakage (N) and “ $A_{\text{film}}$ ” is the initial cross sectional area of the sample ( $\text{cm}^2$ ). The data reported is the mean of 3 film samples.

% elongation was calculated using equation (12).

$$\text{Elongation}(\%) = \frac{(L-L_0)}{L_0} \times 100 \quad (12)$$

where “ $L_0$ ” is the initial length of the specimen (cm) and “ $L$ ” is the length at the moment of rupture (cm).

Young’s modulus was calculated using equation (13).

$$\text{Young's modulus} = \frac{F_{\text{lin}}}{A_{\text{film}}} \times \frac{1}{\epsilon} \quad (13)$$

where “ $F_{\text{lin}}$ ” is the force at corresponding strain of the linear section (N), “ $A_{\text{film}}$ ” is the initial cross sectional area of the film ( $\text{cm}^2$ ), and  $\epsilon$  is the corresponding strain.

(c) *Adhesion strength*: The skin adhesion strength of the LbL thin film was evaluated using C57BL/6 mouse skin as the model. Mice were killed using excess ether anesthesia and the dorsal abdominal skin was carefully harvested after clipping the hair. The excised skin was affixed on a cylindrical Perspex support and was secured with screws. The LbL thin film ( $1 \text{ cm}^2$ ) was adhered to a probe (1/2" cylindrical Delrin with part code P/0.5R) using adhesive tape. The probe was lowered to make a contact with the skin tissue at a force of 0.2 N for a contact time of 30 s. It was then withdrawn at a rate of 0.1 mm/s to a distance of 5mm. The data acquisition (500 points/s) and peak integration were performed using the XTRA Dimension software package of the instrument. All the measurements were repeated at least three times. The work of adhesion and the peak detachment force was used to evaluate the skin adhesion strength of the films. The work of adhesion was calculated from the area under the force-distance curve, and the peak

detachment force was calculated as the maximum force required for detaching the film from the tissue.

#### 4.2.5. Antimicrobial activity of the LbL thin films

The antimicrobial activity of films was evaluated against gram negative (*Escherichia coli*) and gram positive (*Staphylococcus aureus*) bacteria. The antimicrobial activity of CS, SA and LbL thin films was investigated by zone of inhibition method and spectrophotometric method. The pure cultures of *E. coli* and *S. aureus* were sub-cultured in LB medium and Müeller-Hinton medium, respectively. These bacterial suspensions were incubated at 37°C on a rotary shaker at 150 rpm. A cell count of  $10^6$  CFU (optical density of 0.2 at 600 nm wavelength) was achieved after 12h incubation.

For the zone of inhibition measurement, agar plate method was performed. The components of the LB agar included tryptone, yeast extract, sodium chloride and 2% agar. The CS, SA and LbL thin films were cut into discs of 0.8cm diameter and placed over the LB agar seeded with bacterial cultures. A standard antibiotic disc was used as a positive control for bactericidal activity. The standard antibiotic disc contained ampicillin (AMP, 10µg), chloramphenicol (C, 25µg), penicillin G (P, 1 unit), streptomycin (S, 10µg), sulphatriad (S3, 300 µg) and tetracycline (TE, 25µg). The plates were incubated at 37°C for 24h and examined for clear zone of inhibition.

Spectrophotometric method was used to study the growth kinetics of bacterial species. The CS, SA and LbL films were cut into discs of 0.5cm diameter and placed in a 96 well plate. Tetracycline (10µg/ml) was used as positive control and blank cells as negative control. Bacterial

cell suspension (200 $\mu$ l, optical density of 0.2 at 600nm wavelength) was added to the well containing polymer film. At different time intervals 0, 2, 4 and 6h, the optical density was measured at 600nm wavelength using a micro-plate reader (SpectraMax M4, Molecular Devices Inc., USA).

#### 4.2.6. Cell viability studies

Cell viability in the presence of LbL thin film was studied in A431 cells. Cells were grown in DMEM supplemented with 10% fetal bovine serum (FBS) and 1% penicillin/streptomycin solution, and incubated at 37°C with 5% CO<sub>2</sub>. Cells (1x10<sup>5</sup>) were seeded on LbL thin film in 6 well plate and incubated for 24h. MTT was added and incubated for 4h at 37°C. Later, cell viability was measured by recording the absorbance of DMSO solubilized formazan at 595nm wavelength.

#### 4.2.7. In-vitro release study

In-vitro release of PFD from the LbL thin film was performed using a Franz diffusion cell apparatus (PermeGear Inc., USA) with a 5ml receptor compartment (effective surface area of 0.64 cm<sup>2</sup>). Regenerated cellulose membrane (Mwt. cut-off 12 kDa, Spectrum Labs, USA) was placed between the donor and receptor compartments. A circular disc of the PFD loaded LbL thin film (1mg PFD equivalent) was placed in the donor chamber and was hydrated with 0.2ml of PBS. Samples of 300 $\mu$ l were withdrawn from the receptor compartment at a

predetermined time points of 0.08, 0.16, 0.25, 0.5, 1, 2, 3 and 4h. Then the samples were analyzed using the HPLC method described above.

#### 4.2.8. In-vitro cell adhesion studies

Human epidermoid carcinoma cells (A431, procured from National Centre for Cell Science, Pune, India) were used for the cell adhesion studies. The cells were cultured in Dulbecco's modified Eagle's medium (DMEM) supplemented with 10% heat inactivated fetal bovine serum (FBS), 10 U/ml penicillin G and 10 mg/ml streptomycin in a humidified atmosphere with 5% of CO<sub>2</sub>. A431 cells ( $1 \times 10^5$  cells) were seeded on the 1 cm<sup>2</sup> LbL thin film placed in a 6-well plate. These cells were incubated for 24h. Later, the LbL thin film was washed thrice with ice cold PBS and the cells were fixed using 4% paraformaldehyde and were permeabilized using 0.2% Triton X-100. Later, the film with cells was incubated in DAPI (1µg/ml) solution for 5min. A fluorescence microscope (Olympus Corporation Inc., Japan) was used to capture the micrographs of DAPI stained A431 cells adhered to the LbL thin film. DAPI was excited at 358nm wavelength and was observed using 40x objective lens. The images were captured using the Q-imaging system (Q-imaging, Canada).

#### 4.2.9. In-vivo studies in the mouse dermal wound model

Female C57BL/6 mice weighing 20-24g were procured from National Institute of Nutrition, Hyderabad, India, and the experiments were performed with approval from the

institutional animal ethics committee (IAEC). The mice were fed with the standard laboratory diet and were provided with a clean drinking water *ad libitum*.

The excision wounds were made after anaesthetizing the mice by an intraperitoneal injection of ketamine (100mg/kg) xylazine (10mg/kg) mixture. The hair on the dorsal side of mice was clipped and the skin was sterilized with 70% ethanol. A circular wound of 8mm diameter was made using a skin biopsy punch on the left side of the dorsal line. The mice weighing 20-24g were divided into four groups including the control group (without treatment), mice treated with blank film, povidone-iodine and PFD loaded LbL thin film. The povidone-iodine gel, blank film, PFD ointment and the PFD loaded LbL thin film were topically applied on the wounded area once a day for up to 12 days.

#### 4.2.10. Determination of the wound contraction area, total protein and collagen content

The wound contraction area was determined every day by tracing the wound on a transparent paper with a permanent marker. The recorded wound area was then measured with a calibrated scale. The percentage of wound contraction was calculated using Equation (14).

$$\text{Wound contraction (\%)} = \frac{\text{initial wound area} - \text{wound area after treatment}}{\text{initial wound area}} \times 100 \quad (14)$$

The skin tissue samples were collected after sacrificing mice at different time points including 0, 3, 6, 9 and 12<sup>th</sup> day. Then the skin samples were mixed with TRI reagent (1ml per 50mg of the tissue) and subjected to probe sonication. Then chloroform (0.2ml per 1ml of TRI reagent) was added to the homogenized tissue and allowed to stand for 15min at room temperature. Later, the mixture was centrifuged at 12000xg for 15min at 4°C. The organic layer of the mixture was then separated and isopropanol (1.5ml of isopropanol per 1ml of TRI reagent)

was added. The mixture was centrifuged at 12000xg for 15min. Finally, the protein pellet collected was lyophilized and stored at -80°C for further analysis.

The total protein estimation was carried out using the bicinchoninic acid assay (BCA) according to the manufacturer instructions (Promega, USA). For total protein determination, known amount of the protein sample was dissolved in 1% SDS and the BCA working reagent (200µl). These samples were incubated for 30min at 37°C and then the absorbance was recorded at 560nm wavelength (SpectraMax M4, Molecular Devices Inc., California, USA). The sample concentration was determined from the standard calibration curve (100-1000µg/ml concentration range;  $R^2 = 0.996$ ).

Collagen is an extracellular matrix component and a major substrate for matrix metalloproteinases (MMP). The main component of collagen is hydroxyproline. The collagen content in wounded and non-wounded skin samples can be analyzed by measuring hydroxyproline in the samples (Neuman & Logan, 1950). The total protein sample (2mg) was hydrolyzed by heating at 110°C after addition of 2ml of 6N HCl. The hydrolysate was neutralized to pH 7 using NaOH. Later, 0.01M copper sulphate (1 ml), 2.5N NaOH (1 ml) and 6% H<sub>2</sub>O<sub>2</sub> (1 ml) were added to the samples. The mixture was then incubated at 80°C for 5min while shaking. The samples were cooled and 4ml of 3N sulphuric acid was added. Finally, 2ml of 5% p-dimethylaminobenzaldehyde was added to the mixture and incubated at 70°C for 15min. The absorbance at 560nm was recorded for the samples using UV-visible spectrophotometer. The amount of hydroxyproline in the protein samples was calculated using a standard curve prepared using L-hydroxyproline in the range of 2 to 10ppm. Hydroxyproline concentration obtained was correlated to the collagen content in the skin using Equation 15 (Yariswamy et al., 2013).

$$\text{Collagen content} = \frac{\text{amount of hydroxyproline in the sample} \times 7.45}{\text{amount of sample}} \quad (15)$$

#### 4.2.11. TGF-beta protein analysis

Equal quantities of proteins were separated by SDS-PAGE gels and then transferred to nitrocellulose membrane at 4°C for 1h using transfer buffer. After transfer, nonspecific sites were blocked with 5% bovine serum albumin in Tris base–saline-tween (TBST, 20mM Tris, pH 7.5, 150mM NaCl and 0.1% Tween 20) for 1h at room temperature. Later, membranes were incubated overnight at 4°C with primary antibody against  $\beta$ -Actin mouse monoclonal IgG (Santa Cruz Biotechnology) and anti-human/mouse TGF-beta functional grade purified (eBioscience). After three 5min washing steps with TBST, the membranes were incubated with the horseradish peroxidase–conjugated (HRP) goat anti-mouse IgG (Santa Cruz) for 1h at room temperature. Later, the membranes were washed with TBST, specific antigen-antibody complexes were developed by using Super-Signal West pico (Thermoscientific) by transferring the blot in to enhanced chemiluminescence (ECL) substrate for 5 min. Place the blot onto the X-ray film in a cassette for 10min (exposure time depends on intensity of band) in a dark room. Then, blotted X-ray film was transferred to developer solution for 1min and stopper solution (0.3% acetic acid solution) for 30sec. Finally, it was transferred to fixer solution for 30sec and finally washed with water.



#### 4.2.12. Systemic absorption of the PFD after topical application

Female C57BL/6 mice weighing 20-24g were divided into two groups of 3 mice each. Group I included mice wounded using a biopsy punch as described above. Group II included mice without the dermal wounds. The PFD loaded LbL thin film (1 cm<sup>2</sup>) was topically applied on the wounded mice and mice without wounds. After application of the LbL thin film, blood samples (0.3 ml) were collected by puncturing the retro-orbital plexus at time intervals of 0.08, 0.25, 0.5, 1, 2, 3, 4, 5, 6, 7 and 8h. These blood samples were collected into 2ml sample collection tubes containing 3.8% w/v sodium citrate solution. The plasma samples were obtained after centrifugation at 5000rpm for 10min. The supernatant was then carefully collected and methanol was added at 2:1 ratio (methanol: plasma) to precipitate protein. These samples (50µl) were analyzed using the HPLC system as discussed above.

#### 4.2.13. Statistical analysis

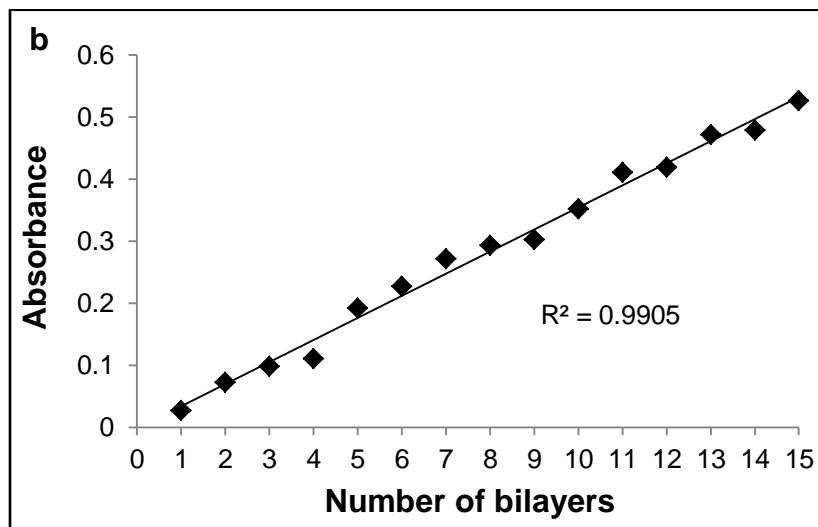
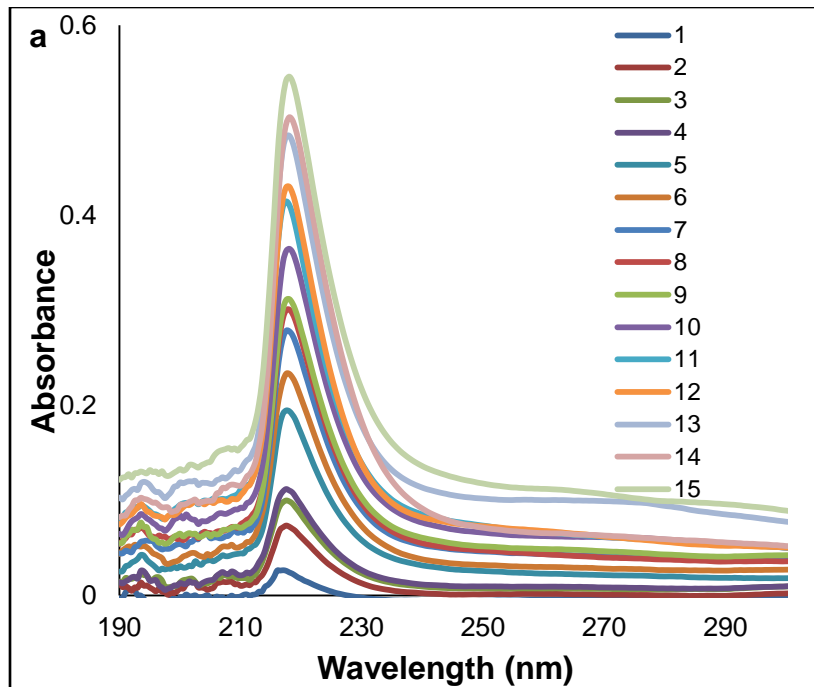
All the results were presented as mean  $\pm$  standard deviation. The significance between groups was determined by Student's t test or analysis of variance (Graphpad Prism, USA), where  $p < 0.05$  was considered to be significant.

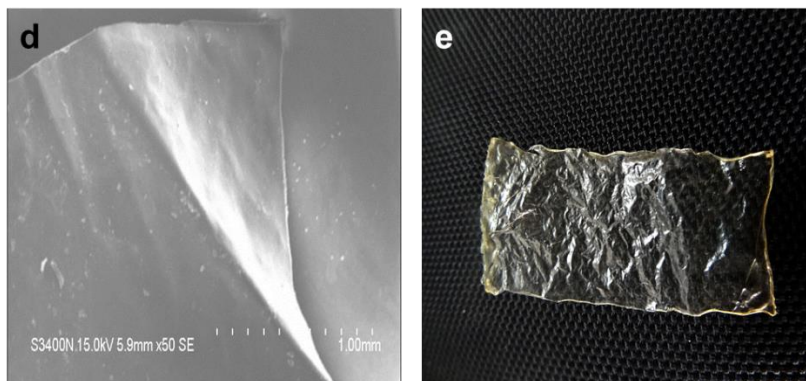
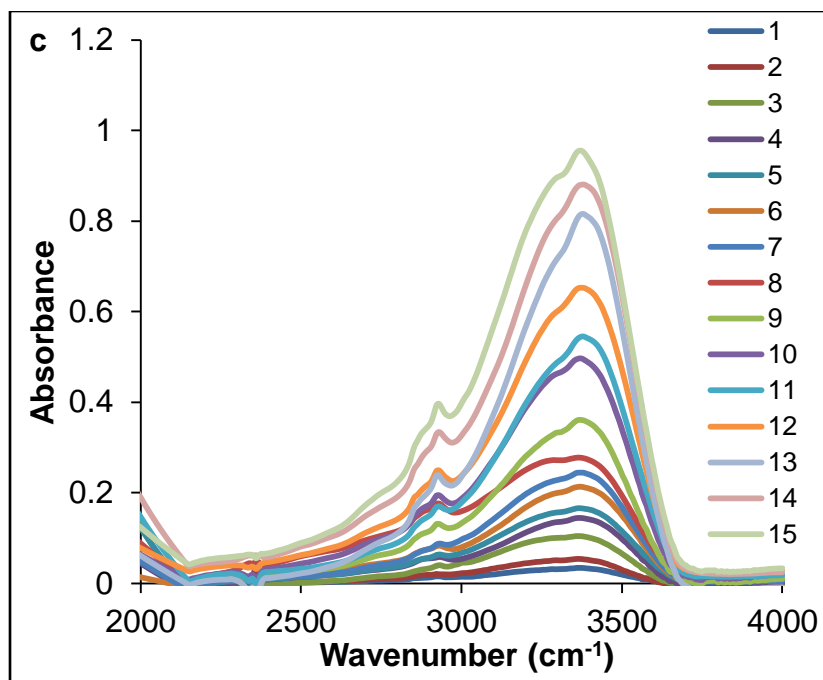
## 4.3. RESULTS

### 4.3.1. Characterization of the free and PFD loaded LbL thin films

The chitosan-sodium alginate LbL thin film formation was optimized for different pH conditions, ionic strength and concentration of polymer. The optimal pH for the LbL thin film formation was found to be 4 and 5 for chitosan and sodium alginate, respectively in the presence of 0.1M NaCl. The adsorption of polymers during the film growth was characterized by UV-visible spectrophotometer and FTIR.

Figure 4.2a shows representative UV-visible absorbance spectra of the LbL thin films recorded after adsorption of each bilayer. It was found that the increase in number of bilayers linearly ( $R^2=0.9905$ ) increased the absorbance at 220nm wavelength (Fig. 4.2b). Figure 4.2c shows representative FTIR spectra of the LbL thin films acquired after adsorption of each bilayer. The broad peak observed at 3000-3500  $\text{cm}^{-1}$  wavenumber represents N-H stretch of chitosan and O-H stretch of sodium alginate. The absorbance at this wavenumber increased with the increase in number of bilayers. The UV-visible spectroscopy and FTIR results confirmed the adsorption of polymers and the growth of LbL thin film.





**Fig. 4.2.** Characterization of LbL assembly and thin films. a. UV-absorbance spectra of the LbL thin films with the increase in number of bilayers. The LbL thin films were dissolved in 0.1N NaOH before recording the spectra. b. Increase in the UV-absorbance of LbL thin films at 220 nm wavelength with the increase number of bilayers. c. FTIR spectra of the LbL thin films with the increase in number of bilayers. d. Scanning electron microscopic image of the chitosan-alginate free standing LbL thin film. e. Digital photograph of the LbL thin film. Images were representative of at least three different experiments.

#### 4.3.1.1. Physical characterization of the LbL thin films

The average thickness of the films was found to be  $15 \pm 2\mu\text{m}$  as measured by digital micrometer. The scanning electron microscopic image and a digital image of the LbL thin film showed an uniform and smooth surface (Fig. 4.2d, e).

The porosity of films was determined by alcohol displacement method. The LbL thin film showed porosity of <50% of the total film volume (Table 4.1). Further, degree of swelling was studied by measuring the difference in weight of the film before and after incubation in PBS. The LbL films showed a percentage swelling ratio of  $32 \pm 3.21$  (Table 4.1).

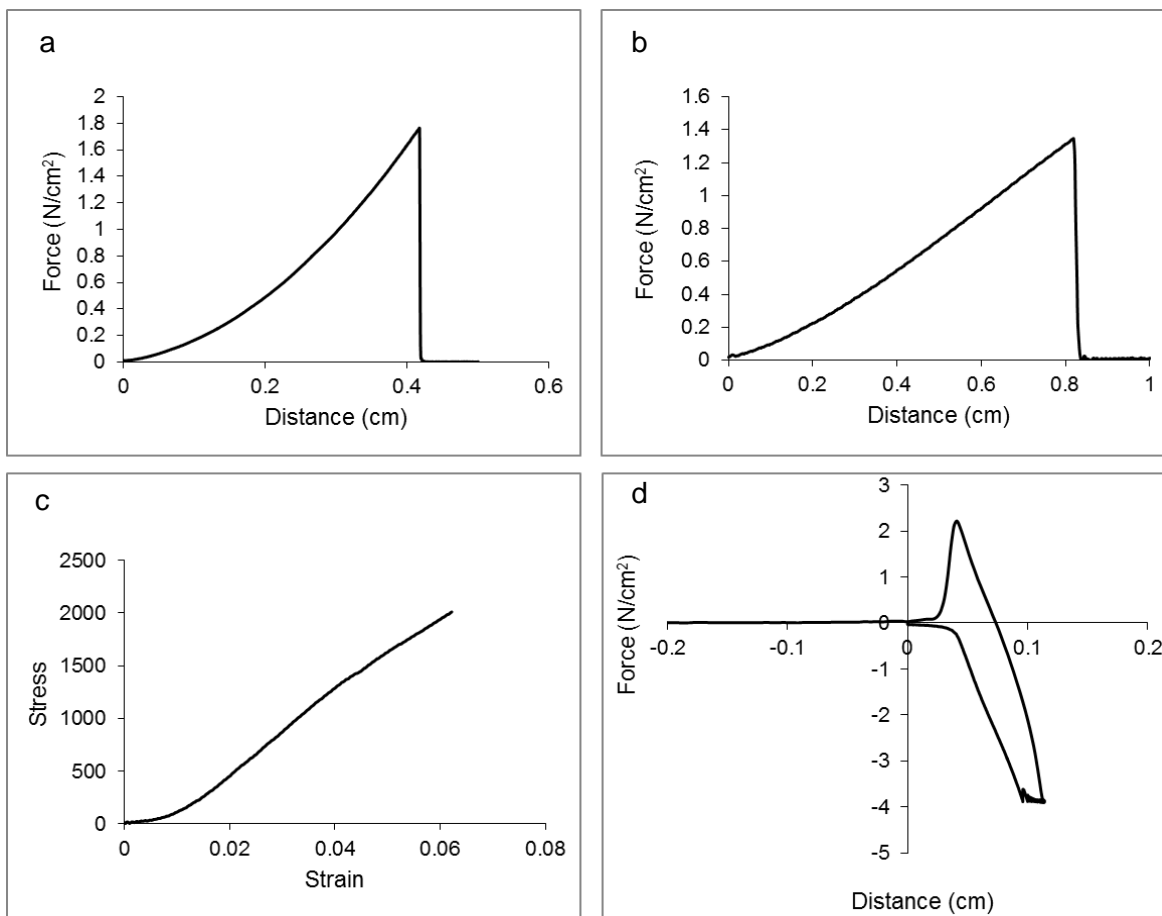
#### 4.3.1.2. Mechanical properties of LbL thin films

The results from texture analyzer showed average burst strength of  $1.76 \pm 0.098 \text{ N/cm}^2$  and an average distance to burst of  $0.41 \pm 0.076 \text{ cm}$ . The tensile strength, elongation and Young's modulus were found to be  $1.30 \pm 0.10 \text{ N/cm}^2$ ,  $3.56 \pm 0.26\%$  and  $39.6 \pm 3.2 \text{ N/cm}^2$  for the LbL thin films. The skin adhesion strength of the LbL thin film was found to be  $2.22 \pm 0.08 \text{ N/cm}^2$  and the work of adhesion was found to be  $0.37 \pm 0.04 \text{ N/cm}^2$  (Fig. 4.3).

**Table 4.1.** Physical and mechanical characteristics of LbL thin films.

<b>Parameter</b>	<b>Value</b>
<b>Thickness (<math>\mu\text{m}</math>)</b>	$15 \pm 1.00$
<b>Porosity (%)</b>	$27 \pm 5.2$
<b>Swelling index (%)</b>	$32 \pm 3.2$
<b>Burst strength (<math>\text{N/cm}^2</math>)</b>	$1.1 \pm 0.09$
<b>Tensile strength (<math>\text{N/cm}^2</math>)</b>	$1.30 \pm 0.1$
<b>Youngs modulus (<math>\text{N/cm}^2</math>)</b>	$39.6 \pm 3.2$
<b>Elongation (%)</b>	$3.56 \pm 0.2$
<b>Adhesion strength (<math>\text{N/cm}^2</math>)</b>	$2.22 \pm 0.08$
<b>Work of adhesion (<math>\text{N/cm}^2</math>)</b>	$0.37 \pm 0.04$

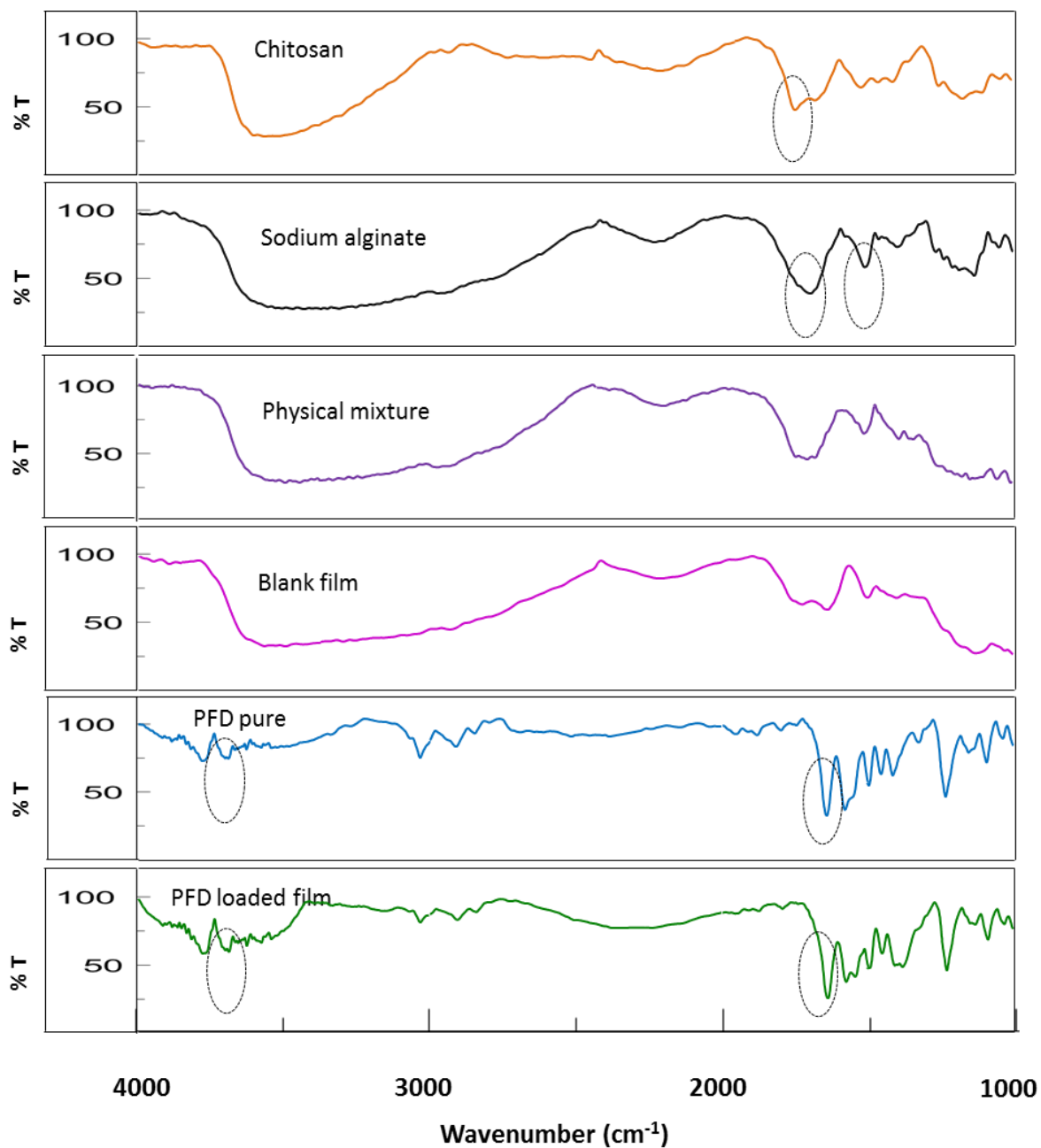
Data are presented as mean ( $n = 3$ )  $\pm$  SD.



**Fig. 4.3.** Representative graphs of the burst strength (a), tensile strength (b), stress-strain curve (c) and mouse skin adhesion strength (d) of LbL thin film.

The PFD loaded LbL thin films were characterized using the HPLC, FTIR and differential scanning calorimeter. The amount of PFD present in the LbL thin film and ointment was found to be  $1.0 \pm 0.1 \text{ mg/cm}^2$  of the film and  $1.0 \pm 0.2 \text{ mg}$  per  $50 \text{ mg}$  of ointment respectively.

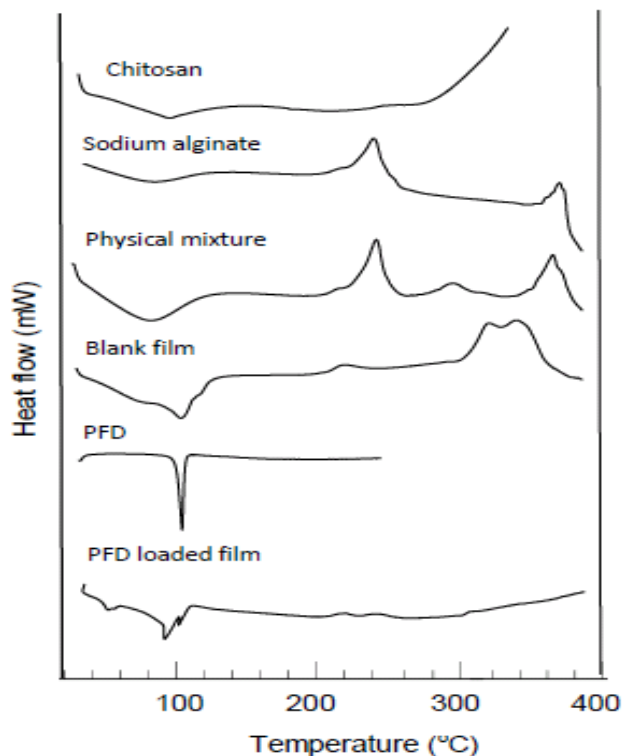
Figure 4.4 shows the FTIR spectra of free chitosan, sodium alginate, PFD, physical mixture of free PFD and film, blank film and the PFD loaded LbL thin film. The characteristic peaks for SA at  $3412 \text{ cm}^{-1}$  wavenumber corresponds to O-H stretch, peaks at  $1615 \text{ cm}^{-1}$  and  $1417 \text{ cm}^{-1}$  wavenumbers are attributed to C-O asymmetric and symmetric stretch respectively. Similarly, for CS, the characteristic peaks were found to be  $3550 \text{ cm}^{-1}$  for N-H stretch,  $1663 \text{ cm}^{-1}$  for C=O stretch of amide bond,  $1584 \text{ cm}^{-1}$  for N-H bending and  $1419 \text{ cm}^{-1}$  for C-H bending. Free PFD showed the characteristic peaks of aromatic C-H stretch and C=O stretch at  $3048 \text{ cm}^{-1}$  and  $1673 \text{ cm}^{-1}$  wavenumbers. The characteristic peaks of the polymers and PFD shifted after LbL thin film formation and PFD entrapment. For chitosan, the peak shift was observed for N-H stretch ( $3458 \text{ cm}^{-1}$ ) and N-H bending ( $1579 \text{ cm}^{-1}$ ). For sodium alginate, the peak shift was observed for the carboxylate group ( $1425 \text{ cm}^{-1}$ ). For PFD, the peak shift was observed for the aromatic C-H stretch ( $3046 \text{ cm}^{-1}$ ).



**Fig. 4.4.** A representative FTIR spectra of neat CS, SA and PFD, physical mixture, blank film and PFD loaded film.



Figure 4.5 shows the DSC thermograms acquired for free chitosan, sodium alginate, PFD, and PFD loaded LbL thin film. The DSC thermogram of sodium alginate showed the thermal transitions for dehydration (100°C), decomposition of biopolymer (249.7°C) and decomposition of carbonaceous material (385°C). For chitosan, the thermal transitions observed were glass transition ( $T_g$ , 90.3°C) and melting endotherm ( $T_m$ , 263°C). Free PFD showed its characteristic melting temperature ( $T_m$ ) at 107.6°C. It was found that the thermal transitions of neat chitosan, sodium alginate and PFD shifted after preparation of the LbL thin films. The PFD loaded film showed a shift in the melting temperature of PFD from 107.6°C to 102.9°C before and after entrapment respectively.

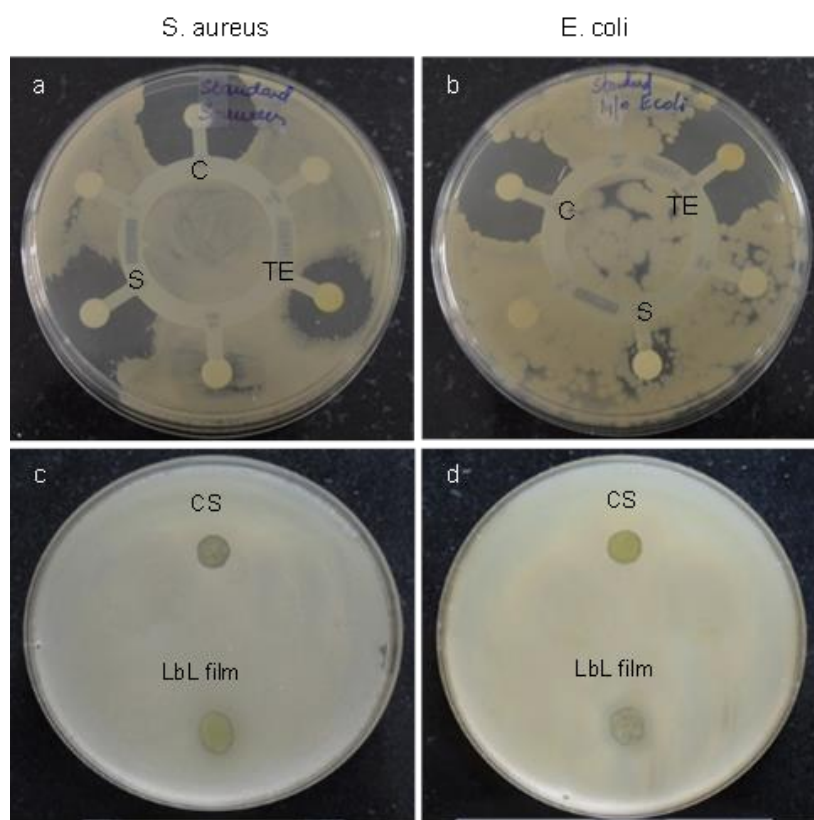


**Fig. 4.5.** A representative thermograms of neat CS, SA, physical mixture, blank film, PFD and PFD loaded film.

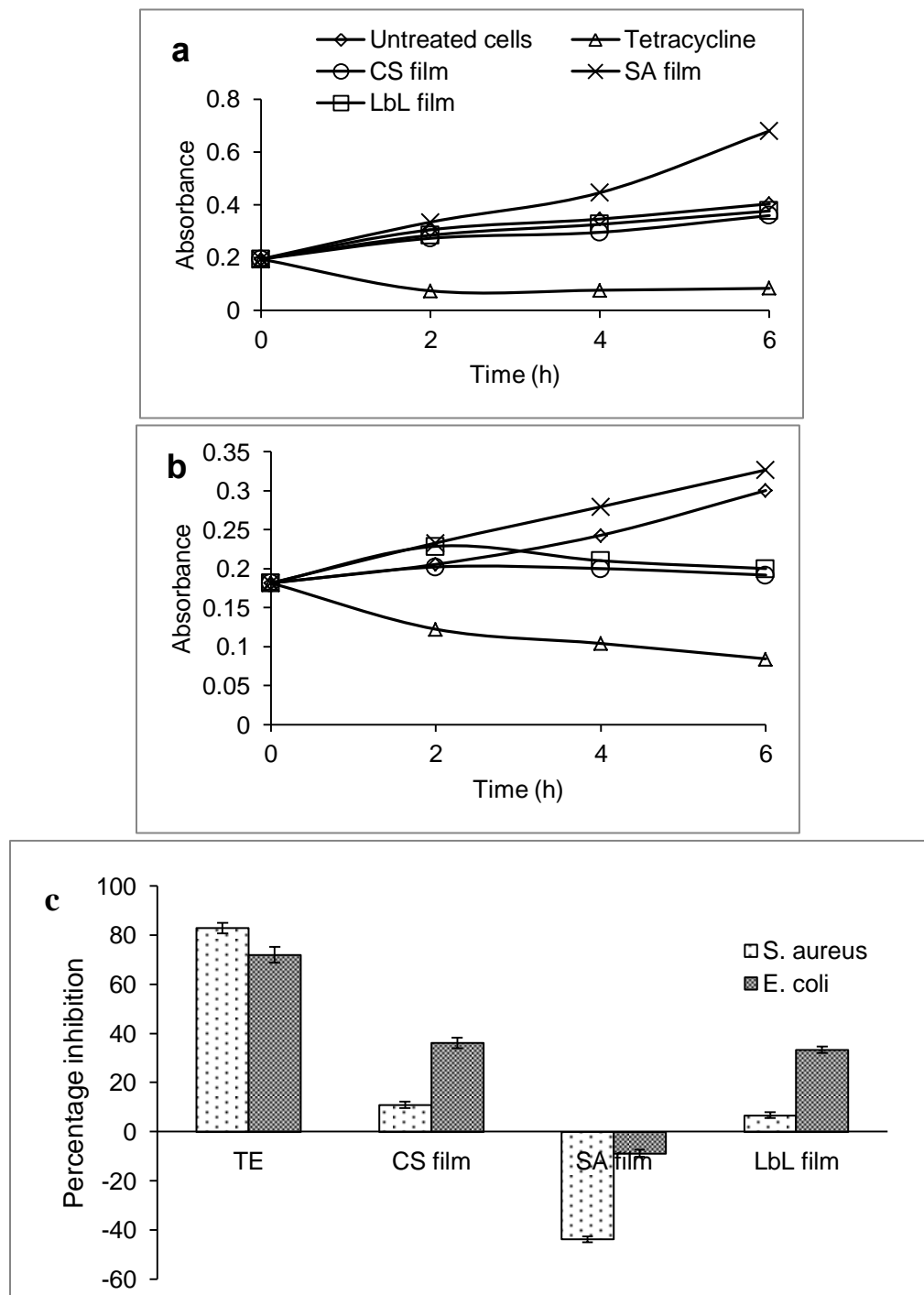
#### 4.3.2. Antibacterial activity of LbL thin films

The antimicrobial activity of polymer films was investigated against *E. coli* and *S. aureus*. Fig. 4.6 shows the zone of inhibition after incubation of CS, SA and LbL films and correlated with standard antibiotic disc. The standards, chloramphenicol, streptomycin and tetracycline showed zone of inhibition of  $1.2\pm 0.2$ cm,  $0.9\pm 0.1$ cm,  $0.8\pm 0.2$ cm against *S. aureus* and  $1\pm 0.2$ cm,  $0.1\pm 0.02$ cm,  $1.1\pm 0.3$ cm against *E. coli*, respectively (Fig. 4.6a and 4.6b). The LbL films showed clear zone of inhibition of  $0.1\pm 0.01$ cm and  $0.1\pm 0.02$ cm against both *S. aureus* and *E. coli*, respectively (Fig. 4.6c and 4.6d).

The bacterial growth kinetics in the presence of CS, SA and LbL films was studied by measuring the optical density of bacterial cell suspension. The bacterial growth in the presence of CS and LbL films was significantly ( $p < 0.05$ ) less at all-time points in comparison with untreated cells. However, in the presence of tetracycline, the growth was significantly ( $p < 0.05$ ) decreased after 2h and plateaued off at subsequent time points. Fig. 4.7 shows growth kinetics of *S. aureus* and *E. coli* up to 6 h. Figure 4.7c shows the percentage growth inhibition by polymer films after 6h incubation. The positive controls of tetracycline showed a growth inhibition of  $82.8\pm 2.14\%$  and  $71.9\pm 3.27\%$  for *S. aureus* and *E. coli*, respectively. The CS film and LbL films showed  $10.9\pm 1.23\%$ ,  $6.6\pm 1.23\%$  and  $36.1\pm 2.21\%$ ,  $33.3\pm 1.32\%$  growth inhibition against *E. coli* and *S. aureus*, respectively. Sodium alginate did not show growth inhibition against both the bacterial strains.



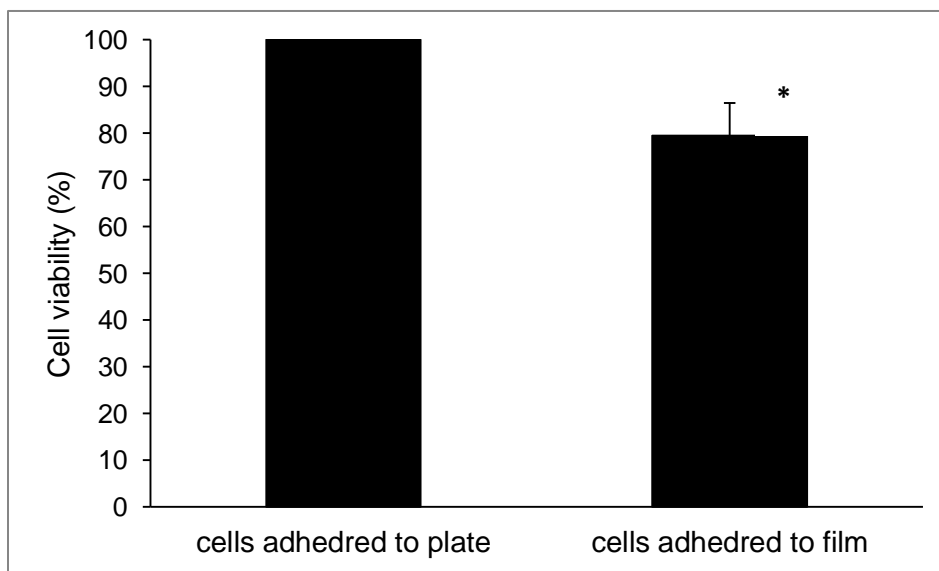
**Fig. 4.6.** Photographs of bacterial zone of inhibition method after incubation with tetracycline (TE), chloramphenicol (C) and streptomycin (S) (a, b) and CS and LbL thin film (c, d) for *S. aureus* (a, c) and *E. coli* (b, d).



**Fig. 4.7.** Growth curves of *S. aureus* ( a) and *E. coli* (b) in the presence of controls, CS, SA and LbL thin films at different time points, (c) Percentage growth inhibition for *S. aureus* and *E. coli* in the presence of tetracyclin (TE), CS, SA, LbL films.

#### 4.3.3. Cell viability in the presence of LbL thin film

Fig. 4.8 showed the percentage cell viability as determined by MTT assay after 24h incubation. It was found that, the cell viability was  $86.2 \pm 0.8\%$  for A431 cells cultured on LbL thin film compared with cells cultured in poly-lysine coated plate.

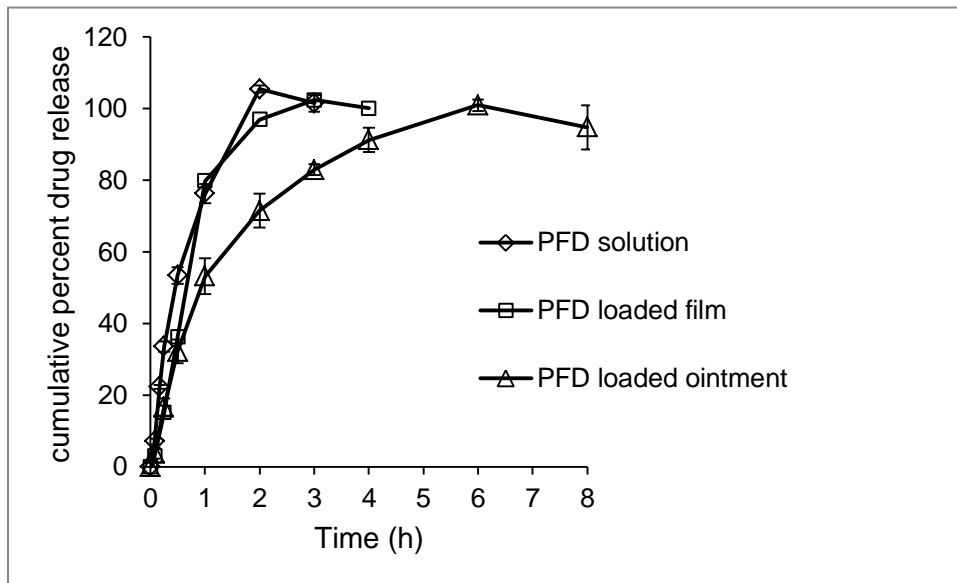


**Fig. 4.8.** A431 cell viability in the presence of LbL thin film. Data was presented as mean (n=4)  $\pm$  SD. \* represents significance between groups at  $P < 0.05$ .

#### 4.3.4. PFD release from the LbL thin film

The release of PFD from the LbL thin film and ointment was compared with diffusion of free PFD through dialysis membrane. The PFD solution showed rapid diffusion across the dialysis membrane and 100% release was achieved within 2h. Whereas, PFD release from the

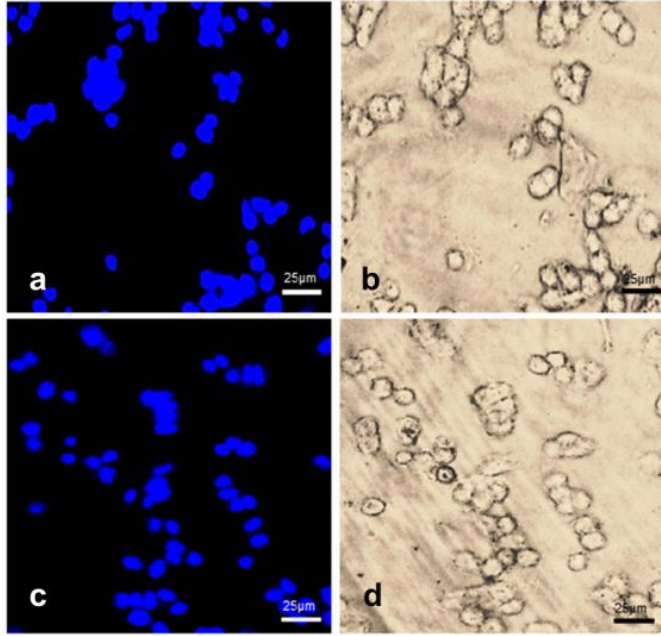
LbL thin film and ointment was slower and released completely in 3h and 6h respectively (Fig. 4.9).



**Fig. 4.9.** Cumulative percent release of pirfenidone in PBS from LbL film and ointment.

#### 4.3.5. A431 cell adhesion of the LbL thin film

The compatibility of the chitosan-sodium alginate LbL thin film with cells was studied using human epidermoid carcinoma cells (A431). Figure 4.10 shows the fluorescence and bright field images of the cells adhered to the films with chitosan surface and sodium alginate surface. The image analysis showed an average of  $3.75 \times 10^3$  cells/mm<sup>2</sup> and  $4.61 \times 10^3$  cells/mm<sup>2</sup> adhered to the chitosan and sodium alginate surfaces of the LbL thin films respectively.



**Fig. 4.10.** Fluorescence micrographs of A431 cell adhesion of the chitosan-alginate LbL thin film. ‘a’ and ‘b’ shows the fluorescence and bright field images of A431 cells adhered to the sodium alginate surface of LbL thin film respectively; ‘c’ and ‘d’ represents the fluorescence and bright field images of A431 cells adhered to the chitosan surface of LbL thin film. DAPI was used to stain cell nucleus. Scale bar represents 25  $\mu\text{m}$ .

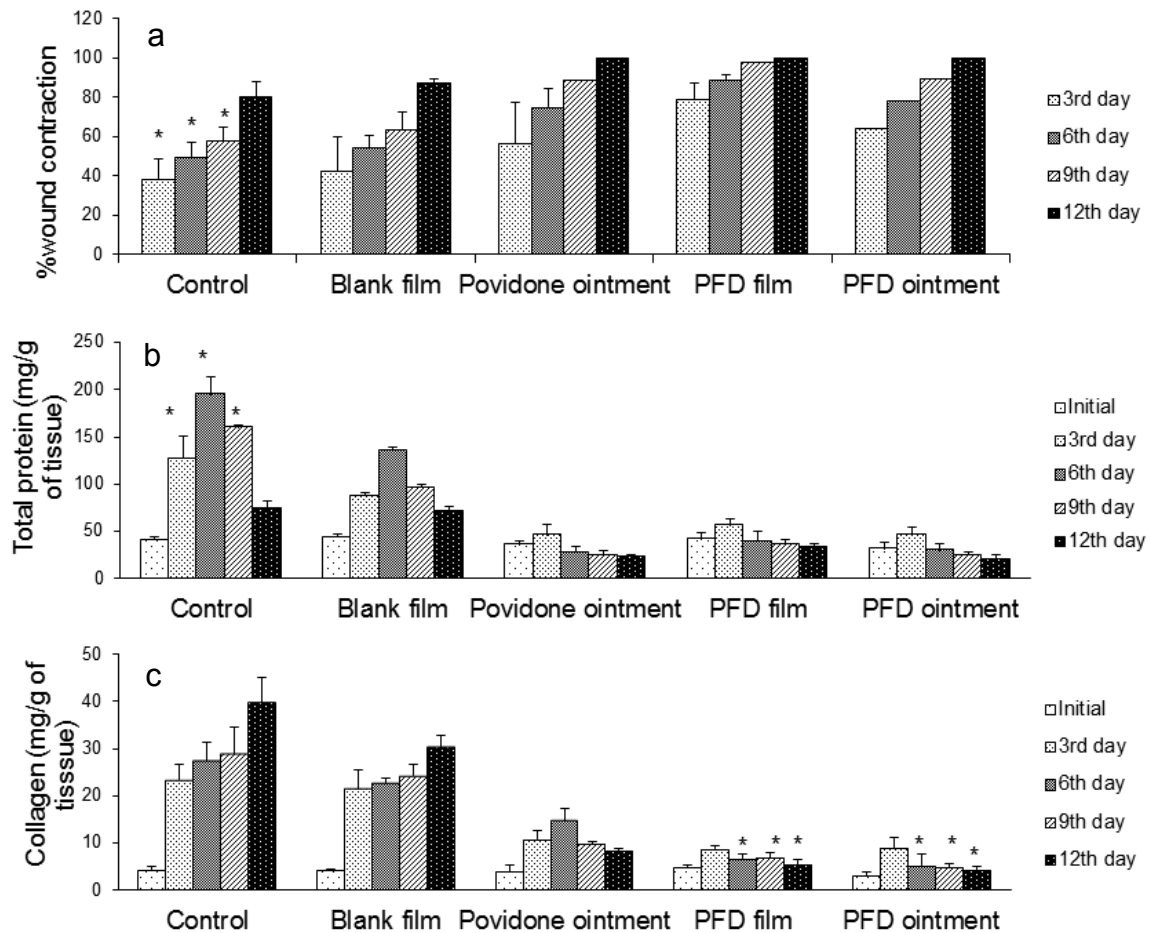
#### 4.3.6. Wound contraction and collagen expression after topical application of the PFD loaded LbL thin film

Fig. 4.11a shows the percentage of wound contraction in the control (without any treatment), and after treatment with povidone-iodine ointment, blank film, PFD ointment and PFD loaded LbL thin film. There was a significant difference in the percentage of wound contraction between the control and all treatment groups. The wound contraction was faster (<9 days) after application of PFD ointment and PFD loaded LbL thin film compared with the commercial povidone-iodine ointment (12 days), blank film and without any treatment (12 days). Fig. 4.12 shows a representative image of wound site and reepithelialization at different time points.

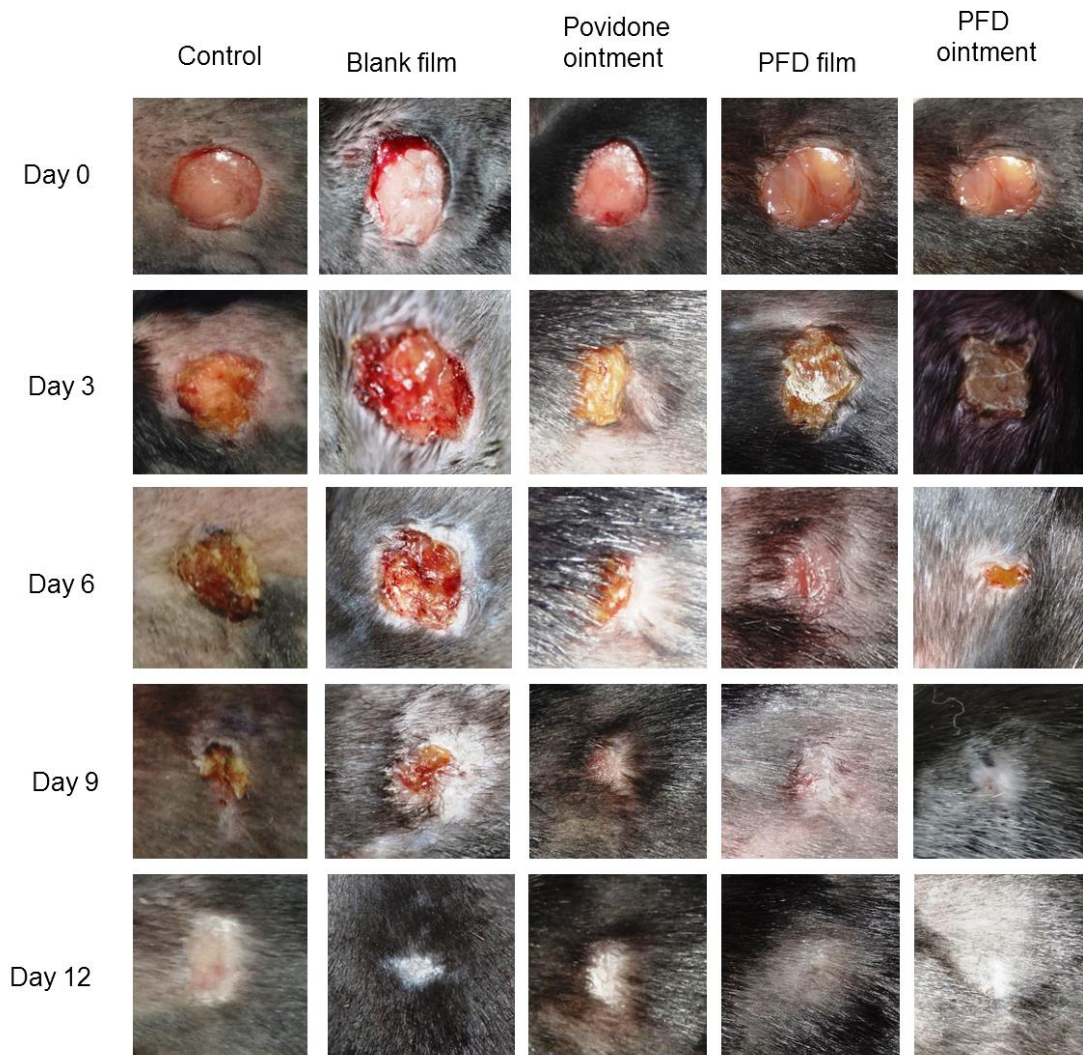
The total protein content within the wound site was measured for all the treatment groups. The total protein content was found to be significantly higher for the control group at all-time points measured compared with groups treated with the povidone-iodine, blank film and PFD loaded LbL thin films (Fig. 4.11b). The total protein content did not significantly change for mice treated with the PFD ointment and PFD loaded LbL thin film at all-time points. On the other hand, the total protein content decreased by 1.5-fold after povidone-iodine application on 12<sup>th</sup> day compared to corresponding 0<sup>th</sup> day (Fig. 4.11b).

Figure 4.11c shows the amount of collagen in the wound tissue at different time points. It was found that the collagen content increased with time in control group and blank film treated group. On the other hand, mice treated with the povidone-iodine and PFD loaded LbL thin films showed a lesser increase in collagen content before decreasing to the amounts present at zero-time point. The ratio of amount of collagen on 12<sup>th</sup> day to 0<sup>th</sup> day was 9.2, 2.1, 7.0, 1.3 and 1.1 for the control, povidone-iodine, blank film, PFD ointment and PFD loaded LbL thin film treatment groups, respectively. Among the treatment groups, the PFD loaded LbL thin films showed a lesser collagen content at all-time points. After 12 days, the collagen content was found to be  $5.45 \pm 1.07\text{mg/g}$  for PFD loaded film treated group,  $4.35 \pm 0.83\text{mg/g}$  tissue for the PFD ointment treated group, while it was  $8.27 \pm 0.67\text{mg/g}$  tissue for povidone-iodine treated group,  $30.25 \pm 2.56\text{mg/g}$  tissue for blank film treated group and  $39.63 \pm 5.39\text{mg/g}$  tissue for control group, respectively.





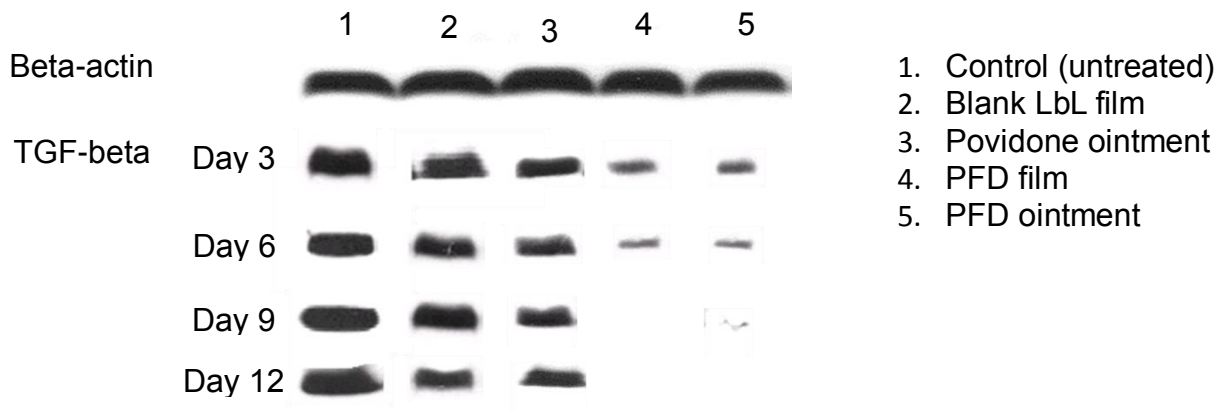
**Fig. 4.11.** Effect of topical application of the blank LbL thin film, mice treated PFD loaded LbL thin film, PFD ointment and povidone ointment on wound contraction (a), total protein (b) and collagen content (c) compared with control (without any treatment). Data were presented as mean (n=4)  $\pm$  standard deviation. \*represents that the values are significantly different at  $p < 0.05$ .



**Fig. 4.12.** Digital photographs of excisional wounds on day 0, 3, 6, 9 and 12 after topical application of the blank LbL thin film, mice treated PFD loaded LbL thin film, PFD ointment and povidone ointment.

#### 4.3.7. TGF-beta protein analysis

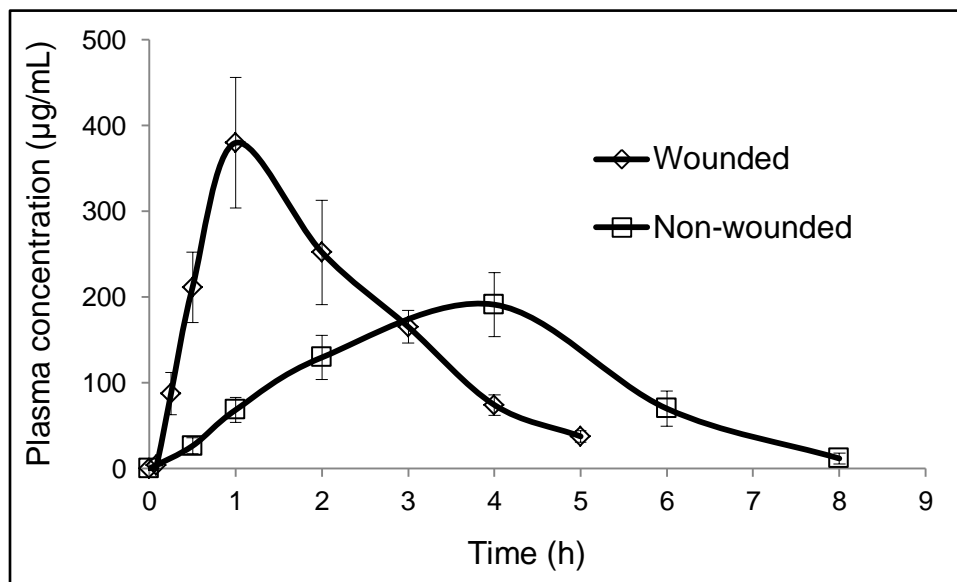
Collagen is an important marker of fibrosis and expression is enhanced in fibrotic process under the influence of highly up-regulated cytokine, TGF-beta with the suppression of collagenase production and activity. Our western blot analysis results showed expression of TGF-beta was increased in the fibrotic process for controls (without any treatment) group, blank thin film and povidone ointment groups. On the other hand, PFD loaded thin film and PFD ointment treated groups showed gradual decrease in TGF-beta expression. PFD loaded thin film treated group showed 50, 66.7, 96.6 and 99.2% inhibition and PFD ointment treated group showed 45.6, 74.5, 92.3 and 99.4% TGF-beta inhibition after 3, 6, 9 and 12<sup>th</sup> day respectively (Fig. 4.13).



**Fig. 4.13.** Western blot analysis of TGF-beta protein expression in skin samples after PFD treatment.

#### 4.3.8. Systemic absorption of PFD after topical application

Fig. 4.14 shows the plasma concentration – time profile of PFD after topical application on wounded and non-wounded site using the LbL thin films. The pharmacokinetic parameters calculated were presented in Table 4.2. The maximum plasma concentration ( $C_{max}$ ) of PFD was significantly ( $p < 0.05$ ) higher after application in the wounded ( $379.9 \pm 76.3 \mu\text{g}$ ) mice in comparison with non-wounded mice ( $191.2 \pm 37.3 \mu\text{g}$ ). The time of maximum plasma concentration ( $T_{max}$ ) was higher for the non-wounded mice (4h) compared with wounded mice (1h). The total amount of PFD bioavailable (AUC) was  $950 \pm 84$  and  $811 \pm 161 \mu\text{g/ml}\cdot\text{h}$  after application on the wounded and non-wounded mice, respectively.



**Fig. 4.14.** The plasma concentration – time profile of PFD in the wounded and non-wounded C57BL/6 mice after topical application of the PFD loaded LbL thin film. Data were presented as mean ( $n=3$ )  $\pm$  standard deviation.

**Table 4.2.** Pharmacokinetic parameters calculated after topical application of PFD loaded LbL thin film.

<b>Parameter</b>	<b>Wounded model</b>	<b>Non-wounded model</b>
<b>Elimination rate constant (<math>\text{h}^{-1}</math>)</b>	$0.686 \pm 0.097$	$0.718 \pm 0.132$
<b><math>t_{1/2}</math> (h)</b>	$1.024 \pm 0.156$	$0.984 \pm 0.164$
<b><math>T_{\max}</math> (h)</b>	$1.00 \pm 0.00$	$4.00 \pm 0.00$
<b><math>C_{\max}</math> (<math>\mu\text{g}/\text{mL}</math>)</b>	$380 \pm 76.3$	$191 \pm 37.3$
<b><math>\text{AUC}_{0-\text{inf\_obs}}</math> (<math>\mu\text{g}/\text{mL} \cdot \text{h}</math>)</b>	$950 \pm 84.1$	$811 \pm 161.7$
<b><math>\text{MRT}_{0-\text{inf\_obs}}</math> (h)</b>	$2.20 \pm 0.145$	$3.78 \pm 0.113$

#### 4.4. DISCUSSION

Chitosan and sodium alginate are obtained from the natural sources of chitin and algae kelp (D'Ayala et al., 2008). Both the polymers are known to be biocompatible and biodegradable, and sodium alginate has been classified as generally recognized as safe (GRAS) (George & Abraham, 2006). The chitosan and sodium alginate have been investigated as wound dressing material and were approved for clinical use (Ilium, 1998; Jayakumar et al., 2011; Paul & Sharma, 2004). Chemically, the amine functionalities in the chitosan and carboxylate in the alginate would allow fabrication of the LbL thin film through their electrostatic interactions. These hydrophilic polymers show high aqueous solubility in free form (George & Abraham, 2006). However, the chitosan-alginate LbL thin film was stable in aqueous medium for at least five days. The stability of these LbL thin films has been attributed to their electrostatic interactions, hydrogen bonding and other weaker van der Waal's interactions (Carneiro-da-Cunha et al., 2010). The important physical properties of thin films for topical application include tensile strength and adhesive strength. The tensile strength of the chitosan-alginate LbL thin films was found to be similar to the reported studies (Silva et al., 2014). Furthermore, adhesion of the LbL thin film to the skin tissue contributes to their user compliance. Chitosan which is the outer layer of our LbL thin film is cationic and is known to possess muco-adhesion properties (Lehr et al., 1992). This adhesion to skin tissue could be attributed to interaction of primary and tertiary amine functionalities of chitosan with negatively charged skin surface. Moreover, the moistness of wound bed would enhance the adhesiveness of the polymer films.

As the hydrophilic polymers upon layering would develop hydrophobic regions within the layers, these films are suitable for loading both the hydrophilic and hydrophobic small molecules. However, only a few studies were reported on the potential of small molecule

entrapment in the LbL thin films (Susan & Christopher, 2004; Smith et al., 2009). PFD shows optimal lipophilicity with the log partition coefficient of 2.14. Traditionally, small molecule drugs are loaded in the LbL thin films by two different strategies, incubation of the preformed LbL thin films in drug solution or layering of charged drug molecules within the LbL thin films. In the present study, we reported entrapment of PFD within the matrix of chitosan and alginate which in turn was layered to produce films. PFD is a neutral molecule with one hydrogen bond acceptor and three hydrophobic interacting groups (determined using Schrodinger molecular modeling software, Schrodinger, Cambridge, USA). Therefore, PFD could be physically entrapped within the polymer layers with possible weaker molecular interactions. The greatest concentration in a traditional transdermal patch is  $5 \text{ mg/cm}^2$  for lidocaine transdermal system (Prausnitz et al., 2004). Here we have obtained  $1 \text{ mg/cm}^2$  of PFD in the LbL thin film. Furthermore, PFD release from the LbL thin films shows a diffusion controlled release mechanism which is a simple mechanism for modelling and prediction of drug release.

The potential application of a biodegradable, transparent, flexible, stable and drug loaded thin film is management of cutaneous wounds. Within a few days of dermal injury, the wound site is infiltrated with diverse immune cells including the neutrophils and macrophages (Sabine et al., 2007). This leads to inflammation at the wound site. Therefore the topically applied formulation is required to be non-irritating and non-immunogenic, and protect the wound site from extraneous contaminants. The human epidermoid carcinoma cells showed compatibility to the chitosan and alginate surfaced LbL thin films. The films can be used for cell adherence and as a scaffold for tissue culture (Hidalgo-Bastida et al., 2007). These films prepared using different polymers have been showed to be compatible with fibroblast and osteoblast cells, where the membranes were proposed to be used as scaffolds (Dhandayuthapani et al., 2011;

Vandrovcova & Bacakova, 2011). The cells were found to adhere to the polymer films and proliferate (Caridade et al., 2013). However, the nature of interactions between the polymers and cells, and the influence of polymer properties on their cell adhesion is an important area yet to be investigated.

Dermal wounds often show excess healing manifested as scar tissue formation (Tuan & Nichter, 1998). This is attributed to an increased production of the extracellular matrix components such as collagen by dermal fibroblast cells (Werner & Grose, 2003). TGF-beta is an important cytokine overexpressed at the wound site during wound contraction and remodeling stage of healing process (Pakyari et al., 2013). The PFD is a TGF-beta inhibitor investigated for its anti-inflammatory and anti-fibrotic properties. While PFD was approved for clinical use against idiopathic pulmonary fibrosis, it is being studied for treatment of renal, hepatic and ocular fibrosis ((Taniguchi et al., 2010; García et al., 2002; Cho & Kopp, 2010; Chowdhury et al., 2013). On the other hand, there were no reports investigating the efficacy of PFD in dermal wound healing. The therapeutics clinically approved for the dermal wound management include passive products (gauze and tulle dressings), interactive products (polymeric films and foams) and bioactive products (dressings constructed from materials with endogenous activity including proteoglycans, collagen, alginates or chitosan) (30). These products are expected to improve the wound healing through occlusive effect, where the dressing is permeable to water vapor and oxygen but impermeable to bacteria. However, these were not effective in controlling the collagen production resulting in the scar tissue formation. On the other hand, there were no marketed TGF-beta inhibitors for topical application in dermal injury. Therefore, PFD is explored for the dermal wound healing using LbL thin films. Our western blot results demonstrate that pirfenidone reduced TGF-beta expression. This further resulted in reduced



collagen expression, resulting in favorable healing process. Pirfenidone was previously shown to reduce TGF-beta secretion, expression of collagen contraction in cardiac fibroblasts and collagen expression induced by TGF-beta in human alveolar epithelial cell line. The skin absorption studies after the application of PFD loaded LbL thin films in the wounded and non-wounded skin showed that PFD is rapidly absorbed into blood circulation. Therefore the effect of PFD in reducing the total protein and collagen content was because of a combination of PFD in blood circulation and in the local skin tissue. The results also suggested that PFD can be delivered using the thin films for systemic application across intact skin. Overall, we have improved the dermal wound healing by reducing the collagen content using the PFD loaded LbL thin films.

#### **4.5. CONCLUSION**

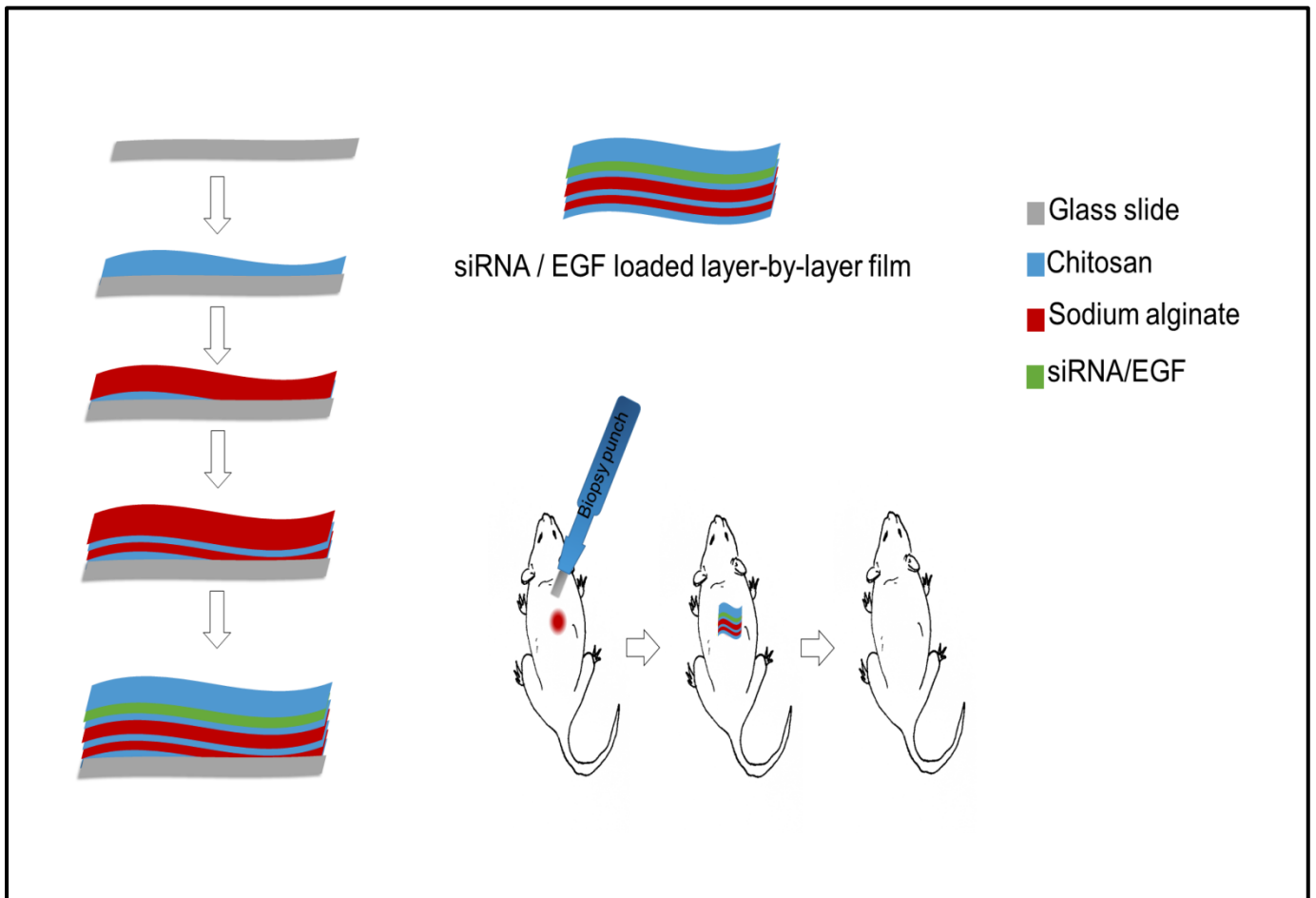
The layer-by-layer thin films can be prepared using biodegradable charged polymers of chitosan and sodium alginate. The chitosan-sodium alginate LbL thin films are stable and possess skin adhesion property. PFD can be entrapped within the LbL thin films at high loading efficiency and PFD shows a diffusion controlled release mechanism. PFD is rapidly absorbed into the systemic circulation after topical application using the LbL thin films on wounded site. The PFD loaded LbL thin films accelerated wound healing while decreasing collagen production.

# Chapter 5

## Layer-by-layer thin films for macromolecule delivery

---

# Graphical abstract



Schematic representation of layer-by-layer thin films loaded with macromolecule for wound management

## 5.1. INTRODUCTION

Layer-by-layer (LbL) assembly is a promising method that has been successfully demonstrated for the topical delivery of biologic therapeutics and biomolecules (Hammond, 2012; Jewell and Lynn, 2008; Shah et al., 2012; Shukla et al., 2012). LbL is the sequential adsorption of oppositely charged polyelectrolytes onto charged substrate via electrostatic, hydrogen bonding, or other complementary interactions (Detzel et al., 2011; Zelikin et al., 2010). Polyelectrolytes of interest can be uniformly coated on a surface with alternate interactions to generate nanometer-scale thin films that can deliver various small molecule drugs, proteins (eg. growth factors), and nucleic acids (DNA and RNA) (Shukla et al., 2010; Shah et al., 2012; Zhao et al., 2012). In the present study, we aimed to assess the potential of self-assembled layer-by-layer thin films for co-delivery of small or short interfering ribonucleic acid (siRNA) and epidermal growth factor (EGF). To test the feasibility of this strategy, we chose to target mouse dermal wound healing as a model.

Dermal injuries are commonly caused by the accidental cuts, burns, diabetic ulcers among others. Macromolecules present in the wound site can trap growth factors within fibrin cuffs in the surrounding capillaries or bind them to ECM. As a result, deficiency of growth factors and cell cycle arrest occurs that leads to delay in wound healing (Higley et al., 1995; Walker, 1999). Hence, it is necessary to provide growth factors either autogenously or externally to accelerate wound healing process. Dermal wounds often result in the scar tissue formation attributed to excessive production of the extracellular matrix components including collagen. TGF-beta is a pro-inflammatory cytokine which is over-expressed at the site of tissue injury. TGF-beta induces the proliferation of fibroblast cells leading to excess

production of collagen. Previous reports showed that the inhibition of TGF-beta controlled wound healing process, resulting in a lesser scar tissue formation (Wang et al., 2014).

Epidermal growth factor (EGF) belongs to a family of growth factors that regulate cell proliferation, migration, and differentiation through binding to receptor kinases on target cells. EGF stimulates the proliferation of various cells, including glial cells, fibroblasts, and keratinocytes results in accelerated re-epithelialization (Vijay et al., 2006; Zieske et al., 2000; Song et al., 2001; Fu-Shin et al., 2010).

RNA interference (RNAi) is one of the important and widely used gene silencing technique for the treatment of various diseases. siRNA mediate the degradation of complementary mRNA, which results in a specific silencing of gene expression. This approach induces gene silencing at a posttranscriptional level and is more specific, reliable and efficient method (Rana, 2007). The limitations associated with siRNA delivery include short half-life and non-target effects (Ballarín-González and Howard, 2012; Wu et al., 2012; Liu et al., 2011; Juliano et al., 2009; Haasnoot et al., 2007). These problems can be overcome by advances in systemic delivery or local administration of siRNA. Topical or local delivery can prevent unwanted systemic side effects and maintain highest payload of therapeutic at target site (Katz et al., 2012; Wolinsky et al., 2012).

There is increasing interest in the stimulatory effect of EGF on wound healing and inhibitory effect of TGF-beta siRNA on scar formation. Here, we have hypothesized that the EGF and TGF-beta siRNA would enhance the wound healing after dermal injury. EGF and siRNA were loaded into LbL thin films prepared using biodegradable chitosan and sodium alginate. These films were applied on an incisional dermal injury mouse model to study the efficacy of EGF and siRNA on proliferation and inhibition of TGF-beta in-vivo.

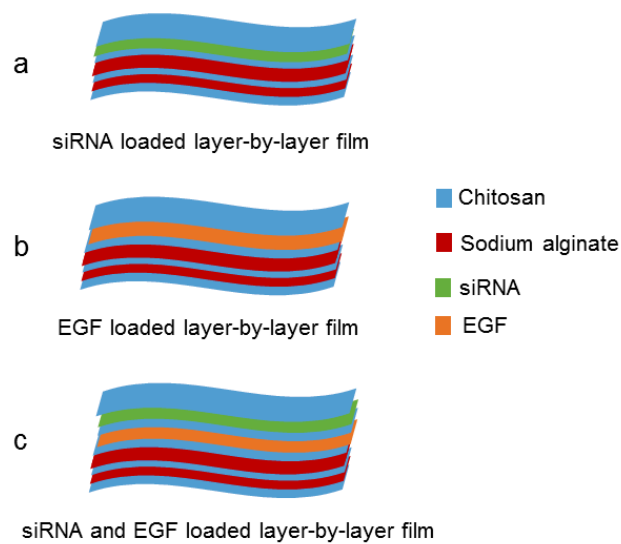
## 5.2. MATERIALS AND METHODS

Chitosan (75-85% deacetylated, MW: 100-300 kDa), sodium alginate (MW: 80 kDa), TGF-beta siRNA (MW: 13.3kDa, Sense: 5' A.A.U.C.A.A.G.U.G.U.G.G.A.G.C.A.A.C.A.U.U 3' and Antisense: 5' 5'-P.U.G.U.U.G.C.U.C.C.A.C.A.C.U.U.G.A.U.U.U.U 3') was purchased from GE Healthcare Dharmacon, USA. Control siRNA (Cat. No. sc-37007) and primary antibody  $\beta$ -Actin mouse monoclonal IgG, Horse radish peroxidase–conjugated (HRP) goat anti-mouse IgG were purchased from Santa Cruz Biotechnology, USA. Anti-human/mouse TGF-beta functional grade purified was purchased from eBioscience, USA. Epidermal growth factor (EGF: 6.2kDa), TRI reagent, isopropanol, sodium dodecylsulfate (SDS), hydroxyproline, hydrogen peroxide, sodium chloride, disodium hydrogen orthophosphate, potassium dihydrogen orthophosphate, sodium citrate, hydrochloric acid, sodium hydroxide, sulphuric acid, potassium bromide, ketamine, xylazine, HPLC grade acetonitrile and ammonium acetate were purchased from Sigma-Aldrich Chemical Company (Bengaluru, India). Dulbecco's modified Eagle's medium (DMEM), Dulbecco's phosphate buffered saline, fetal bovine serum (FBS), penicillin, streptomycin and trypsin were purchased from Himedia labs (Mumbai, India). All the chemicals were used without further purification. Milli-Q (Millipore, USA) water with 18.2 M $\Omega$  resistivity was used for all the experiments.

### 5.2.1. Preparation of the siRNA and EGF loaded layer-by-layer thin film

The LbL thin film was prepared as described in section 4.2.1. Stock solutions of siRNA and EGF were prepared by addition of 50 $\mu$ L HEPES (20 mM, pH 7.4) buffer to the vials containing 265.8  $\mu$ g siRNA and 500  $\mu$ g EGF, respectively. The concentration of the siRNA

was measured at 260 nm wavelength using Biospectrometer (Eppendorf, Germany) and EGF concentration was measured at 560 nm wavelength using BCA assay method against BSA standard. siRNA loaded films were prepared by layering siRNA (54 $\mu$ g/mL, HEPES, pH 7.4) on 14 bilayers of CS and SA. Finally, CS was layered on siRNA. Similar procedure was followed for EGF (54 $\mu$ g/mL, HEPES, pH 7.4) loaded film preparation. In case of siRNA and EGF combination, on top of 13 bilayers of CS and SA, EGF was layered followed by CS, followed by siRNA, and CS was used as final layer (Fig. 5.1).



**Fig. 5.1.** Schematic representation of layer-by-layer thin film loaded with siRNA (a), EGF (b) and combination of siRNA and EGF (c).

### 5.2.2. Characterization of the LbL thin films

The adsorption of polymers during the film growth was characterized by the UV-spectrophotometer and FTIR as described in section 4.2.4.

### 5.2.3. Quantification of siRNA and EGF loaded into LbL thin films

siRNA and EGF loaded LbL thin film were cut into  $1\text{cm}^2$  area and placed in  $500\mu\text{L}$  of nuclease free water. The film was subjected to vigorous agitation and sonication for 30 min to completely dissolve the film. Quantification of siRNA was determined at 260nm wavelength using Biospectrometer. EGF concentration was determined by BCA assay (Sigma-Aldrich BCA1 and B9643 Technical Bulletin); briefly,  $20\mu\text{L}$  protein samples were added to  $200\mu\text{L}$  BCA working reagent (1:8 v/v of copper solution and BCA solution) which was already prepared and placed in 96 wellplate. Samples were incubated for 15min at  $60^\circ\text{C}$  then cooled to room temperature and the absorbance was measured at 560nm using UV-visible spectrophotometer (Spectra Max, M4, Molecular Devices Inc., USA).

### 5.2.4. In-vitro release study

In-vitro release of siRNA and EGF from LbL thin film was performed after suspending in PBS (1 mL, pH = 7.4) in a cuvette incubated at  $37^\circ\text{C}$ . Samples of  $25\mu\text{L}$  were withdrawn from the cuvette at a predetermined time points (0.08, 0.16, 0.25, 0.5, 1, 2, 4, 6 and 8h). The amount of siRNA released was analyzed by measuring the absorbance at 260 nm wavelength. EGF was measured at 560 nm wavelength using BCA assay method as described in section 5.2.3.

To study the integrity of siRNA and EGF loaded in LbL films, tris borate EDTA polyacrylamide gel electrophoresis (TBE-PAGE) and sodium dodecyl sulfate polyacrylamide gel electrophoresis (SDS-PAGE) were performed, respectively. Samples collected after in-vitro release studies were used for gel electrophoresis. Free siRNA and EGF was used as



control. Sample preparation was done by mixing 3  $\mu$ L loading buffer and 10  $\mu$ L of sample and loaded in polyacrylamide gel (5% stacking gel; 10% resolving gel) of 0.75mm thickness. Electrophoresis was performed in vertical gel electrophoresis unit (Hoefer Inc., Holliston, MA) at 100V for 2 h. The gels with siRNA were stained using ethidium bromide for 30 min. Similarly, gels containing EGF were stained using coomassie blue. Then the bands were visualized using Gel DOC (Gel Doc XR+ Imaging system, BIORAD, Hercules, CA).

#### 5.2.5. In-vivo studies in the mouse dermal wound model

Female C57BL/6 mice weighing 20-24 g were procured from National Institute of Nutrition, Hyderabad, India, and the experiments were performed with approval from the institutional animal ethics committee (IAEC). The mice were fed with the standard laboratory diet and were provided with a clean drinking water *ad libitum*.

The excision wounds were made after anaesthetizing the mice by an intraperitoneal injection of ketamine (100 mg/kg) xylazine (10 mg/kg) mixture. The hair on the dorsal side of mice was clipped and the skin was sterilized with 70% ethanol. A circular wound of 8 mm diameter was made using a skin biopsy punch on the left side of the dorsal line. The mice weighing 20-24 g were divided into seven groups as shown in Table 5.1.

**Table 5.1.** Different treatment groups studied for application of TGF-beta and EGF loaded LbL thin films.

<b>Group</b>	<b>Treatment</b>	<b>Application</b>
<b>I</b>	No treatment	Not applicable
<b>II</b>	Blank LbL thin film	Every day
<b>III</b>	Scrambled siRNA control loaded LbL thin film	Alternate day
<b>IV</b>	EGF gel	Every day
<b>V</b>	EGF loaded LbL thin film	Every day
<b>VI</b>	TGF-beta siRNA loaded LbL thin film	Alternate day
<b>VII</b>	TGF-beta siRNA and EGF combination loaded LbL thin film	Alternate day

#### 5.2.6. Determination of the wound contraction, total protein and collagen content

The wound contraction, total protein and collagen content were determined by the procedure as described in section 4.2.10.

#### 5.2.7. Protein analysis

Protein analysis using western blot technique was performed using the procedure as described in section 4.2.11.

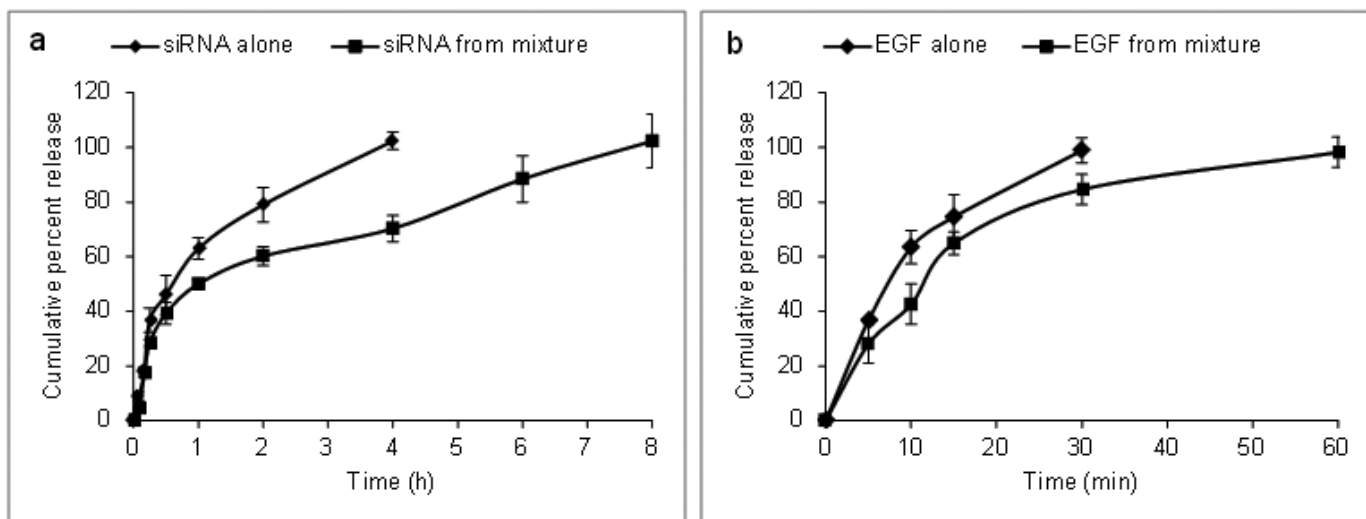
#### 5.2.8. Statistical analysis

All the results were presented as mean  $\pm$  standard deviation. Significance between groups was determined by Student's t test or analysis of variance (Graphpad Prism, USA), where  $p < 0.05$  was considered to be significant.

### 5.3. RESULTS

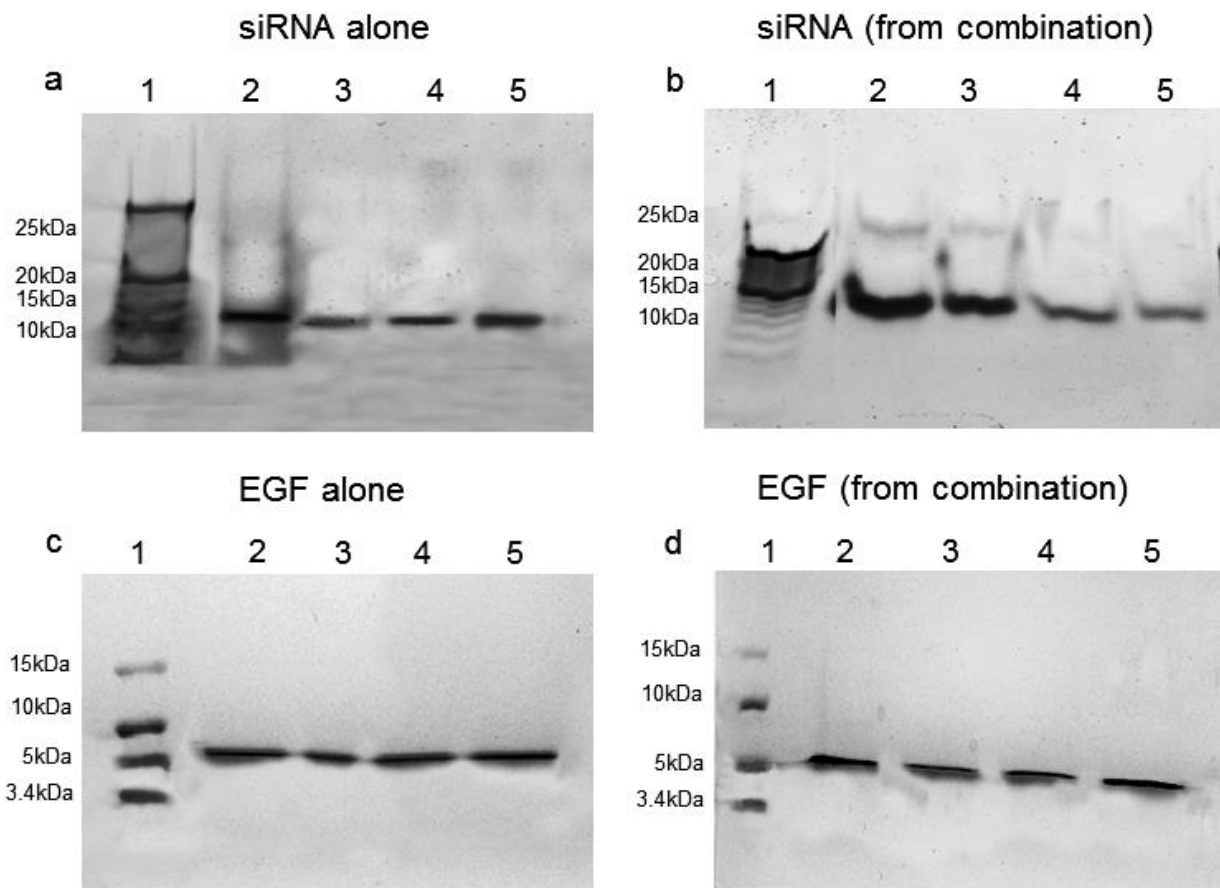
#### 5.3.1. Characterization of the siRNA and EGF loaded LbL thin films

The amount of TGF-beta siRNA and EGF present in 1cm<sup>2</sup> area of LbL thin film was found to be 2.8±0.2µg and 3.0±0.1µg, respectively. Fig. 5.2 shows cumulative percent release of TGF-beta siRNA and EGF as a function of time. The results showed that 100% release was achieved in 4 h for TGF-beta siRNA and 30 min EGF after loading in LbL thin films. For LbL thin films containing both TGF-beta siRNA and EGF, the rate of release was slower at 8 h and 60 min for TGF-beta siRNA and EGF, respectively.



**Fig. 5.2.** Cumulative percent release of a) TGF-beta siRNA and b) EGF in PBS from LbL thin film.

Gel electrophoresis was performed to characterize the integrity of the TGF-beta siRNA and EGF released from LbL thin films. Fig. 5.3 shows that the TGF-beta siRNA released from LbL thin films resulted in a single band at 13kDa. Similarly, the EGF released also showed a single band corresponding to 6kDa molecular weight.



**Fig. 5.3.** Integrity of TGF-beta siRNA released from LbL thin films (a) and combination (b); Lane 1, DNA base pair marker; lane 2, free siRNA; lane 3, 4 and 5 are release sample after 2, 4 and 24h time points. Integrity of EGF released from LbL thin films (c) and combination (d); Lane 1 Protein ladder; lane 2, free EGF; lane 3, 4 and 5 are release sample after 2, 4 and 24h time points.

### 5.3.2. Wound contraction, total protein and collagen content after topical application of the TGF-beta siRNA and EGF loaded LbL thin film

Figure 5.4a shows the percentage of wound contraction in the control (without any treatment), and after treatment with scrambled siRNA film, EGF gel, EGF loaded film, siRNA loaded film and combination of siRNA and EGF loaded film. There was a significant difference in the percentage of wound contraction between the control and all other treatment groups. The wound contraction was accelerated (<9 days) after application of the EGF gel, EGF loaded film, TGF-beta siRNA loaded film and combination of TGF-beta siRNA and EGF loaded film compared with application of blank film, scrambled siRNA loaded film and without any treatment (12 days). Figure 5.5 shows a representative image of excisional wounds at different time points.

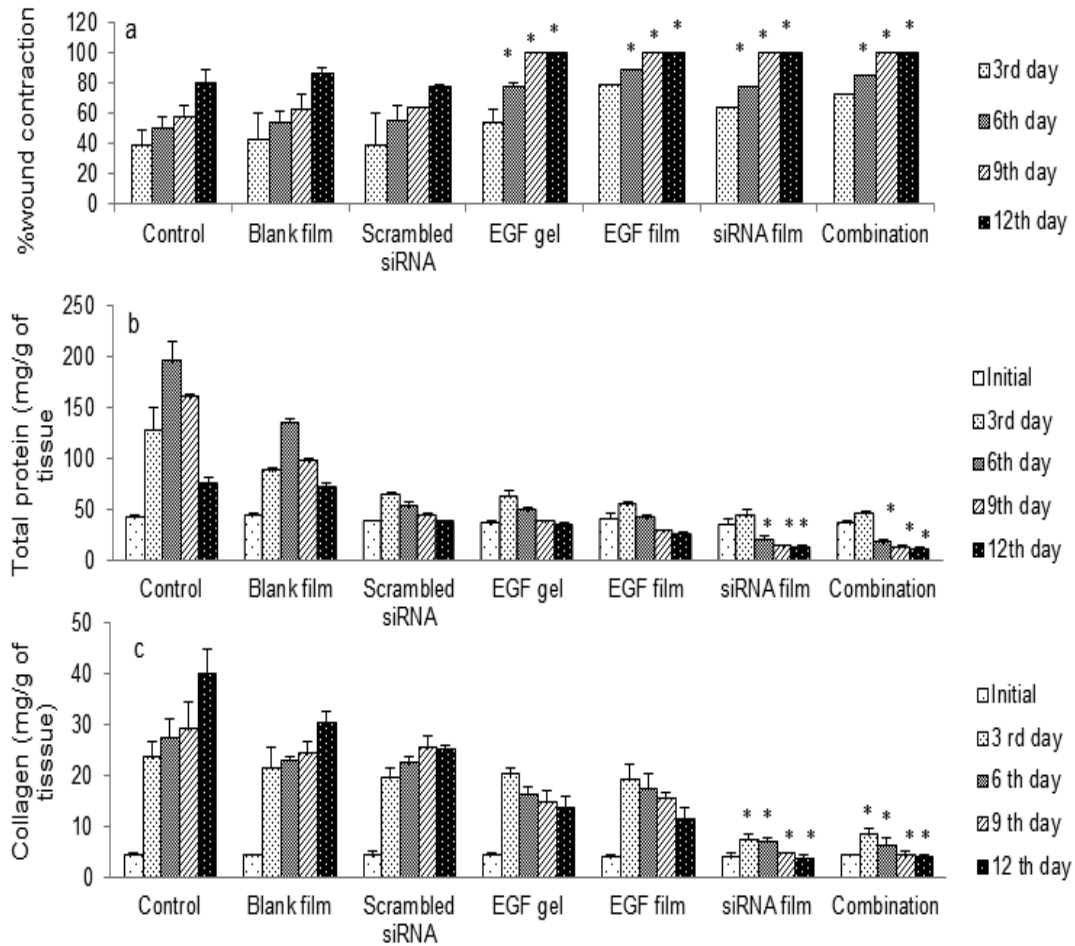
The total protein content within the wound tissue was measured for all the treatment groups. The total protein content was found to be significantly higher for the control group (without any treatment), blank film and scrambled siRNA control at all-time points measured compared with other treatment groups. The total protein content significantly ( $p < 0.05$ ) decreased after 6, 9 and 12<sup>th</sup> day for mice treated with the TGF-beta siRNA film and combination of TGF-beta siRNA and EGF loaded LbL thin film compared with 0 and 3<sup>rd</sup> day. On the other hand, the total protein content decreased significantly ( $p < 0.05$ ) after 9<sup>th</sup> day and 12<sup>th</sup> day for EGF gel and EGF film groups (Figure 5.4b).

Figure 5.4c shows the amount of collagen in the wound tissue at different time points. It was found that the collagen content increased with time in control group (without any treatment and after application of scrambled siRNA loaded film. On the other hand, mice treated with the TGF-beta siRNA loaded LbL thin film and combination of TGF-beta siRNA and EGF

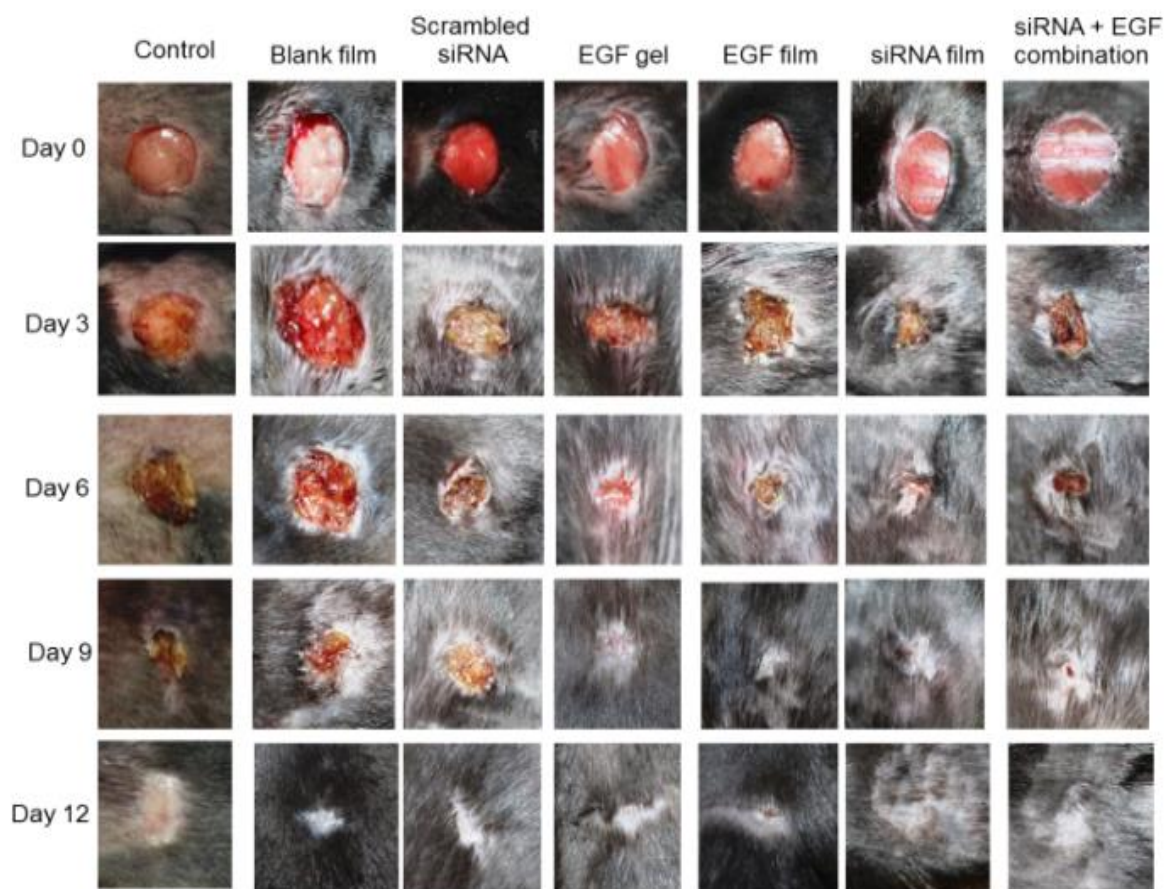
loaded film showed significantly ( $p < 0.05$ ) decreased collagen content compared with films loaded with EGF and EGF gel groups. Among the treatment groups, the TGF-beta siRNA loaded LbL thin films and combination of siRNA and EGF loaded film showed decreased collagen content at all-time points. After 12 days, the collagen content was found to be  $39.6 \pm 5.3$  mg/g tissue,  $30.2 \pm 2.5$  mg/g tissue and  $24.8 \pm 1.2$  mg/g tissue for control, blank film and scrambled siRNA film, respectively. These values are significantly ( $p < 0.05$ ) decreased at  $13.5 \pm 2.4$  mg/g tissue,  $11.3 \pm 2.3$  mg/g tissue,  $3.4 \pm 1.2$  mg/g tissue and  $3.7 \pm 0.8$  for the EGF gel, EGF film, TGF-beta siRNA loaded film and combination of TGF-beta siRNA and EGF loaded films respectively.

### 5.3.3. TGF-beta protein analysis

Western blot results showed that TGF-beta expression increased for mice without any treatment after excisional wounding. Similarly, TGF-beta protein bands were observed after application of blank film and control siRNA (Fig. 5. 6). The TGF-beta band intensity decreased after treatment with EGF gel and EGF film groups. On the other hand, TGF-beta siRNA treated groups (alone and in combination with EGF) showed gradual decrease in TGF-beta expression from 3<sup>rd</sup> day to 12<sup>th</sup> day. Group treated with TGF-beta siRNA showed 81.2, 96.4, 96.6% inhibition of TGF-beta and combination group showed 29.2, 48.6, 92 % inhibition of TGF-beta at 6, 9 and 12<sup>th</sup> day, respectively.

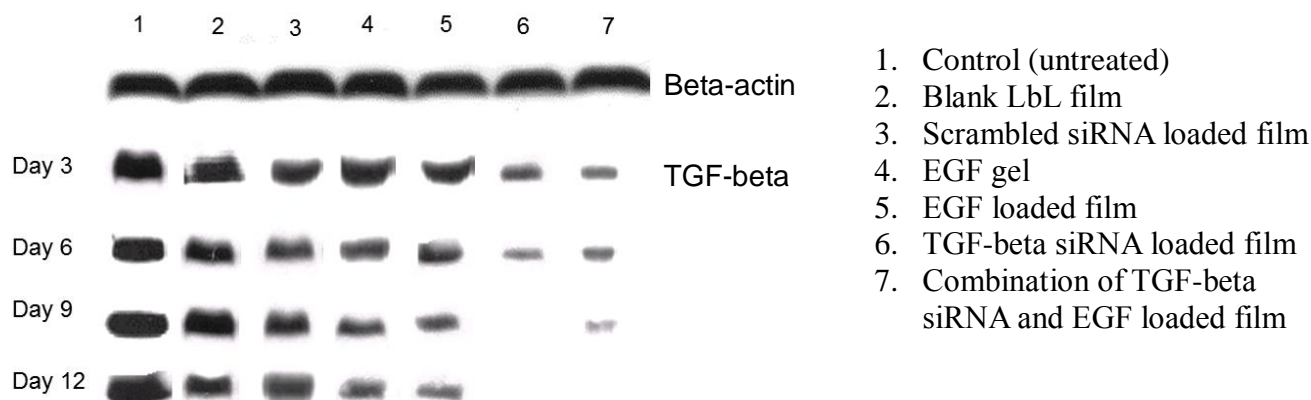


**Fig. 5.4.** Effect of topical application of LbL thin films loaded with siRNA and EGF on wound contraction (a), total protein (b) and collagen content (c). Data were presented as mean (n=4)  $\pm$  standard deviation. \* represents that the values are significantly different at  $p < 0.05$ .



**Fig. 5.5.** Digital photographs of excisional wounds on day 0, 3, 6, 9 and 12 after treatment with LbL thin films loaded with TGF-beta siRNA and EGF.





**Fig. 5.6.** TGF-beta protein analysis in excisional wounds from day 0 to day 12 after treatment with LbL thin films loaded with TGF-beta siRNA and EGF.

#### 5.4. DISCUSSION

Recently, there is increased interest in studying the stimulatory effect on wound healing and inhibitory effect on scar formation. Wound healing is a physiological phenomenon that involves a complex series of integrated cellular and biochemical responses. However, much of its detailed mechanism remains unknown (Kirsten et al., 2013; Clark et al., 2007). In the process of wound healing, the macromolecules present in the wound fluid and bed may trap growth factors within fibrin cuffs or bind them to the extracellular matrix (Trengone et al., 1999; Trengone et al., 2000). As a result, deficiency of growth factors in the wound bed and cell cycle arrest occurs, ultimately delaying the healing process. Hence, it is necessary to provide growth factors either autogenously by utilizing body's platelets/macrophages or can be produced outside the body chemically or biochemically

(recombinant). Studies have suggested that exogenous application of these factors to wound surface may benefit healing process. Growth factors are currently delivered to the wound either topically (such as platelet derived growth factor) or by subcutaneous injections (such as granulocyte colony stimulating factor).

Epidermal growth factor induces cellular proliferation after binding to EGF receptor, and results in EGF receptor dimerization, auto phosphorylation of the receptor and tyrosine phosphorylation of other proteins. Epidermal growth factor receptor activates MAP kinase pathway, ultimately causing phosphorylation of transcription factors, such as c-Fos, to create AP-1 and ELK-1 that contribute to proliferation. Activation of STAT-1 and STAT-3 transcription factors by JAK kinases in response to EGF contributes to proliferative signalling. Phosphatidylinositol signalling and calcium release induced by EGF activate protein kinase C, another component of EGF signalling pathway (Vijay et al., 2006). Thus EGF stimulates the proliferation of various cells, including glial cells, fibroblasts, and epithelium-derived cells such as keratinocytes (Fu-Shin et al., 2010).

In addition to accelerate wound healing process, it is necessary to prevent scar formation using various therapeutics and non-invasive techniques. Gene therapy involving RNA interference (RNAi) technique has shown potential in reduction of overexpressed protein. Small interfering RNA (siRNA) is more suitable for use because it does not require genome integration and can be easily synthesized. Since rational design of siRNA can specifically inhibit endogenous and heterologous gene expression, it can modulate any disease related gene expression.

When dsRNA enters the cell, it is first cleaved into short double stranded fragments of ~20 nucleotide siRNAs by the enzyme Dicer. Then, each double stranded siRNA is split into the passenger strand and the guide strand. After that, the guide strand is incorporated into the RNA-induced silencing complex (RISC), while the passenger strand is degraded. In the RISC, the guide strand of siRNA pairs with a complementary sequence in a messenger RNA molecule and induces cleavage by Argonaute, which causes post-transcriptional gene silencing (Cong-fei Xu and Jun Wang, 2015).

Most commonly used therapeutics, which are clinically approved for the dermal wound management is expected to improve the wound healing through occlusive effect, where the dressing is permeable to water vapor and oxygen but impermeable to bacteria (Aditya Sood et al., 2014; Vanessa Jones et al., 2006). Growth factors are currently delivered to the wound either topically (such as platelet derived growth factor) or by subcutaneous injections (such as granulocyte colony stimulating factor). The topical gel comprised with a recombinant PDGF, becaplermin, EGF is approved by the FDA to treat diabetic wounds (Mohan, 2007; Vijay et al., 2006). However, these were not effective in controlling the collagen production resulting in the scar tissue formation. On the other hand, there were no marketed TGF-beta inhibitors for topical application in dermal injury. Therefore, TGF-beta siRNA and EGF were explored for the dermal wound healing using LbL thin films.

In general, TGF-beta is the inhibitor of epithelial cell proliferation. After excisional wounding, TGF-beta levels will be increased causing cytostatic activity resulting in delayed wound healing. TGF-beta siRNA counteracted TGF-beta lead to enhanced proliferation and accelerated wound healing (Sushovan Chowdhury et al., 2013). Epidermal growth factor (EGF) belongs to a family of growth factors that regulate cell proliferation, migration and

differentiation by binding to receptor kinases on target cells resulting in accelerated wound healing (Zieske et al., 2000; Song et al., 2001; Fu-Shin et al., 2010).

## **5.5. CONCLUSION**

Layer-by-layer thin films can be used to incorporate more than one active molecule (EGF and siRNA) and control the release. We report for the first time the multilayered films-based delivery system containing both siRNA and EGF would significantly reduce collagen production and suppress TGF-beta protein within excisional wounds.

# Chapter 6

## Summary and Conclusions

---

## 6. SUMMARY AND CONCLUSIONS

Layer-by-layer self-assembly systems provide a robust platform to develop novel, drug delivery systems for number of small and macromolecule therapeutics on various nano- to macroscopically-sized systems. Due to its technological ease, low manufacturing cost, avoidance of hazardous chemicals, independent of precise stoichiometry, protection of encapsulated therapeutic agent, facilitation of controlled, triggered and target release, the technique shows potential to be a leading drug delivery technology in future.

In the present study, we developed two types of drug delivery carriers using layer-by-layer technology. The layer-by-layer microcapsules (LbL-MC) and layer-by-layer films were characterized and evaluated for their efficacy under in-vitro and in-vivo conditions.

The present investigation demonstrated that charge of a molecule is an important factor for its encapsulation into LbL-MC. Molecular interactions between LbL-MC and small molecules, including electrostatic interactions and hydrogen bonding enhance the adsorption of molecules. pH for ionic molecules is an important factor to be optimized for encapsulation. Controlled release of small molecules from LbL-MC can be achieved. PEGylation of LbL-MC can lead to reduced liver and spleen disposition. In case of protein, bovine serum albumin (BSA) encapsulation into LbL-MC showed greater encapsulation efficiency through co-precipitation method compared with adsorption method. Encapsulation efficiency and release of BSA were influenced by pH. BSA encapsulated in LbL-MC through co-precipitation method showed lesser degradation compared with adsorption method. Further, PSS/PAH LbL-MC can be developed as pH responsive carriers for controlled release of protein and other macromolecular therapeutics.

The present investigation also showed that the prepared layer-by-layer thin films exhibited good physical, mechanical and skin adhesion properties. The LbL thin films also

showed antimicrobial properties and cyto-compatible. The developed LbL thin films were used to entrap pirfenidone (PFD), epidermal growth factor (EGF) and TGF-beta siRNA and study the efficacy on excisional wound healing in mice. In-vivo wound healing studies showed an accelerated wound contraction after treatment with the PFD, siRNA and EGF loaded LbL thin films compared with blank films and control siRNA. Furthermore, PFD and siRNA treatment groups (alone and in combination with EGF) showed gradual decrease in TGF-beta expression compared to other groups. In conclusion, PFD and EGF & TGF-beta siRNA combination loaded in LbL thin films can be developed for potential wound healing applications.

Overall, this study demonstrated that layer-by-layer technique can be utilized to develop microcapsules and thin films for effective delivery of small and macromolecules for both systemic and topical applications.

## **FUTURE SCOPE AND DIRECTIONS**

The first ten years of layer-by-layer (LbL) self-assembly laid the physicochemical foundation for the fabrication of LbL constructs and the characterization. The robust nature of the self-assembly process, the high encapsulation efficiency, target ability and biocompatibility of LbL self-assembled systems holds great potential in controlled and targeted release of various therapeutic agents i.e small and macromolecule therapeutics (proteins and nucleic acids).

The direct outcome of the present study led to development of potential drug delivery carriers for systemic and topical application. To this end, the drug loaded LbL thin films showed enhanced wound healing and better wound management. Future studies based on this dissertation could include the investigation of applicability of this strategy to incorporate in wound dressings and other skin diseases including psoriasis and skin cancer. New molecular targets and their ligands can be identified to deliver through skin using layer-by-layer assembly technique.

Long-term treatment with biodegradable layer-by-layer implants for low therapeutic index drugs i.e. corticosteroids or anti-cancer drugs could be useful in treatment of tumors. These implants could be situated close to/in the tumor, ensuring long-term sustained release of the drug. The same strategy could probably be applied to deliver genes/DNA fragments to patients with metabolic defects to ensure long-term treatment. The long term focus of our research would be to investigate new methods to deliver small and macromolecules through the skin in a non-invasive fashion to treat systemic and localized diseases.



## REFERENCES

- Aarabi, S.; Longaker, M. T.; Gurtner, G. C. Hypertrophic scar formation following burns and trauma: new approaches to treatment. *PLoS Med.* 2007, 4:e234.
- Aditya, S.; Mark, S. G.; Nancy, L. T. Wound dressings and comparative effectiveness data. *Adv. Wound Care* 2014, 3, 511–529.
- Ai, H.; Jones, S. A.; de Villiers, M. M.; Lvov, Y. M. Nano-encapsulation of furosemide microcrystals for controlled drug release. *J. Controlled Release* 2003, 86, 59-68.
- Ai, H.; Layer-by-layer capsules for magnetic resonance imaging and drug delivery. *Adv. Drug Deliv. Rev.* 2011, 63, 772-788.
- Albertini, B.; Di Sabatino, M.; Calonghi, N. Novel multifunctional platforms for potential treatment of cutaneous wounds: Development and in vitro characterization. *Int. J. Pharm.* 2013, 440, 238–249.
- Allen, C.; Han, J.; Yu, Y.; Maysinger, D; Eisenberg, A. Polycaprolactone-b-poly(ethylene oxide) copolymer micelles as a delivery vehicle for dihydrotestosterone. *J. Controlled Release*, 2000, 63, 275-286.
- Alongi, J.; Carosio, F.; Frache, A.; Malucelli, G. Layer by layer coatings assembled through dipping, vertical or horizontal spray for cotton flame retardancy. *Carbohydr. Polym.* 2013, 92, 114–119.
- Anandhakumar, S.; Nagaraja, V.; Raichur, A. M. Reversible polyelectrolyte capsules as carriers for protein delivery. *Colloids Surf., B* 2010, 78, 266–274.
- Angelatos, A. S.; Radt, B.; Caruso, F. Light-Responsive Polyelectrolyte/Gold Nanoparticle Microcapsules. *J. Phys. Chem. B* 2005, 109, 3071-3076.
- Antipov, A. A.; Shchukin, D.; Fedutik, Y.; Petrov, A. I.; Sukhorukov, G. B.; Mohwald, H. Carbonate microparticles for hollow polyelectrolyte capsules fabrication. *Colloids Surf., A* 2003, 224, 175-183.

- Antipov, A. A.; Sukhorukov, G. B. Polyelectrolyte multilayer capsules as vehicles with tunable permeability. *Adv. Colloid Interface Sci.* 2004, 111, 49-61.
- Antipov, A. A.; Sukhorukov, G. B.; Leporatti, S.; Radtchenko, I. L.; Donath, E.; Mohwald, H. Polyelectrolyte multilayer capsule permeability control. *Colloids Surf., A* 2002, 198, 535-541.
- Antipov, A.A.; Sukhorukov, G. B.; Möhwald, H. Influence of the Ionic article Strength on the Polyelectrolyte Multilayers' Permeability. *Langmuir* 2003, 19, 2444-2448.
- Ariga, K.; Hill, J. P.; Ji, Q. Layer-by-Layer Assembly as a Versatile Bottom-Up Nanofabrication Technique for Exploratory Research and Realistic Application. *Phys. Chem. Chem. Phys.* 2007, 9, 2319–2340.
- Ariga, K.; Hill, J. P.; Lee, M. V.; Vinu, A.; Charvet, R.; Acharya, S. Challenges and breakthroughs in recent research on self-assembly. *Sci. Tech. Adv. Mater.* 2008, 9, 014109.
- Ariga, K.; Ji, Q.; Hill, J. P. Enzyme-encapsulated layer-by-layer assemblies: current status and challenges toward ultimate nanodevices. *Adv. Polym. Sci.* 2010, 229, 51-87.
- Ariga, K.; Ji, Q.; Hill, J.; Vinu, A. Coupling of soft technology (layer-by-layer assembly) with hard materials (mesoporous solids) to give hierarchic functional structures. *Soft Matter* 2009, 5, 3562-3571.
- Ariga, K.; Li, M.; Richards, G. J.; Hill, J. P. Nanoarchitectonics: a conceptual paradigm for design and synthesis of dimension-controlled functional nanomaterials. *J. Nanosci. Nanotechnol.* 2011, 11, 1-13.
- Ariga, K.; Vinu, A.; Ji, Q.; Ohmori, O.; Hill, J. P.; Acharya, S.; Koike, J.; Shiratori, S. A layered mesoporous carbon sensor based on nanopore-filling cooperative adsorption in the liquid phase. *Angew. Chem. Int. Ed.* 2008, 47, 7254-7257.

- Arys, X.; Laschewsky, A.; Jonas, A. M. Ordered polyelectrolyte “multilayers”. 1. Mechanisms of growth and structure formation: a comparison with classical fuzzy “multilayers”. *Macromolecules* 2001, 34, 3318–3330.
- Balabushevitch, N. G.; Sukhorukov, G. B.; Moroz, N. A.; Volodkin, D. V.; Larionova, NI.; Donath, E.; Mohwald, H. Encapsulation of proteins by layer-by-layer adsorption of polyelectrolytes onto protein aggregates: factors regulating the protein release. *Biotechnol. Bioeng.* 2001, 76, 207-213.
- Ballarín-González, B.; Howard, K. A. Polycation-based nanoparticle delivery of RNAi therapeutics: adverse effects and solutions. *Adv. Drug Deliv. Rev.* 2012, 64, 1717–1729.
- Bantchev, G.; Lu, Z.; Lvov, Y. Layer-by-layer nanoshell assembly on colloids through simplified washless process. *J. Nanosci. Nanotechnol.* 2009, 9, 396–403.
- Barker, S. L.; Ross, D.; Tarlov, M. J.; Gaitan, M.; Locascio, L.E. Control of flow direction in microfluidic devices with polyelectrolyte multilayers. *Anal Chem* 2000, 72, 5925–5929.
- Becker, A. L.; Johnston, A. P. R.; Caruso, F. Layer-by-layer-assembled capsules and films for therapeutic delivery. *Small* 2010, 6, 1836-1852.
- Becker, A. L.; Johnston, A. P. R.; Caruso, F. Peptide nucleic acid films and capsules: assembly and enzymatic degradation. *Macromol. Biosci.* 2010, 10, 488–495.
- Bende, G.; Kollipara, S.; Movva, S.; Moorthy, G.; Saha, R. Validation of an HPLC method for determination of imatinib mesylate in rat serum and its application in a pharmacokinetic study. *J Chromatogr Sci* 2010, 48, 334-341.
- Bergbreiter, D. E.; Liao, K. S. Covalent Layer-by-Layer Assembly An Effective, Forgiving Way to Construct Functional Robust Ultrathin Films and Nanocomposites. *Soft Matter* 2009, 5, 23–28.

- Beyer, S.; Bai, J.; Blocki, A. M.; Katak, C.; Xue, Q.; Trau, D. Assembly of biomacromolecule loaded polyelectrolyte multilayer capsules by using water soluble sacrificial templates. *Soft Matter* 2012, 8, 2760–2768.
- Bharadwaj, S.; Montazeri, R.; Haynie, D. T. Direct determination of the thermodynamics of polyelectrolyte complexation and implications thereof for electrostatic layer-by-layer assembly of multilayer thin films. *Langmuir* 2006, 22, 6093–6101.
- Bhattacharjee, J.; Verma, G.; Aswal, V. K.; Date, A. A.; Nagarsenker, M. S.; Hassan, P. A. Tween 80-sodium deoxycholate mixed micelles: structural characterization and application in doxorubicin delivery. *J. Phys. Chem. B* 2010, 114, 16414-16421.
- Bieker, P.; Schönhoff, M. Linear and exponential growth regimes of multilayers of weak polyelectrolytes in dependence on pH. *Macromolecules* 2010, 43, 5052–5059.
- Blacklock, J.; Mao, G.; Oupicky, D.; Mohwald, H. DNA release dynamics from bio-reducible layer-by-layer films. *Langmuir* 2010, 26, 8597-8605.
- Blanazs, A.; Armes, S. P.; Ryan, A. J. Self-assembled block copolymer aggregates: from micelles to vesicles and their biological applications. *Macromol. Rapid Commun.* 2009, 30, 267–277.
- Bo, Q.; Tong, X.; Zhao, Y.; Zhao, Y. A Micellar Route to Layer-by-Layer Assembly of Hydrophobic Functional Polymers. *Macromolecules* 2008, 41, 3562–3570.
- Boncheva, M.; Whitesides, G. M. Making things by self-assembly. *MRS Bull.* 2005, 30, 736–742.
- Brown, J. Q.; Srivastava, R.; McShane, M. J. Encapsulation of Glucose Oxidase and an Oxygen-Quenched Fluorophore in Polyelectrolyte-Coated Calcium Alginate Microspheres: Potential for Implantable Optical Glucose Sensor Systems. *Biosens. Bioelectron.* 2005, 21, 212-216.

- Buck, M. E.; Lynn, D. M. Reactive layer-by-layer assembly of suspended thin films and semipermeable membranes at interfaces created between aqueous and organic phases. *Adv. Mater.* 2010, 22, 994-998.
- Bulwan, M.; Zapotoczny, S.; Nowakowska, M. Robust 'one-component' chitosan-based ultrathin films fabricated using layer-by-layer technique. *Soft Matter* 2009, 5, 4726-4732
- Buron, C. C.; Filiâtre, C.; Membrey, F.; Bainier, C.; Buisson, L.; Charraut, D.; Foissy, A. Surface morphology and thickness of a multilayer film composed of strong and weak polyelectrolytes: effect of the number of adsorbed layers, concentration and type of salts. *Thin Solid Films* 2009, 517, 2611–2617.
- Capito, R. M.; Azevedo, H. S.; Velichko, Y. S.; Mata, A.; Stupp, S. I. Self-assembly of large and small molecules into hierarchically ordered sacs and membranes. *Science* 2008, 319, 1812–1816.
- Caravella, J.; Lugovskoy, A. Design of next-generation protein therapeutics. *Curr. Opin. Chem. Biol.* 2010, 14, 520–528.
- Caridade, S. G.; Monge, C.; Gilde, F.; Free-standing polyelectrolyte membranes made of chitosan and alginate. *Biomacromolecules* 2013, 14, 1653-1660.
- Carneiro-da-Cunha, M. G.; Cerqueira, M. A.; Souza, B.W. S. Physical and thermal properties of a chitosan/alginate nanolayered PET film. *Carbohydr. Polym.* 2010, 82, 153–159.
- Carter, P. J. Introduction to current and future protein therapeutics: a protein engineering perspective. *Exp. Cell. Res.* 2011, 317, 1261–1269.
- Caruso, F.; Caruso, R. A.; Möhwald, H. Nanoengineering of inorganic and hybrid hollow spheres by colloidal templating. *Science* 1998, 282, 1111–1114.
- Caruso, F.; Kurth, D. G.; Volkmer, D.; Koop, M. J.; Müller, A. Ultrathin molybdenum polyoxometalate–polyelectrolyte multilayer films. *Langmuir* 1998, 14, 3462–3465.

- Caruso, F.; Möhwald, H. Preparation and characterization of ordered nanoparticle and polymer composite multilayers on colloids. *Langmuir* 1999, 15, 8276–8281.
- Caruso, F.; Spasova, M.; Susha, A.; Giersig, M.; Caruso, R. A. Magnetic Nanocomposite Particles and Hollow Spheres Constructed by a Sequential Layering Approach. *Chem. Mater.* 2000, 13, 109-116.
- Caruso, F.; Susha, A. S.; Giersig, M.; Möhwald, H. Magnetic Core–Shell Particles: Preparation of Magnetite Multilayers on Polymer Latex Microspheres. *Adv. Mater.* 1999, 11, 950-953.
- Caruso, F.; Yang, W.; Trau, D.; Renneberg, R. Microencapsulation of uncharged low molecular weight organic materials by polyelectrolyte multilayer self-assembly. *Langmuir* 2000, 16, 8932–8936.
- Castleberry, S.; Wang, M.; Hammond, P. T. Nanolayered siRNA dressing for sustained localized knockdown. *ACS Nano* 2013, 25, 5251-5261.
- Chalker, J. M. Prospects in the total synthesis of protein therapeutics. *Chem Biol Drug Des* 2013, 81, 122–135.
- Chang, L.; Kong, X.; Wang, F.; Wang, L.; Schen, J. Layer-by-layer assembly of poly(Nacryloyl-N'-propylpiperazine) and poly(acrylic acid): effect of pH and temperature. *Thin Solid Films* 2008, 516, 2125–2129.
- Chávez, F. V.; Schönhoff, M. Pore size distributions in polyelectrolyte multilayers determined by nuclear magnetic resonance cryoporometry. *J. Chem. Phys* 2007, 126, 104705.
- Chiarelli P. A.; Johal, M. S.; Casson, J. L.; Roberts, J. B.; Robinson, J. M.; Wang, H. L. Controlled fabrication of polyelectrolyte multilayer thin films using spin-assembly. *Adv. Mater.* 2001, 13, 1167–1171.

Cho, J.; Char, K.; Hong, J. D.; Lee, K. B. Fabrication of highly ordered multilayer films using a spin self-assembly method. *Adv. Mater.* 2001, 13, 1076–1078.

Cho, M. E.; Kopp, J. B. Pirfenidone: an anti-fibrotic and cytoprotective agent as therapy for progressive kidney disease. *Expert Opin. Investig. Drugs* 2010, 19, 275-283.

Chowdhury, S.; Guha, R.; Trivedi, R. Pirfenidone nanoparticles improve corneal wound healing and prevent scarring following alkali burn. *PLoS One* 2013, 8:e70528.

Christophe, D.; Sukhorukov, G. B. pH-responsive properties of hollow polyelectrolyte microcapsules templated on various cores. *Langmuir* 2004, 20, 7265–7269.

Chvapil, M.; Kronenthal, R. L.; van Winkle, W. Medical and surgical applications of collagen. *Int. Rev. Connect. Tissue Res.* 1973, 6, 1–61.

Cingolani, R.; Coluccia, A. M. L.; Carlo, G. P.; Gigli, G.; Leporatti, S.; de Luca, E. Imatinib-loaded polyelectrolyte microcapsules for sustained targeting of BCR-ABL<sup>sup</sup>+ leukemia stem cells. *Nanomedicine* 2010, 53, 419-431.

Clark, R. A.; Ghosh, K.; Tonnesen, M. G. Tissue engineering for cutaneous wounds. *J. Invest. Dermatol.* 2007, 127, 1018-1029.

Clark, S. L.; Hammond, P. T. The role of secondary interactions in selective electrostatic multilayer deposition. *Langmuir* 2000, 16, 10206-10214.

Collier, J. H.; Messersmith, P. B. Phospholipid strategies in biomineralization and biomaterials research. *Annu. Rev. Mater. Res.* 2001, 31, 237–263.

Cong-fei, Xu.; Jun Wang. Delivery systems for siRNA drug development in cancer therapy. *Asian J Pharm Sci* 2015, 10, 1–12.

Cranford, S. W.; Buehler, M. J. Mechanomutable properties of a PAA / PAH polyelectrolyte complex: rate dependence and ionization effects on tunable adhesion strength. *Soft Matter* 2010, 6, 4175–4188.

- Dam, H. H.; Caruso, F. Formation and degradation of layer-by-layer-assembled polyelectrolyte polyrotaxane capsules. *Langmuir* 2013, 29, 7203-7208.
- D'Ayala, G. G.; Malinconico, M.; Laurienzo, P. Marine derived polysaccharides for biomedical applications: chemical modification approaches. *Molecules* 2008, 13, 2069-2106.
- De Temmerman, M.; Demeester, J.; De Vos, F.; De Smedt, S. C. Encapsulation performance of layer-by-layer microcapsules for proteins. *Biomacromolecules* 2011, 1283–1289.
- de Villiers, M. M.; Otto, D. P.; Strydom, S. J.; Lvov, Y. M. Introduction to nanocoatings produced by layer-by-layer (LbL) self-assembly. *Adv. Drug Deliv. Rev.* 2011, 63, 701-715.
- Decher, D.; Hong, J. D.; Schmitt, J. Buildup of ultrathin multilayer films by a self-assembly process. III. Consecutively alternating adsorption of anionic and cationic polyelectrolytes on charged surfaces. *Thin Solid Films* 1992, 210, 831-835.
- Decher, G. Fuzzy nanoassemblies: toward layered polymeric multicomposites. *Science* 1997, 277, 1232–1237.
- Decher, G.; Hong, J. D. Buildup of ultrathin multilayer films by a self-assembly process 1: consecutive adsorption of anionic and cationic bipolar amphiphiles on charged surfaces. *Makromol Chem Macromol Symp* 1991, 46, 321-327.
- Decher, G.; Hong, J. D.; Scmitt, J.; Buildup of ultrathin multilayer films by selfassembly process: III. Consecutively alternating adsorption of anionic and cationic polyelectrolytes on charged surfaces. *Thin Solid Films* 1992, 210/211, 831–835.
- Dejugnat, C.; Sukhorukov, G. B. pH-responsive properties of hollow polyelectrolyte microcapsules templated on various cores. *Langmuir* 2004, 20, 7265-7269.
- Delcea, M.; Möhwald, H.; Skirtach, A. G. Stimuli-responsive LbL capsules and nanoshells for drug delivery. *Adv. Drug Deliv. Rev.* 2011, 14, 63(9), 730-747.



- Detzel, C. J.; Larkin, A. L.; Rajagopalan, P. Polyelectrolyte multilayers in tissue engineering. *Tissue Eng Part B* 2011, 17, 101–113.
- Dhandayuthapani, B.; Yoshida, Y.; Maekawa, T. Polymeric scaffolds in tissue engineering application: a review. *Int. J. Poly. Sci.* 2011, 290602, 1-19.
- Donath, E.; Sukhorukov, G. B.; Caruso, F.; Davis, S. A.; Möhwald, H. Novel hollow polymer shells by colloid templated assembly of polyelectrolytes. *Angew. Chem. Int. Ed.* 1998, 37, 2201–2205.
- Dong, W. F.; Ferri, J. K.; Adalsteinsson, T.; Schonhoff, M.; Sukhorukov, G. B.; Mohwald, H. Influence of shell structure on stability, integrity, and mesh size of polyelectrolyte capsules: Mechanism and strategy for improved preparation. *Chem. Mater.* 2005, 17, 2603-2611.
- Dowling, M. B.; Lee, J. H.; Raghavan, S. R. pH-responsive jello: gelatin gels containing fatty acid vesicles. *Langmuir* 2009, 25, 8519-8525.
- Dubas, S. T.; Schlenoff, J. B. Factors controlling the growth of polyelectrolyte multilayers. *Macromolecules* 1999, 32, 8153–8160.
- Erokhina, S.; Berzina, T.; Christofolini, L.; Erokhin, V.; Folli, C.; Konovalov, O.; Marino, I. G.; Fontana, M. P. X-ray reflectivity measurements of layer-by-layer films at the solid/liquid interface. *Langmuir* 2008, 24, 12093–12096.
- Falanga, V. Wound healing and its impairment in the diabetic foot. *Lancet* 2005, 366, 1725-1735. García, L.; Hernández, I.; Sandoval, A.; Armendariz-Borunda, J. Pirfenidone effectively reverses experimental liver fibrosis. *J. Hepatol.* 37, 797–805.
- Fan, Y. F.; Wang, Y. N.; Fan, Y. G.; Ma, J. B. Preparation of insulin nanoparticles and their encapsulation with biodegradable polyelectrolytes via the layer-by-layer adsorption. *Int. J. Pharm.* 2006, 324, 158–167.

- Flessner, R. M.; Jewell, C. M.; Anderson, D. G.; Lynn, D. M. Degradable polyelectrolyte multilayers that promote the release of siRNA. *Langmuir* 2011, 27, 7868-7876.
- Fong, C.; Weerawardena, A.; Sagnella, S. M.; Mulet, X.; Waddington, L.; Krodkiewska, I.; Drummond, C. J. Monodisperse nonionic phytanyl ethylene oxide surfactants: high throughput lyotropic liquid crystalline phase determination and the formation of liposomes, hexosomes and cubosomes. *Soft Matter* 2010, 6, 4727-4741.
- Forster, S.; Schmidt, M. Polyelectrolytes in solution. *Adv. Polym. Sci.* 1995, 120, 51.
- Fou, A.; Onitsuka, O.; Ferreira, M.; Rubner, M.; Hsieh, B. Fabrication and properties of light-emitting diodes based on self-assembled multilayers of poly (phenylene vinylene). *J. Appl. Phys.* 1996, 79, 7501-7509.
- Fu, Y.; Bai, S.; Cui, S.; Qiu, D.; Wang, Z.; Zhang, X. Hydrogen-bonding directed layer by layer multilayer assembly: reformation yielding microporous films. *Macromolecules* 2002, 35, 9451-9458.
- Fujii, N.; Fujimoto, K.; Michinobu, T.; Akada, M.; Hill, J. P.; Shiratori, S.; Ariga, K.; Shigehara, K. The simplest layer-by-layer assembly structure: best paired polymer electrolytes with one charge per main chain carbon atom for multilayered thin films. *Macromolecules* 2010, 43, 3947-3955.
- Fujimoto, H.; Kato, K.; Iwata, H. Layer-by-layer assembly of small interfering RNA and poly(ethyleneimine) for substrate-mediated electroporation with high efficiency. *Anal. Bioanal. Chem.* 2010, 397, 571-578.
- Fukao, N.; Kyung, K. H.; Fujimoto, K.; Shiratori, S. Automatic spray-LbL machine based on in-situ QCM monitoring. *Macromolecules* 2011, 44, 2964-2969.
- Fu-Shin, X. Y.; Jia, Yin.; Keping, Xu.; Jenny, H. Growth factors and corneal epithelial wound healing. *Brain Res. Bull.* 2010, 81, 229-235.

- Gallarate, M.; Carlotti, M. E.; Trotta, M.; Bovo, S. On the stability of ascorbic acid in emulsified systems for topical and cosmetic use. *Int. J. Pharm.* 1999, 188, 233-241.
- Galvin, P.; Thompson, D.; Ryan, K. B.; McCarthy, A.; Moore, A. C.; Burke, C.S.; Dyson, M.; Maccraith, B. D.; Gun'ko, Y. K.; Byrne, M. T.; Volkov, Y.; Keely, C.; Keehan, E.; Howe, M.; Duffy, C.; Mac Loughlin, R. Nanoparticle based drug delivery: case studies for cancer and cardiovascular applications. *Cell. Mol. Life Sci.* 2012, 69, 389-404.
- Gan, L.; Han, S.; Shen, J.; Zhu, J.; Zhu, C.; Zhang, X.; Gan, Y. Self-assembled liquid crystalline nanoparticles as a novel ophthalmic delivery system for dexamethasone: Improving precocular retention and ocular bioavailability. *Int. J. Pharm.*, 2010, 396, 179-187.
- Gao, C. Y.; Donath, E.; Mohwald, H.; Shen, J. C. Spontaneous deposition of water-soluble substances into microcapsules: Phenomenon, mechanism, and application. *Angew. Chem. Int. Ed.* 2002, 41, 3789-3793.
- Gao, C. Y.; Leporatti, S.; Moya, S.; Donath, E.; Mohwald, H., Stability and mechanical properties of polyelectrolyte capsules obtained by stepwise assembly of poly(styrenesulfonate sodium salt) and poly(diallyldimethyl ammonium) chloride onto melamine resin particles. *Langmuir* 2001, 17, 3491-3495.
- Gao, C. Y.; Liu, X. Y.; Shen, J. C.; Mohwald, H. Spontaneous deposition of horseradish peroxidase into polyelectrolyte multilayer capsules to improve its activity and stability. *Chem. Commun.* 2002, 1928-1929.
- Gao, C. Y.; Moya, S.; Donath, E.; Mohwald, H. Melamine formaldehyde core decomposition as the key step controlling capsule integrity: Optimizing the polyelectrolyte capsule fabrication. *Macromol. Chem. Phys.* 2002, 203, 953-960.
- Gao, C. Y.; Moya, S.; Lichtenfeld, H.; Casoli, A.; Fiedler, H.; Donath, E.; Mohwald, H. The decomposition process of melamine formaldehyde cores: The key step in the fabrication

- of ultrathin polyelectrolyte multilayer capsules. *Macromol. Mater. Eng.* 2001, 286, 355-361.
- Gao, C.; Donath, E.; Moya, S.; Dudnik, V. Elasticity of hollow polyelectrolyte capsules prepared by the layer-by-layer technique. *Eur. Phys. J. E* 2001, 5, 21-27.
- Gao, C.; Leporatti, S.; Moya, S.; Donath, E.; Möhwald, H. Swelling and shrinking of polyelectrolyte microcapsules in response to changes in temperature and ionic strength. *Chem. Eur. J.* 2003, 9, 915-920.
- Ge, L. Q.; Mohwald, H.; Li, J. B. Phospholipase A(2) hydrolysis of mixed phospholipid vesicles formed on polyelectrolyte hollow capsules. *Chem. Eur. J.* 2003, 9, 2589-2594
- George, D. W. A Note on Wound Healing Under Dressings with Special Reference to Perforated-film Dressings. *The Journal of Investigative Dermatology* 1965, 45, 299–302.
- George, M.; Abraham, T. E. Polyionic hydrocolloids for the intestinal delivery of protein drugs: Alginate and chitosan — a review. *J. Control Release* 2006, 114, 1–14.
- Georgieva, R.; Dimova, R.; Sukhorukov, G.; Ibarz, G.; Möhwald, H. Influence of different salts on micro-sized polyelectrolyte hollow capsules. *J. Mater. Chem.* 2005, 15, 4301-4310.
- Ghosh, P. K.; Majithiya, R. J.; Umrethia, M. L.; Murthy, R. S. R. Design and development of microemulsion drug delivery system of acyclovir for improvement of oral bioavailability. *AAPS PharmSciTech*, 2006, 7, 77.
- Gittleson, F. S.; Kohn, D. J.; Li, X.; Taylor, A. D. Improving the assembly speed, quality, and tunability of thin conductive multilayers. *ACS Nano* 2012, 6, 3703–3711.
- Gleb, B.; Sukhorukov, M.; Brumen, E.; Donath, H. Mohwald, Hollow polyelectrolyte shells: exclusion of polymers and donnan equilibrium. *J. Phys. Chem. B* 1999, 103, 6434-6440.

- Glinel, K.; Dejumat, C.; Prevot, M.; Scholer, B.; Schonhoff, M.; Klitzing, R. V. Responsive polyelectrolyte multilayers. *Colloids Surf., A* 2007, 303, 3-13.
- Graf, N.; Tanno, A.; Dochter, A.; Rothfuchs, N.; Vörösa, J.; Zambelli, T. Electrochemically driven delivery to cells from vesicles embedded in polyelectrolyte multilayers. *Soft Matter* 2012, 8, 3641-3648.
- Grzybowski, B. A.; Wilmer, C. E.; Kim, J.; Browne, K. P.; Bishop, K. J. M. Self-assembly: from crystals to cells. *Soft Matter* 2009, 5, 1110–1128.
- Guzmán, E.; Ritacco, H.; Rubio, J. E. F.; Rubio, R. G.; Ortega, F. Salt-induced changes in the growth of polyelectrolyte layers of poly(diallyldimethylammonium chloride) and poly(4-styrene sulfonate of sodium). *Soft Matter*. 2009, 5, 2130–2142.
- Haasnoot, J.; Westerhout, E. M; Berkhout, B. RNA interference against viruses: Strike and counterstrike. *Nat. Biotechnol.* 2007, 25, 1435–1443.
- Hale, M. L.; Margolin, S. B.; Krakauer, T.; Roy, C. J.; Stiles, B. G. Pirfenidone blocks the in vitro and in vivo effects of staphylococcal enterotoxin B. *Infect. Immun.* 2002, 70, 2989–2994.
- Hammond, P. T. Building biomedical materials layer-by-layer. *Mater. Today* 2012, 15, 196–206.
- Hammond, P. T. Engineering materials layer-by-layer: challenges and opportunities in multilayer assembly. *AIChE J* 2011, 57, 2928-2940.
- Hammond, P.T. Recent explorations in electrostatic multilayer thin film assembly. *Curr. Opin. Colloid Interface Sci.* 2000, 4, 430–442.
- Hammond, P.T. Polyelectrolyte multilayered nanoparticles: using nanolayers for controlled and targeted systemic release. *Nanomedicine* 2012, 7, 619–622.

- Han, B.; Shen, B.; Wang, Z.; Shi, M.; Li, H.; Peng, C.; Zhao, Q.; Gao, C. Layered microcapsules for daunorubicin loading and release as well as *in vitro* and *in vivo* studies. *Polymer. Adv. Tech.* 2008, 19, 36-46.
- Harris, J. J.; Bruening, M. L. Electrochemical and in situ ellipsometric investigation of the permeability and stability of layered polyelectrolyte films. *Langmuir* 2000,16, 2006–2013.
- Haynie, D. T.; Palath, N.; Liu, Y.; Li, B. Y.; Pargaonkar, N. Biomimetic nanostructured materials: inherent reversible stabilization of polypeptide microcapsules. *Langmuir* 2005, 21, 1136- 1138.
- Hidalgo-Bastida, L. A.; Barry, J. J.; Everitt, N. M. Cell adhesion and mechanical properties of a flexible scaffold for cardiac tissue engineering. *Acta Biomater* 2007, 3, 457-462.
- Higley, H. R.; Ksander, G. A.; Gerhardt, C. O.; Falanga, V. Extravasation of macromolecules and possible trapping of transforming growth factors –beta in venous ulcerations. *Br. J. Dermatol.* 1995, 132, 79–85.
- Hirsjärvi, S.; Peltonen, L.; Hervonen, J. Layer-by-layer polyelectrolyte coating of low molecular weight poly(lactic acid) nanoparticles. *Colloids Surf., A* 2006, 49, 93–99.
- Hong, H. J.; Jin, S. E.; Park, J. S. Accelerated wound healing by smad3 antisense oligonucleotides-impregnated chitosan/alginate polyelectrolyte complex. *Biomaterials* 2008, 29, 4831–4837.
- Hong, H.; Steitz, R.; Kirstein, S.; Davidov, D. Superlattice structures in poly (phenylenevinylene)-based self-assembled films. *Adv. Mater.* 1998, 10, 1104–1108.
- Hong, X.; Li, J.; Wang, M.; Xu, J.; Guo, W.; Li, J.; Bai, Y.; Li, T. Fabrication of magnetic luminescent nanocomposites by a layer-by-layer self-assembly approach. *Chem. Mater.* 2004, 16, 4022–4027.

- Hooda, E.; Gonzalez, M.; Plaas, A.; Strom, J.; Van Auker, M. Immuno-targeting of nonionic surfactant vesicles to inflammation. *Int. J. Pharm.*, 2007, 339, 222-230.
- Hoogeveen, N. G.; Cohen Stuart, M. A.; Fleer, G. J. Formation and stability of multilayers of polyelectrolytes. *Langmuir* 1996, 12, 3675–3681.
- Hu, S. H.; Tsai, C. H.; Liao, C. F.; Liu, D.M.; Chen, S. Y. Controlled Rupture of Magnetic Polyelectrolyte Microcapsules for Drug Delivery. *Langmuir* 2008, 24, 11811-11818.
- Hu, X.; Ji, J. Construction of multifunctional coatings via layer-by-layer assembly of sulfonated hyperbranched polyether and chitosan. *Langmuir* 2010, 26, 2624-2629.
- Hu, Y.; Cai, K.; Luo, Z.; Jandt, K. D. Layer-by-layer assembly of beta-estradiol loaded mesoporous silica nanoparticles on titanium substrates and its implication for bone homeostasis. *Adv. Mater.* 2010, 22, 4146-4150.
- Hu, Y.; Cai, K.; Luo, Z.; Zhang, R.; Yang, L.; Deng, L.; Jandt, K. D. Surface mediated in situ differentiation of mesenchymal stem cells on gene-functionalized titanium films fabricated by layer-by-layer technique. *Biomaterials* 2009, 30, 3626-3635.
- Huynh, D. P.; Im, G. J.; Chae, S. Y.; Lee, K. C.; Lee, D. S. Controlled release of insulin from pH/temperature-sensitive injectable pentablock copolymer hydrogel. *J Controlled Release* 2009, 137, 20-24.
- Ibarz, G.; Dahne, L.; Donath, E.; Mohwald, H. Resealing of polyelectrolyte capsules after core removal. *Macromol. Rapid Commun.* 2002, 23, 474-478.
- Ilium, L. Chitosan and its use as a pharmaceutical excipient. *Pharm Res* 1998, 15, 1326-1331.
- Iyer, S. N.; Gurujeyalakshmi, G.; Giri, S. N. Effects of pirfenidone on transforming growth factor-beta gene expression at the transcriptional level in bleomycin hamster model of lung fibrosis. *J. Pharmacol. Exp. Ther.* 1999, 291, 367–373.

- Izquierdo, A.; Ono, S. S.; Voegel, J. C.; Schaaf, P.; Decher, G. Dipping versus spraying: Exploring the deposition conditions for speeding up layer-by-layer assembly. *Langmuir* 2005, 21, 7558–7567.
- Jang, H.; Kim, S.; Char, K. Multilayer line micropatterning using convective self-assembly in microfluidic channels. *Langmuir* 2003, 19, 3094–3097.
- Jayakumar, R.; Prabakaran, M.; Kumar, P. T. S. Biomaterials based on chitin and chitosan in wound dressing applications. *Biotechnol. Adv.* 2011, 29, 322–337.
- Jeong, Y. I.; Nah, J. W.; Lee, H. C.; Kim, S. H.; Cho, C. S. Adriamycin release from flower-type polymeric micelle based on star-block copolymer composed of poly( $\gamma$ -benzyl L-glutamate) as the hydrophobic part and poly(ethylene oxide) as the hydrophilic part. *Int. J. Pharm.*, 1999, 188, 49-58.
- Jewell, C. M.; Lynn, D. M. Multilayered polyelectrolyte assemblies as platforms for the delivery of DNA and other nucleic acid-based therapeutics. *Adv. Drug Deliv. Rev.* 2008; 60, 979–999.
- Ji, Q.; Honma, I.; Paek, S. M.; Akada, M.; Hill, J. P.; Vinu, A.; Ariga, K. Layer-by-layer films of graphene and ionic liquid for highly selective gas sensing. *Angew. Chem. Int. Ed.* 2010, 49, 9737-9739.
- Jiang, C.; Liu, X.; Luo, C.; Zhang, Y.; Shaoa, L.; Shi, F. Controlled exponential growth in layer-by-layer multilayers using high gravity fields. *J. Mater. Chem. A* 2014, 2, 14048–14053.
- Jiang, X.; Zhou, J.; Yuen, N. K.; Corless, C. L.; Heinrich, M. C.; Fletcher, J. A.; Demetri, G. D.; Widlund, H. R.; Fisher, D. E.; Hodi, F. S. Imatinib targeting of KIT-mutant oncoprotein in melanoma. *Clin. Cancer Res.* 2008, 14, 7726-7732.
- Johnston, A. P. R.; Cortez, C.; Angelatos, A. S.; Caruso, F. Layer-by-layer engineered capsules and their applications. *Curr. Opin. Colloid Interface Sci.* 2006, 11, 203-209.



- Johnston, A. P. R.; Read, E. S.; Caruso, F. DNA multilayer films on planar and colloidal supports: sequential assembly of like-charged polyelectrolytes. *Nano Lett.* 2005, 5, 953–956.
- Juliano, R.; Bauman, J.; Kang, H.; Ming, X. Biological barriers to therapy with antisense and siRNA oligonucleotides. *Mol. Pharmacol.* 2009; 6, 686–695.
- Kabanov, V. *Multilayer Thin Films* (Eds.: G. Decher, J. B. Schlenoff), Wiley-VCH Verlag, Weinheim, 2003.
- Kamineni, V. K.; Lvov, Y. M.; Dobbins, T. A. Layer-by-layer polyelectrolytes using formamide as the working medium. *Langmuir* 2007, 23, 7423–7427.
- Kantak, C.; Beyer, S.; Yobas, L.; Bansal, T.; Trau, D. A ‘microfluidic pinball’ for on-chip generation of layer-by-layer polyelectrolyte microcapsules. *Lab Chip* 2011, 11, 1030–1035.
- Karamitros, C. S.; Yashchenok, A. M.; Möhwald, H.; Skirtach, A. G.; Konrad, M. Preserving catalytic activity and enhancing biochemical stability of the therapeutic enzyme asparaginase by biocompatible multilayered polyelectrolyte microcapsules. *Biomacromolecules* 2013, 14, 4398-4406.
- Katayama, H.; Ishihama, Y.; Asakawa, N. Stable cationic capillary coating with successive multiple ionic polymer layers for capillary electrophoresis. *Anal. Chem.* 1998, 70, 5272–5277.
- Katz, M. G.; Fargnoli, A. S.; Pritchette, L. A.; Bridges, C. R. Gene delivery technologies for cardiac applications. *Gene Ther* 2012,19, 659–669.
- Kazakova, L. I.; Shabarchina, L. I.; Anastasova, S.; Pavlov, A. M. Chemosensors and biosensors based on polyelectrolyte microcapsules containing fluorescent dyes and enzymes. *Anal. Bioanal. Chem.* 2013, 405, 1559–1568.

- Kharlampieva, E.; Kozlovskaya, V.; Sukhishvili, S. A. Layer-by-Layer Hydrogen-Bonded Polymer Films: From Fundamentals to Applications. *Adv. Mater.* 2009, 21, 3053–3065.
- Kharlampieva, E.; Kozlovskaya, V.; Tyutina, J.; Sukhishvili, S. A. Hydrogen-bonded multilayers of thermo-responsive polymers. *Macromolecules* 2005, 38, 10523-10531.
- Khopade, A. J.; Caruso, F. Stepwise Self-Assembled Poly- (amidoamine) Dendrimer and Poly(styrenesulfonate) Microcapsules as Sustained Delivery Vehicles. *Biomacromolecules* 2002, 3, 1154– 1162.
- Khutoryanskaya, O. V.; Potgieter, M.; Khutoryanskiy, V. V. Multilayered hydrogel coatings covalently-linked to glass surfaces showing a potential to mimic mucosal tissues. *Soft Matter* 2010, 6, 551-557.
- Kim, B. S.; Gao, H.; Argun, A. A.; Matyjaszewski, K.; Hammond, P. T. All-star polymer multilayers as pH-responsive nanofilms. *Macromolecules* 2009, 42, 368-375.
- Kim, B. S.; Smith, R. C.; Poon, Z.; Hammond, P. T. MAD (multiagent delivery) nanolayer: delivering multiple therapeutics from hierarchically assembled surface coatings. *Langmuir* 2009, 25, 14086-14092.
- Kim, H. J.; Lee, K.; Kumar, S.; Kim, J. Dynamic sequential layer-by-layer deposition method for fast and region-selective multilayer thin film fabrication. *Langmuir* 2005, 21, 8532–8538.
- Kim, S.; Shi, Y.; Kim, J. Y.; Park, K.; Cheng, J. X. Overcoming the barriers in micellar drug delivery: loading efficiency, in vivo stability, and micelle-cell interaction. *Expert Opin. Drug Del.* 2010, 7, 49-62.
- Kinnane, C.R.; Such, G.K.; Antequera-García, G.; Yan, Y.; Dodds, S. J.; Liz-Marzan, L. M.; Caruso, F. Low-fouling poly(N-vinyl pyrrolidone) capsules with engineered degradable properties. *Biomacromolecules* 2009, 10, 2839–2846.

- Kirsten, A.; Bielefeld, S. A.; Benjamin, A. A. Cutaneous wound healing: recruiting developmental pathways for regeneration. *Cell. Mol Life Sci* 2013, 70, 2059–2081.
- Kittitheeranun, P.; Sanchavanakit, N.; Sajomsang, W.; Dubas, S. T. Loading of curcumin in polyelectrolyte multilayers. *Langmuir* 2010, 26, 6869-6873.
- Kleinfeld, E. R.; Ferguson, G. S. Stepwise formation of multilayered nanostructural films from macromolecular precursors. *Science* 1994, 265, 370-373.
- Ko, S. H.; Su, M.; Zhang, C. A.; Ribbe, A. E.; Jiang, W.; Mao, C. D. Synergistic self-assembly of RNA and DNA molecules. *Nat. Chem.* 2010, 2, 1050–1055.
- Ko, Y. H.; Kim, Y. H.; Park, J.; Nam, K. T.; Park, J. H.; Yoo, P. J. Electric-field-assisted layer-by-layer assembly of weakly charged polyelectrolyte multilayers. *Macromolecules* 2011, 44, 2866–2872.
- Koker, S. D.; Cock, L. J. D.; Rivera-gil, P.; Parak, W. J.; Auzély, R.; Vervaet, C. Polymeric multilayer capsules delivering biotherapeutics. *Adv. Drug Deliv. Rev.* 2011, 63, 748–761.
- Kolarik, L.; Furlong, D. N.; Joy, H.; Struijk, C.; Rowe, R. Building assemblies from high molecular weight polyelectrolytes. *Langmuir* 1999, 15, 8265–8275.
- Kotov, N. A. Layer-by-layer self-assembly: the contribution of hydrophobic interactions. *Nano Struct Mater* 1999, 12, 789-796.
- Kötz, J.; Kosmella, S. *Polyelectrolytes and Nanoparticles*, Springer Publishers, Heidelberg, 2007.
- Kötz, J.; Kosmella, S.; Beitz, T. Self-assembled polyelectrolyte systems. *Prog. Polym. Sci.* 2001, 26, 1199–1232
- Kotz, J.; Kosmella, S.; Beiz, T. Self-assembled polyelectrolyte systems. *Prog. Polym. Sci.* 2001, 26, 1199-1232.

- Krasemann, L.; Tieke, B. Selective ion transport across self-assembled alternating multilayers of cationic and anionic polyelectrolytes. *Langmuir* 2000, 16, 287-290.
- Krishna, G.; Bhattacharyya, A. S. Kinetics and thermodynamics of methylene blue adsorption on neem (*Azadirachta indica*) leaf powder. *Dyes Pigm.* 2005, 65, 51-59.
- Krogman, K. C.; Cohen, R. E.; Hammond, P. T.; Rubner, M. F.; Wang, B. N. Industrial-scale spray layer-by-layer assembly for production of biomimetic photonic systems. *Bioinspir Biomim* 2013, 8, 045005.
- Krogman, K. C.; Lowery, J. L.; Zacharia, N. S.; Rutledge, G. C.; Hammond, P. T. Spraying asymmetry into functional membranes layer-by-layer. *Nat. Mater.* 2009, 8, 512–518.
- Krogman, K. C.; Zacharia, N. S.; Schroeder, S.; Hammond, P. T. Automated process for improved uniformity and versatility of layer-by-layer deposition. *Langmuir* 2007, 23, 3137–3141.
- Kryger, Z. B.; Sisco, M.; Roy, N. K. Temporal expression of the transforming growth factor-beta pathway in the rabbit ear model of wound healing and scarring. *JACS* 2007, 205, 478-488.
- Ladam, G.; Gergely, C.; Senger, B.; Decher, G.; Voegel, J. C.; Schaaf, P.; Cuisinier, F. J. G. Protein interactions with polyelectrolyte multilayers: interactions between human serum albumin and polystyrene sulfonate/polyallylamine multilayers. *Biomacromolecules* 2000, 1, 674-687.
- Ladam, G.; Schaaf, P.; Decher, G.; Voegel, J. C.; Cuisinier, F. J. G. Protein adsorption onto auto-assembled polyelectrolyte films. *Biomol Eng* 2002, 19, 273-280.
- Langereis, E.; Heil, S. B. S.; Knoops, H. C. M.; Keuning, W.; van de Sanden, M. C. M.; Kessels, W. M. M.; In situ spectroscopic ellipsometry as versatile tool for studying atomic layer deposition. *J. Phys. D: Appl. Phys.* 2009, 42, 1–19.

- Laugel, n.; Betscha, c.; Winterhalter, M.; Voegel, J. C.; Schaaf, P.; Ball, V. Relationship between the growth regime of polyelectrolyte multilayers and the polyanion/polycation complexation enthalpy. *J. Phys. Chem. B* 2006, 110, 19443–19449.
- Lee, D.; Rubner, M. F.; Cohen, R. E. All-nanoparticle thin-film coatings. *Nano Lett.* 2006, 6, 2305–2312.
- Lehr, C. M.; Bouwstra, J. A.; Schacht, E. H. In vitro evaluation of mucoadhesive properties of chitosan and some other natural polymers. *Int. J. Pharm.* 1992, 78, 43–48.
- Lensen, D.; Vriezema, D. M.; Hest, J. C. M Van. Polymeric microcapsules for synthetic applications. *Macromol. Biosci.* 2008, 8, 991–1005.
- Li, H. Y.; LaBean, T. H.; Leong, K. W. Nucleic acid-based nanoengineering: novel structures for biomedical applications. *Interface Focus* 2011, 1, 702–724.
- Linford, M. R.; Auch, M.; Möhwald, H. Nonmonotonic effect of ionic strength on surface dye extraction during dye–polyelectrolyte multilayer formation. *J. Am. Chem. Soc.* 1998, 120, 178–182.
- Liu, J.; Guo, S.; Cinier, M.; Shlyakhtenko, L. S.; Shu, Y.; Chen, C.; Shen, G.; Guo, P. Fabrication of stable and RNase-resistant RNA nanoparticles active in gearing the nanomotors for viral DNA packaging. *ACS Nano* 2011, 5, 237–246.
- Liu, J.; Zhang, Y.; Wang, C.; Xu, R.; Chen, Z.; Gu, N. Magnetically sensitive alginate-templated polyelectrolyte multilayer microcapsules for controlled release of doxorubicin. *J. Phys. Chem. C* 2010, 114, 7673–7679.
- Liu, X.; Bruening, M. L. Size-selective transport of uncharged solutes through multilayer polyelectrolyte membranes. *Chem. Mater.* 2004, 16, 351–357.
- Liu, X.; Gao, C.; Shen, J.; Mohwald, H. Multilayer microcapsules as anti-cancer drug delivery vehicle: deposition, sustained release, and *in vitro* bioactivity. *Macromol. Biosci.* 2005, 5, 1209–1219.

- Loh, K. J.; Kim, J.; Lynch, J. P.; Kam, N. W. S.; Kotov, N. A. Multifunctional layer-by-layer carbon nanotube-polyelectrolyte thin films for strain and corrosion sensing. *Smart Mater. Struct.* 2007, 16, 429-438.
- Lvov, Y.; Ariga, K.; Ichinose I, Kunitake T. Assembly of multicomponent protein films by means of electrostatic layer-by-layer adsorption. *J. Am. Chem. Soc.* 1995, 117, 6117-6123.
- Lvov, Y.; Ariga, K.; Ichinose, I.; Kunitake, T. Layer-by-layer architectures of concanavalin A by means of electrostatic and biospecific interactions. *J. Chem. Soc., Chem. Commun.* 1995, 2313-2314
- Lvov, Y.; Haas, H.; Decher, G.; Moehwald, H.; Mikhailov, A.; Mtchedlishvily, B.; Morgunova, E.; Vainshtein, B. Successive deposition of alternate layers of polyelectrolytes and a charged virus. *Langmuir* 1994, 10, 4232-4236.
- Lvov, Y.; Onda, M.; Ariga, K.; Kunitake, T. Ultrathin films of charged polysaccharides assembled alternately with linear polyions. *J. Biomater. Sci., Polym. Ed.* 1998, 9, 345-355.
- Lynn, D. M. Layers of opportunity: nanostructured polymer assemblies for the delivery of macromolecular therapeutics. *Soft Matter* 2006, 2, 269–273.
- Lynn, D. M.; Langer, R. Degradable poly( $\beta$ -amino esters): synthesis, characterization, and self-assembly with plasmid DNA. *JACS* 2000, 122, 10761- 10768.
- Ma, L.; Cheng, M.; Jia, G.; Wang, Y.; An, Q.; Zeng, X.; Shen, Z.; Zhang, Y.; Shi, F. Layer-by-layer self-assembly under high gravity field. *Langmuir* 2012, 28, 9849–9856.
- Madaboosi, N.; Uhlig, K.; Jäger, M. S.; Möhwald, H.; Duschl, C.; Volodkin, D. V. Microfluidics as a tool to understand the build-up mechanism of exponential-like growing films. *Macromol. Rapid Commun.* 2012, 33, 1775–1779.

- Maeda, H. The enhanced permeability and retention (EPR) effect in tumor vasculature: the key role of tumor-selective macromolecular drug targeting. *Adv. Enzyme Regul.* 2001, 41, 189-207.
- Mahanta, D.; Manna, U.; Madras, G.; Patil, S. Multilayer Self-Assembly of TiO<sub>2</sub> Nanoparticles and Polyaniline-Grafted-Chitosan Copolymer (CPANI) for Photocatalysis. *ACS Appl. Mater. Interfaces* 2010, 3, 84–92.
- Maity, S.; Jana, P.; Maity, S. K.; Haldar, D. Mesoporous vesicles from supramolecular helical peptide as drug carrier. *Soft Matter* 2011, 7, 10174-10181.
- Mak, W. C.; Cheung, K. Y.; Trau, D. Influence of different polyelectrolytes on layer-by-layer microcapsule properties: encapsulation efficiency and colloidal and temperature stability. *Chem. Mater.* 2008, 20, 5475-5484.
- Mak, W. C.; Cheung, K. Y.; Trau, D. Influence of different polyelectrolytes on layer-by-layer microcapsule properties: encapsulation efficiency and colloidal and temperature stability. *Chem. Mater.* 2008, 20, 5475-5484.
- Manju, S.; Sreenivasan, K. Hollow microcapsules built by layer by layer assembly for the encapsulation and sustained release of curcumin. *Colloids Surf., B* 2011, 82, 588-593.
- Manna, U.; Patil, S. Dual drug delivery microcapsules via layer-by-layer self-assembly. *Langmuir* 2009, 25, 10515-10522.
- Manna, U.; Patil, S. Glucose-Triggered Drug Delivery from Borate Mediated Layer-by-Layer Self-Assembly. *ACS Appl. Mater. Interfaces* 2010, 2, 1521–1527.
- Mao, Z.; Ma, L.; Gao, C.; Shen, J. Preformed microcapsules for loading and sustained release of ciprofloxacin hydrochloride. *J. Control. Release* 2005, 104, 193-202.
- Matosevic, S.; Paegel, B. M. Layer-by-layer cell membrane assembly. *Nat. Chem.* 2013, 5, 958–963.

- Mehrotra, S.; Lee, I.; Chan, C. Multilayer mediated forward and patterned siRNA transfection using linear-PEI at extended N/P ratios. *Acta Biomater.* 2009, 5, 1474-1488.
- Mehrotra, S.; Lynam, D.; Maloney, R.; Pawelec, K. M.; Tuszynski, M. H.; Lee, I.; Chan, C.; Sakamoto, J. Time controlled protein release from layer-by-layer assembled multilayer functionalized agarose hydrogels. *Adv. Funct. Mater.* 2010, 20, 247-258.
- Mendes, A. C.; Baran, E.T.; Reis, R. L.; Azevedo, H. S. Self-assembly in nature: using the principles of nature to create complex nanobiomaterials. *Wiley Interdiscip Rev Nanomed Nanobiotechnol* 2013, 5(6), 582-612.
- Merrill, M. H.; Sun, C. T. Fast, simple and efficient assembly of nanolayered materials and devices. *Nanotechnology* 2009 20, 075606.
- Mohammed, J. S.; McShane, M. Polymer/ colloid surface micromachining: micropatterning of hybrid multilayers. *Langmuir* 2008, 24, 13796-13803.
- Mohan, V. K. Recombinant human epidermal growth factor (REGEN-D 150): effect on healing of diabetic foot ulcers. *Diabetes Res Clin Pract* 2007, 78, 405-411.
- Mohanta, V.; Madras, G.; Patil, S. Layer-by-Layer Assembled Thin Films and Microcapsules of Nanocrystalline Cellulose for Hydrophobic Drug Delivery. *ACS Appl. Mater. Interfaces* 2014, 6, 20093-20101
- Mohanta, V.; Madras, G.; Patil, S. Layer-by-Layer Assembled Thin Film of Albumin Nanoparticles for Delivery of Doxorubicin. *J. Phys. Chem. C* 2012, 116, 5333–5341.
- Moreno-Villoslada, I.; Gonzalez, R.; Hess, S.; Rivas, B. L.; Shibue, T.; Nishide, H. Complex formation between rhodamine B and poly(sodium 4-styrenesulfonate) studied by <sup>1</sup>H-NMR. *J. Phys. Chem. B* 2006, 110, 21576-21581.
- Mori, T.; Okamoto, K.; Endo, H.; Hill, J. P.; Shinoda, S.; Matsukura, M.; Tsukube, H.; Suzuki, Y.; Kanekiyo, Y.; Ariga, K. Mechanical tuning of molecular recognition to



- discriminate the single-methyl-group difference between thymine and uracil. *J. Am. Chem. Soc.* 2010, 132, 12868-12870.
- Morton, S. W.; Herlihy, K. P.; Shopsowitz, K. E.; Deng, Z. J.; Chu, K. S.; Bowerman, C. J.; Desimone, J. M.; Hammond, P. T. Scalable manufacture of built-to-order nanomedicine: Spray-assisted layer-by-layer functionalization of print nanoparticles. *Adv. Mater.* 2013, 25, 4707–4713.
- Morton, S. W.; Poon, Z.; Hammond, P. T. The architecture and biological performance of drug-loaded LbL nanoparticles. *Biomaterials* 2013, 34, 5328-5335.
- Mulhearn, W. D.; Kim, D. D.; Gu, Y.; Lee, D. Facilitated transport enhances spray layer-by-layer assembly of oppositely charged nanoparticles. *Soft Matter* 2012, 8, 10419–10427.
- Müller, K.; Quinn, J.F.; Jonhston, A. P. R.; Becker, M.; Greiner, A.; Caruso, F. Polyelectrolyte functionalization of electrospun fibers. *Chem. Mater.* 2006, 18, 2397–2403.
- Myers, D. *Surfaces, Interfaces, and Colloids: Principles and Applications* (John Wiley & Sons, 1999).
- Nakazato, H.; Oku, H.; Yamane, S. A novel anti-fibrotic agent pirfenidone suppresses tumor necrosis factor-alpha at the translational level. *Eur. J. Pharmacol.* 2001, 446, 477–485.
- Neuman, R. E.; Logan, M. A. The determination of hydroxyproline. *J. Biol. Chem.* 1950, 184, 299-306.
- Nolte, A. J.; Chung, J. Y.; Walker, M. L.; Stafford, C. M. In situ adhesion measurements utilizing layer-by-layer functionalized surfaces. *ACS Appl. Mater. Interfaces.* 2009, 1, 373–380.
- Nolte, A. J.; Takane, N.; Hindman, E.; Gaynor, W.; Rubner, M. F.; Cohen, R. E. Thin film thickness gradients and spatial patterning via salt etching of polyelectrolyte multilayers. *Macromolecules* 2007, 40, 5479–5486.

Ochs, C.J.; Such, G.K.; Yan, Y.; van Koeeverden, M.P.; Caruso, F. Biodegradable click capsules with engineered drug-loaded multilayers. *ACS Nano* 2010, 4, 1653–1663.

Okahata, Y.; Tsuruta, T.; Ijio, K.; Ariga, K. Preparations of Langmuir-Blodgett films of enzyme-lipid complexes: a glucose sensor membrane. *Thin Solid Films* 1989, 180, 65-72.

Onda, M.; Ariga, K.; Kunitake, T. Activity and stability of glucose oxidase in molecular films assembled alternately with polyions. *J. Biosci. Bioeng.* 1999, 87, 69-75.

Onda, M.; Lvov, Y.; Ariga, K.; Kunitake, T. Sequential actions of glucose oxidase and peroxidase in molecular films assembled by layer-by-layer alternate adsorption. *Biotechnol. Bioeng.* 1996, 51, 163-167.

Pakyari, M.; Farrokhi, A.; Maharlooei, M. K. Critical role of transforming growth factor beta in different phases of wound healing. *Adv Wound Care* 2013, 2, 215-224.

Pargaonkar, N.; Lvov, Y. M.; Li, N.; Steenekamp, J. H.; de Villiers, M. M. Controlled release of dexamethasone from microcapsules produced by polyelectrolyte layer-by-layer nanoassembly. *Pharm. Res.* 2005, 22, 826-835.

Pastoriza-Santos, I.; Schöler, B.; Caruso, F. Core-shell colloids and hollow polyelectrolyte capsules om diazoresins. *Adv. Funct. Mater.* 2001, 11, 122–128.

Paul, W.; Sharma, C. P. Chitosan and alginate wound dressings: a short review. *Trends Biomater Artif Organs* 2004, 18, 18-23.

Pavlov, A. M.; Saez, S.; Cobley, A.; Graves, J.; Sukhorukova, G. B.; Mason, T. J. Controlled protein release from microcapsules with composite shells using high frequency ultrasound-potential for in vivo medical use. *Soft Matter* 2011, 7, 4341-4347.

Pechenkin, M. A.; Mohwald, H.; Volodkin, D. V. pH and salt-mediated response of layer-by-layer assembled PSS/PAH microcapsules: fusion and polymer exchange. *Soft Matter* 2012, 8, 8659-8665.

- Peiffre, D.; Corley, T.; Halpern, G.; Brinker, B. Utilization of polymeric materials in laser fusion target fabrication. *Polymer* 1981, 22, 450–460.
- Peng, H.; Li, K.; Wang, T.; Wang, J.; Wang, J.; Zhu, R. Preparation of hierarchical mesoporous CaCO<sub>3</sub> by a facile binary solvent approach as anticancer drug carrier for etoposide. *Nanoscale Res. Lett.* 2013, 8, 1-11.
- Peng, Z. G.; Hidajat, K.; Uddin, M. S. Conformational change of adsorbed and desorbed bovine serum albumin on nano-sized magnetic particles. *Colloids Surf., B* 2004, 33, 15-21.
- Petersen, H.; Fechner, P. M.; Fischer, D.; Kissel, T. Synthesis, characterization, and biocompatibility of polyethylenimine-graft-poly(ethylene glycol) block copolymers. *Macromolecules* 2002, 35, 6867-6874.
- Petrov, A. I.; Antipov, A. A.; Sukhorukov, G. B. Base-acid equilibria in polyelectrolyte systems: From weak polyelectrolytes to interpolyelectrolyte complexes and multilayered polyelectrolyte shells. *Macromolecules* 2003, 36, 10079- 10086.
- Petrov, A. I.; Volodkin, D. V.; Sukhorukov, G. B. Protein-calcium carbonate co-precipitation: a tool for protein encapsulation. *Biotechnol. Progr.* 2005, 21, 918-925.
- Peyratout, C. S.; Dahne, L. Tailor-made polyelectrolyte microcapsules: from multilayers to smart containers. *Angew. Chem. Int. Ed.* 2004, 43, 3762-3783.
- Picart, C.; Lavalle, P.; Hubert, P.; Cuisinier, F. J. G.; Decher, G.; Schaaf, P.; Voegel, J. C. Buildup mechanism for poly (L-lysine)/hyaluronic acid films onto a solid surface. *Langmuir* 2001, 17, 7414–7424.
- Picart, C.; Schneider, A.; Etienne, O.; Mutterer, J.; Schaaf, P.; Egles, C.; Jessel, N.; Voegel, J. C. Controlled degradability of polysaccharide multilayer films in vitro and in vivo. *Adv. Funct. Mater.* 2005, 15, 1771–1780.

- Prausnitz, M. R.; Mitragotri, S.; Langer, R. Current status and future potential of transdermal drug delivery. *Nat Rev Drug Discov* 2004, 3, 115-124.
- Priest, C.; Quinn, A.; Postma, A.; Zelikin, A. N.; Ralston, J.; Caruso, F. Microfluidic polymer multilayer adsorption on liquid crystal droplets for microcapsule synthesis. *Lab Chip* 2008, 8, 2182–2187.
- Qi, A.; Chan, P.; Ho, J.; Rajapaksa, A.; Friend, J.; Yeo, L. Template-free synthesis and encapsulation technique for layer-by-layer polymer nanocarrier fabrication. *ACS Nano* 2011, 5, 9583–9591.
- Qiu, X.; Leporatti, S.; Donath, E.; Möhwald, H. Studies on the Drug Release Properties of Polysaccharide Multilayers Encapsulated Ibuprofen Microparticles. *Langmuir* 2001, 17, 5375-5380.
- Radt, B.; Smith, T. A.; Caruso, F. Optically addressable nanostructured capsules. *Adv. Mater.* 2004, 16, 2184-2189.
- Raman, N.; Lee, M. R.; Palecek, S. P.; Lynn, D. M. Polymer multilayers loaded with antifungal b-peptides kill planktonic *Candida albicans* and reduce formation of fungal biofilms on the surfaces of flexible catheter tubes. *J. Control Release* 2014, 191, 54–62.
- Rana, T. M. Illuminating the silence: Understanding the structure and function of small RNAs. *Nat. Rev. Mol. Cell Biol.* 2007, 8, 23–36.
- Redkar, M.; Hassan, P. A.; Aswal, V.; Devarajan, P. Onion phases of PEG-8 distearate. *J. Pharm. Sci.* 2007, 96, 2436-2445.
- Reyes, D. R.; Perruccio, E. M.; Becerra, S. P.; Locascio, L. E.; Gaitan, M. Micropatterning neuronal cells on polyelectrolyte multilayers. *Langmuir* 2004, 20, 8805–8811.
- Richardson, J. J.; Björnalm, M.; Caruso, F. Multilayer assembly. Technology-driven layer-by-layer assembly of nanofilms. *Science* 2015, 348, 2491.

- Richardson, J. J.; Ejima, H.; Lörcher, S. L.; Liang, K.; Senn, P.; Cui, J.; Caruso, F. Preparation of nano- and microcapsules by electrophoretic polymer assembly. *Angew. Chem. Int. Ed.* 2013, 52, 6455–6458.
- Richardson, J. J.; Liang, K.; Kempe, K.; Ejima, H.; Cui, J.; Caruso, F. Immersive polymer assembly on immobilized particles for automated capsule preparation. *Adv. Mater.* 2013, 25, 6874–6878.
- Sabine, A. E.; Thomas, K. Jeffrey, M. D. Inflammation in wound repair: molecular and cellular mechanisms. *J. Invest. Dermatol.* 2007, 127, 514-525.
- Saito, G.; Swanson, J. A.; Lee, K. D. Drug delivery strategy utilizing conjugation via reversible disulfide linkages: role and site of cellular reducing activities. *Adv. Drug Deliv. Rev.* 2003, 55, 199-215.
- Salloum, D. S.; Schlenoff, J. B. Protein adsorption modalities on polyelectrolyte multilayers. *Biomacromolecules* 2004, 5, 1089–1096.
- Satarkar, N. S.; Hilt, J. Z. Magnetic hydrogel nanocomposites for remote controlled pulsatile drug release. *J. Controlled Release* 2008, 130, 246-251.
- Sato, K.; Yoshida, K.; Takahashi, S.; Anzai, J. pH and sugar-sensitive layer-by-layer films and microcapsules for drug delivery. *Adv. Drug Deliv. Rev.* 2011, 63, 809–821.
- Sato, M.; Sano, M. van der Waals layer-by-layer construction of a carbon nanotube 2D network. *Langmuir* 2005, 21, 11490–11494.
- Schlenoff, J. B.; Dubas, S. T.; Farhat, T. Sprayed polyelectrolyte multilayers. *Langmuir* 2000, 16, 9968–9969.
- Schonhoff, M. Self-assembled polyelectrolyte multilayers. *Curr. Opin. Colloid Interface Sci.* 2003, 8, 86-95.

- Seo, J.; Lutkenhaus, J. L.; Kim, J.; Hammond, P. T.; Char, K. Effect of the layer-by-layer (LbL) deposition method on the surface morphology and wetting behavior of hydrophobically modified PEO and PAA LbL films. *Langmuir* 2008, 24, 7995–8000.
- Shah M, Foreman DM, Ferguson MW. (1992). Control of scarring in adult wounds by neutralising antibody to transforming growth factor beta. *Lancet* 339:213-14.
- Shah, N. J.; Hong, J.; Hyder, M. N.; Hammond, P. T. Osteophilic multilayer coatings for accelerated bone tissue growth. *Adv. Mater.* 2012, 24, 1445–1450.
- Shchukin, D. G.; Patel, A. A.; Sukhorukov, G. B.; Lvov, Y. M. Nanoassembly of biodegradable microcapsules for DNA encasing. *J. Am. Chem. Soc.* 2004, 126, 3374-3375.
- Shchukin, D. G.; Sukhorukov, G. B. Nanoparticle Synthesis in Engineered Organic Nanaoscale Reactors. *Adv. Mater.* 2004, 16, 671-682.
- Shchukin, D. G.; Sukhorukov, G. B. Selective YF<sub>3</sub> nanoparticle formation in polyelectrolyte capsules as microcontainers for yttrium recovery from aqueous solutions. *Langmuir* 2003, 19, 4427-4431.
- Shen, H.; Shi, H.; Ma, K.; Xie, M.; Tang, L.; Shen, S. Polyelectrolyte capsules packaging BSA gels for pH-controlled drug loading and release and their antitumor activity. *Acta Biomater.* 2013, 9, 6123–6133.
- Shi, L.; Lu, Y.; Sun, J.; Zhang, J.; Sun, C.; Liu, J.; Shen, J. Site-selective lateral multilayer assembly of bienzyme with polyelectrolyte on ITO electrode based on electric field-induced directly layer-by-layer deposition. *Biomacromolecules* 2003, 4, 1161–1167.
- Shim, B. S.; Kotov, N. A. Single-walled carbon nanotube combing during layer-by-layer assembly: From random adsorption to aligned composites. *Langmuir* 2005, 21, 9381–9385.

- Shim, B. S.; Podsiadlo, P.; Lilly, D. G.; Agarwal, A.; Lee, J.; Tang, Z.; Ho, S.; Ingle, P.; Paterson, D.; Lu, W.; Kotov, N. A. Nanostructured thin films made by dewetting method of layer-by-layer assembly. *Nano Lett.* 2007, 7, 3266–3273.
- Shu, S.; Sun, C.; Zhang, X.; Wu, Z.; Wang, Z.; Li, C. Hollow and degradable polyelectrolyte nanocapsules for protein drug delivery. *Acta Biomater.* 2010, 6, 210–217.
- Shukla, A.; Avadhany, S. N.; Fang, J. C.; Hammond, P. T. Tunable vancomycin releasing surfaces for biomedical applications. *Small* 2010, 6, 2392–2404.
- Shukla, A.; Fang, J. C.; Puranam, S.; Jensen, F. R.; Hammond, P. T. Hemostatic multilayer coatings. *Adv. Mater.* 2012, 24, 492–496.
- Shukla, A.; Fleming, K. E.; Chuang, H. F.; Chau, T. M.; Loose, C. R.; Stephanopoulos, G. N.; Hammond, P. T. Controlling the release of peptide antimicrobial agents from surfaces. *Biomaterials* 2010, 31, 2348-2357.
- Silva, H. S.; Uehara, T. M.; Bergamaski, K.; Miranda, P. B. Molecular ordering in layer-by-layer polyelectrolyte films studied by sum-frequency vibrational spectroscopy: the effects of drying process. *J. Nanosci. Nanotechnol.* 2008, 8, 3399–3405.
- Silva, J. M.; Duarte, A. R. C.; Caridade, S. G. Tailored freestanding multilayered membranes based on chitosan and alginate. *Biomacromolecules* 2014, 15, 3817–3826.
- Skirtach, A. G.; Dejugnat, C.; Braun, D.; Susha, A. S.; Rogach, A. L.; Parak, W. J.; Möhwald, H.; Sukhorukov, G. B. The Role of Metal Nanoparticles in Remote Release of Encapsulated Materials. *Nano Lett.* 2005, 5, 1371-1377.
- Skorb, E. V.; Möhwald, H. 5th anniversary article: Dynamic interfaces for responsive encapsulation systems. *Adv. Mater.* 2013, 25(36), 5029-5043.
- Smith, R. C.; Leung, A.; Kim, B. S.; Hammond, P. T. Hydrophobic effects in the critical destabilization and release dynamics of degradable multilayer films. *Chem. Mater.* 2009, 21, 1108-1115.

- Smith, R. C.; Riollano, M.; Leung, A. Layer-by-layer platform technology for small-molecule delivery. *Angew. Chem. Int. Ed.* 2009, 48, 8974-8977.
- Song, Q. H.; Singh, R. P.; Trinkaus-Randall, V. Injury and EGF mediate the expression of alpha6beta4 integrin subunits in corneal epithelium. *J. Cell. Biochem.* 2001, 80, 397-411.
- Steitz, R.; Jaeger, W.; Klitzing, R. Influence of charge density and ionic strength on the multilayer formation of strong polyelectrolytes. *Langmuir* 2001, 16, 4471-4474.
- Stockton, W. B.; Rubner, M. F. Molecular-level processing of conjugated polymers. 4: layer-by-layer manipulation of polyaniline via hydrogen-bonding interactions. *Macromolecules* 1997, 30, 2717-27125.
- Stuart, E.; Joseph, E. G.; Keith, G. H. Recent advances and emerging treatments. *BMJ* 2006, 332, 962-965.
- Su, X.; Kim, B. S.; Kim, S. R.; Hammond, P. T.; Irvine, D. J. Layer-by-layer-assembled multilayer films for transcutaneous drug and vaccine delivery. *ACS Nano* 2009, 3, 3719-3729.
- Sujata, S. Recent advances in topical wound care. *Indian J. Plast. Surg.* 2012, 45, 379-387.
- Sukhorukov, G. B.; Antipov, A. A.; Voigt, A.; Donath, E.; Möhwald, H. pH-controlled macromolecule encapsulation in and release from polyelectrolyte multilayer nanocapsules. *Macromol. Rapid Commun.* 2001, 22, 44-46.
- Sukhorukov, G. B.; Brumen, M.; Donath, E.; Mohwald, H. Hollow Polyelectrolyte Shells: Exclusion of Polymers and Donnan Equilibrium. *J. Phys. Chem. B* 1999, 103, 6434-6440.
- Sukhorukov, G. B.; Donath, E.; Davis, S.; Lichtenfeld, H.; Caruso, F.; Popov, V. I.; Möhwald, H. Stepwise polyelectrolyte assembly on particle surfaces: a novel approach to colloid design. *Polym. Adv. Technol.* 1998, 9, 759-767.



- Sukhorukov, G. B.; Donath, E.; Lichtenfeld, H.; Knippel, E.; Knippel, M.; Budde, A.; Möhwald, H. Layer-by-layer self-assembly of polyelectrolytes on colloidal particles. *Colloids Surf A Physicochem Eng Asp* 1998, 137, 253–266.
- Sukhorukov, G. B.; Volodkin, D. V.; Gunther, A. M.; Petrov, A. I.; Shenoy, D. B.; Mohwald, H. Porous calcium carbonate microparticles as templates for encapsulation of bioactive compounds. *J. Mater. Chem.* 2004, 14, 2073-2081.
- Sun, j.; Gao, M.; Feldmann, J. Electric field directed layer-by-layer assembly of highly fluorescent CdTe nanoparticles. *J Nanosci Nanotechnol* 2001, 1, 133–136.
- Susan, E. B.; Christopher, J. B. pH-Dependent loading and release behavior of small hydrophilic molecules in weak polyelectrolyte multilayer films. *Macromolecules* 2004, 37, 5375-5384.
- Sushovan, C.; Rajdeep, G.; Ruchit, T.; Uday, B. K.; Aditya, K.; Sarbani, H. Pirfenidone nanoparticles improve corneal wound healing and prevent scarring following alkali burn. *PLOS ONE* 2013; 8:e70528.
- Szarpak, A.; Pignot-Paintrand, I.; Nicolas, C.; Picart, C.; Auzély-Velty, R. Multilayer assembly of hyaluronic acid/poly(allylamine): control of the buildup for the production of multilayer capsules. *Langmuir* 2008, 24, 9767–9774.
- Tada, S.; Nakamuta, M.; Enjoji, M.; Sugimoto, R.; Iwamoto, H.; Kato, M. Pirfenidone inhibits dimethylnitrosamine-induced hepatic fibrosis in rats. *Clin. Exp. Pharmacol. Physiol.* 2001, 28, 522–527.
- Takahata, H.; Lavelle, E. C.; Coombes, A. G.; Davis, S. S. The distribution of protein associated with poly(DL-lactide co-glycolide) microparticles and its degradation in simulated body fluids. *J. Control. Release* 1998, 50, 237–246.

- Tang, H. Q.; Ji, S. L.; Gong, L. L.; Guo, H. X.; Zhang, G. J. Tubular ceramic-based multilayer separation membranes using spray layer-by-layer assembly. *Polym. Chem.* 2013, 4, 5621–5628.
- Taniguchi, H.; Ebina, M.; Kondoh, Y. Pirfenidone in idiopathic pulmonary fibrosis. *Eur. Respir. J.* 2010, 35, 821–829.
- Tao, X.; Chen, H.; Sun, X. J.; Chen, J. F.; Roa, W. H. Formulation and cytotoxicity of doxorubicin loaded in self-assembled bio-polyelectrolyte microshells. *Int. J. Pharm.* 2007, 336, 376–381.
- Tao, X.; Li, J. B.; Mohwald, H. Self-assembly, optical behavior, and permeability of a novel capsule based on an azo dye and polyelectrolytes. *Chem. Eur. J.* 2004, 10, 3397–3403.
- Taori, V. P.; Liu, Y.; Reineke, T. M. DNA delivery in vitro via surface release from multilayer assemblies with poly (glycoamidoamine)s. *Acta Biomater* 2009, 5, 925–933.
- Thomas, I. M. Single-layer TiO<sub>2</sub> and multilayer TiO<sub>2</sub>-SiO<sub>2</sub> optical coatings prepared from colloidal suspensions. *Appl. Opt.* 1987, 26, 4688–4691.
- Thu, H. E.; Zulfakar, M. H.; Ng, S. F. Alginate based bilayer hydrocolloid films as potential slow-release modern wound dressing. *Int. J. Pharm.* 2010, 434, 375–383.
- Tian, B.; Tao, X.; Ren, T.; Weng, Y.; Lin, X.; Zhang, Y.; Tang, X. Polypeptide-based vesicles: formation, properties and application for drug delivery. *J. Mater. Chem.*, 2012, 22, 17404–17414.
- Tong, W.; Song, X.; Gao, C. Layer-by-layer assembly of microcapsules and their biomedical applications. *Chem. Soc. Rev.* 2012, 41, 6103–6124.
- Trengone, N. J.; Bielefeldt –Ohmann, H.; Stacey, M. C. Miogenic activity and cytokine levels in nonhealing and healing chronic leg ulcers. *Wound Repair Regen.* 2000, 8, 13–25.

- Trengone, N. J.; Stacey, M. C.; MacAuley, S. Analysis of acute and chronic wound environment: The role of proteases and their inhibitors. *Wound Repair Regen.* 1999, 7, 442–452.
- Tripathy, S. K.; Kumar, J.; Nalwa (Eds.), H. S. *Handbook of Polyelectrolytes and Their Application*, American Scientific Publishers, Los Angeles, 2002.
- Trojer, M. A.; Nordstierna, L.; Bergek, J.; Blanck, H.; Holmberg, K.; Nydén, M. Use of Microcapsules as Controlled Release Devices for Coatings. *Adv. Colloid Interface Sci.* 2014.
- Tuan, T. L.; Nichter, L. S. The molecular basis of keloid and hypertrophic scar formation. *Mol Med Today* 1998, 4, 19-24.
- Tuo, X.; Chen, D.; Cheng, H.; Wang, X. Fabricating water-insoluble polyelectrolyte into multilayers with layer-by-layer self-assembly. *Polym. Bull.* 2005, 54, 427–433.
- Utsel, S.; Malmstrom, E. E.; Carlmark, A.; Wagberg, L. Thermoresponsive nanocomposites from multilayers of nanofibrillated cellulose and specially designed N-isopropylacrylamide based polymers. *Soft Matter* 2010, 6, 342-352.
- Van derveer, W. M.; Bloemen, M. C. T.; Ulrich, M. M. W.; Molema, G.; van Zuijlen, P. P.; Middelkoop, E.; Niessen F. B. Potential cellular and molecular causes of hypertrophic scar formation. *Burns* 2009, 35, 15-29.
- Van Tassel, P. R. Polyelectrolyte adsorption and layer-by-layer assembly: Electrochemical control. *Curr. Opin. Colloid Interface Sci.* 2012, 17, 106–113.
- Vandrovcova, M.; Bacakova, L. Adhesion, growth and differentiation of osteoblasts on surface-modified materials developed for bone implants. *Physiol Res* 2011, 60, 403-417.
- Vanessa, J.; Joseph, E. G.; Keith, G. H. Wound dressings. *BMJ* 2006, 332, 777–780.

- Varki, A. Biological roles of oligosaccharides—all of the theories are correct. *Glycobiology* 1993, 3, 97–130.
- Veerabadran, G. N.; Price, R. R.; Lvov, Y. M. Clay nanotubes for encapsulation and sustained release of drugs. *NANO* 2007, 2, 115-120.
- Vericat, C.; Vela, M. E.; Benitez, G.; Carro, P.; Salvarezza, R.C. Self-assembled monolayers of thiols and dithiols on gold: new challenges for a well-known system. *Chem. Soc. Rev.* 2010 39, 1805-1834.
- Verma, G.; Hassan, P. A. Self-assembled materials: design strategies and drug delivery perspectives. *Phys. Chem. Chem. Phys.* 2013, 15, 17016-17028
- Vijay, V.; Sharad, P.; Sekhar, N.; Murthy, G. S. R. A Phase III study to evaluate the safety and efficacy of recombinant human epidermal growth factor (REGEN-D™ 150) in healing dia . *Wounds* 2006, 18, 186-196.
- Vogel, A.; Venugopalan, V. Mechanisms of Pulsed Laser Ablation of Biological Tissues. *Chem. Rev.* 2003, 103, 577-644.
- Volodkin, D. V.; Larionova, N. I.; Sukhorukov, G. B. Protein encapsulation via porous CaCO<sub>3</sub> microparticles templating. *Biomacromolecules* 2004, 5, 1962-1972.
- Volodkin, D. V.; Madaboosi, N.; Blacklock, J.; Skirtach, A. G.; Möhwald, H. Surface-supported multilayers decorated with bio-active material aimed at light-triggered drug delivery. *Langmuir* 2009, 25, 14037-14043.
- Volodkin, D. V.; Petrov, A. I.; Prevot, M.; Sukhorukov, G. B. Matrix polyelectrolyte microcapsules: new system for macromolecule encapsulation. *Langmuir* 2004, 20, 3398-3406.
- Walker, D. J. Venous stasis wounds. *Orthop. Nurs.* 1999, 18, 65–74.
- Wang, F.; Liu, X.; Li, G.; Lia, D.; Dong, S. Selective electrodisolution of inorganic ions/DNA multilayer film for tunable DNA release. *J. Mater. Chem.* 2009, 19, 286-291.

- Wang, K.; He, Q.; Yan, X.; Cui, Y.; Qi, W.; Duan, L.; Li, J. Encapsulated photosensitive drugs by biodegradable microcapsules to incapacitate cancer cells. *J. Mater. Chem.* 2007, 17, 4018-4021.
- Wang, L.; Chen, D.; Sun, J. Layer-by-layer deposition of polymeric microgel films on surgical sutures for loading and release of ibuprofen. *Langmuir* 2009, 25, 7990-7994.
- Wang, X.; Ji, J. Postdiffusion of oligo-peptide within exponential growth multilayer films for localized peptide delivery. *Langmuir* 2009, 25, 11664-11671.
- Wang, X.; Zhang, X.; Castellot, J.; Herman, I.; Lafrati, M.; Kaplan, D. L. Controlled release from multilayer silk biomaterial coatings to modulate vascular cell responses. *Biomaterials* 2008, 29, 894-903.
- Wang, Y. W.; Liou, N. H.; Cherng, J. H.; Chang, S. J.; Ma, K. H.; Fu, E.; Liu, J. C.; Dai N. T. siRNA-targeting transforming growth factor- $\beta$  type I receptor reduces wound scarring and extracellular matrix deposition of scar tissue. *J. Invest. Dermatol.* 2014, 134, 2016-2025.
- Wang, Y.; Angelatos, A. S.; Caruso, F. Template Synthesis of Nanostructured Materials via Layerby- Layer Assembly. *Chem. Mater.* 2007, 20, 848-858.
- Wang, Y.; Liu, Y.; Cheng, Y.; Kim, E.; Rubloff, G. W.; Bentley, W. E.; Payne, G.F. Coupling electrodeposition with layer-by-layer assembly to address proteins within microfluidic channels. *Adv. Mater.* 2011, 23, 5817-5821.
- Wang, Y.; Yan, Y.; Cui, J.; Hosta-Rigau, L.; Heath, J. K.; Nice, E. C.; Caruso, F. Encapsulation of water-insoluble drugs in polymer capsules prepared using mesoporous silica templates for intracellular drug delivery. *Adv. Mater.* 2010, 22, 4293-4297.
- Wang, Z.; Zhang, X.; Gu, J.; Yang, H.; Nie, J.; Ma, G. Electrodeposition of alginate/chitosan layer-by-layer composite coatings on titanium substrates. *Carbohydr. Polym.* 2014, 103, 38-45.

- Werner, S.; Grose, R. Regulation of wound healing by growth factors and cytokines. *Physiol. Rev.* 2003, 83, 835-870.
- Whitesides, G. M.; Kriebel, J. K.; Mayers, B. T. Self-assembly and nanostructured materials. In: Huck WTS, ed. *Nanoscale Assembly: Chemical Techniques*. New York: Springer. 2005, 217–239.
- Wolinsky, J. B.; Colson, Y. L.; Grinstaff, M. W. Local drug delivery strategies for cancer treatment: gels, nanoparticles, polymeric films, rods, and wafers. *J. Control. Release* 2012, 159, 14–26.
- Wu, Z. W.; Chien, C. T.; Liu, C. Y.; Yan, J. Y.; Lin, S. Y. Recent progress in copolymer-mediated siRNA delivery. *J. Drug Target.* 2012, 20, 551–560.
- Wynn, T. A. Cellular and molecular mechanisms of fibrosis. *J. Pathol.* 2008, 214, 199–210.
- Yair, D. T. T. siRNAs: applications in functional genomics and potential as therapeutics. *Nat. Rev. Drug Discov.* 2004, 3, 318-329.
- Yan, S.; Zhu, J.; Wang, Z.; Yin, J.; Zheng, Y.; Chen, X. Layer-by-layer assembly of poly (L-glutamic acid)/chitosan microcapsules for high loading and sustained release of 5-fluorouracil. *Eur. J. Pharm. Biopharm.* 2011, 78, 336-345.
- Yang, M.; Yang, Y.; Yang, H.; Shen, G.; Yu, R. Layer-by-layer self-assembled multilayer films of carbon nanotubes and platinum nanoparticles with polyelectrolyte for the fabrication of biosensors. *Biomaterials* 2006, 27, 246-255.
- Yang, S. Y.; Rubner, M. F. Micropatterning of polymer thin films with pH-sensitive and cross-linkable hydrogen-bonded polyelectrolyte multilayers. *J. Am. Chem. Soc.* 2002, 124, 2100-2101.
- Yang, Y. J.; Tao, X.; Hou, Q.; Ma, Y.; Chen, X. L.; Chen, J. F. Mesoporous silica nanotubes coated with multilayered polyelectrolytes for pH-controlled drug release. *Acta Biomater.* 2010, 6, 3092-3100.

- Yang, Y.; Ye, Y.; Lin, X. Inhibition of pirfenidone on TGF-beta2 induced proliferation, migration and epithelial-mesenchymal transition of human lens epithelial cells line SRA01/04. *PLoS One* 2013, 8:e56837.
- Yariswamy, M.; Shivaprasad, H. V.; Joshi, V. Topical application of serine proteases from *Wrightia tinctoria* R. Br. (Apocyanaceae) latex augments healing of experimentally induced excision wound in mice. *J Ethnopharmacol* 2013, 149, 377-383.
- Yoo, D.; Shiratori, S. S.; Rubner, M. F. Controlling bilayer composition and surface wettability of sequentially adsorbed multilayers of weak polyelectrolytes. *Macromolecules* 1998, 31, 4309–4318.
- Yoshida, K.; Sato, K.; Anzai, J. Layer-by-layer polyelectrolyte films containing insulin for pH-triggered release. *J. Mater. Chem.* 2010, 20, 1546-1552.
- Yu, B. G.; Okano, T.; Kataoka, K.; Sardari, S.; Kwon, G. S. In vitro dissociation of antifungal efficacy and toxicity for amphotericin B-loaded poly(ethylene oxide)-block-poly(beta benzyl L aspartate) micelles. *J. Controlled Release*, 1998, 56, 285-291.
- Yuri, L.; Antipov, A. A.; Mamedov, A.; Mohwald, H.; Sukhorukov, G. Urease encapsulation in nanoorganized microshells. *Nano Lett.* 2001, 1, 125–128.
- Zebli, B.; Susha, A. S.; Sukhorukov, G. B.; Rogach, A. L.; Parak, W. J. Magnetic Targeting and Cellular Uptake of Polymer Microcapsules Simultaneously Functionalized with Magnetic and Luminescent Nanocrystals. *Langmuir* 2005, 21, 4262-4265.
- Zelikin Iler, R. K. Multilayers of colloidal particles. *J. Colloid Interface Sci.* 1966, 21, 569-594.
- Zelikin, A. N. Drug Releasing Polymer Thin Films: New Era of Surface-Mediated Drug Delivery. *ACS Nano* 2010, 4, 2494–2509.
- Zelikin, A. N. Drug releasing polymer thin films: new era of surface-mediated drug delivery. *ACS Nano* 2010, 4, 2494–2509.

- Zhao, Q.; Feng, X.; Mei, S.; Jin, Z. Carbon-nanotube-assisted high loading and controlled release of polyoxometalates in biodegradable multilayer thin films. *Nanotechnology* 2009, 20, 105101
- Zhao, Q.; Zhang, S.; Tong, W.; Gao, C.; Shen, J. Polyelectrolyte microcapsules templated on poly(styrene sulfonate)-doped CaCO<sub>3</sub> particles for loading and sustained release of daunorubicin and doxorubicin. *Eur. Polym. J.* 2006, 42, 3341-3351.
- Zhao, Z.; Qi, Y.; Wei, M.; Zhang, F.; Xu, S. Layer-by-layer assembly and morphological characterizations of DNA/layered double hydroxide Thin Films. *Mater. Lett.* 2012, 78, 62–68.
- Zhu, H. G.; McShane, M. J. Loading of hydrophobic materials into polymer particles: Implications for fluorescent nanosensors and drug delivery. *J. Am. Chem. Soc.* 2005, 127, 13448-13449.
- Zieske, J. D.; Takahashi, H.; Hutcheon, A. E.; Dalbone, A. C. Activation of epidermal growth factor receptor during corneal epithelial migration. *Invest. Ophthalmol. Vis. Sci.* 2000, 41, 1346– 1355.



## LIST OF PUBLICATIONS AND PRESENTATIONS

### From thesis

1. Praveen K. Mandapalli, Venkata Vamsi K. Venuganti. Layer-by-layer assembled thin films loaded with TGF-beta siRNA and epidermal growth factor for excisional wound healing applications. (Manuscript under preparation).
2. Praveen K. Mandapalli, Jagadeesh Bojja, Venkata Vamsi K. Venuganti. Topical application of pirfenidone loaded layer-by-layer assembled thin films: preparation, characterization and in-vivo evaluation of dermal wound management. (Manuscript under communication).
3. Praveen K. Mandapalli, Venkata Vamsi K. Venuganti. Layer-by-layer microcapsules for pH-controlled delivery of small molecules. *Journal of Pharmaceutical Investigation*, 2015; 45:131-141.
4. Praveen K. Mandapalli, Suman Labala, Deekshith Vanamala, Manali P. Koranglekar, Lakshmi A. Sakimalla, Venkata Vamsi K. Venuganti. Influence of charge on encapsulation and release behavior of small molecules in self-assembled layer-by-layer microcapsules. *Drug Delivery*, 2014; 21(8): 605–614.

### Other publications

1. Praveen Kumar Mandapalli, Suman Labala, Sumeet Chawla, Renuka Reddy Janupalli, Sriram Dharmarajan, Venkata Vamsi Krishna Venuganti. Polymer – Gold Nanoparticle Composite films for Topical Application: Evaluation of Physical Properties and Antibacterial Activity. (Manuscript under communication).
2. Anup Jose, Praveen K. Mandapalli, Venkata Vamsi K. Venuganti. Liposomal hydrogel formulation for transdermal delivery of pirfenidone. *Journal of Liposome Research* (early online, DOI: 10.3109/08982104.2015.1060611).
3. Suman Labala, Praveen K. Mandapalli, Abhinav Kurumaddali, Venkata Vamsi K. Venuganti. Layer-by-layer polymer coated gold nanoparticles for topical delivery of imatinib mesylate to treat melanoma. *Molecular Pharmaceutics*, 2015; 12 (3), 878-888.
4. Suman Labala, Praveen K. Mandapalli, Shubhmita Bhatnagar, Venkata Vamsi K. Venuganti. Encapsulation of albumin in self-assembled layer-by-layer microcapsules: comparison of co-precipitation and adsorption techniques. *Drug Development and Industrial Pharmacy* (early online, 2014, DOI: 10.3109/03639045.2014.947509).

## **Papers accepted/presented in conference**

### **From thesis**

1. Praveen Kumar Mandapalli, Jagadeesh Balija, Suman Labala, Venkata Vamsi Krishna Venuganti. Preparation, characterization and in vivo evaluation of pifrenidone loaded layer-by-layer films for dermal wound management. AAPS Annual Meeting and Exposition, Nov' 2-6, 2014, San Diego, USA.
2. Praveen Kumar Mandapalli, Venkata Vamsi Krishna Venuganti. Influence of charge on encapsulation and release of small molecules from PSS/PAH layer by layer microcapsules. 65th Indian Pharmaceutical Congress, Dec' 20-22, 2013, New Delhi, India.
3. Praveen Mandapalli, Deekshith Vanamala, Lakshmi Sakimalla, Venkata Vamsi K. Venuganti. Layer-by-layer encapsulated imatinib mesylate: in-vitro release, cell viability and bio-distribution studies. AAPS Annual Meeting and Exposition, Nov' 10-14, 2013, San Antonio, USA.
4. Mandapalli P. K., Koranglekar M. P., Venuganti V. V. K. Influence of physico-chemical properties of model molecules on encapsulation into self-assembled layer-by-layer microcapsules. CRS - Indian Chapter 13th International Symposium, Jan' 2013, Mumbai, India.
5. Mandapalli Praveen Kumar, Venkata Vamsi Krishna Venuganti. Fabrication of self-assembled layer-by-layer microcapsules for encapsulation of model charged lipophilic molecule. 64th Indian Pharmaceutical Congress, Dec' 7-9, 2012, Chennai, India.

### **Other presentations**

1. P. K. Mandapalli, S. Labala, D. Sriram, J. Renuka, V.V.Venuganti. Polymeric composites containing gold nanoparticles as antimicrobial agents for topical applications. Biomaterials International, June 1-5, 2015, Kenting, Taiwan.
2. Praveen Kumar M., Suman L., Sumeet C., Venkata Vamsi Krishna V. Evaluation of antimicrobial activity of gold nanoparticle loaded polymeric films for topical applications. 66th Indian Pharmaceutical Congress, Jan' 21-23, 2015, Hyderabad, India.
3. Anup Jose., Praveen Kumar M., Venkata Vamsi Krishna V. Feasibility study for transdermal delivery of pifrenidone using liposomes. 66th Indian Pharmaceutical Congress, Jan' 21-23, 2015, Hyderabad, India.

4. Suman Labala, Praveen Kumar Mandapalli, Venkata Vamsi Krishna Venuganti. Layer-by-layer polymer coated gold nanoparticles for topical delivery of imatinib mesylate to treat melanoma. AAPS Annual Meeting and Exposition, Nov' 2-6, 2014, San Diego, USA.
5. Suman Labala, Praveen Kumar Mandapalli, Shubhmita Bhatnagar, Venkata Vamsi Krishna Venuganti. Preparation, characterization and protein deliverability of layer-by-layer microcapsules. AAPS Annual Meeting and Exposition, Nov' 2-6, 2014, San Diego, USA.
6. Rahul Sharma, Mandapalli Praveen Kumar and Venkata Vamsi Krishna Venuganti. Fabrication of self-assembled layer-by-layer microcapsules for encapsulation of model charged lipophilic molecule. 2nd International Conference and Exhibition on Pharmaceutical Regulatory Affairs, Nov' 2012, Hyderabad, India.
7. Manali P Koranglekar, Mandapalli Praveen Kumar and Venkata Vamsi Krishna Venuganti. Fabrication of self-assembled layer-by-layer microcapsules for encapsulation of model charged hydrophilic molecule. 2nd International Conference and Exhibition on Pharmaceutical Regulatory Affairs, Nov' 2012, Hyderabad, India.

## **AWARDS AND RECOGNITIONS**

1. Awarded International Travel Award by Indian Council of Medical Research (ICMR), Govt. of India to present a paper at Biomaterials International 2015, Kenting, Taiwan. Jun' 2015.
2. Awarded International Travel Support (ITS) Grant by Science and Engineering Research Board (SERB), Dept. of Science and Technology, Govt. of India to present a paper at AAPS Annual Meeting and Exposition 2014, San Diego, USA. Nov' 2014.
3. Awarded International Travel Award by Indian Council of Medical Research (ICMR), Govt. of India to present a paper at AAPS Annual Meeting and Exposition 2014, San Diego, USA. Nov' 2014.
4. Awarded International Travel Award by Centre for International Co-operation in Science (CICS), Govt. of India to present a paper at AAPS Annual Meeting and Exposition 2014, San Diego, USA. Nov' 2014.
5. Graduate Student Travel Award sponsored by Formulation Design and Development (FDD) section, AAPS Annual meeting and Exposition, San Antonio, TX, USA, NOV' 2013.
6. Awarded Senior Research Fellowship (SRF) to pursue Ph.D by Council of Scientific & Industrial Research (CSIR), Human Resource Development Group (HRDG), New Delhi, India.

### **Biography of Praveen Kumar Mandapalli**

Mr. Praveen Kumar Mandapalli has completed his B. Pharm (2006) and M. Pharm (2009) from Kakatiya University, Warangal. Later, he worked as a research assistant in Suven Life Sciences Pvt Ltd., in pre-formulation department. He joined BITS-Pilani, Hyderabad campus as a PhD scholar in Jan 2011. He has authored/co-authored research papers in renowned international and national peer-reviewed journals. He has also presented scientific posters/papers in reputed international and national conferences. Mr. Praveen Kumar received “Senior Research Fellowship” from CSIR-New Delhi. He also received various travel grants from SERB, Department of Science and Technology (DST), Indian Council of Medical Research (ICMR) and Centre for International Co-operation in science (CICS) to present his research work.

### **Biography of Dr. Venkata Vamsi Krishna Venuganti**

Dr. Venkata Vamsi Krishna Venuganti is currently working as Assistant Professor in Department of Pharmacy, BITS-Pilani, Hyderabad Campus. He received his B. Pharm degree (2004) from Kakatiya University, India. He was awarded with PhD degree from South Dakota State University, USA (2010) in Pharmaceutical Sciences. He has been working as a faculty member in BITS-Pilani, Hyderabad Campus since July, 2010. He has 10 publications to his credit and authored a book chapter in “Nanosystems for skin drug delivery. In. Nanoparticulate delivery systems II. Formulation and Characterization” published by Informa Healthcare Inc, New York, NY, USA. Currently he has four government sponsored research projects. He has successfully completed two projects funded by BITS-Pilani (Research initiation grant) and Department of Science and Technology - SERB Young Scientist Award, India.